MONASH University

Investigating the effect of Soil Moisture, Temperature and Precipitation Extremes on Fire Risk and Intensity in Australia

Alexander William Holmes

MSc Atmospheric and Climate Sciences ETH Zürich, Switzerland
BSc Monash University, Australia
alexander.holmes@monash.edu

A thesis submitted for the degree of *Doctor of Philosophy*
at Monash University in 2018
3291: Doctor of Philosophy (Faculty of Engineering)

February 16, 2018

Copyright Notice

Abstract

Fire risk and fire intensity are increasingly important in semi-arid regions such as Australia where extreme conditions are expected to increase in both intensity and frequency under the influence of climate change. Conditions such as extreme temperature or prolonged precipitation deficits provide ample conditions for forest fires. As evident by the recent devastating fires in California in 2017 and infamously the 'Black Saturday' fires in Victoria in 2009, forest fires can have a devastating effect on land, property, livestock and even human life. Therefore, this thesis investigates the effect soil moisture, temperature, and precipitation deficits have on fire risk and fire intensity in Australia. At present there are no studies that combine high resolution remotely sensed soil moisture data, precipitation-driven drought indices, temperature extremes, and Fire Radiative Power (FRP) to produce fire risk. Also, there are many fire danger indices used to quantify the likelihood of a fire, with the most common, the McArthur Forest Fire Danger Index (FFDI), used in Australia. Most of these indices, and in particular the FFDI, are produced using spatially low resolution data and only include soil moisture in the form of the Keetch-Byram Drought Index (KBDI). This is an oversight, as soil moisture deficits are not only linked to vegetation moisture deficits but also to temperature extremes which in turn affect the resultant FFDI.

As the representation of soil moisture within the current FFDI uses an out-dated empirically derived precipitation-driven drought index (the KBDI), this thesis initially assesses several of the most commonly used precipitation-based moisture indices, as well as the remotely sensed ESA CCI soil moisture, and AWAP's modelled surface soil moisture products. This thesis builds on previous comparisons of precipitation-driven moisture indices by comparing them against ground observations and also against remotely sensed products, providing an overview of the spatial variation across Australia between 2000 to 2015 (*in situ*), and 1979 to 2015 (ESA CCI). Generally, API (Antecedent Precipitation Index) and MSDI (Mount's Soil Dryness Index) showed the largest correlation to *in situ* surface soil moisture (both normalised and the anomalies of the normalised data) with the highest correlations observed in the OzNet network, compared to the OzFlux and CosmOz network sites. Beyond this, API and MSDI tend to resemble the gridded reference soil moisture the closest with little bias towards either wetter or drier conditions, whereas KBDI and 14-day SPI show a large wet bias.

Furthermore, as precipitation and temperature are two of the key variables used in determining fire risk, their relationship with each other and their feedbacks are of particular relevance. To this extent, the influence of the location of the'Transitional Zone' on the Tx90-SM (Tx90; Hot-Days, SM; Soil Moisture) relationship is investigated in this thesis.

The transitional zone paradigm explains the influence of soil moisture on the overlying energy partitioning between sensible and latent heat in the context of evapotranspiration drivers and vegetation conditioning. Not only does this thesis show that, contrary to previous studies, the semi-arid region is moisture limited, indicating that it is largely not within the transitional zone, but also that, large areas of the temperate and savanna regimes enter the transitional zone resulting in a larger correlation between changes in moisture and Tx90 in these regions. This suggests that Australia exhibits differing conditions in relation to the Tx90-SM relationship than other similar climate regions.

The spatial variation in the strength of this relationship is a key factor in the magnitude of the resultant FFDI and more so the FRP. In particular, the most intense fires appear to occur in the temperate/transitional regime, specifically, in alpine south-east Australia, and are generally characterised as having very few fires per year compared to the north of the country. Typically, there is a larger number of fires occurring in the north of Australia but on average they have a far lower FFDI and FRP. This suggests that the current use of the FFDI should be adjusted to take into account the spatial differences in what constitutes fire risk in Australia. Furthermore, both MSDI and API best correspond to observed changes in the relationship between soil moisture and FRP with a clear logarithmic increase in FRP with decreasing moisture. When substituting the API (and other indices) in place of the KBDI in the drought component of the FFDI there is little difference in the resultant FFDI further suggesting that API is a more parsimonious measure of soil moisture.

Finally, API is used as the sole input into the drought component in the FFDI to assesses the change in FFDI derived from past and future projections of selected CMIP5 models for Australia between 1979 and 2100. Overall, FFDI is projected to increase substantially throughout the twenty-first century, particularly for the highest radiative forcing pathway (RCP 8.5). However, these changes are expected to vary greatly across Australia and seasonally, in line with observations from current trends in FFDI. By the end of the century the change in cumulative annual FFDI is estimated to increase by about 20% and 30% for medium (RCP 4.5) and high climate pathways, respectively (estimates of FFDI derived from monthly means). This underlines the importance of the FFDI and the use of soil moisture as a prognostic tool for estimating fire risk in Australia.

The research presented in this thesis contributes to a better understanding of the land-climate processes leading to forest fires and their intensity and also their likely change due to the effect of climate change. By strengthening this understanding, better prevention and mitigation of events and better allocation of water resources in the Australian region can be achieved.

Declaration

This thesis contains no material which has been accepted for the award of any other degree or diploma at any university or equivalent institution and that, to the best of my knowledge and belief, this thesis contains no material previously published or written by another person, except where due reference is made in the text of the thesis.

Print Name: Alexander Holmes

Signature: 

Date: 16/02/2018

Publications

I hereby declare that this thesis contains no material which has been accepted for the award of any other degree or diploma at any university or equivalent institution and that, to the best of my knowledge and belief, this thesis contains no material previously published or written by another person, except where due reference is made in the text of the thesis.

This thesis includes 2 original papers published in peer reviewed journals. The core theme of the thesis is to investigate *"The Effect of Soil Moisture, Temperature and Precipitation Extremes on Fire Risk and Intensity in Australia"*. The ideas, development and writing up of all the papers in the thesis were the principal responsibility of myself, the student, working within the unit: Doctor of Philosophy - 3291, under the primary supervision of Dr. Christoph Rüdiger.

In the case of chapters: 5 and Appendix-A.1 my contribution to the work involved the following:

Thesis Chapter	Publication Title	Status	Student Contribution	Co-author name(s) and contribution	Monash Student [Y/N]
5	Variability of Soil Moisture Proxies and Hot Days Across the Climate Regimes of Australia	Published	Alex Holmes* 70%	Chris Rudiger† 10% Brigitte Mueller⋆ 10% Martin Hirschi⋆ 5% Nigel Tapper‡ 5%	No No No No
A.1	Determining the Minimum Sampling Frequency for Ground Measurements of Burn Severity	Published	1. Alex Holmes* 75%	Chris Rudiger⋆ 10% Sarah Harris⋆ 10% Nigel Tapper‡ 5%	No No No

*Conceptual, data analysis and writing.
⋆Conceptual, writing and revision.
†Writing and revision.
‡ Manuscript revision.

I have renumbered sections of submitted or published papers in order to generate a consistent presentation within the thesis.

Student name: Alexander Holmes

Student signature: [redacted] Date: 16/02/2018

The undersigned hereby certify that the above declaration correctly reflects the nature and extent of the student's and co-authors' contributions to this work. In instances where I am not the responsible author I have consulted with the responsible author to agree on the respective contributions of the authors.

Main supervisor name: Christoph Rüdiger

Main supervisor signature: [redacted] Date: 16/02/2018

Acknowledgements

First and foremost, I would like to express my sincere gratitude to my main supervisor, Chris Rüdiger, for his scientific guidance and generous support throughout my candidature. His direction, vast knowledge and attention to detail has not only helped me though the course of my candidature but also provided me the feedback necessary to continually improve my research and writing. Thank you for pushing me to become a better scientist. I would also like to thank my co-supervisor, Professor Nigel Tapper for his insightful contribution to my work and his constant support and encouragement. He has always been readily available despite his busy schedule and eager to offer his time for discussion. I greatly appreciate both of you and thank you for your support through the ups and downs of my candidature.

Thank you also to Sarah Harris for her contribution and generosity throughout my candidature. Despite not being an official supervisor, she has always maintained contact to see how I was going and supported me with any queries and problems that arose. I would also like to thank the thesis reviewers and my candidature panel, Edo Daly, Valentijn Pauwels, Shayne McGregor, and Sarah for their comments and recommendations during each milestone.

To all my friends and colleagues at both the department of civil engineering and at the school for Earth, Atmosphere and the Environment, I thank you for sharing and the collaboration with data and knowledge, as well as your personal support and friendship. A particular thank you to my friend and office colleague, Sajjad Hosseini, who has shared the journey of our candidatures together and for countless hours of discussions and conversations along the way.

I acknowledge the World Climate Research Programme's Working Group on Coupled Modelling, responsible for the CMIP project, as well as Peter Briggs from CSIRO for making the AWAP data available to me, and any other groups responsible for the data used herein. Furthermore, I am grateful for the support of the Bushfire and Natural Hazards Cooperative Research Centre for their financial support as well as great opportunities through facilitating meetings, career-development opportunities, workshops, and conferences that I otherwise would not have been exposed to. Likewise, I would like to thank the Department of Civil Engineering, Monash, for their contribution via a half-scholarship to my candidature. I would also like to thank the Department of Environment, Land, Water and Planning (DELWP) for project management and facilitation as well as partly funding a component of this research.

Last, but not least, thank you to my family for their endless support and love throughout not only my Ph.D candidature but through life in general. I am truly grateful to my mum, my dad, my sister, and my grandparents for encouraging me always. I would also like to thank Andrea, for your love, patience and support throughout my candidature. Not only have you been the greatest inspiration to my research, as well as contributing with technical support, but your encouragement to pursue a scientific career has led me to undertake this Ph.D.

List of Abbreviations

API Antecedent Precipitation Index

AWAP Australian Water Availability Project

CMIP5 Coupled Model Intercomparison Project Phase 5

CosmOz Australian Cosmic-ray Neutron Soil Moisture Monitoring Network

DF Drought Factor

ERA-INTERIM European Centre for Medium-Range Weather Forecasts' re-analysis

ESA CCI European Space Agency Climate Change Initiative

ECV Essential Climate Variable

FFDI McArthur Forest Fire Danger Index

FRE Fire Radiative Energy

FRP Fire Radiative Power

IPCC Intergovernmental Panel on Climate Change

KBDI Keetch-Byram Drought Index

MODIS Moderate-Resolution Imaging Spectroradiometer

MSDI Mount's Soil Dryness Index

OzFlux Terrestrial Ecosystem Research Network: OzFlux

OzNet OzNet hydrological monitoring network

PDSI Palmer Drought Severity Index

pr Daily Precipitation

s0 AWAP Surface Soil Moisture

sfcWind Near Surface Wind Speed

SM Soil Moisture

SPI Standardized Precipitation Index

ss AWAP Soil Moisture

RH & hurs Near Surface Relative Humidity

Tx & tasmax Near Surface Maximum Daily Temperature

Tx90 & HD Number of Hot Days per Month

TX90pct 90^{th} Percentile of Maximum Daily Temperature

Contents

List of Figures

List of Tables

CHAPTER 1

Introduction

Overview With the likelihood of extreme events such as forest fires expected to increase due to climate change, it is critical to better understand the mechanisms promoting conditions leading to forest fires. These conditions, namely soil moisture, temperature, relative humidity, and wind speed are yet to be studied in relation to fire intensity; therefore an opportunity exists to not only investigate these conditions with respect to fire danger in Australia, but also improve on the resources for accurately calculating the McArthur Forest Fire danger Index (FFDI). In this thesis, in order to facilitate this, an investigation of the use and accuracy of various moisture indices for characterizing soil moisture is necessary and is the focus of the initial research task. Following this, since the partitioning between sensible and latent heating at the surface governs the strength of the relationship between soil moisture deficits and extreme temperature, the region in which this is expected to be maximised is analysed. This leads to a better understanding of the spatial variation between differences in FFDI, fire intensity (Fire Radiative Power; FRP) and relevant conditions, allowing for further research into improving the classification of fire danger through the FFDI. It is expected that in doing so a simpler formulation of the drought factor (a component within the FFDI) can be developed, further increasing our skill in forecasting fire danger in fire prone regions such as Australia.

1.1 Motivation

With acknowledgement that the climate system is changing due to anthropogenic forcing (IPCC, 2013a), differences in the mean state of the climate can have a drastic effect on the frequency and duration of extreme events. Due to this, the climate system has gained increasing attention during the last several decades, with the study of extreme events becoming the focus of research. Extreme events such as droughts and heat waves are regular occurrences on a large scale in semi-arid regions such as Australia, and are predicted to further increase in their frequency and severity (Cowan et al., 2014) in a warming climate. Conditions such as extreme temperature or prolonged precipitation deficits lead to these events and provide ample precursor conditions for catastrophic events such as forest fires. Forest fires can have a devastating effect on land, property, livestock, and even human life (Teague et al., 2010).

The 'Black Saturday' fires in Victoria in 2009 are a prime example of the extent of destruction such fires can cause and are generally considered among the worst in Australian recorded history (Teague et al., 2010). Teague et al. (2010) reported that these fires resulted in 173 deaths along with over 400 injuries and in excess of 11,800 livestock lost, with the physical damage of these fires including damage to over 5,000 homes and structures with a total of 2029 homes destroyed. Beyond this, over $60,000\ tonnes$ of produce and about $70,000\ ha$ of crops were destroyed during the fires. Overall, the fires burned an area of $4,500\ km^2$ (roughly 2% of the total size of Victoria) across 13 locations with temperatures in excess of $1200\ C°$. All of this culminated in the total cost of damages in excess of $4.4 billion with $645 million being attributed to the loss of life alone. However, the longer lasting effects of the fires are not considered in these estimates (Teague et al., 2010). Not only do forest fires occur on a large scale in Australia, but fire events are of significance worldwide, with devastating fires in Bolivia in 2010, Greece in 2012, Russia in 2010 and 2015, and more recently in California and Portugal in 2017, in which 44 and 64 people were killed, respectively. Furthermore, extreme conditions and weather events contribute to a raft of far-reaching socio-economic issues, including stress on industry, transportation systems, food, and energy production as well as political and social issues that are particularly vulnerable to shifts in the climate system as a whole.

Droughts in the form of soil moisture deficits influence multi-scale feedbacks (Miralles et al., 2008; Seneviratne et al., 2010; Miralles et al., 2012) as well as land-atmosphere interactions (Koster et al., 2003; Koster et al., 2014; Koster et al., 2016; Schubert et al., 2016b; Schubert et al., 2016a). It is therefore essential to understand exactly how soil moisture varies both spatially and temporally in order to accurately forecast and improve its

predictions in order to better mitigate risks (Draper et al., 2009). The importance of soil moisture on the climate system and as an environmental variable has recently been highlighted by its inclusion into the GCOS (Global Observing System for Climate) Essential Climate Variable (ESV) index under land interactions (Seneviratne et al., 2013). Not only is soil moisture an important variable in land dynamics such as subsurface flow, infiltration, and groundwater recharge, it influences photosynthesis and evapotranspiration through vegetation moisture and is also a key component in land-atmosphere feedbacks associated with the hydrological cycle at both weather and climate time-scales (Koster et al., 2003; Koster et al., 2014; Koster et al., 2016; Liu et al., 2012). Soil moisture affects the energy partitioning between sensible and latent heat from the land into the atmosphere potentially affecting local temperature and precipitation extremes (Seneviratne et al., 2010; Fischer et al., 2007; Hirschi et al., 2010). Similar to extreme events, changes in soil moisture can have a significant socio-economic effect both directly through water resource management, agricultural productivity, forest and ecosystem health, as well as indirectly through exacerbated temperature extremes and their associated risks such as forest fires (Hirschi et al., 2014; Han et al., 2014; Herold et al., 2016).

Soil moisture is currently used in land surface model assimilation (Koster et al., 2009; van Dijk et al., 2014) including agricultural drought models (e.g. Han et al., 2014), numerical weather forecasting (e.g. Draper et al., 2009; Dharssi et al., 2011), flood forecasting (e.g. Wanders et al., 2014), forest fire danger forecasting (represented by a drought component, e.g. Liu et al., 2003; Finkele et al., 2006; Bartsch et al., 2009; Chaparro et al., 2016), and long-term hydrological trends and drought monitoring and evaluation (e.g. Heim, 2002; Teuling et al., 2006; Hubbard et al., 2007; van Dijk et al., 2013; Perkins et al., 2015). Soil moisture is also used extensively in the assessment of hydrological feedbacks in climate modelling (Dirmeyer et al., 2016; Schubert et al., 2016b) such as in the CMIP5 projections (e.g. Seneviratne et al., 2013).

Forest fires are often associated with moisture deficits, extreme temperature and low fuel moisture, culminating in exacerbated fire danger (Pereira et al., 2005; Chaparro et al., 2016). During the Black Saturday fires, the maximum temperature was in excess of 48 C° more than 20 C°above the February long-term average, relative humidity was as low as 9 %, and wind gusts were in excess of 80 kmh^{-1} resulting in record values for FFDI. The royal commission charged with investigating the conditions and effects of the fires concluded that the current FFDI was not suitable for extreme fire events. Based on their recommendations, there was a revision of the FFDI in which a new category ('catastrophic') was introduced, representing values in excess of the previous maximum (Teague et al., 2010). Despite that the FFDI is said to be directly related to the chance of a fire igniting, its rate of spread, and the difficulty of suppression(Nobel et al., 1980), in

its current form the FFDI does not quantify a relationship to either the intensity of a fire nor soil moisture directly. Fire Radiative Power (FRP) can be a useful tool to quantify the impact and intensity of fires and it is directly affected by temperature, moisture and vegetation conditions (Kaufman et al., 1998). The Black Saturday fires burned with a total intensity (FRP) of $70,000 - 80,000\ MW$ (Xu et al., 2017), compared to a controllable intensity of about $3,500 - 4,000\ MW$ (Teague et al., 2010), and compared to the median FRP of $42\ MW$ in Australian tropical savanna (for a single fire; Oliveira et al., 2015, or $\approx 2,000\ MW$ for a comparable sized fire), further highlighting the importance of FRP when assessing the impact and intensity of a fire.

Not only does the risk of fire increase with weather-exacerbated changes in the conditions leading to forest fires, but also changes to the climate system as a whole (Hennessy et al., 2005). As the Earth's climate changes due to anthropogenic forcing (Charlson et al., 1992), there is expected to be an increase in temperature extremes, deficits in precipitation (although, it is expected there to be an increase in global mean precipitation), and generally changes to the parameters associated with high fire risk, each of which are projected to change significantly in the future (Sherwood et al., 2010; Dai, 2013; Wang et al., 2013; Gibson et al., 2017b). More so, it has been identified in both observations and model projections, that spatial patterns and the extent of changes in temperature extremes and precipitation differ globally and on a regional scale (Donat et al., 2017). Specifically, Seneviratne et al. (2016) used ensemble means of CMIP5 projections to show that changes in regional temperature extremes can differ significantly from the global mean trend. Partly, these regional increases in hot extremes have been identified as a result of the land-atmosphere feedbacks which amplify aridity over land (Berg et al., 2016). This is particularly the case with feedbacks of projected soil moisture decreases on land surface temperature, relative humidity, and precipitation (Berg et al., 2016). This has also been identified by Seneviratne et al. (2013) using GLACE-CMIP5 projections. In this work, projected soil moisture changes were found to substantially exacerbate temperature extremes in several regions in both boreal and austral summer (Seneviratne et al., 2013). These regional increases in hot extremes, relative humidity, precipitation deficits all have a significant effect on fire risk.

1.2 Statement of Problem

The McArthur FFDI is used operationally to quantify fire danger in Australia, but the drought component of this index is often criticised for its lack of dynamic range as it is empirically derived using 50-year old assumptions. The drought factor within the FFDI also does not necessarily accurately represent changes in soil moisture across the vari-

ous climate regimes of Australia. Beyond this, the moisture index used in the drought factor is not universal, with both the Keetch-Byram Drought Index (KBDI) and Mount's Soil Dryness Index (MSDI) being used depending on which state the FFDI is formulated in. Furthermore, particularly with KBDI, this calculation can be computationally complex, whereas in climates with similar conditions, other moisture indices such as: the Antecedent Precipitation Index (API), the Rainfall Anomaly Index (RAI), the Standardized Precipitation Index (SPI), and the Standardized Precipitation Evaporative Index (SPEI), have been proven to more accurately represent soil moisture and are far simpler to calculate (Van Rooy, 1965; Oladipo, 1985; Heim, 2002; Liu et al., 2010; Vicente-Serrano et al., 2010). Lastly, unlike similar extreme indices, FFDI does not include an indication of scale or intensity. In particular, the FFDI and soil moisture have not been previously investigated in relation to the rate of energy consumption (quantified through FRP), a key indicator to the intensity of a fire.

1.3 Research Question and Aims

This research investigates the effect of conditions leading to forest fires and their effect on fire intensity at various spatial scales. The intention is to quantify the strength of coupling between soil moisture and high-temperature anomalies leading to forest fire vulnerability and in doing so, investigate how these vary with the forest fire danger indices (FFDI) across Australia. By including high resolution remotely sensed soil moisture from the ESA CCI product (see section 3.3.2) and indices of soil moisture (see sections 2.2 and 3.4), the aim is to increase the accuracy and scalability of the index and risk analysis. By strengthening the understanding of conditions leading to severe events, improved prevention and mitigation strategies and a better allocation of resources in the Australian region can be achieved.

Specifically, the aims of this research can be stated:

1. How accurately do commonly used indices for soil moisture used in fire-related studies perform against each other and how do they vary across Australia. Is this related to the location of the 'Transitional Zone' and energy partitioning in Australia? Are Tx90 days the only days associated with forest fires?

2. Can remotely sensed soil moisture data be used to improve the current approaches to predict fire risk and danger? What is the spatial variability of soil moisture, moisture indices, temperature and FRP data across the climate regimes of Australia? How is this impact to the operationally used FFDI in Australia? Can the

drought factor be simplified using different moisture indices, whilst maintaining accuracy?

3. Using the results from the above research goals, how does the risk of forest fires change in response to climate change and also how has it changed in the past?

1.4 Structure of Thesis

Including the introduction chapter, this thesis is comprised of a total of eight chapters. The main body of analysis is presented in Chapters 4-7 with each of these introduced with a brief overview of the chapter and concluded with a bridging summary of findings. As field sampling and measurements of burn severity and burn extent are essential to accurately assess remotely sensed products of fire activity an independent analysis on the minimum sampling rate required to accurately measure fire severity from ground sampling are presented in Appendix A. Furthermore, any additional information and plots not directly discussed throughout the thesis are presented in B.

The remaining seven chapters are outlined as follows:

Chapter 2 Literature Review

An overview of the background and current state of research for this thesis is presented in this chapter. More specifically, the mechanisms and processes behind the relationship between soil moisture deficits and heat extremes are discussed in detail, including the link between the terrestrial water and energy balances. A thorough overview of the most commonly used soil moisture and drought indices and their strengths, weaknesses, and applications is discussed as well as the common practices and methods for the retrieval and quantification of fire intensity. Finally, an overview of the current research in relation to the trends in FFDI, both historically and projected through to 2100 is presented in this chapter. A review of the differences in the key variables used to calculate the FFDI between various radiative forcing, and climate pathways due to climate change (produced from CMIP5 model projections), is also conducted.

Chapter 3 Methods

Any methods or data common to the main body of analysis are outlined here, particularly, the moisture indices used, the retrieval methods of *in situ*, modelled or remotely sensed measurements, as well as the main statistical methods used throughout the thesis. Any methods or data specific to a certain chapter are discussed therein.

Chapter 4 Comparison of Soil Moisture Proxies Across Australia

This chapter assesses and quantifies the differences in the moisture indices and a reference soil moisture (*in situ* and gridded remotely sensed) across various climate regimes in Australia.

Chapter 5 Variability of Soil Moisture Proxies and Hot Days

The difference in the strength of coupling between soil moisture and the moisture indices are then placed in the context of the identification and location of the transitional zone, as discussed in the literature review. Furthermore, this chapter investigates the relationship between these various products and temperature extremes in the form of Tx90, both when influenced by ENSO conditions and at all times during the study period.

Chapter 6 Improving Fire Risk Estimation by Investigating Fire Intensity, and Moisture and Temperature Extremes

This chapter introduces both fire danger (FFDI) and fire intensity (FRP) and how each is affected by moisture deficits and temperature extremes. This chapter also investigates the merit of simplifying the current FFDI replacing the drought factor component with each of the moisture indices.

Chapter 7 FFDI in a Changing Climate

This final analysis chapter investigates the historical and future trends of FFDI using CMIP5 modelled data output under a moderate and high radiative climate forcing.

Chapter 8 Conclusions

The key conclusions and findings for each chapter are outlined and summarised in this chapter, as well as the potential opportunity for future work developed from this thesis.

CHAPTER 2

Review of Literature

Overview In this literature review, the linking mechanisms between soil moisture states and temperature extremes will be discussed, along with their potential use in producing a high-resolution fire danger index throughout the twentieth and twenty-first centuries. This will be compared to current methods for producing fire risk indices and the potential advantages gained by including soil moisture will be discussed. A review of various soil moisture indices will be conducted, highlighting their strength and weaknesses as well as how they compare with the KBDI used in the McArthur Forest Fire Danger Index (FFDI). Furthermore, the methods for calculating high-resolution indices of soil moisture as well as the methods to determine fire risk and its mapping will also be explored. Following this, Fire Radiative Power (FRP) data retrieval methods will be investigated and whether FRP and fire occurrence should be considered in relation to FFDI to simplify its formulation for forecasting. Finally, the main concepts and gaps in knowledge in this field will be critically reviewed, providing a sound justification for this research.

2.1 Background

Drought and heat wave events are regular occurrences on a large scale in semi-arid regions of the world, such as Australia, and are predicted to further increase in their frequency and severity (Cowan et al., 2014). Much of Australia has been heavily affected by drought conditions in recent years (Perkins-Kirkpatrick et al., 2016) and as such, a large stress has been placed on the allocation of water resources. Understanding the changes in the hydrological conditions and water balance in a region is essential for understanding the distribution of droughts and any consequent forcing of extreme temperatures. This leads to more accurate predictive skills and forecasting of extreme events for an improvement in the ability to plan mitigation strategies.

High maximum temperatures and low moisture content in the vegetation provide favourable conditions leading to fires, which is well documented in numerous studies (Barbosa et al., 1999; Ainuddin et al., 2008; Bartsch et al., 2009; Dolling et al., 2005; Gellie et al., 2010; Kala et al., 2015; Turco et al., 2017; Urbieta et al., 2015). As drought severity (as expressed as PDSI; Palmer Drought Severity Index) is a function of temperature and precipitation, Balling Jr et al. (1992) found that when winter precipitation decreased and summer mean temperatures increased, soil moisture in the region decreased substantially. This was significantly related to the increased fire activity over the period investigated and increases/decreases in soil moisture correlated well to decreases/increases in fire activity. Balling Jr et al. (1992) found that in the Yellowstone national park over one-third of the temporal variance in burnt area is explained by drought severity. This was also found in a study by Westerling et al. (2006) where a large increase in fire duration and frequency in the 1980's was attributed to a warmer spring and summer period with a substantial decrease in winter precipitation. These conditions led to a decrease in soil moisture and vegetation moisture increasing the availability of dry fuel as well as affecting associated land-climate interactions.

Therefore, understanding the underlying physics of the water and energy balance are essential for better understanding these land-climate interactions and their effect on the conditions leading to forest fires. More particularly, the exchange of water between the atmosphere and the land surface as well as the energy balance are illustrated in Figure 2.1a. The amount of water stored in reservoirs (in various forms in terrestrial, atmosphere, ocean, and lake reservoir environments) varies greatly, therefore, changes in state between reservoirs will have a large effect on the energy balance, particularly through evapotranspiration (E or the latent heat flux λE where λ is the latent heat of vaporisation). The terrestrial water balance for the surface soil layer including vegetation (Figure 2.1a, left) can be expressed as:

$$\frac{dS}{dt} = P - E - R_s - R_g \tag{2.1}$$

where the amount of water entering a given soil layer through precipitation (P) is balanced by the evapotranspiration (E), the surface runoff (R_s), and the drainage (R_g). The rate of change of water is denoted by $^{dS}/_{dt}$ and includes changes to the soil moisture, surface water, snow, ice, and groundwater. The evapotranspiration term includes evaporation from bare soil, surface water or from water intercepted and stored in the canopy, as well as through plants' transpiration, and snow/ice sublimation. The terrestrial water

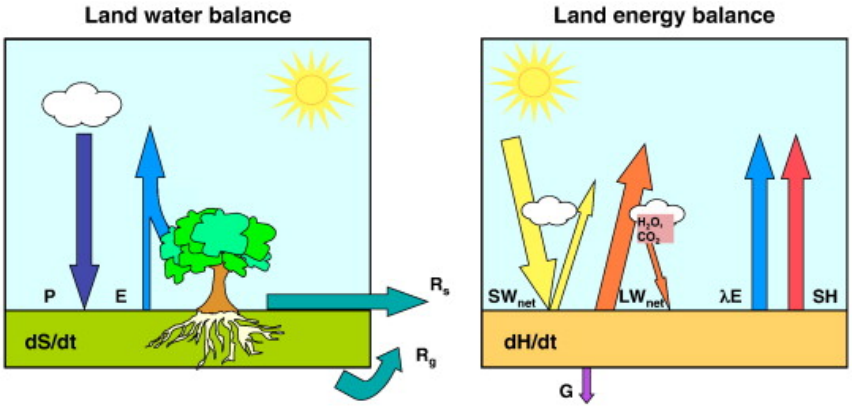

(a)

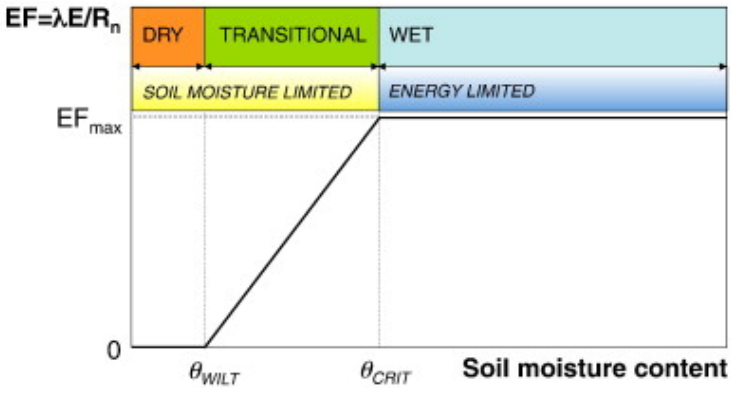

(b)

Figure 2.1: Figure and caption taken from (Seneviratne et al., 2010), pages 129 and 130. (a) Schematic of the land water balance (left) and land energy balance (right) for a given surface soil layer. $^{dS}/_{dt}$ refers to the change in water content within the layer (soil moisture, surface water, snow; depending on the depth of the layer, this may include ground water changes), while $^{dH}/_{dt}$ refers to the change of energy within the same layer. $SWnet$ refers to the net shortwave radiation ($SW_{in}SW_{out}$) and LW_{net} refers to the net longwave radiation ($LW_{in}LW_{out}$). Note that H_2O and CO_2refer to atmospheric water vapour and atmospheric CO_2 and their role as greenhouse gases. (b) Definition of soil moisture regimes and corresponding evapotranspiration regimes. EF denotes the evaporative fraction, and EF_{max} its maximal value. θ_{WILT} is the wilting point and θ_{CRIT} is the critical saturation point.

balance is coupled with the energy balance through the evapotranspiration term and given as:

$$\frac{dH}{dt} = R_{net} - \lambda E - SH - G \tag{2.2}$$

Here, the evaporation of water is related to the exchange of energy, expressed as the latent heat flux (λE where λ is the latent heat of vaporization or sublimation). The amount of energy entering the system via net radiation R_{net} is balanced by the change in heat stored in the system ($^{dH}/_{dt}$) and is the sum of incoming and outgoing radiation components, both in the form of longwave-infrared (LWIR) radiation and the shortwave near-infrared (SW-NIR) radiation. The transfer of heat directly into the atmosphere via changes in temperature is called the sensible heat flux (SH), otherwise, heating is a result of an associated phase change in water and is defined as the latent heat flux (LH). The transfer of heat from the soil layers to the adjacent atmosphere is defined as the ground heat flux (G) (Seneviratne et al., 2010).

As changes in either of the energy or water balance are interrelated via evapotranspiration through their calculation, the amount of evapotranspiration in the system is not only constrained by the amount of water available (through soil moisture), but also by the amount of available energy which governs temperature. Due to this, changes in the amount of the evapotranspiration has been investigated in the form of the relationship between soil moisture and Hot-Days (the number of days exceeding the 90th percentile of the climatology, HD; Fischer et al., 2007; Hirschi et al., 2010). More specifically, the SM-HD relationship is postulated to be the result of the effect of soil moisture on the surface energy balance (land-climate coupling linking soil moisture and surface/air temperature). That is that the soil moisture of a region determines the partitioning between sensible and latent heating resulting in direct changes to the temperature.

Regional studies on changes in the water balance (through the terrestrial water storage of a basin) typically focus on the influx and outflow of water in this system (Potter et al., 2009). However, the variability in terrestrial water balance and the feedback with climate has also been investigated by Leblanc et al. (2009). They determined that the response of Total Water Storage (TWS) and soil moisture was due to changes in precipitation and temperature in the Murray-Darling Basin (South-east Australia). Furthermore, through investigating the relationship between actual and potential evapotranspiration, Budyko (1974) showed that the mean annual actual evapotranspiration of a basin is controlled by its mean annual precipitation and potential evapotranspiration. Based on a conceptual model of the controls on moisture limited and radiation limited basins (for large-scale basins with an area greater than 1000 km^2; Budyko, 1974), Hirschi et al. (2010) and Fis-

cher et al. (2007) indicated that a soil moisture deficit could also precede above-average temperatures in a region.

The mechanism through which this occurs is due to the interaction between the water and energy balances, as sensible heat dominating latent heat will cause a localised temperature change as a result of the direct heating above the surface. However, latent heat dominating sensible heat will result in a larger amount of evapotranspiration and a decrease in the near-surface temperature (Seneviratne et al., 2010). Evapotranspiration in a region can be either moisture or radiation limited. In the case of moisture limitation, the lack of available water prevents evapotranspiration. Conversely, radiation limitation occurs where moisture is abundantly available while the amount of evapotranspiration is limited by the incoming radiation (Teuling et al., 2006). When soil moisture is below the wilting point (θ WILT) then evapotranspiration will be at a minimum (adirect relationship between temperature and radiation resulting in only sensible heating). Likewise, if the surface is saturated (θ CRIT) then evapotranspiration will be at a maximum (latent heating is at a maximum) and only dependent on available energy. However, a region that is normally soil moisture limited between the wilting point and critical level is known as a 'Transitional Zone' (Seneviratne et al., 2010). A schematic of the soil moisture regimes and corresponding evapotranspiration regimes is presented in Figure 2.1b. Transitional zones lie between wet and dry climates or semi-arid regions, such as large parts of Australia.

2.2 Soil Moisture / Drought Indices

The impact and intensity of droughts can be assessed using various definitions (Heim, 2002). The American Meteorological Society (AMS) groups drought definitions into four main categories: meteorological or climatological, agricultural, hydrological, and socio-economical, each with different metrics as well as onset duration (Heim, 2002). For example, a socio-economical drought will usually be associated with a reduction in the supply of economic goods due to limited water resources. In this case, the onset duration will be determined by the length of time for water stress to occur in agricultural commodities, as a direct result of drought. Agricultural droughts refer to crop failure as a result of evapotranspiration far exceeding the available precipitation and consequently soil moisture in the root zone. This can develop over a relatively short period of time (weeks to months) as a result of a prolonged meteorological drought. Meteorological droughts are generally defined as a reduction or lack of precipitation compared to average conditions over a time frame and can have a relatively short onset period (days to weeks), depending on temperature, soil conditions, and the local climatology. Finally,

hydrological droughts occur when the soil surface and subsurface water stores are affected by meteorological droughts causing a lack of water supply to not only the root zone but to streams, groundwater, reservoirs, and lakes. These occur for a far longer period of time (months to years) and can persist long after a meteorological drought has ended.

As there are several definitions for droughts, each with varying duration, cause and prevailing conditions, particularly referring to water resources (through soil moisture, groundwater, snowpack, river discharges, and reservoir storages), there are many indices that define the intensity, severity and spatial extent of droughts (such as: API, PDSI, RAI, KBDI, MSDI, SWSI, SPI, VCI, SMI, and SPEI to name a few; and are defined below). As a consequence, the moisture memory may vary substantially between indices. Hence, it is commonly accepted that droughts are multiscalar phenomena (Vicente-Serrano et al., 2010). As such, each index will have a different relationship to precipitation, and soil moisture and have a different physical application as well as strengths and weaknesses (detailed descriptions of the indices cited throughout this thesis is outlined in Table 2.1, including their formulation, the main variables required, and applications).

Early drought indices were based on the meteorological drought definition indicating a deficit in precipitation over a given time period (Tannehill, 1947). These typically relied on determining the length of period that precipitation was below a certain threshold in precipitation (Munger, 1916; Blumenstock, 1947) and could reasonably depict short-term droughts. Originally produced to estimate soil moisture for flood forecasting, the Antecedent Precipitation Index (API) was the first drought index that defined a moisture depletion rate reducing from the field capacity (Kohler et al., 1951). Empirically derived, the API is computed at a daily scale multiplying the index from the previous day by the depletion factor (commonly 0.9) and adding the current daily precipitation. Any snowfall is included on the day it melted. It is often used in various watershed analysis studies (Liu et al., 2011). However, the depletion rate has a considerably large spatial variation due to several factors including soil type, soil density, vegetation, exposure, hill slope etc. Although recently re-defined to address this by introducing the daily maximum temperature into the depletion rate (Crow et al., 2005; Crow et al., 2012; Holgate et al., 2016; Kumar et al., 2017), the API was surpassed by indices that included a water balance model (Heim, 2002).

Following the original formulation of the API, the first widely used index, the Palmer Drought Severity Index (PDSI; Palmer, 1965), defined relative dryness based on temperature and precipitation data. Standardised between -10 (dry) and $+10$ (wet) it has been shown to successfully reflect characteristics in long-term drought through using a

physical water balance model comprising of temperature, precipitation, moisture supply, runoff, and evaporation demand at the surface level (Dai et al., 1997; Dai, 2011b; Dai, 2011a; Trenberth et al., 2013; Mishra et al., 2010; Edwards, 1997; Vicente-Serrano et al., 2010; Sims et al., 2002). The calculation procedure was based on a set of three formulas and made several assumptions: i) that the top soil layer has a field capacity of 2.54 cm, ii) that moisture does not filtrate to the 'root zone' layer until the top layer becomes saturated, iii) that runoff only occurs once all layers are saturated, and iv) that any precipitation exceeding the evapotranspiration and soil moisture demand will be lost through runoff (Vicente-Serrano et al., 2010). Due to these reasons, the spatial comparability of PDSI is often questioned and requires calibration and standardisation (McKee et al., 1993). Furthermore, the main issue with the PDSI relates to its fixed temporal scale (between 9 and 12 months) and its lengthy antecedent behaviour in which the PDSI can be affected by previous years conditions (Guttman, 1998).

The Rainfall Anomaly Index (RAI; Van Rooy, 1965) aimed to improve spatial comparability by introducing climatology into its formulation. Similar to the API in its simplicity, the RAI is computed by determining the difference between the average precipitation over a given period and the mean of the ten highest and ten lowest records from the climatology of a location. Oladipo (1985) found that there were only negligible differences between RAI and the complicated PDSI, however, a complete time-series of data for any specific location is required. Often several indices are combined to reduce the deficiencies of a specific index. For example as snowpack, reservoir storage, and streamflow dynamics had not previously been incorporated into the PDSI, the Surface Water Supply Index (SWSI; Shafer et al., 1982) was developed to complement the PDSI. While both indices were empirically derived, they have been used extensively to assess the surface water supply of river basins (Doesken et al., 1991). However, as the SWSI is also calculated per basin, issues in spatial variability and comparability are observed.

Initially developed as an alternative to the PDSI for Colorado, the Standardized Precipitation Index (SPI; McKee et al., 1993) was produced to characterise drought and flood severity using solely precipitation data. Guttman (1999) found that the spectral characteristics of the PDSI indicated large spatial variability (as previously mentioned) whilst SPI was spatially invariant, meaning that it is comparable between locations. Guttman (1999) also found that PDSI was affected by previous values such that they caused a 'memory' as opposed to SPI with a moving average. Hence, the SPI can be used to directly compare moisture of both spatially different climates and regions with large temporal variation. Furthermore, the different time-scales for which SPI can be computed at (typically 1-48 months) refer to the various definitions of drought. E.g. the shorter scales (1-3 months) indicate agricultural and meteorological droughts and longer (six plus) in-

dicate hydrological drought (Hirschi et al., 2010). 3-month SPI has been widely used to investigate the association between soil moisture and temperature extremes in Europe (Hirschi et al., 2010) and globally (Mueller et al., 2012). Due to its ease of calculation, SPI is increasingly used for drought-related studies (Bonaccorso et al., 2003; Livada et al., 2006; Naresh Kumar et al., 2009; Mohammad Amin Asadi et al., 2015).

As the SPI is driven solely by precipitation data it has drawn much criticism due to lack of consideration of other variables that influence droughts, such as; temperature, evapotranspiration, and wind speed. However, SPI is based on the assumption that the variability of precipitation is far greater than these variables and that they are temporally in-variate, such that their effect on droughts is negligible, whereas SPI assumes that droughts are controlled by the temporal variability in precipitation. Secondly, SPI is also undefined at regions with long-term precipitation averages below 1 mm, and thus may not be appropriate in arid regions. Regardless, precipitation has been shown to be the main variable in determining the onset, duration, and intensity of droughts (Heim, 2002).

An extension to the SPI was developed to address some of the shortcomings of the SPI. The Standardized Precipitation Evapotranspiration Index (SPEI) also considers the sensitivity to changes in potential evapotranspiration (PET) as well as precipitation (as SPI does). As with API, the SPEI captures the response in drought conditions to variations in daily maximum temperature through evapotranspiration. Due to this though, the SPEI is sensitive to uncertainties in the variables used to derive PET, such as; wind speed, surface humidity, and solar radiation (Vicente-Serrano et al., 2010). As such, at shorter temporal scales, a simplified PET is calculated based on the Thornthwaite approximation (Thornthwaite, 1948). Similar to the SPI, the SPEI can be produced at various temporal scales between $1 - 48$ months. Again, a minimum of 30 years of data is required to provide a robust distribution (McKee et al., 1993). As the SPEI has been shown to correlate well with PDSI at longer time scales ($\geq \approx 18\, months$ Vicente-Serrano et al., 2010), it is better suited for detecting and monitoring fluctuations in drought conditions due to global warming (Vicente-Serrano et al., 2010). The SPEI is becoming more commonly used in drought and extreme event (e.g forest fire) studies, with Urbieta et al. (2015) and Turco et al. (2017) investigating its use in determining the effect of drought conditions of fire activity and burned area. This follows on from the evaluation of drought indices that suggest that SPEI shows a slightly higher correlation with observationally based soil moisture over SPI, particularly in arid regions (McEvoy et al., 2012).

Each of these indices is similar in that they are precipitation and/or temperature based often using water balance models to determine soil moisture. However, in each case, they do not use soil water observations directly nor do they use modern remotely sensed

techniques to estimate soil moisture. The Soil Moisture Index (SMI; Hubbard et al., 2007) was developed to address the former and it represents the onset of agricultural droughts by observing the dryness of a soil relative to a plant's ability to extract water as scaled from the difference between the wilting point and field capacity for a given plant (Hunt et al., 2009). The primary issue with this is that it still requires some inherent information of moisture content and that it is limited in its temporal scale referring to an agricultural drought. Similarly, the Vegetation Condition Index (VCI; Liu et al., 1996) has been developed to utilise remotely sensed data from the Advanced Very High Resolution Radiometer (AVHRR). It likewise indirectly infers moisture content and its effect on agricultural droughts through the dependence of vegetation on the climate. Quiring et al. (2010) found that VCI was strongly correlated to 6-and-9-month SPI and to PDSI, indicating that it is most suited to hydrological droughts and less sensitive to short-term precipitation deficiencies.

Due to the relationship between drought conditions and burn severity Balling Jr et al. (1992), the Keetch-Byram Drought Index (KBDI; Keetch et al., 1968) was developed for use by fire control managers within the United States Department of Agriculture. The KBDI has been incorporated into the United States National Fire Danger Rating System to estimate moisture and the inferred quantity of available fuel for burning, however, it is also used operationally in Australia for forest fire danger prediction (Finkele et al., 2006). The KBDI drives the moisture component of the drought factor within the commonly used McArthur Forest Fire Danger Index (FFDI; discussed in Section 2.3). Mapping of KBDI and its subsequent fire danger has been used operationally in the United States (Johnson et al., 2001; Lorimer et al., 1988; Dolling et al., 2005), the Mediterranean (Petros et al., 2011; Garcia-Prats et al., 2015), Malaysia (Ainuddin et al., 2008), South Africa (Verbesselt et al., 2006), and as mentioned in Australia (in context with changes in FFDI; Fox-Hughes et al., 2014; Pitman et al., 2007; Clarke et al., 2011; Hennessy et al., 2005; Clarke et al., 2012). Furthermore, it has also been used to assess the effect of climate change on forest fires (Liu et al., 2010; Sherwood et al., 2010; Dai, 2013; Wang et al., 2013; Gibson et al., 2017b). Similar in nature to API, in that only precipitation and temperature are required, the major assumption behind KBDI is that the evapotranspiration rate is a function of the mean annual rainfall meaning that it is spatially dependent on the precipitation. Also, KBDI assumes that the water holding capacity is at a maximum of 20 cm. However, for clay soils, this equates to a soil depth of 80 cm indicating that soil depth is not particularly well defined. Conversely, the KBDI is relatively simple to calculate and is widely used.

Table 2.1: Summary of the most commonly used drought/moisture indices, including their abbreviation, the year introduced, the formula used for their calculation, and key variables and applications in which they are used.

Index	Year	Formula	Variables & Applications
API	1954	$(API_{n-1} + P_{n-1})e^{-\alpha\Delta t}$ $(\gamma \times API_{n-1}) + P_n$	Precipitation based and modulated using a temperature controlled soil moisture depletion, typically used for flood forecasting.
PDSI	1965	Multiple	Precipitation and temperature analysed in a physical water balance model.
RAI	1965	$\pm 3\frac{P - \bar{P}}{\bar{E} - \bar{P}}$	Snowpack, reservoir storage, streamflow, and Supply Index precipitation.
KBDI	1968	$\frac{[203.2 - Q]\left[0.968e^{0.0875T+1.5552} - 8.3\right]}{[1 + 10.88e^{-0.001736R} \times 10^{-3}]}$	Precipitation and soil moisture analysed in a water budget model used by fire managers.
MSDI	1972	$P_{eff} + ET$ $P_{eff} = rain - interception - runoff$ $ET = a_i T_{max} + b_i$	Precipitation and soil moisture analysed in a water budget model using run-off data and used by fire managers.
SWSI	1982	$\frac{aP_{snow} + bP_{prec} + cP_{strm} + dP_{resv} - 50}{12}$	Snowpack, reservoir storage, streamflow, and Supply Index precipitation.
SPI	1993	$\pm\left(t - \frac{c_0 + c_1 t + c_2 t^2}{1 + d_1 t + d_2 t^2 + d_3 t^3}\right)$	A statistical distribution fit to the precipitation time series producing a deficit/surplus index.
VCI	1996	$100\frac{5\,(NDVI - NDVI_{min})}{(NDVI_{max} - NDVI_{min})} - 5$	Determines moisture using remotely sensed differences in vegetation radiances from NDVI.
SMI	2008	$\left[\frac{5\,(SM - WP)}{(FC - WP)} - 5\right]$	Normalised soil moisture, derived using the idealistic water availability for plants calculated from the difference between the field capacity and the wilting point.
SPEI	2010	$W - \frac{c_0 + c_1 W + c_2 W^2}{1 + d_1 W + d_2 W^2 + d_3 W^3}$	Precipitation and Temperature based and using a climatic water balance to produce a deficit/surplus index at different time scales from a log-logistic probability distribution over the time series.

Similar to the KBDI, Mount's Soil Dryness Index (MSDI; Mount, 1972) is also used by fire control managers. In Tasmania and Western Australia it is used in exchange for the KBDI in the drought factor component of the FFDI, and like the KBDI it is an empirically derived cumulative SM deficit index. However, it differs from the KBDI in the estimation of evapotransporation which is determined by applying a vegetation filtration model. The MSDI is essentially a water balance model that takes into account rainfall, run-off, and interception. The retrieval of vegetation for defining evapotransporation is derived utilizing the MODIS leaf area index (LAI) product (MCD15A2H; Myneni, 2015). For each vegetation category, parameters are defined for the canopy rainfall interception fraction, the canopy storage capacity, wet evaporation rates, and flash-runoff fraction using a linear relationship to LAI as per (Finkele et al., 2006). One drawback of the MSDI is that the regression coefficients used are based on *in situ* observations of evapotranspiration from capital cities in the Australian states of Victoria, Tasmania, and South Australia. This means that both the calculation of MSDI is computationally time-consuming and that values are spatially dependent.

Each one of the indices has their drawbacks and advantages, with a number of studies comparing various of the indices against remotely sensed and modelled products and *in situ* soil moisture both in Australia and abroad (e.g. Holgate et al., 2016; Kumar et al., 2017; Heim, 2002; Keyantash et al., 2002; Mishra et al., 2010; Vicente-Serrano et al., 2010; Sims et al., 2002; Quiring et al., 2010) in order to identify their efficiency and characteristics. Keetch et al. (1968) discussed the further analysis of these indices in relation to FFDI using various fuel loadings and vegetation types adding to their simple water balance model (precipitation - evaporation). However, despite the vast improvements and differences in estimating soil moisture, seldom have these indices been compared to each other in relation to their possible use in the drought factor of the FFDI and in their relationship to fire occurrence and intensity.

2.3 Fire Danger and the Retrieval of Fire Metrics

Forest fires occur regularly on a large-scale across semi-arid regions such as southeastern Australia (Hennessy et al., 2005). These fires cause significant strain on forest management services attempting to mitigate their impact on both the community and the economy. Forest and fire management services throughout the world have long used vegetation management in the form of controlled burning to minimise fuel load and to mitigate potential fire danger in a region at risk. Forest fires, either through long- or short-term ecological impact, alter the vegetation and soil attributes from burning of surface litter to changing the species composition throughout a forest (Cocke et al., 2005;

Keeley, 2009), and if applied as a preventive measure, reduce future large-scale fire risks.

'Fire severity' or 'burn severity' describe the immediate effects of a fire on organic matter such as vegetation, soil, and litter (Key et al., 2006; Keeley, 2009). In other words, burn severity is a function of the ecological change due to fire (Cocke et al., 2005). Likewise, fire intensity or 'burn intensity' are generally described as the rate of combustion of fuel of a given fire in progress (Byram, 1959). The quantification of fire intensity ranges from the energy released from a fire to fire-line, to burned area versus fuel consumption, and to burn scarring. However, when assessing the likelihood or risk of fire in a region several terms and methods for its quantification can be used. Economical (or technical) risk assessors consider not only risk as the probability of fire, but also socio-economic loss and infrastructure value; this is compared to fire management services which typically defines risk as the likelihood of ignition (Hardy, 2005). 'Hazard' is also used commonly and refers to the state of the fuel load, whilst burn severity specifically describes the impact of a fire on the wildland system (Hardy, 2005; Key et al., 2006; Keeley, 2009). Lastly, Beall (1946) describes fire 'danger' as including all the items which quantify how and whether fires will start, what the spread and damage are, as well as their ability to be contained. However, fire danger and risk can also be defined using metrics, such as spread, damage, and ability to be contained. These are typically associated with incipient fires and their conditions and do not present the likelihood or potential of fire. To this extent, forest fire danger is typically quantified using indices that incorporate atmospheric conditions such as, surface air temperature, precipitation, relative humidity, and wind speed to name a few, as well as fuel moisture. Various fire danger indices exist, including the McArthur Forest Fire Danger Index (FFDI; McArthur, 1967), the McArthur Grassland Fire Danger Index (GFDI; McArthur, 1967), the Canadian Fire Weather Index (FWI; Van Wagner, 1987), the United States National Fire Danger Ratings System (NFDRS; Deeming et al., 1972), and the Fosberg Fire Weather Index (FFWI; Fosberg, 1978).

In Australia, the FFDI is used operationally by the Bureau of Meteorology and fire management services and is applied in many studies to directly asses the level of forest fire risk. Recently, there has been a large effort to increase the accuracy of FFDI using the methods as mentioned above and from various remotely sensed products. However, it has been found that there is a significant variation in the classification of risk categories between such indices (FFDI and FWI) at low index values (Dowdy et al., 2009). More particularly, several studies have investigated improvements to the drought factor component of the FFDI, such as Griffiths (1998). This introduced a smoothing function for the drought factor and was introduced into operational use thereafter. Alternate drought factors have also been investigated such as by Snyder et al. (2006), which presented a fuel dryness index based on biophysical principles associated with energy exchange, defined

as the daily ratio of sensible heat to available energy. They determined that the index was more responsive to daily changes than most of the other indices, including the KBDI and the fuel moisture code in the FWI, providing more accurate fuel dryness conditions of live vegetation. Similarly, the KBDI (used within the drought factor) was modified for a better adaptation to Mediterranean conditions, also producing a faster response to daily to meteorological conditions (Petros et al., 2011).

Fire danger indices are used to quantify the risk of fire danger based on meteorological, climate and fuel information. These are then used to forecast risk and issue warnings in regions likely to be affected. The most commonly used FDI globally is the Canadian Forest Fire Weather Index (FWI) System (Van Wagner, 1987) and is calculated based on daily observations of weather conditions. The FWI determines the risk of fire based on three moisture components incorporating temperature, relative humidity, wind, rain, as well as the wind itself. The three moisture components are numeric ratings of moisture content in i) the surface litter, characterised by the Fine Fuel Moisture Content (FFMC; used to determine fire spread), ii) the lower organic layer of the forest vegetation calculated by the Duff Moisture Code (DMC; used to determine fuel consumption), and iii) the deeper organic layers comprised of larger woody vegetation and is indicated by the Drought Code (DC; an indication of the overall drought conditions of the vegetation; Van Wagner, 1987). However, in Australia, the MacArthur FFDI is used to assess the likelihood and severity of forest fires (McArthur, 1967). The Australian Bureau of Meteorology issues forecasts of the FFDI and the grassland curing levels to local fire authorities. Dowdy et al., 2009 compared the FFDI and FWI across Australia from various case studies and found that both FFDI and FWI performed similarly with the main variation between the two occurring in regions where the index values were typically low (temperate and tropical regions). Dowdy et al., 2009 determined that the FFDI typically indicated lower severity than that of FWI in these regions, with the FFDI generally performing within one standard deviation or about 15% of the FWI value. They concluded that since the indices do not provide a direct physical relationship with any specific aspect of fire danger or fire behaviour, it is to be expected that the significance of an index value will show some degree of variation between different locations" (Dowdy et al., 2009, pg.75). They conclude that substantial improvements could be made in particular to the drought factor, but would require substantial validation against known fire activity. Similarly, a study by Cruz et al., 2007 determined that for pine plantations in Australia the FWI also outperformed the FFDI in indications of extreme fire behaviour, indicating that the FWI is more appropriate in heavily forested regions such as semi-arid and temperate regions of Australia .

The FFDI framework as provided by McArthur, 1967 for forest fire prediction using al-

ternative moisture indices was introduced by Liu et al., 2003. They compared the original framework which uses observational data, with high-resolution data retrieved from the HIRES model and also investigated using the Antecedent Precipitation Index (API) as a proxy for the drought factor (DF). Liu et al., 2003 found that using the HIRES NWP model provided a more structured soil moisture field resulting in improvements to FFDI prediction. Secondly, Liu et al., 2003 found that replacing DF with the simplified API yielded a more direct relationship between the FFDI and precipitation. This could be largely contributed to the API being a function of precipitation, and as such, provided more stability in prediction from high-resolution datasets. Using products such as API and SPI (and aforementioned moisture indices) to infer fire risk allows for calculations of risk to be made at various spatial and temporal resolutions as well as heavily forested areas and areas affected by retrieval limitations. Similarly, Sharples et al. (2009) investigated the use of a simple fire danger index based on antecedent conditions. Their comparisons suggested that their fire danger index may be a useful pedagogical tool in the context of fire danger and fire weather, providing similar results to the FFDI and the FWI, but as mentioned, this still does not take into account the expected intensity of fires.

During forest fires, the concentration of pyrogenic emissions is directly proportional to the amount of biomass consumed and provides an estimate of fire intensity (Delmas et al., 1995). There are many methods to determine fire intensity through the amount of energy released by a fire resulting from the combustion of fuels with a common method, e.g. fire-line intensity being a measure of the energy released along the front of the fire itself (Byram, 1959). Quantification of most methods such as the fire-line intensity poses substantial challenges with large uncertainty in estimating, combustion efficiency, fuel load and type, and the spread or propagation of the fire itself (French, 2004; Arnett et al., 2015; Hudak et al., 2016). Beyond this, complex burn patterns resulting from a multitude of ignition points can lead to stationary fires which have both a significant heat release and extreme turbulence for which fire-line intensity cannot be defined. Similarly, ember spotting may induce multiple fire-lines meaning that the estimation of the total fire energy released from fires according to fire-line intensity may be inaccurate over short (minutes) temporal scales. Within the same context, simple estimates of biomass combustion can result in large uncertainties due to the variation in fire propagation, therefore estimates typically ignore the inter-dependence of smouldering and flame combustion. Simple biomass combustion can be defined from Eq 2.3 Seiler et al., 1980

$$M = A \times B \times C \tag{2.3}$$

where, A is the burned area (km^2), B is fuel load ($^{kg}/_{km^2}$), C the fraction of available fuel burned, and M the estimated amount of dry fuel burned (kg) (Ellicott et al., 2009). The

total emissions of direct pyrogenic carbon released can be then calculated by multiplying M by the fraction of volatile carbon contained in the fuel (Eq 2.4):

$$E_x = EF_x \times M \tag{2.4}$$

Where E_x is the total emission load (g); EF_x is the emission factor for the specific vegetation type ($^g/_{kg}$) and M is the fuel burned in Eq 2.3 (Ellicott et al., 2009). Despite improvements with remote sensing techniques the parametrisation of E has typically been proved inaccurate, as estimates of the B and C parameters have not been readily available and any estimates contained large uncertainties (Barbosa et al., 1999; French, 2004). Furthermore, this has made remotely sensed emission estimates through this method very imprecise, resulting in large differences with earth observations (Barbosa et al., 1999). On top of this, there is a lack of agreement in the algorithm to characterise burned area from remotely sensed data and Korontzi et al. (2004) and Korontzi et al. (2004) showed that this can lead to a difference in the estimate of biomass consumed by a factor of two (Ellicott et al., 2009).

Andreae et al. (2001) suggested that the development of a new method to accurately estimate the energy emitted by fires and the amount of fuel combusted could be achieved through Fire Radiative Power (FRP) and Fire Radiative Energy (FRE; Wooster et al., 2005). Both FRP and FRE have equivalent units to fire-line intensity and fire power and, similar to E, FRP and FRE are a measure of the severity and intensity of a fire through the energy emitted. FRP is defined as the quantification of the radiant heat output from the fire (Roberts et al., 2005; Ichoku et al., 2008) with Freeborn et al. (2008) showing that it is related to smoke emissions released. FRP is a direct result of the combustion process, where carbon is oxidised to CO_2 (and other compounds) releasing energy stored in the fuel as heat (Wooster et al., 2005; Ellicott et al., 2009). FRP is the rate of release of the radiative component and Wooster et al. (2005) found that it is highly correlated to the combustion rate, however, radiant heat from smouldering fuel beds can significantly contribute to FRP where burning has ceased. Integrating FRP over the whole fire results in the total energy released or the Fire Radiative Energy (FRE) and hence, Wooster et al. (2005) found that FRE should be linearly proportional to the total biomass of fuel consumed. As remotely sensed retrievals improve, FRP and FRE are becoming more commonly used in studies to describe fire severity and intensity (Wooster et al., 2005; Roberts et al., 2005; Ellicott et al., 2009). The rate of fuel combustion can be described from Eq 2.5:

$$(C_6H_{10}O_5)n + O_2 + ignition\ temperature \rightarrow H_2O + CO_2 + heat\ yield \tag{2.5}$$

From the Stefan-Boltzmann Law, the radiant component released is emitted as electromagnetic waves and is proportional to the absolute temperature of the fire (assumed to be a black body) raised to the fourth power (Wooster et al., 2005; Ellicott et al., 2009). The relationship between fire temperature and spectral radiance was subsequently shown to closely match the Stefan-Boltzmann Law ($Radiance = \sigma T^4$). Therefore FRP and FRE are derived from a simple equation combining the sample size, emissivity of the fire and Stefan-Boltzmann's constant (Kaufman et al., 1998). As a result, FRP is ultimately calculated from the difference in brightness temperature of the fire pixel and the background pixels (Kaufman et al., 1998; Wooster et al., 2005), where A is the area of a fire pixel:

$$FRP = (4.34 \times 10^{-19} MWK^{-8} km^{-2}) \times (T^8_{4\mu m} - T^8_{4\mu m.background}) \times A \tag{2.6}$$

As mentioned above, fire alters the vegetation, soil, and litter composition as well as exposing and altering the colour and brightness of the surface soil. This causes changes in the spectral response and as such can be detected through the NIR and MIR wavelengths via remote sensing satellites (van Wagtendonk et al., 2004; Chuvieco et al., 2006). As the accuracy of remotely sensed data has improved during recent years, it has become a more common approach to determine burn metrics(Keeley, 2009). Various satellite sensors (e.g. MODIS, ASTER, Landsat, RapidEye) are commonly used, with the Landsat Thematic Mapper identified as the most accurate instrument used to estimate burn severity. However, the spatial coverage is substantially limited (van Wagtendonk et al., 2004; Brewer et al., 2005; Cocke et al., 2005; Chuvieco et al., 2006; Kokaly et al., 2007; French et al., 2008).

Furthermore, there are many difficulties in determining the combustion efficiency, fuel load and fire behaviour propagation of the fire itself from other methods. Therefore the determination of FRP and FRE through remotely sensed data is far more effective and accurate (spatially and temporally) than other methods for determining fire severity and intensity. This can not only be used for determining fire intensity but also to define thresholds between classes within the FFDI. A study by Maier et al. (2013) determined fire detection thresholds using remotely sensed data from MODIS-based FRP in fire-prone savanna in the Northern Territory. Maier et al. (2013) found that a steep increase in the number of detections with increasing FRP indicated a clear detection threshold (3.6 MW to 16.3 MW). However, they warn that minimum FRP is very sensitive to outliers and that perhaps a better measure is the median FRP value and that further work on thresholds of FRP for fire detection should be conducted. Similarly, Roberts et al. (2005) determined that FRP retrievals from SEVIRI (Spinning Enhanced Visible and Infrared Imager) are strongly comparable with those derived from near-coincident MODIS overpasses on a per-fire base. However, due to SEVIRI's inability to detect fire pixels with an FRP < 100

MW, SEVIRI typically underestimated FRP with respects to MODIS at the regional scale. ASTER has also been used for FRP retrieval by Giglio et al. (2008), where they statistically analysed 100 ASTER scenes determining that detection rates were between 80-90% with false alarms varying between 9×10^{-8} (India) and 2×10^{-5} (USA/Canada). Giglio et al. (2008) also found that ASTER FRP was accurate to within 20%, with the exception of one (of 20) fire partially obscured by heavy soot. Satellite 'overpasses' will not necessarily coincide with either clear skies or the appropriate time (Keeley, 2009) and it is possible that several days to weeks may pass before an image can be acquired. This is one significant limitation in the retrieval of FRP from remotely sensed sources.

Similar to FRP and FRE, fire indices (such as FFDI) and fire risk can be spatially represented using remotely sensed data for easier interpretation by both weather forecasters and local fire authorities. Despite significant fire activity occurring in only a small portion of the areal extent of maps, fire can have a wider impact spatially, particularly in semi-arid regions (Moreno et al., 2013). The use of remotely sensed data for use in hazard mapping and fire risk mapping has been introduced by Chuvieco et al., 1989. With the development of Geographical Information Systems (GIS) techniques, processing large data volumes has become increasingly easy and common. Many studies have been conducted to monitor active fires and visualise predictions of fire hazards and danger. These use a range of variables to approximate fire hazard ranging from vegetation moisture, fuel types, wind direction and speed among many others (Chuvieco et al., 2007). Remotely sensed products have also been used to assess the effects of fire on vegetation characteristics via the reflected visible, near infrared, and short-wave infrared wavelengths. For example, Chuvieco et al. (2006) estimated fire effects from determining the composite burn index (CBI) through applying a radiative transfer model to predict how the spectral reflection from a vegetated surface will change due to fire. They showed that fires alter the electromagnetic spectrum, specifically in the near infrared range and consequently vegetation indices that are derived from spectral reflection produce correlations with CBI. Likewise, a study by Chuvieco et al., 2004 investigates the use of Normalized Differenced Vegetation Index (NDVI) and temperature to infer live fuel moisture content for use in fire danger indices. However, there are few studies that include the use of soil moisture to infer fire risk and danger.

Similarly to Balling Jr et al. (1992, who determined that the PDSI accounted for approximately one-third of the temporal variance in the burn area) and Liu et al. (2003), Chaparro et al. (2016) investigated the use of soil moisture for determining fire risk, specifically for producing high resolution ($1km$) fire risk maps over Spain. From fire pre-conditions using simple thresholds of temperature and soil moisture, fire risk maps with two categories of low and high risk were produced. That is, the higher the surface temperature

and lower the soil moisture at a location, the higher the risk of fire (Chaparro et al., 2016; Chuvieco et al., 2014; Petros et al., 2011). These fire risk data were then compared with MODIS derived fire detections to determine the success of predictions. This initial study produced promising results with success ranging from 46% to 85% of fires falling within high-risk zones (Chaparro et al., 2016). Likewise, Petros et al. (2011) suggested that the drought factor/index should be based on the drought conditions of the previous day in the form of an antecedent moisture index, which may also be expressed as a function of potential evapotranspiration (PET). They also suggested that this empirical drought index should have a cumulative form and be able to be produced using a simple function of basic and easily available meteorological variables (Petros et al., 2011).

2.4 Past and Future Changes In SM, Tx and FFDI

The relationship between forest fires and atmospheric conditions is relatively well understood (Pereira et al., 2005; Trigo et al., 2006; Potter, 2012). Changes in fire risk can be affected through large-scale dynamics as well as through inter-annual variability such as the El Nino Southern Oscillation (Williams et al., 1999). However, exacerbated fire risk is associated with changes in the synoptic weather conditions, in particular, wind direction and speed, temperature, relative humidity, and precipitation. Likewise, as mentioned previously, deficits in soil moisture are strongly related to an increase in temperature extremes and in the number of hot days (Fischer et al., 2007; Hirschi et al., 2010; Mueller et al., 2012). This can, in turn, exacerbate the aforementioned conditions through land-climate feedbacks, leading to a higher fire danger, as well as being directly related to an increase in fire intensity. Fire risk can also be affected by changes in the climate system as a whole (Hennessy et al., 2005); for example as the Earth's climate changes due to anthropogenic forcing (Charlson et al., 1992), it is expected that an increasing number of temperature extremes, precipitation deficits, and consequently the parameters associated with high fire risk will occur.

Each of these has changed throughout the 20th-century Williams et al. (2001), Hennessy et al. (2005), Pitman et al. (2007), Dai (2011b), Clarke et al. (2012), Sheffield et al. (2012), and Fox-Hughes et al. (2014), and in line with the Intergovernmental Panel on Climate Change (IPCC) Fifth Assessment Report Summary for Policy Makers, climate extremes are projected to change significantly in the future (IPCC, 2013b). In particular, the number of warm days is likely to increase (Perkins et al., 2012; Seneviratne et al., 2013; Gibson et al., 2017a), as well as the number of prolonged precipitation and soil moisture deficits (Sherwood et al., 2010; Sherwood et al., 2014; Dai, 2013; Wang et al., 2013), in turn compounding the resultant fire danger. Changes in the global mean temperature throughout

the 20th and 21st century as simulated by the CMIP3 (Coupled Model Intercomparison Project Phase 3) and CMIP5 models is shown in Figure 2.2. Each of the last iterations of the CMIP project indicated a similar pattern of global warming. However, the simulated twentieth-century warming is less gradual in the CMIP5 model mean compared to CMIP3. This is due to the radiative forcings that drive the model being more complete, including solar and volcanic forcings, and indirect aerosol effects (Knutti et al., 2012). The twenty-first-century warming is not as comparable between the models because the CMIP5 models use the new Representative Concentration Pathways (RCPs), whereas the CMIP3 models used the Special Report on Emissions Scenarios (SRES) B1, A1B and A2 scenarios. However, despite this, each of the SRES and RCP simulations indicates substantial warming throughout the century (Figure 2.2). Both iterations indicate a similar mean and range of the climate sensitivity and the transient climate response and share consistent projection uncertainties.

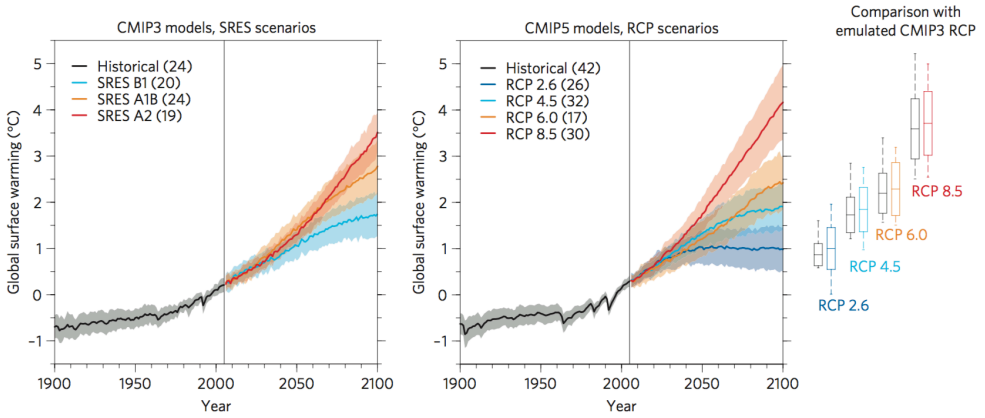

Figure 2.2: Figure and caption taken from Knutti et al. (2012), page 370. Global temperature change (mean and one standard deviation as shading) relative to 1986 – 2005 for the SRES scenarios run by CMIP3 and the RCP scenarios run by CMIP5. The number of models is given in brackets. The box plots (mean, one standard deviation, and minimum to maximum range) are given for 2080 – 2099 for CMIP5 (colours) and for the MAGICC model calibrated to 19 CMIP3 models (black), both running the RCP scenarios.

Through simulations from climate models, increases in temperature extremes have been attributed to anthropogenic forcing at global and regional scales (Morak et al., 2011; Knutti et al., 2012; Morak et al., 2013; Kim et al., 2015). Likewise, the effect of anthropogenic forcing on temperature extremes at smaller spatial and temporal scales has been extensively studied (Wang et al., 2013; Perkins, 2015; Perkins et al., 2015; Lorenz et al., 2016; Gibson et al., 2017a), with a large inter-model spread observed at the local to regional scale for both heat wave trends and climatology (Gibson et al., 2017a). Simulated increases in temperature extremes will continue regardless of the emission path chosen, however, reductions in carbon dioxide emissions will significantly influence the magnitude of heat extremes later this century (e.g. Figure 2.2; Knutti et al., 2012; Tebaldi et al.,

2016). Unremitting, an increase in emissions will drive heat extremes such as the 2003 European heatwave, which was associated with strong soil moisture deficits (Fischer et al., 2007), such that current heat extremes will be considered standard or in fact cool by the end of the century (Christidis et al., 2014).

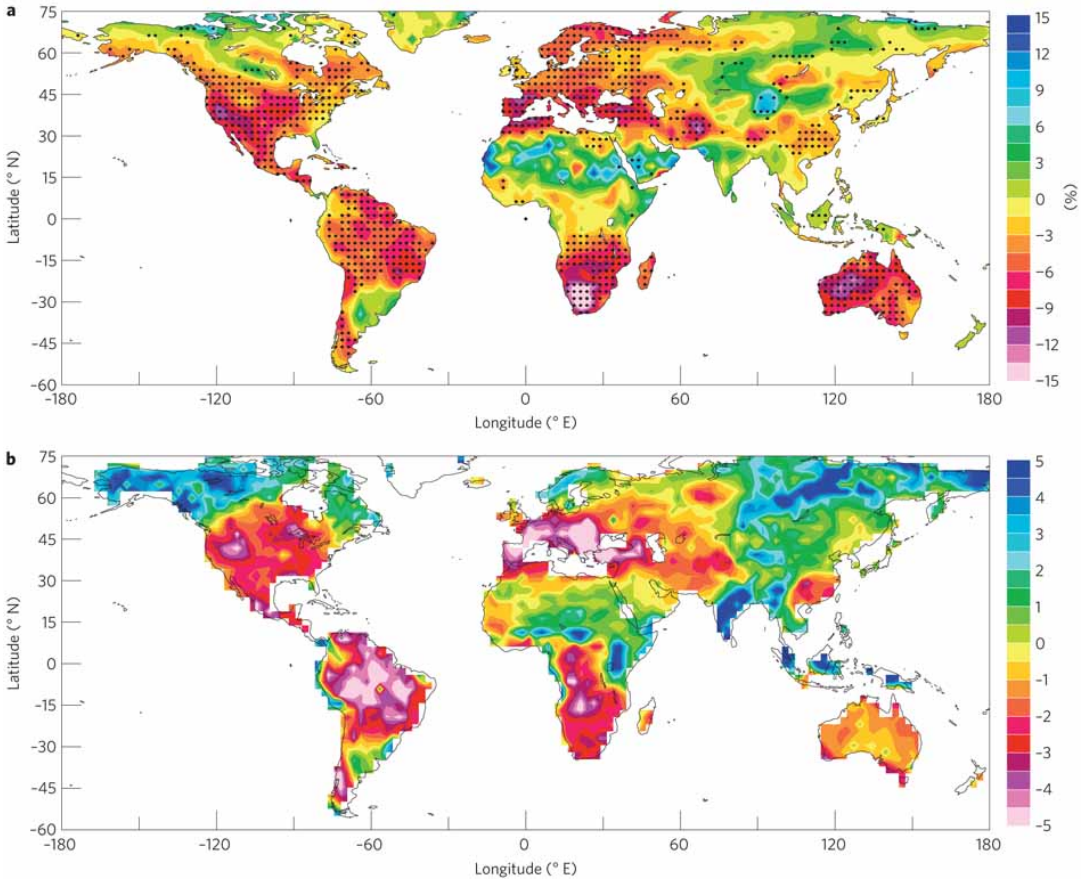

Figure 2.3: Figure and caption taken from Dai (2013), page 53. (a) Percentage changes from 1980 – 1999 to 2080 – 2099 in the multimodel ensemble mean soil moisture content in the top 10 cm layer (broadly similar for the whole soil layer) simulated by 11 CMIP5 models under the RCP 4.5 emissions scenario. Stippling indicates at least 82% (9 out of 11) of the models agree on the sign of change. (b) Mean PDSI averaged over 2090 – 2099 computed using the 14 model ensemble mean climate (including surface air temperature, precipitation, wind speed, specific humidity and net radiation) from the CMIP5 simulations under the RCP 4.5 scenario. A PDSI value of −3.0 or below indicates severe to extreme droughts for the present climate.

Likewise, it is well documented that changes in precipitation extremes (both positive and negative) will occur as well as consequent changes in soil moisture and drought conditions (Purich et al., 2013; Sippel et al., 2017). Through many studies, PDSI, a measure of drought or aridity has been identified to increase during the last 60-years (IPCC, 2013a). This is particularly the case in mid-latitude semi-arid regions (Feng et al., 2013). Sherwood et al. (2014) and Fu et al. (2013) concluded that this was due to the change in temperature during this time as a result of the relationship between the earth and the atmosphere. Future projections of changes (comparing the 1980-1999 and 2080-2099

time periods) soil moisture and mean PDSI are illustrated in Figure 2.3 (Dai, 2011b; Dai, 2013), identifying a strong increase globally throughout the 20th and 21st centuries. This was suggested to be a result of the intrinsic overestimation in PDSI, and consequently, Sheffield et al. (2012) and Cook et al. (2014) found that a modified PDSI (using a more robust estimator of potential evaporation) had a smaller trend throughout the 20th century.

These are similar to trends seen in projected precipitation and evapo[transpi]ration. As mentioned previously, evapotranspiration is the common factor in both the energy and water balance and drives the relationship between soil moisture and temperature extremes, meaning that trends in evapotranspiration will significantly influence trends in both soil moisture and temperature. Historically, evapotranspiration was generally found to increase globally since the 1980s (Zeng et al., 2012; Zeng et al., 2014; Wang et al., 2010), but both Miralles et al. (2013) and Mueller et al. (2013) also identified a decline in global evapotranspiration after 1998. Douville et al. (2012) showed that historical changes in evapotranspiration were attributed to the effect of anthropogenic radiative forcing and could increase with higher radiative forcing in the future.

Changes in precipitation, drought, and evapotranspiration under climate change conditions can have a large influence on the coupling with temperature extremes (Douville et al., 2016). In turn, this can lead to changes in the fuel moisture and the resultant observed fire frequency and extreme fire weather days throughout the twenty-first century (Flannigan et al., 2015). This outlines the influence of not only climate conditions but vegetation conditions have on fire activity. Forkel et al. (2017), also investigated anthropogenic controls, as well as, climate and vegetation controls of fire activity between 1997 and 2011. They concluded that the spatial variation in the relationship between controls is not homogeneous, in particular for Australia. As Figure 2.4 indicates, fire activity in arid-central Australia is mostly controlled by a combination of climate and vegetation conditions, whereas, in alpine and coastal south-eastern Australia, fire activity is largely controlled by vegetation conditions. This leads to varying trends in fire activity across Australia. In particular, Andela et al. (2017) indicated that global burned area declined by $24.3 \pm 8.8\%$ over the previous 18 years and suggested that the decrease in fire activity may be as a result of the expansion and intensification of agricultural land use and its effect on vegetation. However, Andela et al. (2017) also shows that there are contrasting trends in fire activity depending on the product used and spatially. In Australia, on average, the MODIS MCD64A1 product indicated a 1.53% (2003-2015) increase in burned area per year, whereas, the GFED4 (Global Fire Emissions Database version 4) and FireMIP (Fire Model Inter-comparison Project) products indicate a trend of -2.53% (1998-2015) and -0.5% (1997-2013) per year, respectively.

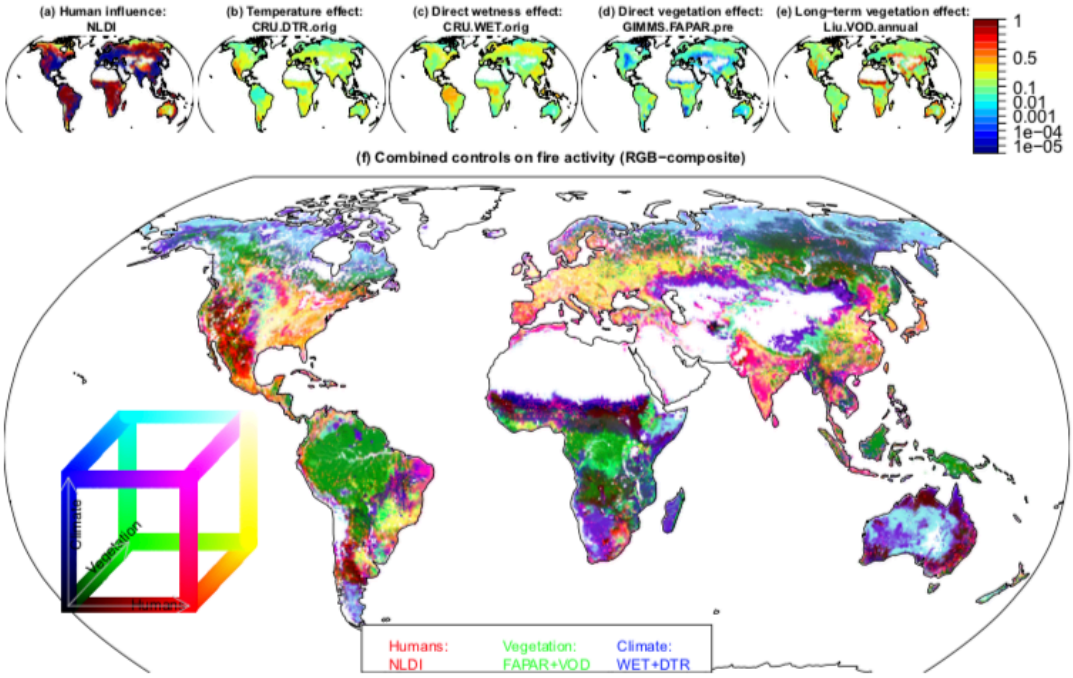

Figure 2.4: Figure and caption taken from Forkel et al. (2017), page 19. Example of combined climate, vegetation, and human controls on fire activity based on the SOFIA model SF.124421. The maps in (a-e) show the average response value for each functional relationship for the period 1997-2011. High values (1, red) indicate that this factor allows unlimited burning and low values (0, blue) indicate that this factor restricts burning. The map in (f) is a red-green-blue composite of the human influence (map in a, red channel), the combined direct and long-term vegetation effect (mean of d and e, green channel), and the climate effect (mean of b and c, blue channel). Bright and dark colours indicate a strong restriction and allowance of fire activity, respectively.

Not only has there been studies on the change in fire activity over the past 20-50 years but also there have been several studies that have investigated fire danger in the 20th century and projected through the 21st century both globally and regionally. Liu et al. (2010) investigated the potential of global wildfire under climate change using KBDI which is analogous to fire potential. They compared historically derived KBDI, driven by observed maximum temperature and precipitation, to projected changes for 2070-2100. Using four GCMs, each with four emission scenarios, it was determined that future fire potential increased significantly in the United States, South America, central Asia, southern Europe, southern Africa, and Australia. Similarly, Flannigan et al. (2013) used three GCMs and three emission scenarios to determine that fire season and fire severity increased for most of the globe, in particular, for the Northern Hemisphere. Here, fire potential was determined using the Cumulative Severity Rating (CSR) and the 1971-2000 baseline was compared to mid-century (2041-2050) and late-century (2091-2100) values. Regionally, many studies have focused on Canada and the United States, with Stocks et al. (1998), Brown et al. (2004), and Wotton et al. (2010) in agreement that there is a large increase in the areal extent and magnitude of fire danger in both countries between base-

line periods and late 21st century values, using various metrics to assess fire potential applied to different numbers of GCM and RCMs.

Similarly, several studies have investigated fire danger both in previous decades and projected through the 21st century in Australia. Williams et al. (2001) quantified the impact of climate change on fire risk through analysing daily and seasonal FFDI produced using model simulations. They used two different CO_2 concentration forcings from the CSIRO 9-level general circulation model (CSIRO9 GCM) for a 30-year period between 1960 and 1992. They found that there was an increase in the number of days with very high and extreme fire danger when the CO_2 was doubled and that the seasonal fire danger increases in response to the doubling of CO_2's through its effect on maximum temperature. Following this, the historical change in annual cumulative FFDI between 1973 and 2010 at 38 *in situ* observational sites was investigated by Clarke et al. (2012). They found that at 16 of the 38 sites, cumulative FFDI increased significantly and for 24 sites, the annual 90th percentile FFDI increased significantly. They also found that increases were greatest during the spring and autumn austral seasons and in the interior of the continent.

Simulated projected changes in FFDI have been studied across multiple regions and scales (Hennessy et al., 2005; Pitman et al., 2007; Clarke et al., 2011; Fox-Hughes et al., 2014) .Hennessy et al. (2005) investigated the change in FFDI and the Grassland Fire Danger Index (GDFI) using two RCMs as input for climate change scenarios for the years 2020 and 2050, across 17 sites. These results were in agreement with global studies showing an increase in fire-weather risk for both 2020 and 2050. This included the average number of days when the FFDI rating is very high or extreme. Similarly, Pitman et al. (2007) investigated the change in FFDI and GDFI using gridded data produced by RCMs for 2050 and 2100. As with Hennessy et al. (2005), Pitman et al. (2007) showed that there was a consistent increase in fire risk over Australia and that this was principally driven by warming and reductions in relative humidity. Further regional studies by Clarke et al. (2011) and (Fox-Hughes et al., 2014) investigated the change in FFDI using the CSIRO-Mk3-0-0 RCM and GCMs across four regions along the east coast of Australia and in Tasmania, respectively, with the former focusing on the seasonality of FFDI changes over time. Furthermore, Flannigan et al. (2015) concluded that the sensitivity in the changes in fuel moisture due to an increase in temperature extremes from climate change would result in drier fuels and an increase in the fire frequency and fire extremes. In summary, the importance of understanding the relationship between changes in precipitation, temperature, evapotranspiration, fuel moisture, and soil moisture and their influence on fire conditions and extremes is underpinned by the continued influence of climate change on the earth system and climate extremes.

2.5 Summary

The literature on FFDI, FRP and fire occurrence as well as moisture indices, and climate extremes have been critically reviewed. From this review, it is apparent that:

1. Whilst much research has been undertaken on the use of fire risk indices for fire forecasting, few studies have used high spatial resolution daily and monthly data. This extends to limited studies on the use of soil moisture, which has long been associated with forest fires and fire risk. Often simple measures of precipitation which are used to produce indices of soil moisture are available at the daily time scale whereas other remotely sensed soil moisture products have a temporal retrieval of several days, yet these proxies are not included in calculations for fire risk indices. One caveat is of course that [drought] indices of soil moisture do not necessarily correlate perfectly with *in situ* or remotely sensed measurements soil moisture. Therefore, it is important to compare the performance of all available products used to calculate FFDI. Furthermore, the relationship between indices and temperature extremes has not been investigated in context with the transitional zone in Australia.

2. Likewise, little research has been conducted on the relationship between soil moisture, FFDI, and FRP, not only to determine minimum fire detection thresholds but also to better understand the effect of fire pre-conditions on fire intensity and severity.

3. Lastly, despite the effect of climate change on fire risk being investigated by several sources, studies have so far focused on a specific region within Australia or used data from local stations for comparisons across various climates within Australia and either look into historical changes or future projections but not both consistently. Whilst there are global studies indicating the overall changes in fire danger for Australia, FFDI itself, which is used operationally, has yet to be studied using an ensemble of GCM's

From this review and using the previous studies as a framework, the relationship of various soil moisture indices to the number of hot days and FFDI in Australia and how this is related to fire intensity and frequency will be investigated. Fire intensity as determined from FRP will be compared against the FFDI both spatially and temporally through the twentieth and twenty-first century. Through investigation of these relationships, we will ascertain the potential usefulness of remotely sensed data for forecasting forest fires and improve on the current framework for calculating FFDI as well as investigating the effect of climate change on FFDI.

CHAPTER 3

Methods

Overview This chapter presents the methodologies and data-sets that are common to analysis throughout this thesis. *In situ* data that are collated for this study form the reference for comparison with satellite and modelled data from which various indices are computed. The *in situ* data were obtained from the OzNet, OzFlux and the CosmOz networks in Australia. Further datasets used throughout this study include; AWAP and ERA-Interim (land surface model derived datasets), CMIP5 (intercomparison study of various climate models), SOI (inter-annual variability index), MODIS (remotely sensed datasets) and the ESA CCI (collaborative initiative including various datasets, such as SM, fire, cryosphere, etc). API, SPI, KBDI, MSDI and other indices were calculated using a combination of the aforementioned datasets. Additionally, statistical methods used in this study, as well as the methods used to calculate indices and their specifications, are discussed in this chapter in detail.

3.1 *In situ* Datasets

3.1.1 OzNet hydrological monitoring network

In situ soil moisture data were retrieved from several observational soil moisture networks. The Australian monitoring network for soil moisture and micrometeorology (OzNet) operated in collaboration between Monash University and The University of Melbourne consists of 64 dedicated soil moisture sites in the Murrumbidgee (Smith et al., 2012) and Goulburn (Rüdiger et al., 2010) River catchments, in New South Wales (available at http://www.oznet.org.au). The OzNet soil moisture observations record soil water content at multiple depths between 0-90 cm (0-7 cm, 0-30 cm, 30-60 cm, 60-90 cm) and are quality controlled by comparing with rainfall observations (Smith et al., 2012). Measurements are recorded using Campbell Scientific time/frequency-domain reflectometers (older sites) and Stevens Hydraprobe sensors (newer sites), and tipping bucket rain gauges at between 20- to 30-minute intervals depending on the site (Smith et al., 2012). Measurements infer volumetric soil moisture from the soil's dielectric constant and conductivity (for further of these methods see; Rüdiger et al., 2009; and Robinson et al., 2008). The OzNet sites span a range of climate regimes, soil types, vegetation and land use as well as a range in elevation from 50 m to up to 1000 m. The location of OzNet sites, as well as a detailed overview of their attributes, can be found in Figure 3.1 and Table 3.1.

3.1.2 Terrestrial Ecosystem Research Network: OzFlux

The Australian flux tower network (OzFlux) is part of the FluxNet global network of over 500 micrometeorological flux tower sites that primarily use eddy covariance methods to measure the exchanges of carbon dioxide, water vapour, and energy between the atmosphere and biosphere (Cleverly, 2011). OzFlux consists of 27 active (as of August 2017) observational sites and 10 inactive sites that measure energy and atmospheric fluxes as well as soil moisture, soil temperature, air temperature, wind profiles and precipitation. Soil moisture is measured at each site typically using either frequency-domain reflectometers (generally Campbell Scientific CS-616 probes) or time-domain reflectometers (generally Campbell Scientific CS-610 probes) at 30-minute intervals. Data are available at four levels of processing; level three provides quality controlled soil moisture content at various depths (depending on site and probe type; Beringer, 2014) and are used here. OzFlux data are available for both active and inactive sites for varying periods between 2008-2017 via the online portal (http://data.ozflux.org.au/portal/home.jspx).

3.1.3 Australian Cosmic-ray Neutron Soil Moisture Monitoring Network

The Australian cosmic-ray probe network (CosmOz) provides continuous estimates of soil moisture at 17 locations (16 calibrated) around Australia, with each location containing a CRP-1000b Hydroinnova cosmic-ray probe (Hawdon et al., 2014). Unlike gravimetric measurements and conventional dielectric reflectometry measurements, cosmic-ray probes passively measure the near-earth-surface (2 m) fast neutron flux produced by cosmic rays (Zreda, 2016). The fast neutron flux is sensitive to changes in surface moisture as it is inversely correlated to the presence of hydrogen. That is, the higher the moisture content, the lower the neutron count as a consequence of a greater amount of scattering. Due to this, and the insensitivity to soil chemistry (bulk density, surface roughness, and soil texture), cosmic-ray probes are ideal to measure variations in surface soil moisture. Cosmic-ray probes have a horizontal footprint of up to 660 m and estimate soil moisture at depths of between 12 to 76 cm (Hawdon et al., 2014). The effective depth depends strongly on soil moisture itself, decreasing non-linearly with increasing moisture content. Cosmic-ray probe measurements require a correction to account for the effects of atmospheric pressure changes and water vapour pressure changes on variation in the incoming fast neutron flux, and each probe has been modulated by the soil moisture conditions at each location. These corrected values are converted to a volumetric soil moisture using a calibration function based on the known local wet and dry moisture conditions. As with both AWAP and OzFlux, the CosmOz observational network is managed by CSIRO and is available freely online (http://cosmoz.csiro.au/), with only level 4, calibrated, hourly data used for analysis. Further details outlining the methods of data processing and calibration of sites are described by (Hawdon et al., 2014). The locations of the CosmOz sites, used here, are shown in Figure 3.1 as well as the details in Table 3.1.

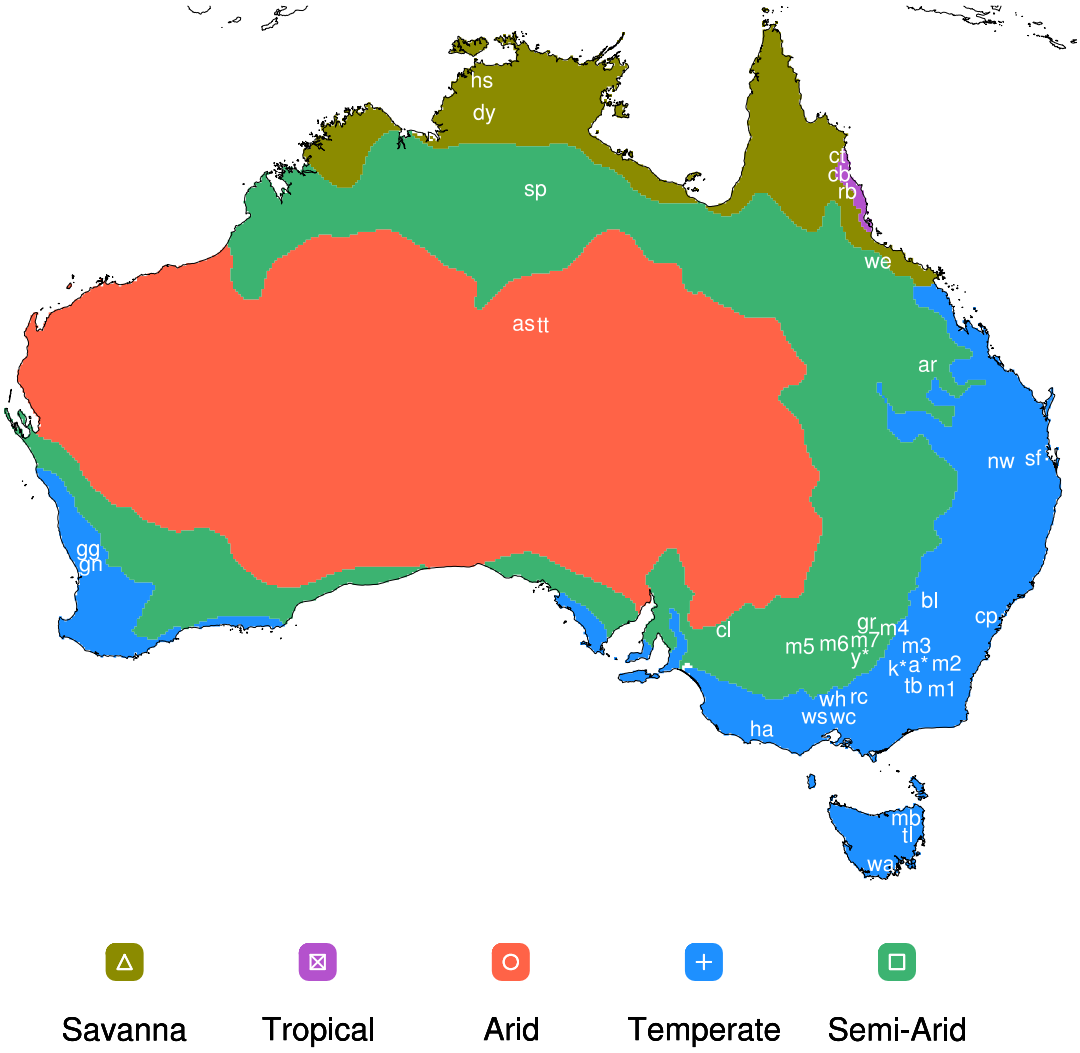

Figure 3.1: Köppen-Geiger climate regimes as produced by Peel et al. (2007). Sites from the OzNet, OzFlux and CosmOz networks are indicated using double-lettered codes. Yanco, Kyemba and Adelong sites are denoted with y*, k* and a* respectively. Full details of sites and codes are given in Table 3.1

Table 3.1: Summary of soil moisture *in situ* sites from the OzNet, OzFlux, and CosmOz networks. Information includes: site name, code, location, altitude, data period, number of observations, measurement depth, and Köppen-Geiger climate regime.

	Site Name	Code	Coordinates	Alt [m]	Data Period	Obs	Depth [cm]	Koeppen Regime		Reference
OzNet	Murrumbidgee 1	m1	36.29 S, 148.97 E	937	14/09/01 - 31/05/11	3579	0-7, 0-30, 30-60, 60-90	15	Temperate	Smith et al. (2012)
	Murrumbidgee 2	m2	35.31 S, 149.20 E	639	14/09/01 - 31/05/11	3579	0-7, 0-30, 30-60, 60-90	15	Temperate	Smith et al. (2012)
	Murrumbidgee 3	m3	34.63 S, 148.04 E	333	15/09/01 - 31/05/11	3021	0-7, 0-30, 30-60, 60-90	14	Temperate	Smith et al. (2012)
	Murrumbidgee 4	m4	33.94 S, 147.20 E	258	16/09/01 - 31/05/11	3578	0-7, 0-30, 30-60, 60-90	11	Temperate	Smith et al. (2012)
	Murrumbidgee 5	m5	34.66 S, 143.55 E	62	28/09/01 - 28/02/11	3473	0-7, 0-30, 30-60, 60-90	7	Semi-Arid	Smith et al. (2012)
	Murrumbidgee 6	m6	34.55 S, 144.87 E	90	28/09/01 - 31/05/11	3565	0-7, 0-30, 30-60, 60-90	7	Semi-Arid	Smith et al. (2012)
	Murrumbidgee 7	m7	34.25 S, 146.07 E	137	29/09/01 - 31/05/11	3564	0-7, 0-30, 30-60, 60-90	7	Semi-Arid	Smith et al. (2012)
	Yanco 1	y1	34.63 S, 145.85 E	120	28/12/03 - 31/05/11	2710	0-7, 0-30, 30-60, 60-90	7	Semi-Arid	Smith et al. (2012)
	Yanco 2	y2	34.65 S, 146.11 E	130	17/01/04 - 31/05/11	2690	0-7, 0-30, 30-60, 60-90	7	Semi-Arid	Smith et al. (2012)
	Yanco 3	y3	34.62 S, 146.42 E	144	29/09/01 - 31/05/11	3564	0-7, 0-30, 30-60, 60-90	7	Semi-Arid	Smith et al. (2012)
	Yanco 4	y4	34.72 S, 146.02 E	130	22/12/03 - 31/05/11	2716	0-7, 0-30, 30-60, 60-90	7	Semi-Arid	Smith et al. (2012)
	Yanco 5	y5	34.73 S, 146.29 E	136	10/12/03 - 31/05/11	2728	0-7, 0-30, 30-60, 60-90	7	Semi-Arid	Smith et al. (2012)
	Yanco 6	y6	34.84 S, 145.87 E	121	22/12/03 - 31/05/11	2624	0-7, 0-30, 30-60, 60-90	7	Semi-Arid	Smith et al. (2012)
	Yanco 7	y7	34.85 S, 146.12 E	128	18/12/03 - 31/05/11	2627	0-7, 0-30, 30-60, 60-90	7	Semi-Arid	Smith et al. (2012)
	Yanco 8	y8	34.85 S, 146.41 E	149	12/12/03 - 31/05/11	2633	0-7, 0-30, 30-60, 60-90	7	Semi-Arid	Smith et al. (2012)
	Yanco 9	y9	34.97 S, 146.02 E	122	18/12/03 - 31/05/11	2627	0-7, 0-30, 30-60, 60-90	7	Semi-Arid	Smith et al. (2012)
	Yanco 10	y10	35.01 S, 146.31 E	119	10/01/04 - 31/05/11	2604	0-7, 0-30, 30-60, 60-90	7	Semi-Arid	Smith et al. (2012)
	Yanco 11	y11	35.11 S, 145.94 E	113	09/01/04 - 31/05/11	2605	0-7, 0-30, 30-60, 60-90	7	Semi-Arid	Smith et al. (2012)
	Yanco 12	y12	35.07 S, 146.17 E	120	12/12/03 - 31/05/11	2633	0-7, 0-30, 30-60, 60-90	7	Semi-Arid	Smith et al. (2012)
	Yanco 13	y13	35.09 S, 146.31 E	121	12/12/03 - 31/05/11	2633	0-7, 0-30, 30-60, 60-90	7	Semi-Arid	Smith et al. (2012)
	Kyeamba 1	k1	35.49 S, 147.56 E	437	16/11/01 - 31/05/11	3516	0-7, 0-30, 30-60, 60-90	14	Temperate	Smith et al. (2012)
	Kyeamba 2	k2	35.44 S, 147.53 E	351	17/11/01 - 28/02/11	3423	0-7, 0-30, 30-60, 60-90	14	Temperate	Smith et al. (2012)
	Kyeamba 3	k3	35.43 S, 147.57 E	318	17/11/01 - 31/05/11	3515	0-7, 0-30, 30-60, 60-90	14	Temperate	Smith et al. (2012)
	Kyeamba 4	k4	35.43 S, 147.60 E	296	16/11/01 - 31/05/11	3516	0-7, 0-30, 30-60, 60-90	14	Temperate	Smith et al. (2012)
	Kyeamba 5	k5	35.42 S, 147.60 E	306	15/11/01 - 28/02/11	3425	0-7, 0-30, 30-60, 60-90	14	Temperate	Smith et al. (2012)
	Kyeamba 6	k6	35.39 S, 147.46 E	317	06/11/03 - 31/05/11	2762	0-7, 0-30, 30-60, 60-90	14	Temperate	Smith et al. (2012)
	Kyeamba 7	k7	35.39 S, 147.57 E	259	06/11/03 - 31/05/11	2762	0-7, 0-30, 30-60, 60-90	14	Temperate	Smith et al. (2012)
	Kyeamba 8	k8	35.32 S, 147.34 E	326	06/11/03 - 31/05/11	2577	0-7, 0-30, 30-60, 60-90	14	Temperate	Smith et al. (2012)
	Kyeamba 10	k10	35.32 S, 147.53 E	232	07/12/03 - 31/05/11	2546	0-7, 0-30, 30-60, 60-90	14	Temperate	Smith et al. (2012)
	Kyeamba 11	k11	35.27 S, 147.43 E	327	07/11/03 - 31/08/09	2123	0-7, 0-30, 30-60, 60-90	14	Temperate	Smith et al. (2012)
	Kyeamba 12	k12	35.23 S, 147.49 E	220	06/11/03 - 31/05/11	2762	0-7, 0-30, 30-60, 60-90	14	Temperate	Smith et al. (2012)
	Adelong 1	a1	35.50 S, 148.11 E	772	02/12/01 - 31/05/11	3500	0-7, 0-30, 30-60, 60-90	15	Temperate	Smith et al. (2012)
	Adelong 2	a2	35.43 S, 148.13 E	595	02/12/01 - 31/05/11	2018	0-7, 0-30, 30-60, 60-90	15	Temperate	Smith et al. (2012)
	Adelong 3	a3	35.40 S, 148.10 E	472	02/12/01 - 31/05/11	3220	0-7, 0-30, 30-60, 60-90	15	Temperate	Smith et al. (2012)
	Adelong 4	a4	35.37 S, 148.07 E	457	02/12/01 - 31/05/11	3591	0-7, 0-30, 30-60, 60-90	15	Temperate	Smith et al. (2012)
	Adelong 5	a5	35.36 S, 148.09 E	379	26/11/01 - 28/02/11	3229	0-7, 0-30, 30-60, 60-90	15	Temperate	Smith et al. (2012)
CosmOz	Baldry	bl	32.87 S, 148.53 E	438	30/03/11 - 13/03/14	1078	Variable ≈ 15	14	Temperate	Hawdon et al. (2014)
	Tumbarumba	tb	35.66 S, 148.15 E	1200	03/04/11 - 31/12/15	1501	Variable ≈ 10	15	Temperate	Hawdon et al. (2014)
	Weany	we	19.88 S, 146.54 E	287	02/12/10 - 31/12/15	1855	Variable ≈ 15	6	Semi-Arid	Hawdon et al. (2014)
	Robson	rb	17.12 S, 145.63 E	715	28/10/10 - 31/12/15	1890	Variable ≈ 15	2	Tropical	Hawdon et al. (2014)
	Gnangara	gn	31.38 S, 115.71 E	50	16/05/11 - 06/12/15	1133	Variable ≈ 50	8	Temperate	Hawdon et al. (2014)
	Daly	dy	14.16 S, 131.39 E	75	07/06/11 - 31/12/15	1646	Variable ≈ 50	3	Savanna	Hawdon et al. (2014)
	Norwin	nw	27.57 S, 151.31 E	361	12/05/11 - 25/06/13	758	Variable ≈ 15	14	Temperate	Hawdon et al. (2014)
	Hamilton	ha	37.83 S, 142.09 E	199	01/07/15 - 31/12/15	184	Variable ≈ 10	15	Temperate	Hawdon et al. (2014)
	Tullochgorum	tl	41.67 S, 147.91 E	285	15/12/10 - 31/12/15	1842	Variable ≈ 15	15	Temperate	Hawdon et al. (2014)
	Mineral Banks	mb	41.26 S, 147.79 E	284	06/12/13 - 31/12/15	748	Variable ≈ 15	15	Temperate	Hawdon et al. (2014)
	Griffith	gr	34.25 S, 146.12 E	127	01/10/11 - 09/05/13	541	Variable ≈ 15	7	Semi-Arid	Hawdon et al. (2014)
	Yanco	yc	35.01 S, 146.30 E	124	01/04/11 - 31/12/15	1735	Variable ≈ 20	7	Semi-Arid	Hawdon et al. (2014)
OzFlux	Alice Springs Mulga	as	22.28 S, 133.25 E	606	03/09/10 - 01/08/14	1428	0-10	4	Arid	Cleverly (2011)
	Arcturus	ar	23.86 S, 148.47 E	170	01/01/11 - 01/01/14	1096	2.5, 5, 15	6	Semi-Arid	Schroder (2014)
	Calperum	cl	34.00 S, 140.59 E	64	01/08/10 - 21/10/15	1907	0-10	7	Semi-Arid	Calperum-Tech (2013)
	Cape Tribulation	ct	16.11 S, 145.38 E	66	01/01/10 - 03/09/15	2071	10, 75, 150	2	Tropical	Liddell (2013a)
	Cow Bay	cb	16.10 S, 145.45 E	86	01/01/09 - 12/05/15	2322	4, 50 100, 200	2	Tropical	Liddell (2013b)
	Cumberland Plain	cp	33.62 S, 150.72 E	200	19/10/12 - 31/10/15	1108	5, 30	15	Temperate	Pendall (2015)
	Gingin	gg	31.38 S, 115.71 E	51	01/01/11 - 07/11/15	1771	10, 20, 40, 80, 160	8	Temperate	Silberstein (2015)
	Howard Springs	hs	12.49 S, 131.15 E	64	01/01/01 - 03/09/15	5356	10-100	3	Savanna	Beringer (2013a)
	Riggs Creek	rc	36.65 S, 145.58 E	152	18/12/10 - 06/07/15	1661	10, 20, 40, 80, 120, 200	14	Temperate	Beringer (2014)
	Samford	sf	27.39 S, 152.88 E	71	01/01/10 - 31/12/15	2190	10, 30, 50, 80	14	Temperate	Rowlings (2011)
	Sturt Plains	sp	17.15 S, 133.35 E	250	01/01/08 - 01/01/15	2556	5, 50	6	Semi-Arid	Beringer (2013b)
	Ti Tree East	tt	22.29 S, 133.64 E	553	01/01/13 - 01/08/14	578	Various	4	Arid	Cleverly (2013)
	Wallaby Creek	wc	37.43 S, 145.19 E	720	01/01/09 - 01/01/14	1826	10, 15, 20, 40, 80, 150	15	Temperate	Beringer (2013c)
	Warra	wa	43.10 S, 146.65 E	100	05/03/13 - 17/02/15	715	10, 20, 40, 80	15	Temperate	Phillips (2015)
	Whroo	wh	36.67 S, 145.03 E	165	01/01/12 - 03/09/15	1341	10, 20, 40, 80, 150	14	Temperate	Beringer (2013d)
	Wombat State Forest	ws	37.42 S, 144.09 E	713	01/01/10 - 01/01/13	1096	10, 20, 40, 80, 150	15	Temperate	Arndt, 2013

3.2 Modelled Datasets

3.2.1 Australian Water Availability Project (AWAP)

Gridded data of daily maximum 2 m air temperature, precipitation, evaporation, transpiration, potential evaporation, shortwave radiation, as well as modelled SM produced by the Australian Water Availability Project (AWAP; Jones et al., 2009) are used here, both for analysis, and to produce SPI, API, MSDI, and KBDI. AWAP is a gridded dataset derived from *in situ* data collected at automated weather stations sourced from the Australian Data Archive for Meteorology (ADAM; Jones et al., 2009). Data anomalies in AWAP are generated using an optimal two-dimensional Barnes successive correction analysis procedure. The weighting function is obtained using the iterative Barnes algorithm (Jones et al., 2000) along with cross-validation parameters described by Seaman (1989). Finally, AWAP values are given from standard summing and multiplying of the weighting functions of precipitation of the climatological and anomaly analyses from the decomposition of the raw station data respectively (Jones et al., 2007). The 30-minute temporal resolution *in situ* data are incorporated into a simple water balance model (which includes SM) and projected onto an equirectangular 5 km grid across Australia (Jones et al., 2009). Despite the Australia-wide spatial coverage, large uncertainties exist in central Western Australia due to low station density, with this region being commonly masked for analysis. AWAP is commonly used for 20th-century Australian climatology studies (Perkins, 2015; Herold et al., 2016) due to its superior spatiotemporal coverage compared to other products. Both daily and monthly means are available from the CSIRO's (Commonwealth Scientific and Industrial Research Organisation) AWAP model run 26j (historical dataset between 1900 and current; Jones et al., 2009).

3.2.2 ECMWF ERA-INTERIM (ERA-INTERIM)

The European Centre for Medium-Range Weather Forecasts' re-analysis (ERA) of observational datasets into a Numerical Weather Prediction (NWP) models has been developed since 1975. They incorporate land and atmospheric observational datasets within an NWP-framework to reconstruct sea- and land-surface conditions over a specific time (Dee et al., 2011). The first re-analysis (ERA-15) was produced for 15 years between 1978 and 1994. The second re-analysis product (ERA-40; intended to span 40 years) covered a period of 45 years until 2002. The most recent re-analysis product produced by the ECMWF is the ERA-Interim, which covers the period from 1979 to present using the IFS (Cy31r2) data assimilation system. This system includes a 4-dimensional variational analysis (4D-Var) with a 12-hour analysis window and a spatial resolution of approximately 80 km at 60 various vertical levels from the surface layer to 0.1 hPa (Dee et al.,

2011). The temporal resolution of ERA-Interim is 6-hourly and is used for relative humidity, the u and v wind components, the daily maximum 2 m air temperature, and the precipitation flux (mm per unit time).

3.2.3 Coupled Model Intercomparison Project Phase 5 (CMIP-5)

In order to investigate and address scientific questions arising from the IPCC AR4 (Intergovernmental Panel on Climate Change 4th Assessment Report) assessment due to the effects of climate change, the Coupled Model Intercomparison Project Phase 5 (CMIP-5) was established by the Working Group on Coupled Modelling (WGCM; Taylor et al., 2012). This is a set of experimental protocols for studying the output of coupled atmosphere-ocean general circulation models (AOGCMs) both historically and predictively using various emission scenarios. CMIP is essentially a peer-supported infrastructure to analyse, compare, and validate climate models in order to improve model output. Since its inception in 1995, there have been five major iterations of the protocols with the latest phase of experiments produced during the period 2010-2014 (Taylor et al., 2012).

Coupled atmosphere-ocean general circulation models allow for the simulated climate to adjust to time-varying parameters of climate forcing, such as increasing/decreasing atmospheric carbon dioxide among other greenhouse gas emissions. Typically, these adjusted scenarios are compared against control runs in which anthropogenic radiative forcing is held constant for the given base period (or forced only by changes in natural forcings; Taylor et al., 2012). There are five main scenarios or Representative Concentration Pathways (RCPs), the historical, RCP-2.6, RCP-4.5, RCP-6.0, and RCP-8.5, each coming with varying greenhouse gas emissions and forcing. The number attached to the RCP describes the value of the anthropogenic radiative forcing at the end of the century in Wm^{-2} (Taylor et al., 2012). Models are typically run at either the global or region scale, and for each of the RCP's, have multiple runs with varying forcing parameters. The historical runs are available for the period 1850-2005, whilst the RCP's are available between 2006-2300 (Taylor et al., 2012). Further details of models, ensembles and scenarios used are outlined in Chapter 7.

3.3 Satellite Datasets

3.3.1 Moderate-Resolution Imaging Spectroradiometer (MODIS)

A number of products are retrieved using the Moderate Resolution Imaging Spectroradiometer (MODIS) satellite and datasets. MODIS is a sensor with 36 bands ranging from $0.4\mu m$ to $14.4\mu m$ and is installed on the Terra and Aqua satellites (Barnes et

al., 1998) with derived products ranging from temperature, to evapotranspiration and vegetation cover (for a full list of MODIS version 4-6 products see: https://lpdaac.usgs.gov/dataset_discovery/modis/modis_products_table/). This study uses the MODIS Collection 6 datasets, which have recently replaced collection 5.1. Collection 6, level 3, monthly, and daily processed data are available at various spatial (250m, 500m, 1km and 5.6km) and temporal resolutions (5-minute, daily, 8-daily, 16-daily, monthly and annually) depending on the dataset used. The thermal anomalies/fire locations MCD14DL product is used for both FRP and fire hotspot retrieval. MCD14DL is processed by the Land, Atmosphere Near real-time Capability for EOS (LANCE) Fire Information for Resource Management System (FIRMS), using swath products (MOD14/MYD14) rather than the tiled MOD14A1 and MYD14A1 products (Giglio, 2015). FRP retrieval is performed using the approach of Wooster et al. (2005), and is flagged by the MODIS MOD14/MYD14 fire and thermal anomalies algorithm (Giglio et al., 2003) as containing one or more fires within the pixel and also indicating confidence levels. As described in section 3.4.4, the MODIS leaf area index product (MCD15A2H; Myneni, 2015) is used to calculate the vegetation/evapotranspiration component within the MSDI and is available at 500 m resolution per 8-days. Likewise, the MODIS MOD13Q1 product is used for determining vegetation through NDVI (Normalized Differenced Vegetation Index) at 16-day intervals at 250 m resolution (Didan, 2015). Data are obtained from the Land Processes Distributed Active Archive Center (LPDAAC; https://lpdaac.usgs.gov/) and are upscaled to 5 km and 25 km to match the spatial resolution of various other datasets used for analysis in this study.

3.3.2 European Space Agency Climate Change Initiative (ESA CCI)

Following the inclusion of soil moisture as an Essential Climate Variable (ECV), a consortium of research institutes funded by the European Space Agency (ESA) Climate Change Initiative (CCI) have developed a soil moisture dataset comprising several active and passive microwave satellite retrieval datasets (ESA CCI Liu et al., 2012; Dorigo et al., 2017; Gruber et al., 2017). This was in order to provide a complete and consistent soil moisture dataset including both active (scatterometer) and passive (radiometer) microwave observations. These include the C-band scatterometers on ERS1/2 between 1991-2011, MetOp's ASCAT from 2006, and the multi-frequency radiometers on Acqua's AMSR-E from 2002, Coriolis Windsat from 2003 (as well as: TRMM-TMI from 1997, DMSP SSM/I from 1987 and Nimbus-7/SMMR between 1978-1987; Wagner et al., 2012). Data are retrieved according to the original satellite specifications with temporal retrievals between 1-8 days and datasets are listed below (3.2). The overall spatial resolution of the ESA CCI project is upscaled to 50km and 25km and depict a soil moisture depth between 0.5-2 cm. For the purposes of this research version 2.1 of the ESA CCI product has been

used. Each of the contributing products/sensors are discussed in more detail below and outlined in Table 3.2.

Table 3.2: List of datasets used for the composite ESA CCI SM dataset and their details.

Sensor	Agency	Type	SM Depth	Operational Period	Spatial Resolution	Temporal Resolution
ASCAT	EUMETSAT	Active @ 5.255 GHz	0.5-2 cm	2007 - 2015	12.5 km	≈ 2 days
AMI-WS	EUMETSAT	Active @ 5.255 GHz	0.5-2 cm	1991 - 2006	12.5 km	≈ 2 days
AMSR-E	JAXA	Passive @ 6.9, 10.65, 18.7, 23.8, 36.5, 89.0 GHz	0-1 cm	2002 - 2011	25 km	≈ 3 days
AMSR2	JAXA	Passive @ 6.9/7.3, 10.65, 18.7, 23.8, 36.5, 89.0 GHz	0-1 cm	2012 - 2015	25 km	≈ 3 days
WindSat	NRL	Passive @ 6.9, 10.7, 18.7, 23.8, 36.5 GHz	2-5 cm	2007 - 2010	25 km	≈ 8 days
TRMM-TMI	NASA / JAXA	Passive @ 10.7, 19.4, 21.3, 37, 85.5 GHz	0-1 cm	1998 - 2002	25 km	1 day
DMSP SSM/I	NASA DAAC	Passive @ 19.35, 23.235, 37, 85.5 GHz	0-7 cm	1987 - 1997	25 km	1 day
Nimbus-7 SMMR	NASA DAAC	Passive @ 6.6, 10.7, 18, 21, 37 GHz	0-7 cm	1978 - 1987	25 km	2 days

AMI-WS & ASCAT

The Vienna University of Technology's (TU-Wien) wind scatterometer (AMI-WS) product is a soil moisture product that amalgamates the radar backscattering coefficients as measured by the European Remote Sensing satellites ERS-1 and ERS-2. The AMI-WS has the greatest temporal range of all the remote sensing products available, with coverage from 1991 to mid-2007 (including periods of overlap between the products). This coverage has since been extended to present, with the ASCAT (Advanced SCATterometer; beginning from 2007) dataset on board the MetOp satellites (technical aspects do not differ from AMI-WS; Liu et al., 2011; Albergel et al., 2012). The ERS-1 and ERS-2 Solar synchronous satellites operate at the 5.255 GHz frequency (C-Band). Together they provide three radar images of the Earth's surface with a total swath of about 500 km (50 km spatial resolution; Albergel et al., 2012; de Jeu et al., 2008; Liu et al., 2011). The satellites have a morning/descending overpass (10:30 am local time) and afternoon/ascending overpass (10:30 pm local time), to produce a daily average measurement. Total revisit time is 1-7 days (Table 3.2). The TU-Wien dataset models the incidence angle dependency of the radar backscattering signal σ^0. From this, the backscattering coefficients

are normalised to the referencing angle of $40°$ (Wagner et al., 2012). Surface soil moisture and the surface water index are derived from the scaling of the normalised backscattered coefficients $\sigma^0(40°)$. SSM and SWI values range between 0% and 100% (0 and 1), where the lowest/highest values correspond to the driest/wettest conditions. The derived SSM (SWI) represent the uppermost 2 cm (100 cm) of the soil and is then resampled to a 12.5 km resolution grid using the Discrete Global Grid index (for DGG resampling see ; Sahr et al., 2002).

AMSR-E/AMSR2

Developed by the Japan Aerospace Exploration Agency (JAXA) the Advanced Microwave Scanning Radiometer-Earth Observing System (AMSR-E) is a twelve-channel, six-frequency, passive-microwave radiometer system. It measures brightness temperatures at 6.9 GHz, 10.7 GHz, 18.7 GHz, 23.8 GHz, 36.5 GHz, and 89.0 GHz modified for Aqua and is onboard the Japanese ADEOS-2 satellite (Njoku, 2004). The spatial resolution of the individual measurements varies between 5.4 km at 89 GHz to 56 km at 6.9 GHz, however, the mean resolution is roughly 56 km. AMSR-E has a morning/descending overpass (1:30 am local time at the equator) and afternoon/ascending overpass (1:30 pm local time at the equator), to produce a daily average measurement (Njoku, 2004). The AMSR-E product ceased operation in 2011 and was replaced by the AMSR2 sensor.

WindSat

Operated by both NASA (National Aeronautics and Space Administration) and NOAA (National Oceanic and Atmospheric Administration), the WindSat passive-microwave radiometer operating in 5 discrete channels: 6.8, 10.7, 18.7, 23.8 and 37.0 GHz was set up for the retrieval of sea-surface wind speed direction and temperature (Gaiser et al., 2004). All channels are fully polarimetric except the 6.8 and 23.8 GHz channels that have only dual polarization. The WindSat sensor operates on the Coriolis satellite which is in a near-polar orbit. WindSat has a morning/descending overpass at 6 am (local time at the equator) and afternoon/ascending overpass 1:30 pm (local time at the equator), to produce a daily average measurement. Unlike other radiometers, the WindSat sensor records observations during both the forward and aft scans. This provides WindSat with a wider swath than comparable sensors (Gaiser et al., 2004).

3.3.3 Köppen-Geiger Regions

The strength of land-climate feedbacks such as the coupling of soil moisture with temperature is largely dependent on the local climate of a region. As Australia is host to various climate regions, it is important to define those regions for analysis of locations with

similar conditions. The Köppen-Geiger climate classifications, as proposed by Köppen (1884), is one such method allow to identify the different regions spatially. The Köppen-Geiger climate classification scheme, divides climates into five main groups (Tropical, Dry, Temperate, Continental and Polar) each with sub-categories describing the variation of the climate therein (Köppen, 1884; Kottek et al., 2006; Peel et al., 2007). These climate regimes are defined by thresholds of the mean monthly precipitation, temperature, and evapotranspiration. Australia is predominately categorised as arid, semi-arid, temperate, tropical wet or tropical dry (savanna) (see Figure 3.1). Arid climate regions have a monthly precipitation less than half of their potential evapotranspiration and semi-arid regions have a monthly precipitation between 50% and 100% of their potential evapotranspiration (Kottek et al., 2006; Peel et al., 2007) with average annual temperature above $18°$. The temperate climate regions have an average summer temperatures above $10°C$ and between $3°C - 18°C$ in winter (Kottek et al., 2006; Peel et al., 2007).

Table 3.3: Overview of datasets including: variables recorded, soil depth for which data are represented, operational period of dataset and spatial and temporal resolution of dataset. Variables used include maximum daily temperature (Tx), precipitation (Pr), soil moisture (SM), Soil Water Content (SWC), Fire Radiative Power (FRP), Leaf Area Index (LAI), Normalized Differenced Vegetation Index (NDVI), relative humidity (RH), u & v wind components and the SOI (Southern Oscillation Index)

Datasets	Type	Variables	Soil depth	Operational Period	Spatial Resolution	Temporal Resolution	Reference
AWAP	Modelled/*in situ*	Pr, Tx, SM	0-2 cm	1900 -	0.05°	Daily	Jones et al. (2009)
Oznet	*in situ*	SM Pr	0-7 cm 0-30 cm 30-60 cm 60-90 cm	2001 -	Station	20-30 min	Smith et al. (2012)
OzFlux	*in situ*	SM	Table 3.1	2005 -	Station	30 min	Hawdon et al. (2014)
CosmOz	*in situ*	SM, SWI	Table 3.1	2010 -	Station	1 hour	Table 3.1
MODIS	Remotely Sensed	FRP, LAI, NDVI		2000 -	500m	1-8 days	
CMIP-5	Modelled	RH, u, v, Tx, Pr		1850 - 2100	Table ??	Daily Monthly Yearly	(Taylor et al., 2012)
ERA-Interim	Remotely Sensed	RH, u, v, Tx, Pr		1979 -	0.25°	3-hourly	(Dee et al., 2011)
ESA CCI	Remotely Sensed	SM	0.5-2cm (SSM) 0-100cm (SWI)	1978 - 2015	0.25°	1-8 days	(Liu et al., 2011) (Dorigo et al., 2017) (Gruber et al., 2017)
SOI	*in situ*	SOI		1876 -	Global value	Monthly	(Ropelewski et al., 1987)
Koeppen-Geiger	*in situ*	Climate Regions		N/A	0.1°	N/A	(Peel et al., 2007)

Finally, the difference between tropical and savanna climate regions is that during the

driest months the minimum precipitation is 60 mm for tropical regions and below that for savanna regions (Kottek et al., 2006; Peel et al., 2007). Historical data of temperature, precipitation and evapotransporation used to determine the climate regimes are retrieved from the Global Historical Climatology Network (GHCN-Monthly Version 2). This is a network of observational stations worldwide extending back to 1950 and updated monthly, of which, 4,844 stations for temperature and 12,396 stations for precipitation are used for calculating the Köppen-Geiger index (Peel et al., 2007).

3.4 Moisture Indices

3.4.1 Standardised Precipitation Index (SPI)

As previously mentioned, the SPI is a commonly used proxy for soil moisture to provide a high-resolution dataset that is comparable in both time and space (Guttman, 1998; Hayes et al., 1999). and it can be calculated at different time scales to monitor droughts with respect to relative water resources and depending on the desired period of soil moisture memory. Most commonly it is calculated at one, three, six or twelve months. Short to mid-term deficits i.e droughts are of particular interest and are indicated through a 3- or 6-month SPI (McKee et al., 1993). The SPI is calculated from the transformation of a fitted gamma distribution function that describes a time series of precipitation data with a standard normalised distribution (z-distribution; Abramowitz et al., 1964; Edwards, 1997). Due to the fitting of a standardised normal distribution to the precipitation time series, the frequency of events is not dependent on seasonality, allowing for comparative analysis of seasons. However, a drawback to this method is that high-resolution data are required with a minimum of 30 years to provide a robust distribution (McKee et al., 1993). Table 3.4 defines the SPI values for corresponding drought or flood characteristics and their occurrence probability as calculated according to the fitted standard normalised distribution. SPI ranges from 3 to -3, or extremely wet to extremely dry conditions respectively.

More specifically, Equation 3.1 describes the cumulative density function (CDF) of the gamma distribution (Γ), where x and $\bar{x}$ are the precipitation and mean precipitation from the time series, respectively, and $\hat{\alpha}$ and $\hat{\beta}$ are the shape and scale parameters, respectively.

$$G(x) = \int_0^x g(x)\mathrm{d}x = \frac{1}{\hat{\beta}^{\hat{\alpha}}\Gamma(\hat{\alpha})} \int_0^x x^{\hat{\alpha}} e^{\frac{-x}{\hat{\beta}}}\,\mathrm{d}x \tag{3.1a}$$

with

$$\hat{a} = \frac{1}{4A}\left(1 + \sqrt{1 + \frac{4A}{3}}\right) \tag{3.1b}$$

and

$$\hat{\beta} = \frac{\bar{x}}{\hat{a}} \tag{3.1c}$$

and

$$A = ln(\bar{x}) - \frac{\sum ln(x)}{n} \tag{3.1d}$$

The gamma cumulative distribution function is not defined for zero precipitation, and as such, zero precipitation (under 1 mm) events are removed from the time series and the resulting gamma distribution is modulated using the probability of this occurrence. The following equation describes the adjustment to the gamma cumulative distribution function (*G(x)*) where *q* is the probability of zero precipitation. As applied by McKee et al. (1993, Equation 3.1), the calculated gamma cumulative distribution function is then transformed into a standard normal distribution for SPI values. This is done simply by overlaying a standard normal distribution over the top of the gamma CDF and then reading the values from the CDF. Note that this approach is impractical for large datasets, and an approximate conversion is provided by Abramowitz et al. (1964), as seen in Edwards (1997) (here, Equation 3.2).

$$SPI = \begin{cases} -\left(t - \dfrac{c_0 + c_1 t + c_2 t^2}{1 + d_1 t + d_2 t^2 + d_3 t^3}\right) & \text{if} \quad 0 < \ H(x) \leq 0.5 \\ \\ +\left(t - \dfrac{c_0 + c_1 t + c_2 t^2}{1 + d_1 t + d_2 t^2 + d_3 t^3}\right) & \text{if} \quad 0.5 < H(x) < 1 \end{cases} \tag{3.2a}$$

where

$$H(x) = q + (1 - q).G(x) \tag{3.2b}$$

and

$$t = \begin{cases} \sqrt{ln\left[\dfrac{1}{(H(x))^2}\right]} & \text{if} \quad 0 < \ H(x) \leq 0.5 \\ \\ \sqrt{ln\left[\dfrac{1}{(1 - H(x))^2}\right]} & \text{if} \quad 0.5 < H(x) < 1 \end{cases} \tag{3.2c}$$

with

$$c_0 = 2.515517 \quad c_1 = 0.802853 \quad c_2 = 0.010328$$
$$d_1 = 1.432788 \quad d_2 = 0.189269 \quad d_3 = 0.001308$$

where c_0 to c_2 and d_0 to d_2 are empirically derived constants used to approximate the conversion from the gamma CDF to a normal distribution.

Table 3.4: Precipitation anomaly classification based on SPI values and corresponding event probabilities

SPI Value	Category	Probability %
2.00 or more	Extremely Wet	2.3
1.50 to 1.99	Severely Wet	4.4
1.00 to 1.49	Moderately Wet	9.2
0 to 0.99	Mildly Wet	34.1
0 to -0.99	Mild Drought	34.1
-1.00 to -1.49	Moderate Drought	9.2
-1.50 to -1.99	Severe Drought	4.4
-2 or less	Extreme Drought	2.3

3.4.2 Antecedent Precipitation Index (API)

Similar to the SPI, the Antecedent Precipitation Index (API) is an empirical method for indirectly estimating SM from precipitation output. While the SPI is calculated based on a fitted distribution of a moving average of the precipitation time series, API provides a current precipitation-driven SM employing a constant SM depletion rate. API estimates the current SM by multiplying the previous API by a depletion factor and adding the previous day's precipitation. API was initially defined by Kohler et al. (1951) to determine drought conditions and has also been used in various watershed analysis studies (Equation 3.3; Liu et al., 2011).

$$API_n = (API_{n-1} + P_{n-1})e^{-\alpha \Delta t} \tag{3.3}$$

where API_n and API_{n-1} are the current and previous day's API, Δt represents the time-step of the measurement (in most cases it is equal to 1) and $\alpha(day^{-1})$ is the inverse of the characteristic soil moisture depletion (Kohler et al., 1951). As the depletion rate

has a considerably large spatial variation due to several factors including soil type, soil density, vegetation, exposure, hill slope etc. it is further simplified to be a function of the daily maximum temperature. The API has most recently been calculated using the form of Equation 3.4 (Crow et al., 2005; Crow et al., 2012; Holgate et al., 2016; Kumar et al., 2017).

$$API_n = (\gamma \times API_{n-1}) + P_n \tag{3.4a}$$

where

$$\gamma = 0.85 + \delta(20 - T_x) \tag{3.4b}$$

and

$$\delta = 0.0075$$

where API_{n-1} is modulated by the depletion rate (γ), and P_n is the current day's precipitation depth. The depletion rate is calculated using a sensitivity parameter (δ) and an offset to the maximum daily temperature (T_x Crow et al., 2005). As API is representative of soil moisture, values are capped to 50 mm to indicate full saturation (Kumar et al., 2017).

3.4.3 Keetch-Byram Drought Index (KBDI)

As discussed in Chapter 2, another alternative to SPI is the KBDI (also used in the current FFDI formulation). The KBDI describes the soil moisture deficit in the root-zone and surface litter layers expressed in mm. The soil moisture deficit is defined by Keetch et al. (1968), ranging from 0 (saturated) to 203.2 mm (severe drought). In essence, the KBDI is a simple water balance model calculated daily and is expressed as:

$$dQ = \frac{[203.2 - Q]\left[0.968 \times e^{0.0875T_{max}+1.5552} - 8.3\right] dt}{1 + 10.88e^{-0.001736R}} \times 10^{-3} \tag{3.5a}$$

and

$$Q_n = Q_{n-1} + dQ \tag{3.5b}$$

where dQ is rate of change of the index, Q is the KBDI based on the previous day's calculations, T_{max} is the daily maximum temperature (°C), R is the mean annual precipitation (mm), and dt is the time increment (set to 1 day). Keetch et al. (1968) limited the calculation of drought conditions to periods that consistently exceeded $21°C$ with little to no rainfall. Strong precipitation events can result in negative dQ values and light events

are generally defined as $dQ = 0$. These thresholds define drought for the case region, but do not consider varied climate regions and vegetation types. Equation 3.5 is based on the assumption provided by Keetch et al. (1968) that soil moisture is at field capacity at 203.2 mm of water depth for all soil types and that vegetation density is a function of the inverse exponent of mean annual precipitation, inferring the rate of moisture loss. It also assumes that the evaporation rate with time is the exponent of the daily maximum temperature.

3.4.4 Mount's Soil Dryness Index (MSDI)

Similarly to the KBDI, Mount's Soil Dryness Index (MSDI; Mount, 1972) is also an empirically derived cumulative SM deficit index. However, it differs from the KBDI in the estimation of evapotransporation which is determined through using a vegetation filtration model. The MSDI is essentially a soil moisture model that takes into account rainfall, run-off, and interception. The retrieval of vegetation for defining evapotransporation is derived using the MODIS leaf area index (LAI) product (MCD15A2H; Myneni, 2015). For each vegetation category, parameters are defined for the canopy rainfall interception fraction, the canopy storage capacity, wet evaporation rates, and flash-runoff fraction using a linear relationship to LAI as per (Finkele et al., 2006). Regression coefficients used are based on *in situ* observations of evapotranspiration from capital cities in the Australian states of Victoria, Tasmania and South Australia. In general MSDI is given as:

$$\frac{dMSDI}{dt} = P_{eff} + ET \tag{3.6a}$$

where

$$P_{eff} = rain - interception - runoff \tag{3.6b}$$

and

$$ET = a_i T_{max} + b_i \tag{3.6c}$$

where evapotranspiration (ET) is a linear function of maximum daily temperature (T_{max}), and where a_i and b_i are derived from the relationship between mean monthly pan evaporation and mean monthly maximum temperature (Finkele et al., 2006). As MSDI is used operationally in various states in Australia in place of KBDI in the formulation of FFDI, MSDI is scaled to between 0 mm and 203.2 mm, where 0 mm is considered the saturated moisture content and 203.2 mm considered as extremely dry.

3.5 McArthur Forest Fire Danger Index (FFDI)

As mentioned in Chapter 2, in Australia, the McArthur FFDI is used operationally and will be also be used here to describe fire danger. The FFDI quantifies fire danger with a scale between 0 and 100+ for low to catastrophic risk respectively (see Table: 3.5). It was originally derived empirically by (McArthur, 1967; Nobel et al., 1980) and is expressed as:

$$FFDI = 2\,D^{0.987} e^{[-0.45 + 0.0338\,T - 0.0345\,RH + 0.0234\,v]} \tag{3.7}$$

$$DF = \frac{0.19\,[KBDI + 104]\,[DSLR + 1]^{1.5}}{3.52\,[DSLR + 1]^{1.5} + LR - 1} \tag{3.8}$$

Table 3.5: McArthur Forest Fire Danger categories and their index values.

Fire Danger Rating	FFDI
Low - Moderate	0-11
High	12-24
Very High	25-49
Severe	50-74
Extreme	75-99
Catastrophic	100+

where *DF* is the Drought factor, given as a number between 0 and 10, T is the daily maximum temperature ($^{\circ}C$), *RH* is daily minimum relative humidity, v is the daily-mean wind speed, *LR* (mm) is the total rainfall during the previous rain event and *KBDI* (mm) is the amount of rain needed to restore the soil moisture content to a maximum field capacity of 203.2 mm (constant depth) and a minimum of 0 m m(Nobel et al., 1980). As with Liu et al. (2003), D can be derived empirically as provided by McArthur (1967) or through a more recent simplification by Griffiths (1998). Both of these formulae require actual soil moisture content, limiting resolution and the scalability of the index. Commonly the soil moisture deficit used for calculating the drought factor is calculated either from the KBDI (Keetch et al., 1968) or from Mount's Soil Dryness Index (MSDI) (Mount, 1972). It should be noted that values in excess of 100 were only included in the classifications (catastrophic) in response to the 2009 "Black Saturday Fires" in south-east

Australia. Prior to this, a maximum value of 100 was set for extreme fire conditions in 1939 (Nobel et al., 1980).

3.6 Statistical Methods

In order to compare daily time steps of the API, SPI, KBDI, MSDI to remotely sensed soil moisture, *in situ* soil moisture observations were converted to daily averages and scaled using a standard min/max normalisation (between 0-1) for each time series. As this rescaling method can be sensitive to outlier observations, each observational soil moisture dataset time-series has been visually inspected to remove erroneous measurements (negative values, values exceeding realistic maxima, etc.). Any variable from which anomalies have been computed used a 31-day sliding mean, similar to the calculation of hot days and to studies such as; Perkins et al. (2012). The magnitude and sign of the relationship between datasets are compared through calculating the Pearson correlation. Correlation coefficients were then compared using several methods, including Taylor diagrams which display the correlation coefficient, a normalised standard deviation and an unbiased RMSD (Root Mean Squared Difference). The Pearson correlation coefficients were calculated using Equation 3.9:

$$r = \frac{\sum_i (X_i - \bar{X})(Y_i - \bar{Y})}{\sqrt{\sum_i (X_i - \bar{X})^2 \sum_i (Y_i - \bar{Y})^2}} \tag{3.9}$$

where r represents the correlation coefficient, X is the first variable and Y is the second variable. Typically, correlation coefficients are spatially averaged by taking the mean over a given area (Perkins, 2015; Holgate et al., 2016). However, this can lead to a large sample distribution bias depending on the number of correlation coefficients to be averaged. Corey et al. (1998), suggest using the Fisher z-transformation to normalise values, then average these values before converting those back into the familiar correlation coefficients. This study presents findings using this method, calculated using:

$$z' = 0.5ln\frac{1+r}{1-r} \tag{3.10a}$$

and

$$r_{z'} = \frac{e^{2.\bar{z'}} - 1}{e^{2.\bar{z'}} + 1} \tag{3.10b}$$

where r is the correlation coefficient, and z' is the Fisher z-transformation value. Finally, significance testing of the correlation coefficients is also presented using a stricter

approach than that of using the 5% level (used for stippling significance in maps). Conventionally, in order to evaluate the significance of a correlation, a nominal threshold of 5% is chosen, a value above which the probability of the resultant randomly occurring correlation should not exceed. The statistical power of this is greatly reduced due to the discrete nature of the test statistic and Wilks (2006) suggests using the false discovery rate (FDR) threshold for significance testing. The FDR method calculates a single global threshold based on the distribution of p-values in a field obtained from multiple local significance tests. The field significance criteria are met if the local test is below this global threshold. The FDR threshold is calculated using Equation 3.11 for each significance test.

$$\rho^*_{FDR} = \max_{i=1,\ldots,N} \left[\rho_{(i)} : \rho_{(i)} \geqslant (\frac{i}{n}) \alpha_{FDR} \right] \tag{3.11}$$

where, α_{FDR} is the nominal threshold, and the threshold ρ^*_{FDR} for rejecting the local null hypotheses is the largest ρ_i that is no larger than the fraction of α_{FDR} specified by i/n.

Chapter Summary

This chapter presented the methodologies and datasets that are common to analysis throughout the following chapters. More specifically, the specifications and details of the *in situ* soil moisture datasets from the OzNet, OzFlux and CosmOz networks, the ERA-Interim and CMIP5 modelled datasets, the MODIS and ESA CCI remotely sensed datasets, and soil moisture indices, namely, the API, SPI, KBDI and MSDI derived from the AWAP gridded observationally based datasets were all outlined in this chapter. The following chapters will explore the relationships discussed in Chapter 2 using the datasets and methods introduced here. Specific methods not discussed in this chapter will be outlined in further detail at the beginning of each chapter where pertinent.

CHAPTER 4

Comparison of Soil Moisture Proxies Across Australia

Overview This chapter investigates the relationship between soil moisture and various moisture precipitation-driven indices and models in Australia. This is done at both a monthly and daily scale for observational (Cosmic-ray detection network, Time-domain reflectometer network, and Frequency-domain sensor networks) and gridded datasets. More specifically, the degree of association between soil moisture derived from the CosmOz, OzNet and OzFlux sites with the API, SPI, KBDI and MSDI moisture indices is compared in this chapter in context with regional soil and climatological characteristics. Furthermore, this chapter then compares these indices against the remotely sensed ESA CCI soil moisture product, and AWAP's surface soil moisture product spatially across Australia.

4.1 Introduction

The importance of soil moisture on the climate system and as an environmental variable has been highlighted by its inclusion into the GCOS (Global Observing System for Climate) Essential Climate Variable (ESV) index under land interactions (GCOS, 2010). Not only is soil moisture an important variable in land dynamics such as subsurface flow, infiltration, and groundwater recharge as well as influencing photosynthesis and evapotranspiration through vegetation moisture, but it is also a key component in land-atmosphere feedbacks associated with the hydrological cycle at both weather and climate time-scales (Seneviratne et al., 2010). As highlighted in Chapter 2 and following in Chapter 5.1, soil moisture is known to influence the energy partitioning between sensible and latent heat from the land into the atmosphere, and as a consequence affecting local temperature and precipitation extremes (Seneviratne et al., 2010; Fischer et al., 2007; Hirschi et al., 2010). Changes in soil moisture can have a significant socio-economic effect both directly through water resource management, agricultural productivity, forest and ecosystem health, as well as indirectly through exacerbated temperature extremes and their associated risks (Hirschi et al., 2014; Han et al., 2014; Herold et al., 2016).

As soil moisture influences multi-scale feedbacks (Seneviratne et al., 2010) as well as land-atmosphere interactions (Brocca et al., 2011; Albergel et al., 2012), it is essential to understand how it varies both spatially and temporally. In doing so, the accuracy of predictions can be improved in order to better mitigate potential risks (Draper et al., 2009). To this end soil moisture is currently used in land surface model assimilation (van Dijk et al., 2014) including agricultural drought models (e.g. Han et al., 2014), numerical weather forecasting (e.g. Draper et al., 2009; Dharssi et al., 2011), flood forecasting (e.g. Wanders et al., 2014), forest fire danger forecasting (e.g. Liu et al., 2003; Finkele et al., 2006; Bartsch et al., 2009), and long-term hydrological trends and drought monitoring and evaluation (e.g. Heim, 2002; Teuling et al., 2006; Hubbard et al., 2007; van Dijk et al., 2013; Perkins et al., 2015). Soil moisture is also used extensively in the assessment of hydrological feedbacks in CMIP5 projections (e.g. Seneviratne et al., 2013) and other climate studies.

Soil moisture is available through various products, typically via observational networks such as the OzNet, OzFlux and CosmOz (Chapter 3.1) or via remotely sensed products such as the ESA CCI dataset (Liu et al., 2011), as well as through modelled data such as AWRA-L (Australian Water Resource Assessment Landscape model) or CABLE (Community Atmosphere Biosphere Land Exchange). Each of these has varying advantages and disadvantages due to individual temporal and spatial resolutions. Alternatively, soil moisture can be derived using; water balance indices where high resolution data are

unavailable. Commonly-used indices include the Antecedent Precipitation Index (API; Kohler et al., 1951), Palmer Drought Severity Index (PDSI; Palmer, 1965), Keetch-Byram Drought Index (KBDI; Keetch et al., 1968), Mount's Soil Dryness Index (MSDI; Mount, 1972), Surface Water Supply Index (SWSI; Shafer et al., 1982), Standardized Precipitation Index (SPI; McKee et al., 1993), Vegetation Condition Index (VCI; Liu et al., 1996), Soil Moisture Index (SMI; Hubbard et al., 2007), and the Standardized Precipitation Evapotranspiration Index (SPEI; Vicente-Serrano et al., 2010), among many more (further detail has been documented in Chapter 2.2 and summarised in Table 2.1).

A number of previous studies have compared several of the aforementioned remotely sensed and modelled products with *in situ* soil moisture globally and in Australia (e.g. Albergel et al., 2012; Brocca et al., 2011; Draper et al., 2009; Hawdon et al., 2014; Liu et al., 2011; Dorigo et al., 2015). Although there is a general agreement between products, these studies limit analysis to similar products compared against *in situ* measurements located primarily in the south-east of Australia using the OzNet network. Often these comparisons occur using a relatively short observational period or utilise very coarse resolution data. Both Su et al. (2013), Holgate et al. (2016), and Kumar et al. (2017), provide an extended analysis using three networks in Australia (OzNet, OzFlux, and CosmOz) comparing various types of products, but in both cases, detail is limited by both the spatial and temporal resolution as well as through a sub-selection of available sites. Additionally, the latter two studies have not provided a detailed analysis in context with known differences in the climate regimes, vegetation and soil types across Australia.

This chapter compares the API, SPI, KBDI, MSDI precipitation-based moisture indices, the remotely sensed ESA CCI product, and AWAP's surface soil moisture product. Generally, studies have compared a number of these products over a subset of the available time series (Holgate et al., 2016; Kumar et al., 2017). However, this chapter builds on previous comparisons using all three *in situ* networks as a reference for the entire available time range. For *in situ* networks, this is between 2001 and 2015 and between 1979-2015 for the ESA CCI product. Furthermore, comparisons are not only analysed at *in situ* locations but also for gridded at 25 km resolution. This provides a spatially more consistent and detailed analysis of the association between products under various climate regimes, vegetation, and soil types.

4.2 Data and Methodology

Direct comparison between the *in situ*, remotely sensed and modelled datasets is challenging due to the systematic differences between each data source. Measurements differ

in terms of the temporal and spatial resolutions and observational depths measured. As discussed in Chapter 3.1, soil moisture measured from the OzNet, OzFlux and CosmOz networks vary in observation depth, ranging from the surface soil moisture of between 0-5 cm or 0-10 cm to a much deeper layer between 0-200 cm (using several measurements). In addition to this, due to the technical aspects of CosmOz, measurements are considered as variable estimates usually between 0-30 cm. Typically, remotely sensed moisture products have an observational depth of between 0-2 cm to 0-5 cm. Soil moisture measurements also differ in their sampling frequency across the three networks, and range from 20 min to 30 min in the OzFlux and OzNet networks, to hourly in the CosmOz network. For comparable analysis with the modelled AWAP dataset, daily precipitation averages are calculated between 9 am - 9 am. AWAP provides gridded data at 5km resolution spatially for Australia for several variables including precipitation, temperature, and soil moisture. Regions that recorded less than 1 mm precipitation over a 50 year period were masked from the analysis. For comparison with the ESA CCI derived soil moisture, AWAP derived variables and indices were up-scaled from 5 km to 25 km resolution to match the ESA CCI product. This was done using a bilinear interpolation from the post-processed datasets. Prior to this, where not previously provided, each product has been converted to volumetric units (m^3/m^3) of soil moisture then normalised (min/max) to provide values between 0 and 1 for direct comparison:

$$z_i = \frac{x_i - min(x)}{max(x) - min(x)} \tag{4.1}$$

Different sources of uncertainty and error are associated with each different data source preventing an absolute agreement between the different products (Brocca et al., 2011; Draper et al., 2013). In order to measure the association between moisture indices and the reference (both *in situ* and remotely sensed) soil moisture, three classical metrics were applied, similarly to other soil moisture studies (Draper et al., 2013; Albergel et al., 2013). These include i) the Pearson correlation coefficient (r; as calculated by Eq. 3.9), ii) the bias, and iii) the unbiased root mean squared error/difference (RMSE or RMSD). The equations for the calculation of the RMSE and the bias are given as follows (Brown, 1947; Chatfield, 1988; Armstrong et al., 1992; Brocca et al., 2011; Draper et al., 2013):

$$RMSE = \sqrt{\frac{\sum_{i=1}^{n} (x_i - y_i)^2}{n}} \tag{4.2}$$

$$bias = \frac{1}{n} \sum_{i=1}^{n} (x_i - y_i) \tag{4.3}$$

where n is the number of data pairs between the reference (x) and the index (y) used, and x_i and y_i are the values at individual points for each dataset. Simply put, these are a measure of how different the two comparable datasets are in both magnitude and sign.

Similarly, these metrics were also determined to evaluate temporal anomalies of each data set. This is done in order to highlight the agreement of soil moisture and remove any seasonality from the dataset (Rüdiger et al., 2009; Brocca et al., 2011; Albergel et al., 2013; Draper et al., 2013; Dorigo et al., 2015) which particularly affects the upper soil layer (Albergel et al., 2013). Generally, temporal anomalies within the time series are calculated by determining the difference between a single measurement in time and its reference mean. However, as mentioned, each dataset to be compared contains varying temporal periods. Therefore, anomalies of varying temporal periods can be calculated using a moving average for each individual dataset. Typically, soil moisture studies (Brocca et al., 2011; Albergel et al., 2013; Draper et al., 2013; Perkins, 2015; Dorigo et al., 2015) define anomalies using either 29, 31 or a 35-day sliding mean (i.e. 14, 15 or 17 days plus/minus). Provided at least five measurements within this range are available, soil moisture anomalies are calculated here using a sliding window of 31-days corresponding to the time interval ($t \pm 15\,days$). The difference between the soil moisture estimate at any given day i and the sliding mean is then scaled to the standard deviation of the reference data within the time window. The dimensionless anomaly *(anom)* is given by Eq. 4.4

$$anom_i = \frac{SM_i - \bar{SM}_F}{\sigma[SM_F]} \tag{4.4}$$

where $F = [i - 15, i + 15]$ and σ is the standard deviation of the dataset. As defined in Chapter 3.6, significance testing of correlation coefficients is produced using the False Discovery Rate threshold, and averages of correlations are computed using the Fisher z-transformation value.

4.2.1 API Calibration

Similarly to Kumar et al. (2017), daily API as defined in Chapter 3.4.2 is capped to 50 mm indicating a fully saturated surface soil layer (Kumar et al., 2017). However, this may not be applicable for comparison for all soil types and locations across Australia, and as such, it is necessary to identify the effect of changing this metric has on API and its relationship to soil moisture. For this, the normalised correlation coefficients between API and *in situ* soil moisture (from the OzNet, OzFlux and CosmOz networks) were compared with limiting values set between 0 and 150 mm.

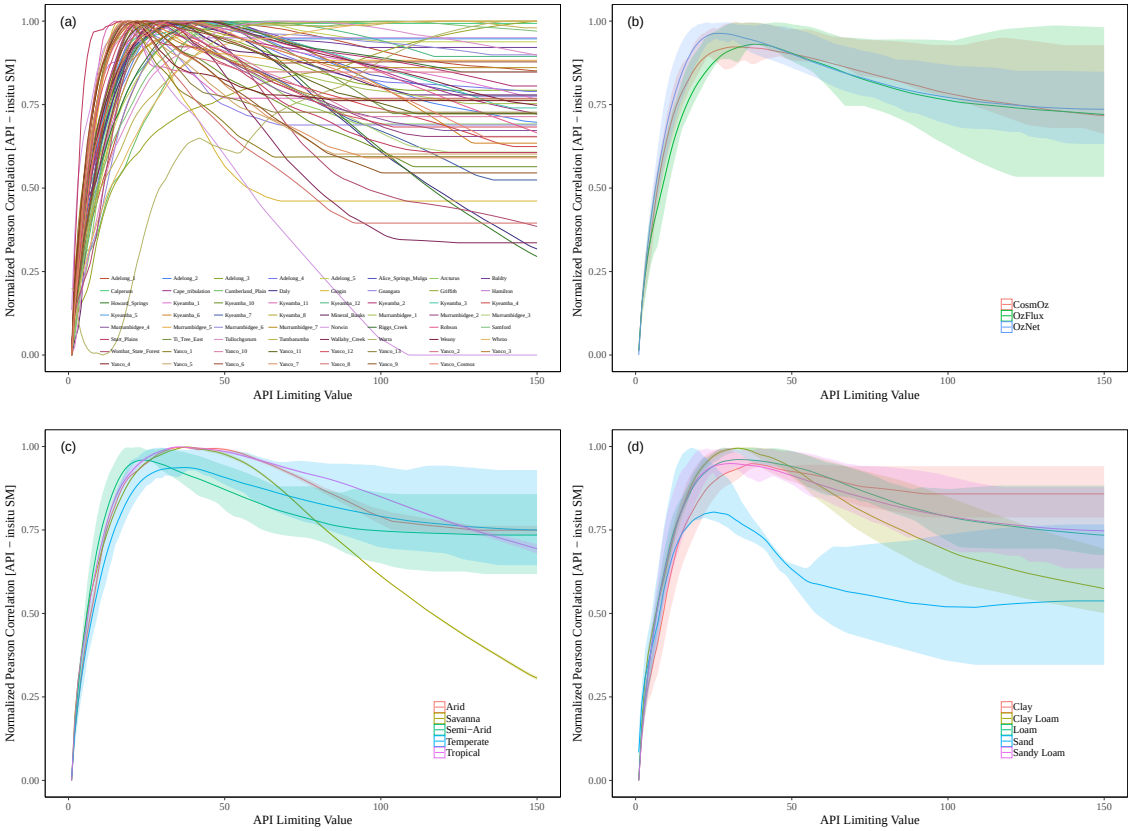

Figure 4.1: Comparison of normalised correlation coefficients between soil moisture and API with a limiting factor varying between 0 and 150 mm. (a) each *in situ* site compared against each other, (b) averages of the CosmOz, OzFlux and OzNet networks. (c) averages across Köppen-Geiger regimes. (d) averages across soil types. (b-d) also include the mean and 0.25 to 0.75 confidence interval.

Figure 4.1 shows correlation coefficients for each site, as well as averages across the networks, the Köppen-Geiger regimes as well as the soil types. Generally, maximum correlation coefficients are achieved between 10-75 mm depending on location. As each network spans a variety of climate regimes and soil types, each network on average exhibits similar maximum coefficients between 20-30 mm. When comparing various soil types, coarser soils such as sand and sandy-loam have much lower limiting values than finer soils such as loam and clay. Semi-arid and temperate regimes typically have maxima at a lower limiting value indicating that soils in these regions are coarser with higher filtration rates, conversely, savanna and arid regions typically have much higher limiting values. In each case correlation coefficients decrease substantially at limiting values greater than 75 mm. For the purpose of this chapter and future chapters, API is limited to 50 mm, as this just exceeds the expected maxima in each case. This allows for consistency when comparing *in situ* sites with gridded data across Australia, as grid cells span various soil types due to the coarseness of the available spatial resolution. This also allows for direct comparison to other studies which use 50 mm as the limit, namely, Holgate et al. (2016) and Kumar et al. (2017).

4.2.2 SPI Temporal Scales

SPI is calculated at various temporal scales and is typically calculated using monthly data with a scale of between 1 and 24 months. However, for the purpose of this study, SPI has also been calculated using daily values. Here, SPI at 7-, 14-, 30-, and 60-days as well as at 1-, 3-, 6-, and 12-months have been calculated and compared across for all available *in situ* sites for daily and monthly data, respectively. That is, SPI is calculated based on the sum of the previous 7-day to 12-months (depending on desired temporal scale) cumulative precipitation record. Both, 14- and 30-day SPI have the largest correlation coefficients to soil moisture with values of 0.595 and 0.574 (refer to Table 4.1). Similarly, normalised 3-, 6- and 12-month SPI were calculated and correlated to the *in situ* normalised soil moisture. Both 3-month and 6-month (especially for the OzNet and CosmOz networks) SPI generally show higher correlation coefficients across the *in situ* sites than the longer and shorter temporal scale of 1- and 12- months. As SPI is calculated using a fitted distribution based on historical differences, individual precipitation events appear to have little effect on values, whereas more weight is given to persistent precipitation events. Both very long and very short temporal scales of SPI have much lower correlation coefficients with their respective daily or monthly soil moisture. 3-month SPI is commonly used as a proxy for soil moisture, for example, Mueller et al. (2012) and Hirschi et al. (2014) who all use 3-month SPI in their comparison with hot days. Results are also in agreement with studies by Hallack-Alegria et al. (2012) and Jung et al. (2012) that indicate that a 3-month SPI best correlates to soil moisture.

Table 4.1: Correlation coefficients between SPI and soil moisture at various temporal scales, averaged across multiple *in situ* sites.

Length	OzNet	CosmOz	OzFlux	Overall
7-Day	0.618	0.555	0.547	0.573
14-Day	0.646	0.577	0.561	0.595
30-Day	0.611	0.567	0.545	0.574
60-Day	0.559	0.584	0.521	0.554
1-Month	0.417	0.329	0.321	0.356
3-Month	0.479	0.422	0.288	0.396
6-Month	0.462	0.437	0.084	0.328
12-Month	0.357	0.384	0.266	0.336

4.3 Results

4.3.1 OzNet, CosmOz and OzFlux *in situ* Sites

KBDI (Keetch-Byram Drought Index), MSDI (Mount's Soil Dryness Index), API (Antecedent Precipitation Index) and SPI (Standardized Precipitation Index) derived from 5km resolution AWAP precipitation data as well as AWAP's soil moisture data between 2000 and 2015 were compared against *in situ* soil moisture from 64 sites from the OzNet, CosmOz and OzFlux networks (full details regarding sites is provided in Table 3.1). Table 4.3 displays a full list of the Pearson correlation coefficient, the RMSE, the bias, the temporal period, and the number of observations used for each of the *in situ* sites. As it is difficult to compare sites, networks and the index used in this format, Taylor plots (Figure 4.2) were produced for both daily and monthly data. This displays the correlation statistics for each *in situ* site graphically.

Shown in Figure 4.2, there is a large variation between the correlation statistics across *in situ* sites, however, indices at each site generally fall within two normalised standard deviations of the reference. On average API best correlates to the observed daily (monthly) soil moisture with a coefficient of 0.72 (0.78) compared to 0.69 (0.68), 0.60 (0.72), 0.59 (0.78) and 0.46 (0.40) for MSDI, s0, KBDI and SPI, respectively (Table 4.2). Correlation coefficients are typically higher for monthly data than daily data. This is to be expected as daily variations and the effects of soil moisture memory are minimised over this scale and is evident in results by the lower observed RMSE and biases. On average KBDI shows a large bias towards wet conditions as does MSDI and SPI, albeit both to a lesser degree. Conversely, s0 tends towards drier conditions with API having either minimal or a slight dry bias to observed soil moisture. When comparing monthly and daily results, there is a reversal of the bias for MSDI, SPI and s0 (Table 4.2). SPI used in this analysis is based on a soil moisture memory from the preceding 14-days precipitation for daily data and for monthly SPI, it is based on the preceding 3-months precipitation. As mentioned previously, SPI is typically calculated using a memory of 3-months (the temporal period associated with hydrological droughts) when comparing to soil moisture and is usually calculated only on the monthly scale. However, for the purpose of this study, 14-day daily data has also been produced in order to determine if SPI can be computed at the daily scale and compared with other daily precipitation-based indices. Both KBDI and MSDI intrinsically include a soil moisture memory component as does API as discussed in Chapters 2 and 3. This partially explains the difference in the observed bias. Each of KBDI, MSDI, and SPI overestimate soil moisture compared to s0 and API. API tends to have a far smaller bias and a more direct relationship to any given day's precipitation, owing to a smaller soil moisture memory than the other indices.

Generally, there is a much higher correlation for each index for the OzNet sites compared to the CosmOz and OzFlux sites, this is mostly due to the fact that the temporal coverage of the OzFlux and CosmOz sites are very limited, usually, only 1 to 5 years compared to up 15 years for OzNet sites. On average for each index, there is also a larger bias and RMSE for OzFlux and CosmOz sites compared to OzNet sites. This difference is considerably less when comparing the correlation coefficients for anomalous data. As the soil moisture anomaly was calculated using the difference from a sliding 31-day mean ($\pm 15\,days$), the effect of a limited temporal coverage is somewhat negated. Again API correlates best to *in situ* soil moisture, however, each of the other indices shows improved correlation coefficients. Several sites appear to have anomalously low correlation coefficients predominately within the OzFlux sites including Cow Bay, Norwin, Cumberland Plain and Calperum. For instance, Cow Bay is located in a rainforest, in which the soil moisture is observed below a deep vegetation mat. This may contribute to the lower average correlation coefficients and also differences in bias and RMSE seen between networks. However, differences in measurement depth, soil type and metrics, and climate regimes are also expected to contribute to observed differences. These are further examined in the following sections.

Table 4.2: Correlation statistics between observational soil moisture and indices/models at CosmOz, zFlux, OzNet *in situ* sites for both daily and monthly data.

		KBDI		**MSDI**		**API**		**SPI**		**AWAP-s0**		**AWAP-ss**		**ESA CCI**	
		Daily	Monthly	Daily	Monthly	Daily	Monthly	Daily	Monthly	Daily	Monthly	Daily	Monthly	Daily	Monthly
CosmOz	Correlation	0.68	0.75	0.74	0.81	0.73	0.80	0.37	0.43	0.64	0.72	0.75	0.84	0.72	0.64
	RMSE	0.44	0.43	0.28	0.26	0.20	0.15	0.26	0.39	0.22	0.20	0.24	0.22	0.16	0.13
	BIAS	0.38	0.39	0.18	0.18	-0.02	-0.02	0.19	0.30	-0.17	-0.16	0.07	0.07	0.08	0.07
OzFlux	Correlation	0.62	0.68	0.71	0.75	0.70	0.74	0.36	0.32	0.60	0.68	0.67	0.73	0.60	0.58
	RMSE	0.35	0.34	0.27	0.24	0.24	0.20	0.29	0.29	0.29	0.27	0.26	0.25	0.23	0.19
	BIAS	0.25	0.25	0.11	0.11	-0.08	-0.08	0.14	0.06	-0.22	-0.21	0.02	0.02	0.01	-0.01
OzNet	Correlation	0.58	0.62	0.73	0.77	0.79	0.82	0.51	0.41	0.70	0.77	0.74	0.80	0.75	0.67
	RMSE	0.33	0.31	0.21	0.19	0.20	0.18	0.26	0.36	0.28	0.26	0.21	0.18	0.17	0.14
	BIAS	0.21	0.22	0.05	0.05	-0.12	-0.11	0.16	0.26	-0.20	-0.21	-0.04	-0.09	-0.04	-0.04

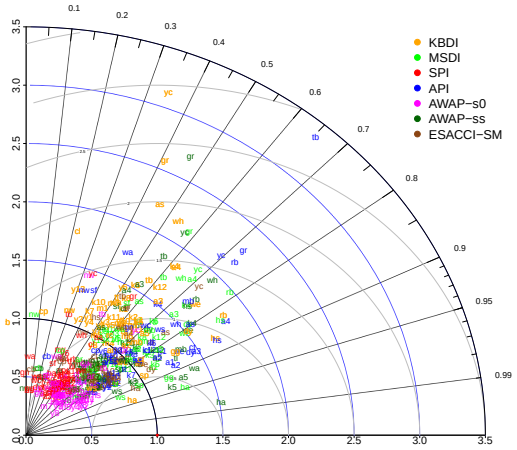

(a) DailyUpper Soil Moisture [Varied 0-20 cm]

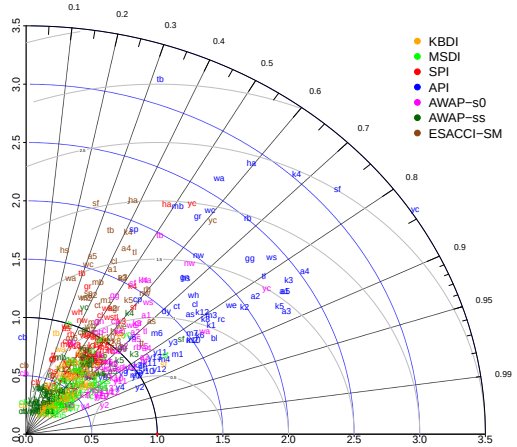

(b) Daily Upper Soil Moisture Anomaly [Varied 0-20 cm]

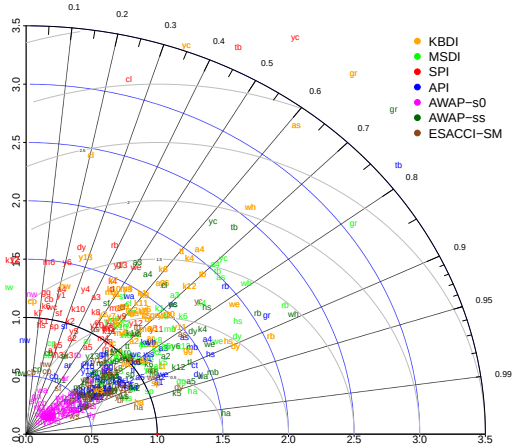

(c) Monthly Upper Soil Moisture [Varied 0-20 cm]

Figure 4.2: Taylor plots of correlation coefficients between daily SPI API, MSDI, KBDI as well as AWAP soil moisture with *in situ* soil moisture data from OzNet, CosmOz and OzFlux sites between 2000 and 2015. (a) normalised daily soil moisture. (b) normalised daily anomalous soil moisture. (c) normalised monthly soil moisture.

Table 4.3: Summary of correlation, RMSE, Bias, as well as the number of observations used and the temporal period of data used, for *in situ* soil moisture against each soil moisture indices (KBDI, MSDI, API, SPI , AWAP s0, AWAP ss and ESA CCI soil moisture). Data have been normalised between 0 - 1 for direct comparison.

Site	Correlation							RMSE							Bias							Period	Obs
	KBDI	MSDI	API	SPI	s0	ss	ESA	KBDI	MSDI	API	SPI	s0	ss	ESA	KBDI	MSDI	API	SPI	s0	ss	ESA		
Murrumbidgee_1	0.47	0.57	0.67	0.57	0.48	0.51	0.63	0.37	0.22	0.28	0.19	0.37	0.36	0.18	0.26	-0.03	-0.22	0.06	-0.32	-0.30	-0.00	14/09/01 - 31/05/11	3579
Murrumbidgee_2	0.60	0.68	0.74	0.54	0.52	0.75	0.56	0.37	0.19	0.23	0.20	0.33	0.18	0.19	0.30	-0.00	-0.17	0.07	-0.27	-0.08	-0.01	14/09/01 - 31/05/11	3579
Murrumbidgee_3	0.51	0.61	0.75	0.48	0.57	0.67	0.63	0.39	0.23	0.21	0.26	0.32	0.22	0.19	0.29	0.06	-0.14	0.17	-0.25	-0.14	-0.07	15/09/01 - 31/05/11	3021
Murrumbidgee_4	0.62	0.78	0.79	0.62	0.66	0.78	0.78	0.27	0.18	0.27	0.25	0.35	0.24	0.22	0.13	-0.07	-0.21	0.13	-0.27	-0.17	-0.14	16/09/01 - 31/05/11	3578
Murrumbidgee_5	0.53	0.77	0.81	0.65	0.79	0.75	0.75	0.22	0.20	0.26	0.23	0.29	0.25	0.19	0.02	-0.11	-0.21	0.15	-0.23	-0.19	-0.11	28/09/01 - 28/02/11	3473
Murrumbidgee_6	0.67	0.78	0.68	0.56	0.67	0.68	0.70	0.22	0.15	0.23	0.22	0.25	0.24	0.16	0.11	-0.05	-0.16	0.12	-0.18	-0.17	-0.04	28/09/01 - 31/05/11	3565
Murrumbidgee_7	0.69	0.80	0.68	0.53	0.53	0.79	0.66	0.19	0.23	0.32	0.23	0.39	0.28	0.28	0.02	-0.15	-0.26	0.08	-0.32	-0.22	-0.20	29/09/01 - 31/05/11	3564
Yanco_1	0.43	0.67	0.79	0.52	0.83	0.60	0.80	0.26	0.16	0.19	0.30	0.20	0.21	0.15	0.12	0.03	-0.13	0.24	-0.14	-0.13	-0.07	28/12/03 - 31/05/11	2710
Yanco_2	0.38	0.64	0.84	0.54	0.88	0.61	0.74	0.29	0.18	0.20	0.27	0.21	0.23	0.18	0.15	-0.02	-0.15	0.18	-0.16	-0.14	-0.08	17/01/04 - 31/05/11	2690
Yanco_3	0.53	0.74	0.77	0.54	0.71	0.73	0.76	0.28	0.15	0.21	0.23	0.27	0.19	0.15	0.17	-0.04	-0.15	0.13	-0.21	-0.12	-0.07	29/09/01 - 31/05/11	3564
Yanco_4	0.45	0.67	0.83	0.58	0.85	0.58	0.79	0.26	0.17	0.21	0.25	0.25	0.23	0.17	0.13	-0.00	-0.17	0.17	-0.20	-0.14	-0.09	22/12/03 - 31/05/11	2716
Yanco_5	0.57	0.71	0.82	0.58	0.86	0.69	0.81	0.28	0.15	0.20	0.24	0.22	0.24	0.16	0.18	-0.02	-0.15	0.16	-0.18	-0.17	-0.09	10/12/03 - 31/05/11	2728
Yanco_6	0.51	0.64	0.64	0.39	0.67	0.67	0.71	0.27	0.16	0.17	0.32	0.17	0.15	0.13	0.16	0.08	-0.09	0.27	-0.10	-0.03	-0.01	22/12/03 - 31/05/11	2624
Yanco_7	0.52	0.69	0.79	0.56	0.81	0.69	0.80	0.27	0.18	0.24	0.26	0.26	0.24	0.18	0.10	-0.02	-0.18	0.16	-0.20	-0.16	-0.10	18/12/03 - 31/05/11	2627
Yanco_8	0.55	0.67	0.81	0.59	0.78	0.73	0.80	0.32	0.21	0.22	0.28	0.31	0.28	0.20	0.18	-0.00	-0.14	0.16	-0.21	-0.17	-0.08	12/12/03 - 31/05/11	2633
Yanco_9	0.52	0.68	0.79	0.55	0.81	0.63	0.80	0.27	0.20	0.28	0.24	0.28	0.26	0.21	0.04	-0.07	-0.23	0.11	-0.23	-0.18	-0.14	18/12/03 - 31/05/11	2627
Yanco_10	0.61	0.71	0.80	0.56	0.81	0.67	0.79	0.28	0.16	0.17	0.26	0.21	0.21	0.13	0.18	0.02	-0.11	0.20	-0.15	-0.14	-0.02	10/01/04 - 31/05/11	2604
Yanco_11	0.68	0.78	0.81	0.60	0.84	0.66	0.83	0.27	0.16	0.14	0.35	0.16	0.18	0.12	0.18	0.08	-0.07	0.30	-0.09	-0.08	0.03	09/01/04 - 31/05/11	2605
Yanco_12	0.63	0.74	0.84	0.59	0.81	0.72	0.83	0.26	0.15	0.17	0.29	0.21	0.19	0.12	0.15	0.01	-0.12	0.23	-0.16	-0.12	-0.02	12/12/03 - 31/05/11	2633
Yanco_13	0.31	0.56	0.72	0.49	0.74	0.56	0.68	0.22	0.20	0.24	0.22	0.27	0.27	0.19	-0.01	-0.10	-0.19	0.13	-0.22	-0.21	-0.11	12/12/03 - 31/05/11	2633
Kyeamba_1	0.57	0.66	0.82	0.48	0.61	0.75	0.69	0.40	0.28	0.18	0.25	0.33	0.18	0.18	0.31	0.16	-0.07	0.15	-0.26	-0.05	-0.05	16/11/01 - 31/05/11	3516
Kyeamba_2	0.63	0.79	0.80	0.45	0.56	0.88	0.78	0.39	0.21	0.18	0.28	0.31	0.15	0.15	0.31	0.12	-0.09	0.18	-0.23	-0.10	-0.01	17/11/01 - 28/02/11	3423
Kyeamba_3	0.66	0.81	0.74	0.41	0.49	0.87	0.76	0.40	0.23	0.19	0.29	0.30	0.14	0.16	0.32	0.15	-0.07	0.19	-0.22	-0.08	0.01	17/11/01 - 31/05/11	3515
Kyeamba_4	0.62	0.74	0.67	0.41	0.49	0.80	0.70	0.44	0.27	0.20	0.27	0.24	0.17	0.15	0.36	0.19	-0.04	0.21	-0.18	0.00	0.04	16/11/01 - 31/05/11	3516
Kyeamba_5	0.66	0.85	0.80	0.47	0.60	0.94	0.81	0.38	0.19	0.17	0.28	0.29	0.11	0.14	0.29	0.12	-0.08	0.17	-0.21	-0.04	-0.01	15/11/01 - 28/02/11	3425
Kyeamba_6	0.54	0.71	0.77	0.44	0.58	0.78	0.74	0.46	0.25	0.15	0.31	0.24	0.13	0.15	0.39	0.18	-0.03	0.25	-0.17	-0.03	0.05	06/11/03 - 31/05/11	2762
Kyeamba_7	0.42	0.57	0.84	0.49	0.70	0.68	0.72	0.45	0.28	0.17	0.29	0.31	0.21	0.18	0.33	0.14	-0.09	0.17	-0.23	-0.08	0.02	06/11/03 - 31/05/11	2762
Kyeamba_8	0.55	0.73	0.76	0.53	0.63	0.81	0.74	0.45	0.25	0.14	0.34	0.20	0.13	0.18	0.38	0.19	-0.01	0.29	-0.11	0.02	0.10	06/11/03 - 31/05/11	2577
Kyeamba_10	0.44	0.63	0.69	0.34	0.58	0.70	0.75	0.39	0.21	0.22	0.28	0.30	0.20	0.16	0.27	0.07	-0.13	0.16	-0.22	-0.09	0.02	07/12/03 - 31/05/11	2546
Kyeamba_11	0.55	0.80	0.78	0.37	0.67	0.78	0.83	0.31	0.15	0.20	0.29	0.28	0.22	0.13	0.20	0.01	-0.13	0.19	-0.21	-0.15	-0.02	07/11/03 - 31/08/09	2123
Kyeamba_12	0.63	0.77	0.79	0.55	0.69	0.81	0.71	0.40	0.21	0.13	0.33	0.18	0.12	0.16	0.33	0.15	-0.03	0.30	-0.12	-0.00	0.08	06/11/03 - 31/05/11	2762
Adelong_1	0.81	0.86	0.87	0.38	0.53	0.65	0.73	0.34	0.26	0.18	0.27	0.37	0.23	0.19	0.29	0.20	0.00	0.06	-0.27	0.02	-0.03	02/12/01 - 31/05/11	3500
Adelong_2	0.70	0.75	0.89	0.44	0.59	0.83	0.71	0.38	0.32	0.19	0.27	0.35	0.22	0.20	0.30	0.23	0.03	0.08	-0.26	0.10	-0.02	02/12/01 - 31/05/11	2018
Adelong_3	0.66	0.73	0.87	0.46	0.68	0.55	0.74	0.27	0.22	0.26	0.20	0.41	0.28	0.21	0.13	-0.01	-0.20	-0.05	-0.38	-0.09	-0.15	02/12/01 - 31/05/11	3220
Adelong_4	0.62	0.69	0.84	0.47	0.69	0.52	0.67	0.45	0.35	0.20	0.23	0.19	0.23	0.18	0.37	0.25	0.04	0.17	-0.14	0.01	0.08	02/12/01 - 31/05/11	3591
Adelong_5	0.72	0.81	0.83	0.40	0.61	0.92	0.70	0.36	0.24	0.18	0.26	0.31	0.14	0.19	0.27	0.15	-0.05	0.11	-0.22	0.05	0.03	26/11/01 - 28/02/11	3229
Baldry	0.64	0.84	0.74	0.51	0.65	0.80	0.81	0.44	0.11	0.19	0.28	0.24	0.19	0.12	0.39	0.00	-0.12	0.21	-0.19	-0.15	0.00	30/03/11 - 13/03/14	1078
Tumbarumba	0.58	0.61	0.65	0.30	0.49	0.56	0.53	0.55	0.51	0.39	0.17	0.24	0.42	0.16	0.53	0.49	0.25	0.11	-0.21	0.39	0.10	03/04/11 - 22/12/15	1492
Weany	0.76	0.81	0.85	0.61	0.79	0.81	0.83	0.34	0.18	0.14	0.28	0.18	0.16	0.12	0.27	0.08	-0.07	0.24	-0.14	0.00	0.06	02/12/10 - 22/12/15	1846
Robson	0.83	0.79	0.73	0.49	0.72	0.74	0.76	0.23	0.28	0.26	0.17	0.28	0.30	0.13	0.13	0.18	-0.05	0.09	-0.26	0.23	0.03	28/10/10 - 22/12/15	1881
Daly	0.81	0.79	0.87	0.21	0.86	0.72	0.86	0.21	0.22	0.15	0.23	0.16	0.19	0.16	0.10	0.10	-0.00	0.08	-0.11	0.06	0.11	07/06/11 - 22/12/15	1637
Norwin	0.30	0.06	0.34	0.34	0.33	-0.02	0.44	0.33	0.27	0.33	0.17	0.28	0.41	0.20	0.26	-0.17	-0.26	0.06	-0.16	-0.37	-0.11	12/05/11 - 25/06/13	758
Hamilton	0.94	0.95	0.80	0.35	0.62	0.98	0.90	0.55	0.35	0.15	0.24	0.26	0.25	0.14	0.55	0.34	-0.06	0.15	-0.20	0.22	0.11	01/07/15 - 22/12/15	175
Tullochgorum	0.60	0.71	0.77	0.45	0.49	0.87	0.62	0.59	0.35	0.15	0.30	0.23	0.16	0.26	0.55	0.30	0.02	0.25	-0.16	0.10	0.21	15/12/10 - 22/12/15	1833
Mineral_Banks	0.73	0.72	0.73	0.19	0.47	0.85	0.55	0.45	0.36	0.21	0.24	0.34	0.24	0.18	0.42	0.33	0.01	0.16	-0.31	0.20	0.09	06/12/13 - 22/12/15	739
Griffith	0.41	0.58	0.73	0.57	0.72	0.47	0.58	0.56	0.22	0.15	0.37	0.08	0.23	0.14	0.52	0.16	0.00	0.36	-0.05	0.10	0.10	01/10/11 - 09/05/13	541
Yanco_Cosmoz	0.35	0.68	0.70	0.35	0.69	0.57	0.72	0.51	0.19	0.13	0.33	0.08	0.14	0.20	0.46	0.15	0.00	0.31	-0.03	0.01	0.17	01/04/11 - 22/12/15	1726
Alice_Springs_Mulga	0.46	0.60	0.80	0.55	0.78	0.53	0.77	0.46	0.20	0.13	0.30	0.09	0.14	0.16	0.39	0.13	0.01	0.28	-0.05	0.04	0.11	03/09/10 - 01/08/14	1428
Arcturus	0.66	0.53	0.70	0.66	0.71	0.42	0.67	0.30	0.21	0.26	0.20	0.26	0.31	0.19	0.23	-0.06	-0.20	0.08	-0.20	-0.23	-0.07	01/01/11 - 01/01/14	1096
Calperum	0.22	0.57	0.78	0.54	0.62	0.56	0.57	0.29	0.13	0.12	0.29	0.14	0.12	0.19	0.23	0.07	-0.08	0.27	-0.10	0.01	0.12	01/08/10 - 21/10/15	1907
Cape_tribulation	0.80	0.76	0.86	0.51	0.79	0.66	0.61	0.29	0.38	0.22	0.24	0.29	0.45	0.22	0.24	0.34	0.09	0.09	-0.24	0.40	0.02	01/01/10 - 03/09/15	2071
Cow_Bay	-0.16	0.15	0.23	0.30	0.22	0.18	0.07	0.36	0.39	0.48	0.27	0.49	0.48	0.38	0.00	-0.28	-0.39	-0.11	-0.42	-0.38	-0.25	01/01/09 - 12/05/15	2322
Cumberland_Plain	0.13	0.35	0.59	0.45	0.60	0.24	0.40	0.43	0.23	0.18	0.37	0.18	0.22	0.25	0.30	0.07	-0.01	0.31	0.02	-0.04	0.15	19/10/12 - 31/10/15	1108
Howard_Springs	0.87	0.83	0.87	0.06	0.84	0.74	0.47	0.19	0.25	0.20	0.23	0.23	0.25	0.28	0.02	0.11	-0.04	0.05	-0.20	0.08	0.16	01/01/01 - 03/09/15	5356
Riggs_Creek	0.60	0.75	0.69	0.30	0.53	0.74	0.74	0.49	0.26	0.21	0.29	0.28	0.19	0.17	0.43	0.19	-0.10	0.16	-0.19	-0.07	0.01	18/12/10 - 06/07/15	1661
Samford	0.61	0.56	0.38	0.32	0.28	0.53	0.36	0.22	0.29	0.46	0.25	0.55	0.28	0.28	-0.01	-0.15	-0.35	-0.12	-0.51	-0.12	-0.18	01/01/10 - 22/12/15	2181
Sturt_Plains	0.87	0.90	0.73	0.49	0.75	0.79	0.77	0.15	0.17	0.28	0.27	0.34	0.23	0.21	0.01	-0.11	-0.19	0.06	-0.26	-0.14	-0.10	01/01/08 - 01/01/15	2556
Ti_Tree_East	0.51	0.64	0.80	0.47	0.74	0.59	0.76	0.21	0.12	0.13	0.23	0.16	0.14	0.11	0.09	-0.01	-0.09	0.18	-0.12	-0.07	-0.03	01/01/13 - 01/08/14	578
Wallaby_Creek	0.76	0.78	0.70	0.17	0.41	0.76	0.66	0.39	0.34	0.24	0.26	0.44	0.30	0.24	0.35	0.30	0.02	0.05	-0.38	0.25	-0.14	01/01/09 - 01/01/14	1826
Warra	0.52	0.62	0.44	0.05	0.33	0.91	0.38	0.64	0.57	0.35	0.38	0.22	0.38	0.29	0.62	0.55	0.23	0.31	-0.12	0.38	0.23	05/03/13 - 17/02/15	715
Whroo	0.53	0.66	0.77	0.44	0.61	0.73	0.62	0.58	0.32	0.14	0.37	0.11	0.28	0.22	0.53	0.27	0.06	0.35	-0.02	0.21	0.18	01/01/12 - 03/09/15	1341
Wombat_State_Forest	0.78	0.91	0.75	0.16	0.43	0.88	0.69	0.38	0.26	0.23	0.26	0.47	0.23	0.25	0.35	0.24	-0.07	-0.01	-0.42	0.20	-0.17	01/01/10 - 01/01/13	1096

4.3.2 Comparison at Various Layer Depths

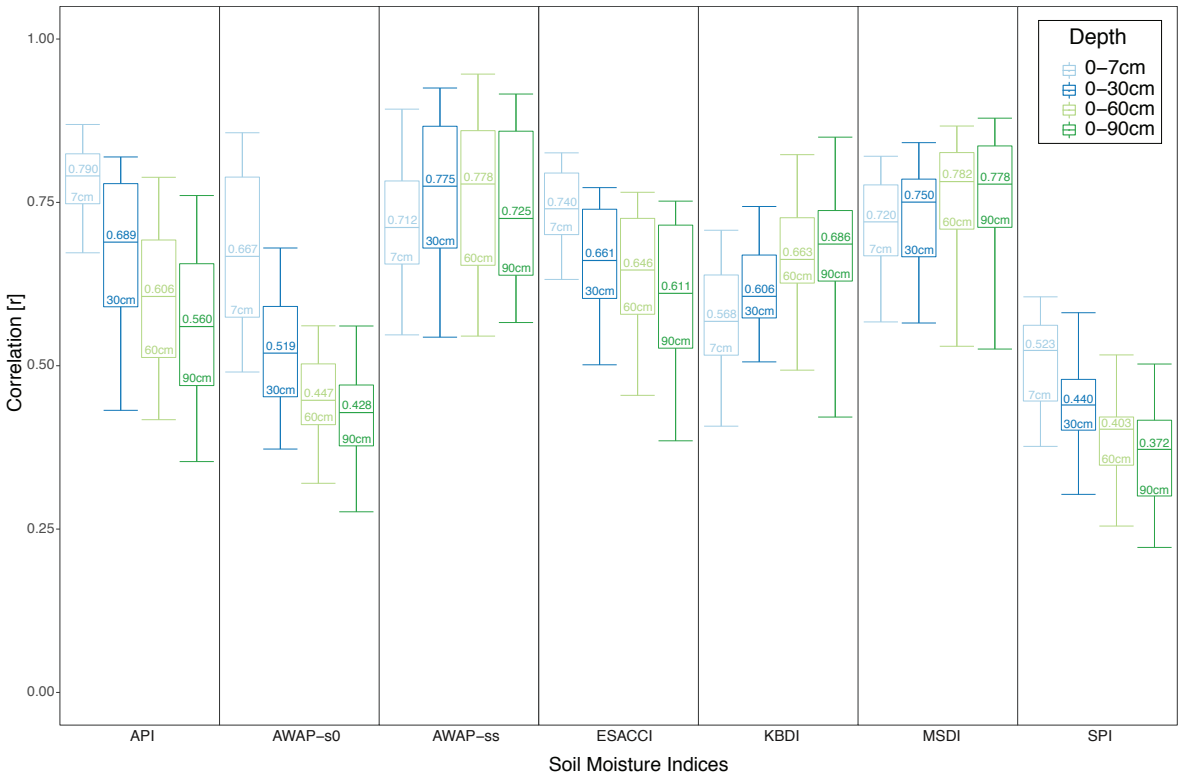

Figure 4.3: Box plots of correlation coefficients between daily SPI API, MSDI as well as KBDI with *in situ* soil moisture data at various measurement depths from OzNet sites between 2000 and 2015.

As discussed in the previous section and in Chapter 2, each index represents soil moisture at different soil layer depths. In order to compare the strength of the relationship between these indices and *in situ* soil moisture, correlation coefficients were compared at four depths, 0-7 cm, 0-30 cm, 0-60 cm and 0-90 cm. These depths were chosen as they are common for all OzNet sites, with other networks having either various measurement depths or just the surface soil moisture available. These depths represent the weighted averages from the corresponding sum of individual soil layers. Figure 4.3 presents box plots of daily correlation coefficients between the *in situ* soil moisture and each product separated by soil layer and the product itself. As previously stated, API and MSDI have the largest values on average for all sites at the surface layer as does ss, with SPI performing particularly weakly. Most strikingly, each of API, SPI, and s0 have a large decrease in correlation coefficients with deeper soil layers. Conversely, values for KBDI, MSDI, and ss show a marginal increase for larger depths, in particular, KBDI which appears much better suited at 0-90 cm. This is largely due to the calculation of each index. API and SPI are purely precipitation based whereas KBDI and MSDI represent evapotranspiration within their water balance models allowing for a better representation of soil moisture beyond the surface layer. For each index, as the layer depth increases the

variance in the values between sites increases substantially. A possible reason for this is the difference in the infiltration rate between soil layers (horizons) at the various sites. It would be expected that for each index, correlation coefficients decrease with increasing soil depth due to the fact that they are calculated based on precipitation data or models which generally only consider the surface layer, however, this would not account for the difference seen.

4.3.3 Gridded Comparison of AWAP Derived Indices versus ESA CCI Soil Moisture

To further compare each moisture index, the indices were computed for Australia at a resolution of 5 km between 1979-2015 using AWAP precipitation, temperature, and other variables. In order to compare against an independent reference soil moisture, the ESA CCI combined remotely sensed soil moisture product was used. As this product is available at a resolution of 25 km between 1979-2015, the AWAP derived moisture indices were up-scaled to match this resolution and are used for the remainder of this section.

Prior to comparing the Pearson correlation coefficients between indices, Hovmöller diagrams were produced. These visually present the one-dimensional spatial variation in soil moisture over a given period of time. This can be computed over either latitudes (Refer to appendix; Figure B.1) or longitudes (Figure 4.4), providing detail in each coordinate plane. For ease of comparison, the standard deviation from the mean soil moisture was produced for each index with negative values represent dry anomalies and conversely, positive values, wet anomalies. Anomalies were calculated for the entire time series, but for graphical purposes, the period 2010-2015 was used as it spans the most current known wet and dry periods. Inter-seasonal periods of wet and dry conditions are reflected in Figures 4.4 & B.1. Both figures indicate the typical seasonal variability between 2012-2015 with a distinct wetter period in the two years prior. This is particularly noticeable with KBDI which appears to have less temporal variation than each other index as well as the ESA CCI soil moisture product. SPI and API appear to best reflect anomalies seen in ESA CCI soil moisture over both latitudes and longitudes, however, API shows more extreme wet anomalies in higher latitudes and across longitudes. Likewise, AWAP derived soil moisture appears to have more extreme wet and dry anomalies compared to the ESA CCI soil moisture.

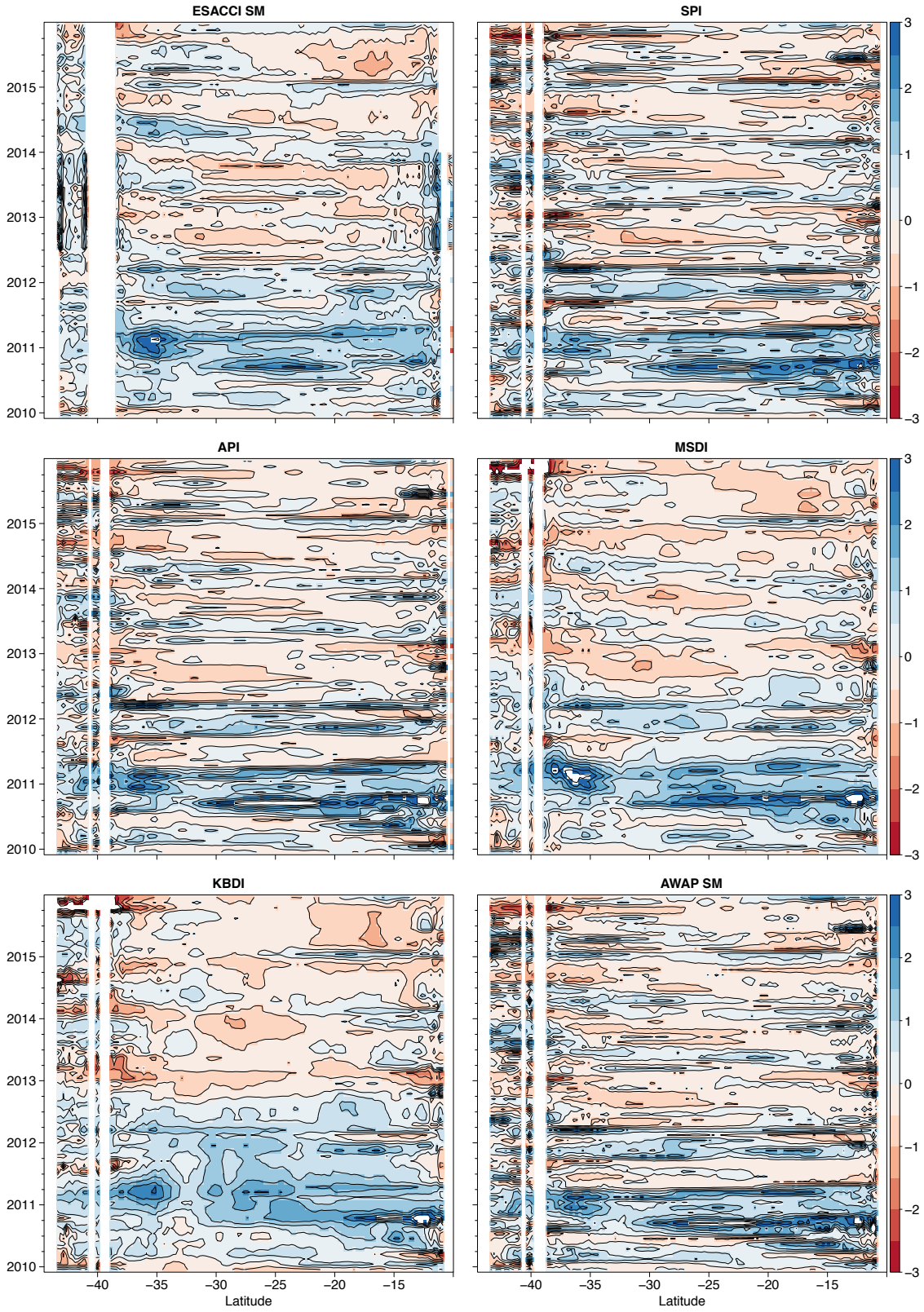

Figure 4.4: Time-longitude Hovmöller diagrams of anomalous monthly soil moisture (compared to the 1979-2015 climatological mean) for each moisture index averaged between $112°E$ and $156.25°E$ longitudes during the 2010-2015 period.

These results are reflected in Figure 4.5, which displays the correlation coefficients of

the normalised soil moisture, the normalised anomalous soil moisture, the RMSE, and the bias for each index compared to the ESA CCI soil moisture product. Again, KBDI appears to have vastly different values over central Australia, with coefficients typically between 0.2 and 0.5. Also, the RMSE and bias are the largest of all the indices in these regions due to the lack of precipitation. To maintain consistency, any regions with a mean annual precipitation of less than 1 mm have been masked out. It appears that correlation coefficients around the masked regions are heavily influenced by the reduced density of observational data and precipitation data was interpolated near the edges. Similarly, the Nullarbor plains typically have very little precipitation and consequently, correlation coefficients are lower on average than other regions of Australia as well as larger RMSE and biases in this region. Regions such as the tropical north and alpine south-east Australia, that have a far greater variability in maximum and minimum precipitation, however, they show the largest correlation coefficients and lowest RMSE and biases. This is to be expected, as there are a larger number of "dry-down" periods, where the dynamical range and behaviour can be better represented by products. Due to this, there is a higher correlation among these regions. These "dry-down" periods are represented in the patterns seen in the Hovmöller diagrams for each index.

Average correlation coefficients, the number of observations and the adjusted alpha significance level are inset to each plot of Figure 4.5. Correlation coefficients on average are between 0.483 and 0.611 for daily normalised data and considerably lower, ranging between 0.325 and 0.592 for anomalies. Similarly as with Section 4.3.1, API has the largest correlations along with MSDI. Surprisingly, AWAP derived soil moisture has very high values for both normalised daily and for anomalies. This is due to the relatively low RMSE and biases compared to the other products, and maybe a result of corrections to the hydrological model used for its computation in low-precipitation regions.

These results are similarly reflected for monthly data as shown in Figure 4.6. As in Section 4.3.1, monthly correlation coefficients are consistently higher on average than daily values, which, as suggested, is a result of a "smoothing" of the daily variation in soil moisture. Correlation coefficients are between 0.659 and 0.739 for normalised monthly data and between 0.455 and 0.648 for monthly anomalies. Monthly API and AWAP soil moisture perform are consistent with values seen for daily data, however, MSDI and KBDI show clear improvements in the overall correlation coefficients, particularly for KBDI, which performed the worst over the daily domain. The spatial variation is relatively consistent between daily and monthly values with the weakest correlations again, in central Australia.

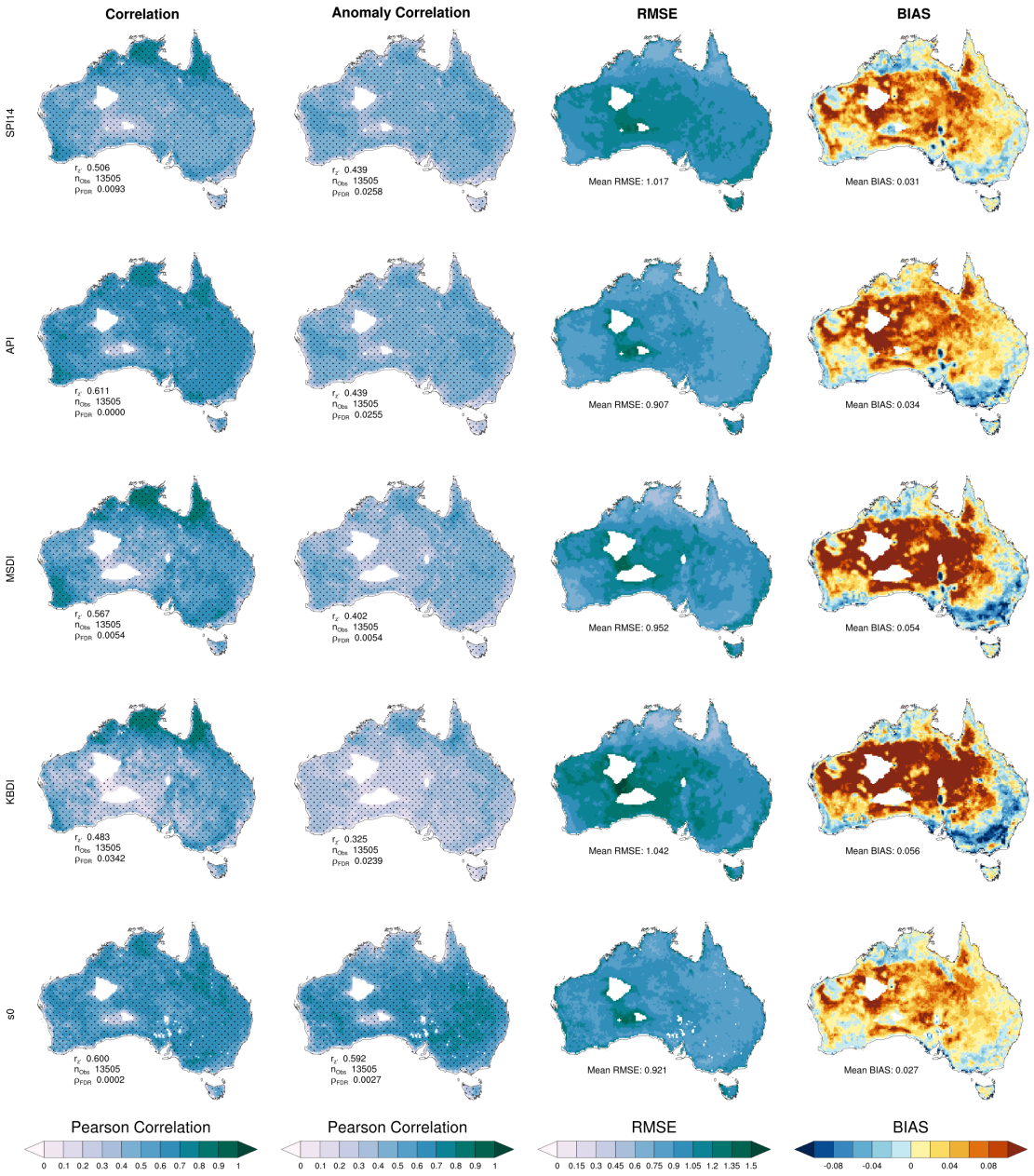

Figure 4.5: Correlation, anomaly correlation, bias and RMSE of daily soil moisture for each index compared to ESA CCI soil moisture. Data are standardised and values are calculated for the period, 1979-2015. Stippling is indicated for significant correlation coefficients using the False Discovery Rate transformation (level is denoted as ρFDR). Also shown are the mean correlation coefficients across Australia using the Fisher-Z transformation ($r_{z'}$) and the number of observations (n_{Obs}) used for calculations.

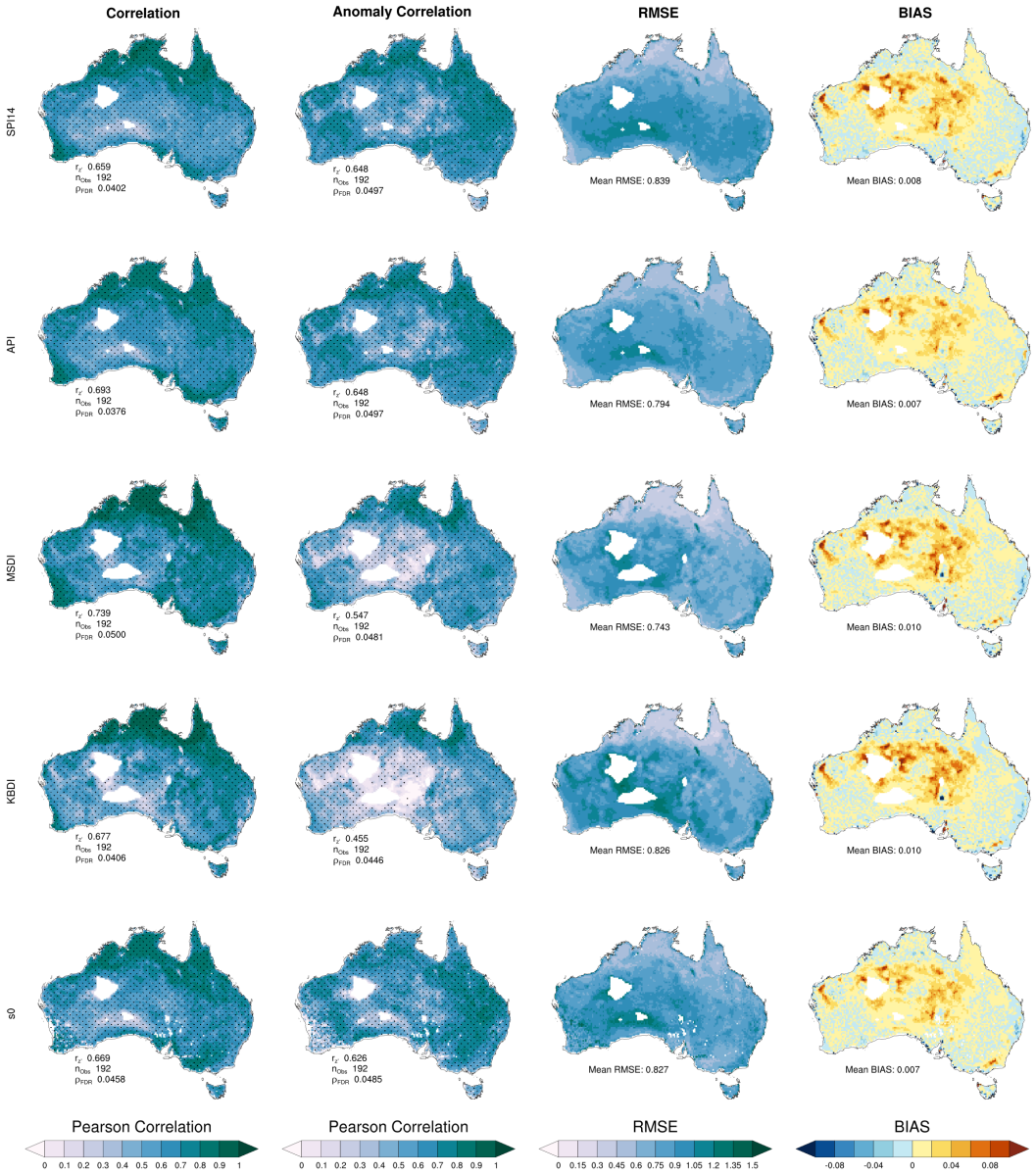

Figure 4.6: Correlation, anomaly correlation, bias and RMSE of monthly soil moisture for each index compared to ESA CCI soil moisture. Data are standardised and values are calculated for the period, 1979-2015. Stippling is indicated for significant correlation coefficients using the False Discovery Rate transformation (level is denoted as ρFDR). Also shown are the mean correlation coefficients across Australia using the Fisher-Z transformation ($r_{z'}$) and the number of observations (n_{Obs}) used for calculations.

4.3.4 Gridded Comparison of Correlation Coefficients and Soil Properties

As suggested in Section 4.3.2, the influence that various soil properties and climate regimes have on the relationship between soil moisture and precipitation-driven moisture indices is investigated here. As done previously, the dominant soil type was extracted from the ASRIS product and rescaled to 25 km resolution to match the ESA CCI soil moisture product. The gridded data allows for the comparison of the full gamut of soil types (12) rather than the three types that were previously used, now ranging from sands and silts to loams and clays. Also as before, the Köppen-Geiger climate regions are defined using the five dominant regimes: savanna, tropical, arid, semi-arid and temperate. Finally, porosity, vegetation optical depth, and topographic complexity are also compared. Each of these variables are included in the ESA CCI product and are used to interpret spatial differences in the soil moisture therein. The porosity is a measure of the space between the soil material as a fraction of the total volume, given as a percentage; the vegetation optical depth (VOD) is proportional to the vegetation water content of the above-ground biomass and is generally used as a proxy for biomass content given as a fraction between 0-1; lastly the topographic complexity is defined as the normalised standard deviation of elevation within a grid cell.

Figure 4.7 presents bivariate choropleth maps with the correlation coefficient between ESA CCI soil moisture and moisture indices on the y-axis and the VOD, topographic complexity, climate regimes, and soil properties on the x-axis. Each set of maps has independent legends with colours chosen to best reflect the spatial variation seen, with the exception of the Kööppen-Geiger climate comparison which uses the previously defined colours set for each regime. From the soil types, it is clear that the dominant soil types throughout Australia are sands and loamy soils with only small regions in north-western Queensland and south-east Australia with a higher clay content. For each soil type, as the correlation approaches a minimum, the colour fades to white. As previously, we see that the lowest correlations are in the central Australia region and portions of South Australia and far Western Australia. These regions generally have sandy or silty soils which are very coarse, but, this is not necessarily the case throughout Australia. The Margaret River region of south-west Western Australia generally has silty/sandy soils as does tropical Northern Australia and correlation coefficients are much higher in these regions, meaning that in these regions correlation coefficients are influenced by other mechanisms, such as the dynamical range of precipitation as discussed previously.

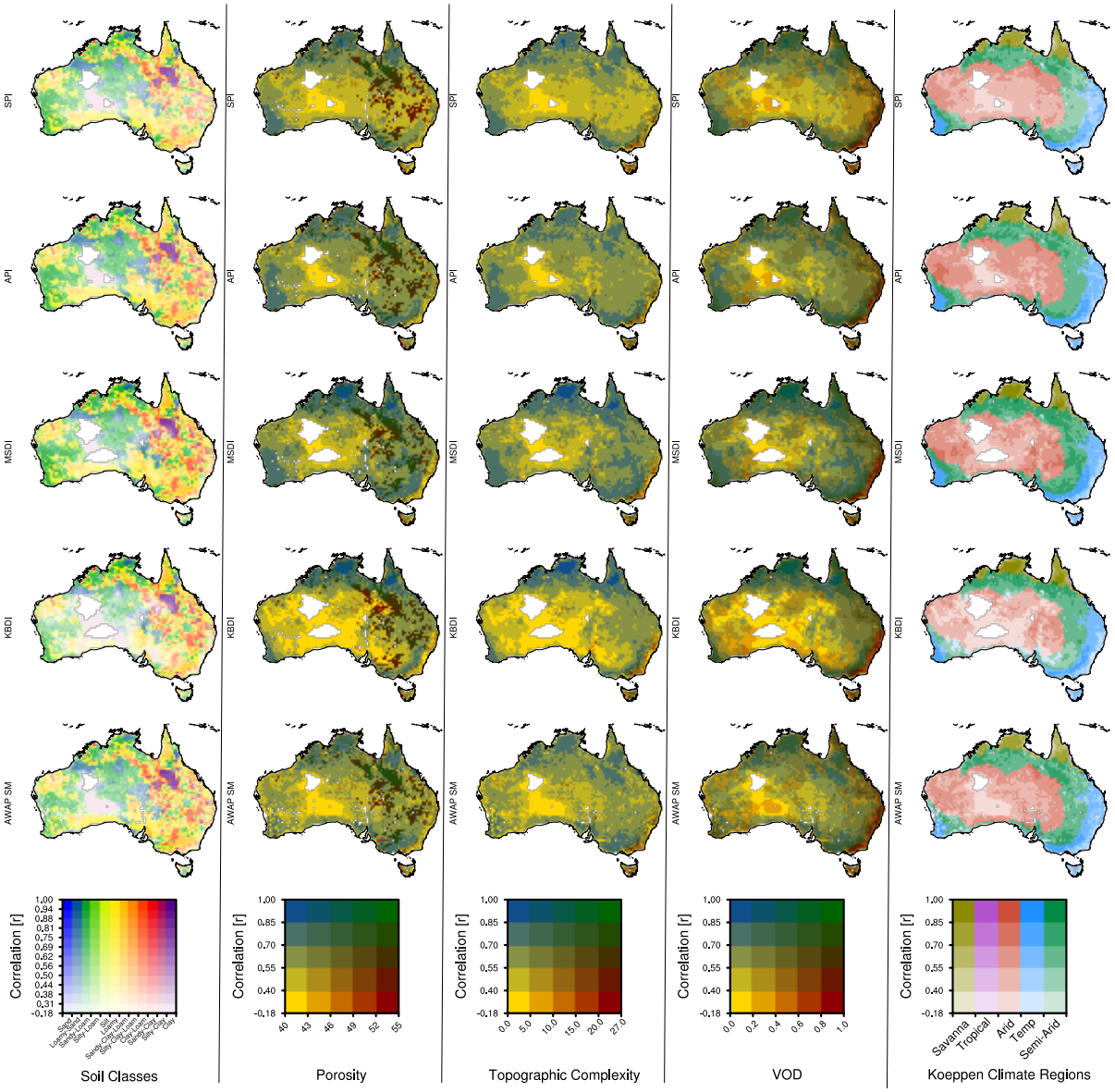

Figure 4.7: Bivariate choropleth maps of correlation coefficients between each indices (rows) and ESA CCI derived soil moisture plotted against; soil types (first column), soil porosity (second column), topographic complexity (third column), vegetation optical depth (fourth column), and Köppen-Geiger climate regimes (fifth column).

These results are similar to what is seen with the porosity which is directly related to soil type. Porosity is inversely proportional to grain size with sands representing soils with typically low porosity (Certini, 2005). Again, the least porous soil and lowest correlation coefficients are seen in central Australia, conversely, the most porous soil is located in north-eastern Australia. KBDI appears to be particularly influenced by porosity and has the largest extent of low correlations compared to the other indices, in contrast, MSDI performs best in regions that generally have low porosity. The most noticeable difference between index correlations and the porosity is in western Queensland, where there are predominately more porous clay soils seeing a large variation in the correla-

tion coefficients between indices. Large areas with predominately clay soils typically have a high correlation for AWAP s0, MSDI, and SPI, whereas, API and in particular KBDI tend to have low correlations in these regions. For all soil types and porosities, it appears that the greatest contrast in correlation coefficients occur with porous clay soils.

Topographic complexity, as well as, VOD has also been compared for Australia with the most noticeable differences across moisture indices occurring in the south-east and south-west of Australia. In the south-west of Australia, correlation coefficients for AWAP s0 appear to be far lower in regions with low topographic complexity and a low VOD. Likewise, in south-east alpine Australia where the topographic complexity is low and the VOD is high, correlation coefficients are typically higher. However, this distinctly differs on the eastward edge of the alpine region running along the coast of south-east Australia. This essentially due to the ESA CCI product performing poorly in the east of the Great Dividing Range where surface conditions (i.e. mountains, forests) hinder microwave sensors in these regions because of the topographic roughness and the high vegetation cover

Essentially, the ESA CCI SM product is not doing well east of the Great Dividing Range, because of the surface conditions (mountains, forests) - microwave sensors simply do not perform well in those regions because of the topographic roughness and the vegetation cover. I.e. the topographic complexity is far higher, coupled with a large VOD and hence correlation coefficients in this region are relatively low in comparison to other regions. These observations are most noticeable for KBDI which appears to have a large difference in the sensitivity to these variations compared to the ESA CCI product and with the other indices, as does MSDI albeit to a lesser extent.

Finally, correlation coefficients were compared for each of the Köppen-Geiger climate regions. For each moisture index, the savannas appear to have the most consistent correlation coefficients, as does the semi-arid region. In both regimes, there are few subregions to exhibit low correlations. In contrast, the temperate and arid regions appear to show the largest variation in observed values, particularly in the aforementioned regions of coastal south-east Australia and central Australia. These results are summarised in Figure 4.8, in which the Fisher-Z transformation was used to produce averages per climate region for daily and monthly data. Again, in both daily and monthly data that the savanna regions has the largest correlation coefficients with the exception of AWAP s0 with values generally between 0.7 and 0.8. The Arid region typically performs the worst over each temporal domain, particularly for KBDI, in which values are approximately a third of the savanna regime. The least variation between regimes occurs for API and AWAP s0, particularly in the daily domain.

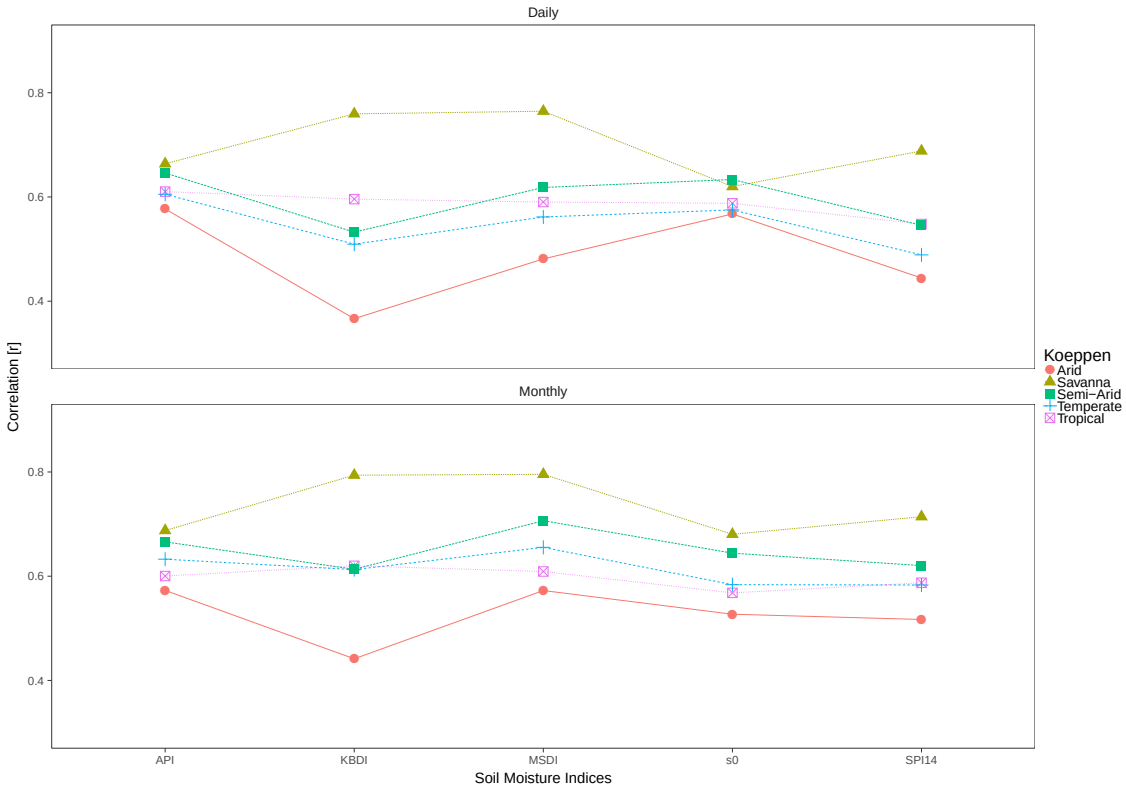

Figure 4.8: Averaged correlation coefficients of daily and monthly moisture Indices versus ESA CCI soil moisture at each major Köppen-Geiger regime. Averaged correlation coefficients are calculated using the Fisher-Z transformation ($r_{z'}$).

4.4 Discussion

The primary focus of this chapter was to compare commonly used moisture indices against *in situ* and a remotely sensed reference soil moisture in relation to differences in soil, vegetation and climate characteristics across Australia. Whilst this study shares similarities with previous studies such as Su et al. (2013), Holgate et al. (2016), and Kumar et al. (2017), this study vastly expands on this work, providing a larger number of *in situ* sites from various networks at several soil depths, gridded comparisons as well as comparing these results to spatially variable characteristics such as VOD, topographic complexity, porosity, soil type, and Köppen-Geiger climate regimes.

More so, a general caveat when comparing satellite observations and *in situ* measurements is the spatial representativeness and temporal stability of *in situ* measurements used as validation for satellite products (Brocca et al., 2009). That is, the longer the temporal period used and the number of measurements used to represent a moisture at any given location the more accurate the validation of products (Brocca et al., 2009). Therefore, this chapter analyses the difference between moisture indices and a reference soil

moisture over a longer time-range than the aforementioned studies, as well as, further extending this analysis temporally by comparing the indices to a remotely sensed reference soil moisture (which has a longer temporal record than *in situ* observations).

The ESA CCI product, used here, has been thoroughly evaluated against ground based-observations globally (Dorigo et al., 2015). Dorigo et al. (2015) found that correlation coefficients between the product and *in situ* measurements were 0.46 for the absolute values and 0.36 for the soil moisture anomalies, with biases on average around 0.04 and 0.05 m^3m^{-3}, respectively. The results presented in this chapter are in agreement with this work, across similar sites, but an increase in quality is shown at all sites with our results indicating that correlation coefficients are on average between 0.6 and 0.75. Whilst the ESA CCI product does not have a perfect agreement with *in situ* measurements of soil moisture and varies spatially, this data set has been used for comparison of gridded data due to its common use in regional and global studies and to determine the comparative spatial strengths of API, MSDI, KBDI, SPI and AWAP s0 across Australia.

The results presented in this chapter compare well with the previously mentioned studies, in particular, that of Holgate et al. (2016) which compared 11 various soil moisture products including MSDI, KBDI and API at 7 OzFlux, 2 OzNet and 4 CosmOz sites. (Holgate et al., 2016) found that for the 2001-2014 period, API performed consistently better (0.63-84) across all Australian sites although the highest correlations occurred for MSDI (0.44-0.87) with KBDI performing poorly at some sites (0.25-0.86), namely at the Yanco CosmOz site. This is similar to the results of the present study where API tends to have the highest degree of association with daily soil moisture across sites on average (0.72) with correlation coefficients between 0.23-0.89 compared to MSDI between 0.15-0.95 (0.69; average), KBDI between -0.16-0.97 (0.59; average), SPI between -0.66-0.66 (0.41; average) and between 0.22-0.88 AWAP s0 (0.60; average). Similarly, the CosmOz Yanco site showed correlations as low as 0.35, but, the Cow Bay and Norwin sites were clearly the worst performing, recording negative correlations and almost no association. The Norwin site has a limited period of data of just over two years and the Cow Bay site a rainforest site, is situated in the tropical climate with an extremely large variation in daily precipitation, which may account for the poor performances at these sites.

Similarly, Kumar et al. (2017) compared KBDI, MSDI, and API at 38 OzNet sites and at nine CosmOz sites. KBDI (0.40-0.74) and MSDI (0.42-0.76) outperformed API (0.43-0.67) across all sites in this study. As vegetation plays an important role in the control of fire activity (Forkel et al., 2017) due to the relationship between biomass production and root zone soil moisture (Werf et al., 2006). The representation of soil moisture at various depths and its subsequent relationship on the sensible heat flux at the surface (as investi-

gated in the following chapter) is particularly important. This chapter assessed the relationship between various soil moisture products at various soil depths. API had largely contrasting correlations between depths with coefficients as low as 0.43-0.58 compared to MSDI and KBDI which only slightly differed between layers. The results presented in here in this chapter are in agreement with Kumar et al. (2017) where API correlations continuously decreased through each of the four layers with averages of 0.77, 0.74, 0.48 and 0.30 for the 0-7 cm, 0-30cm, 30-60 cm and 60-90 cm layers, respectively. This compares with MSDI and KBDI which only slightly differ through each layer, indicating that they represent soil moisture at deeper layers. This is to be expected as the MSDI and KBDI models include an infiltration component within their formulation. Conversely, API and SPI and are precipitation-based models which generally only consider the surface soil layer. In the case of AWAP s0, this is a more complex hydrological model, and as expected there was a stark contrast in the relationship at various soil depths depending which of the two products were used. The surface soil moisture product generally was outperformed at each of the layers compared to the shallow layer product, most particularly at 0-30 cm, 0-60 cm and 0-100 cm. It was also found that correlations vary considerably depending on both the depth and the soil type at *in situ* sites. For instance, API performed better at deeper layers in sandy soils with a higher filtration. Conversely, the advantage of both KBDI and MSDI is lessened in clay soils which typically hold a larger content of water and lower filtration properties. This is most noticeable with KBDI, and particularly so when comparing clay soils with high porosities in Figure 4.7. Here we can see that AWAP s0, API, and SPI have larger correlations in these regions compared to both KBDI and MSDI.

In addition, KBDI shows a large wet bias across all sites for both monthly and daily data as well as for gridded data. As mentioned by Kumar et al. (2017), it is well established that KBDI indicates significantly wetter conditions than MSDI (Finkele et al., 2006). With our results, this is particularly the case in comparison to API, SPI, and AWAP s0. This difference is partly due to the drying component of the KBDI model. KBDI is computed using ET which is driven by the vegetation cover and in turn, is a function of the mean annual precipitation (Holgate et al., 2016). This is in agreement with observed differences in correlation coefficients between the climate regimes. I.e. the largest difference between correlation coefficients of KBDI occurs between the savanna and the arid regimes. KBDI and to a lesser degree MSDI perform exceptionally strongly in the savanna regime with the highest average (gridded data) correlations of in excess of 0.8 seen. Similarly, (Holgate et al., 2016) also found that for KBDI and MSDI the highest correlation coefficients occurred in grassland (savanna) regimes. However, KBDI displayed the greatest variability in this regime. (Holgate et al., 2016) also found that MSDI showed a much lower variation in the correlation between sites compared to KBDI; this is also the case for the results in

this study which found on average across all grid boxes within each climate regime that there is a far smaller variation in observed values. Again this is due to the difference in the models drying component. Where KBDI's infiltration is statically set at 5 mm regardless of vegetation cover, MSDI assigns vegetation via seven classes, each with a separate interception, canopy storage and wet evaporation rates (Finkele et al., 2006). Therefore, any variations in the correlations seen spatially and across climate regimes are also a result of other mechanisms. Similar to MSDI, AWAP-derived soil moisture uses a water balance model which dynamically considers the transpiration, evapo[transpi]ration, runoff, drainage, and precipitation. Likewise, for the savanna regime, it outperforms API and SPI and again has a far smaller variability between regimes than KBDI. Across the Australian *in situ* sites, AWAP s0 performs strongly only being outperformed by API and MSDI.

Finally, differences in the topographic complexity and the VOD have been shown to greatly affect the observed spatial variation in the correlation coefficients. VOD has been shown to be an effective proxy for estimating biomass (Tian et al., 2016) and it has been found that there are low similarities between soil moisture products in regions with both dense vegetation as well as in topographically complex terrain (Nicolai-Shaw et al., 2015). This was also suggested by Rebel et al. (2012) who suggested that accurate soil moisture estimates are limited to regions with low-to-moderate VOD (< 0.6). The results indicate that the low correlations seen for each index in coastal south-east Australia are due to a high topographic complexity and high relative VOD despite highly porous sandy-loam soils dominating.

Chapter Summary

This chapter evaluates the relationship between soil moisture indices/models and *in situ* soil moisture at both daily and at a monthly scale. It was found that API and MSDI show the largest correlation to *in situ* surface soil moisture (normalised and normalised anomaly) with the highest correlations observed in the OzNet network. Both KBDI and 14-day SPI observe a large wet bias across all sites and AWAP surface soil moisture showing a large dry bias compared to *in situ* sites. However, these results are not reflected in deeper soil moisture layers with KBDI and MSDI best representing soil moisture at 30, 60 and 90 cm compared to API, SPI, and AWAP s0. Average correlation coefficients between *in situ* sites and both KBDI and MSDI are generally consistent with varying depths indicating that these might be better suited for root zone studies. These results are consistent with the comparison of gridded products. Again, both API and MSDI outperform the other indices and models, but, spatial variations appears to be largely due to the soil and climate characteristics. From this chapter, further comparisons of the effect of these moisture indices have on both temperature and fire metrics can be interpreted in the context of the spatial variability of their relationship to soil moisture.

CHAPTER 5

Variability of Soil Moisture Proxies and Hot Days

Sections of this chapter have been published as: Holmes, A., C. Rüdiger, B. Mueller, M. Hirschi, and N. Tapper (2017). "Variability of soil moisture proxies and hot days across the climate regimes of Australia." Geophysical Research Letters 44 (14): 7265-7275.

Overview The large-scale weather dynamics of heat waves are well documented. However, studies have only recently indicated a link between soil moisture deficits and hot extremes, focusing on the strength of coupling between the two. This chapter continues on from the investigation of various soil moisture indices in Australia in the previous chapter. Here, the effect of observed soil moisture deficits on temperature extremes is investigated. In particular, this chapter investigates the relationship between hot-days (Tx90) and the various soil moisture products (i.e. the Standardized Precipitation Index, Antecedent Precipitation Index, Mount's Soil Dryness Index, and the Keetch-Byram Drought Index) previously introduced and the variation of this relationship's strength changes for the different climate regimes within Australia. It is shown that a strong negative-correlation between Tx90 and each moisture index exists, particularly for the tropical savanna and temperate regimes. However, the magnitude of the increase in Tx90 with decreasing moisture is strongest in semi-arid and arid regions of the country. In addition, it was found that the magnitude of the correlation coefficient between Tx90 and moisture is highly affected by the strength of La Niña's impact on precipitation. Linking the effects of soil moisture on precursory fire weather conditions, such as extreme temperatures, an improved understanding of how soil moisture indirectly influences fire risk is achieved.

5.1 Identification of the Transitional Zone and Energy Partitioning

5.1.1 Introduction

Drought and heat wave events are regular occurrences on a large scale in semi-arid regions of the world, such as Australia, and are predicted to further increase in their frequency and severity (Cowan et al., 2014). Much of Australia has been heavily affected by drought conditions in recent years and as such, a large stress has been placed on the allocation of water resources. Understanding the changes in the hydrological conditions and water balance in a region is essential for understanding the distribution of droughts and any ensuing forcing of extreme temperatures. Without such an understanding, potential mitigation through accurate forecasting of these extreme events cannot be reasonably achieved.

As mentioned in Chapter 2, the soil moisture of a region determines the partitioning between sensible and latent heating. Sensible heat dominating latent heat will cause a localised temperature change as a result of the direct heating at the surface. However, latent heat dominating sensible heat will result in a larger amount of evapotranspiration and a decrease in surface temperature (Seneviratne et al., 2010). Evapotranspiration in a region can be either moisture or radiation limited. In the case of moisture limitation, the lack of available water prevents evapotranspiration. Conversely, radiation limitation occurs where moisture is abundantly available while the amount of evapotranspiration (ET) is dependent on incoming radiation Teuling et al. (2006). When soil moisture is below the wilting point (θ_{WILT}) then evapotranspiration will be at a minimum (direct relationship between temperature and radiation resulting in only sensible heating) and likewise if the surface is saturated (θ_{CRIT}) then evapotranspiration will be at a maximum (latent heating is at a maximum) and only dependent on available energy. However, a region that is normally soil moisture limited between the wilting point and critical level is known as the transitional zone (Seneviratne et al., 2010). Transitional zones lie between wet and dry climates or semi-arid regions such as large parts of Australia. Hirschi et al. (2010) indicate that for soil moisture to affect the surface energy balance, a region needs to be in the transitional zone.

Typically, changes in climate regimes, which depict differences in the energy partitioning, precipitation, and evapotranspiration are assessed using the P - E metric (e.g. Dai, 2013; Liu et al., 2013). This can be seen primarily using the Köppen-Geiger climate classification scheme. As mentioned in Chapter 3.3.3, this divides climate regimes into five main categories: arid, semi-arid, temperate, savanna or dry tropics, and wet tropics, with

further sub-categories describing the variation of the climate therein, using thresholds of the mean monthly precipitation, temperature, and evapotranspiration (Kottek et al., 2006; Peel et al., 2007). By definition, arid climate regimes have a monthly precipitation less than half of the potential evapotranspiration, semi-arid regions have a monthly precipitation between 50% and 100% of their potential evapotranspiration, and temperate regimes a monthly precipitation in excess of 100% of the potential evapotranspiration. Mathematically speaking, $P - E > 0$ implies a 'wet [climate] regime' and $P - E < 0$ a 'dry [climate] regime'. However, because of this, the climate regime paradigm as defined by Köppen (1884), Kottek et al. (2006), and Peel et al. (2007), may not be sufficiently accurate for comparisons of land-climate interactions between regions which are otherwise categorised as similar climate regimes. In the case of the influence of soil moisture on hot extremes through changes in the energy balance in the transitional zone, it is not sufficient to simply conclude that this relationship will hold true in all semi-arid regions because these are typically defined as within the transitional zone. Due to this, prior to investigating the variation of soil moisture within Australia or its relationship to Tx90, it is essential to investigate the spatial variation of the energy partitioning and consequently the position of the transitional zones in Australia.

5.1.2 Data and Methodology

Changes in hydroclimatological conditions and the transitional zone are examined using yearly averages of precipitation, evapotranspiration and net radiation (R_n) estimates for each climate regime as well as spatially across Australia. Furthermore, as discussed in Chapter 2, Budyko (1974) proposed an empirical relationship between the actual evapotranspiration ratio ($\frac{ET}{P}$) and the dryness index, determined by the potential evapotranspiration ratio ($\frac{R_n}{P}$), as defined by Eq. 5.1 (where ϕ is the dryness index).

Depending on the limiting regime of this relationship a positive feedback to temperature is expected to be seen. Using the Budyko framework (Budyko, 1974) this relationship can be investigated to determine if the region is limited by moisture or radiation, by plotting values of actual evapotranspiration ($\frac{ET}{P}$) and potential evapotranspiration ($\frac{R_n}{P}$) against each. The Budyko curve as provided by Eq. 5.1 is an estimate of the relationship between the amount of moisture versus the amount of radiation based on the average of world basins and does not account for the differences in soil moisture storage for various basins. Pike (1964) and Choudhury (1999) proposed variations of Eq. 5.1, accounting for different soil moisture storages using a shape parameter (υ, where the magnitude describes the amount of soil moisture storage). This relationship is given by Eq. 5.2.

$$f(\phi) = \phi[1 - exp(-\phi)].tanh(\frac{1}{\phi})^{\frac{1}{2}} \tag{5.1}$$

$$f(\phi) = (1 + \phi^{-\upsilon})^{\frac{-1}{\upsilon}} \tag{5.2}$$

5.1.3 Results

Fitted Turc-Pike curves provide an easy method for the comparison against the Budyko curve (ideal watershed) and for identifying how the climate characteristics differ for particular watersheds from their generic regime classification. This was produced for each Köppen climate regime with each data point representing the ratio between the dryness and the evaporative index for each year between 1950 and 2015 (Figure 5.1). As mentioned the transitional zone occurs between the field capacity $(PET/P < 1)$ and the wilting point ($PET/P > 3$, depending on vegetation and root zone (Seneviratne et al., 2010; Rouholahnejad et al., 2016). Typically, the semi-arid region is described as being within the transitional zone (Seneviratne et al., 2010), however, in 34 out of 46 years, the semi-arid region has a dryness index exceeding 3 and is thus moisture limited.

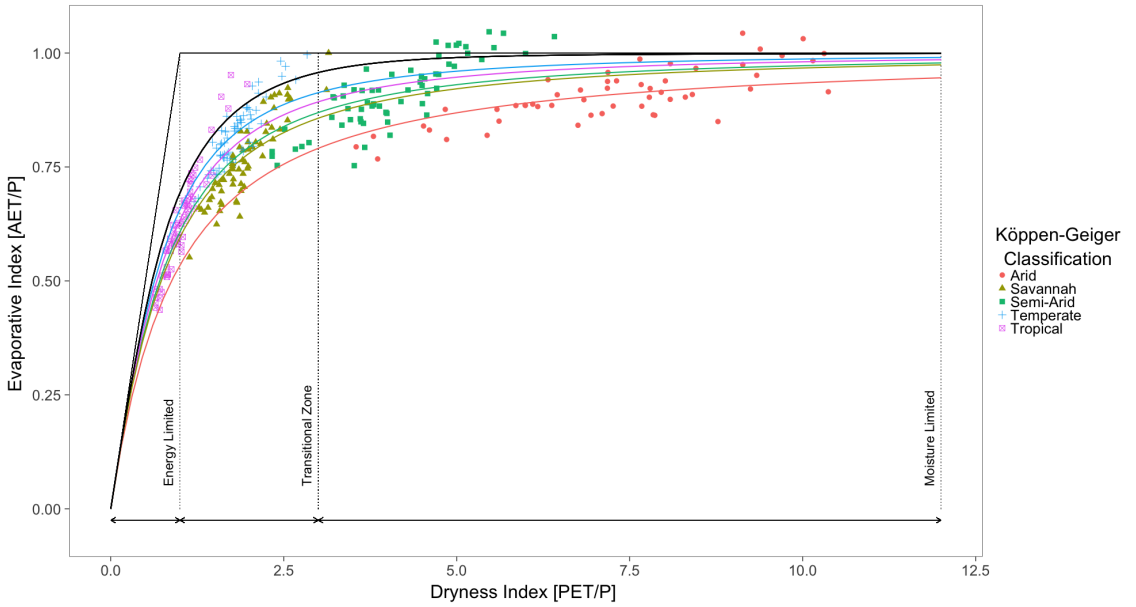

Figure 5.1: Budyko scatter plot of evaporation index versus the dryness index for each Köppen-Geiger region based on yearly averages between 1950 and 2015.

As expected, all and roughly half the years for the arid and tropical regimes, respectively, fall outside the transitional zone. Both the temperate and savanna regimes have values that largely fall within the transitional zone. This is reflected in the fitted Turk-Pike

curves where these regimes have parameters closest to that of the ideal Budyko curve (Figure 5.1).

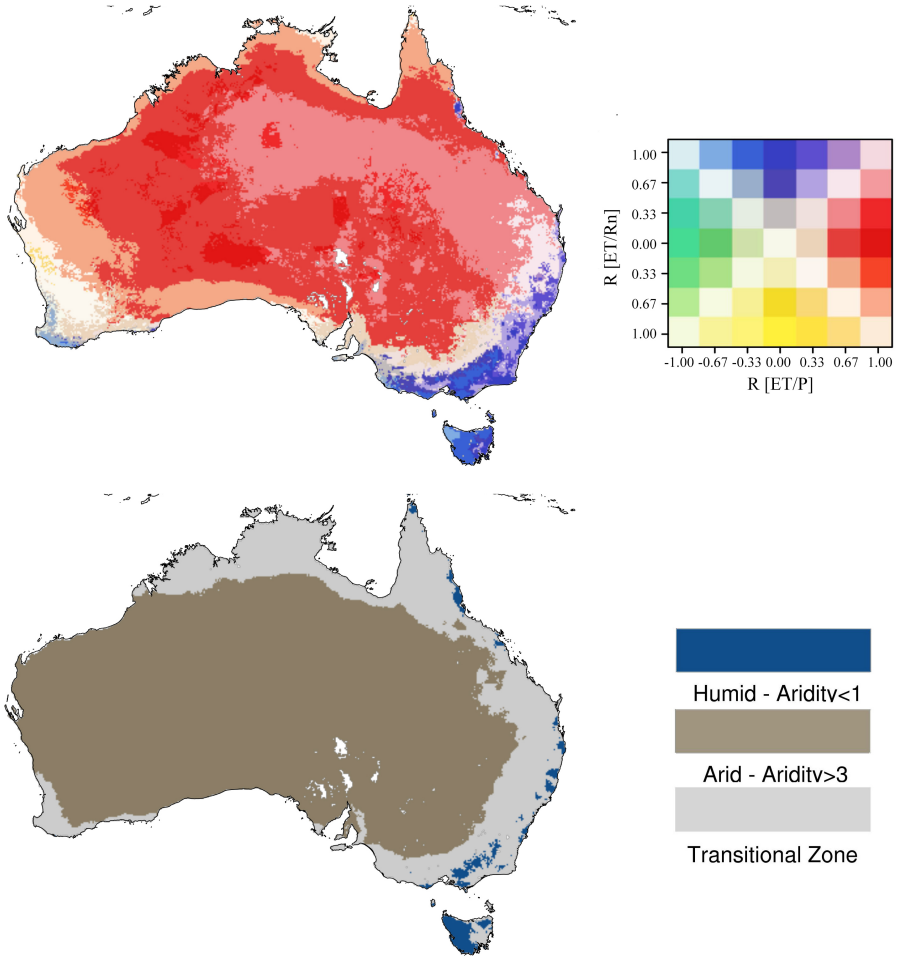

Figure 5.2: Climate drivers using yearly averages between 1950 and 2015 at 5km resolution. (Top) Bivariate map of evapotranspiration drivers, i.e. correlation coefficients between evapotranspiration, incoming solar radiation and precipitation indicating the distribution of moisture and radiation limited regions. (Bottom) Distribution of arid (brown) and humid (blue) zones as well as the "transitional' regime (grey).

These results are also outlined spatially when comparing the dryness and the evaporative index across Australia (Figure 5.2;top). Similarly to Teuling et al. (2009), the correlation coefficients of yearly ET with shortwave solar radiation (Rn) and the precipitation (P) for all of Australia are shown in Figure 5.2;top. Comparing these using a bivariate choropleth legend, two distinct regions can be identified: i) the moisture limited region characterised by high correlation coefficients (ρ) between P and ET but low correlation between Rn and ET (red-coloured areas), and ii) the energy limited region which is characterized by low correlation between P and ET and a high correlation between Rn and ET (blue-coloured areas). Areas that are neither strongly moisture nor energy limited are within the transitional zone (pale-coloured areas), this is in strong agreement with

Figure 5.2, showing similar transitional zone patterns as outlined previously. From this, we can see that there is no strong limiting regime in far northern savanna, the southwest and coastal east and south-east of Australia. This is in strong agreement to the patterns seen from the Köppen-Geiger classifications where parts of the semi-arid and savanna regions are within the transitional zone. Conversely, alpine Australia and the majority of inland Australia are radiation and moisture limited, respectively.

Finally, as from Figure 5.1, the different aridity (dryness) index values are spatially presented for Australia in Figure 5.2;bottom. This separates the aridity (dryness) index into the three zones; the humid (blue), arid (brown) and the transitional zones (gray). From this, the transitional zone can be clearly spatially identified and coincides with the regions which are neither strongly moisture nor energy limited in Figure 5.2;top. Similarly to Figure 5.2;top, alpine and inland Australia fall outside the transitional zone.

5.2 Soil Moisture and its Relationship to Tx90 (Hot-Days)

5.2.1 Introduction

Following the investigation of the distribution of energy partitioning, the location of the transitional zone and the link between soil moisture and temperature extremes are investigated here. As established in Chapter 2, deficits in soil moisture have the largest effect on temperature extremes through amplified sensible heating in regions that are considered to be within the transitional zone (as these regions are most sensitive to changes in soil moisture resulting in differences in evapotranspiration). Furthermore, heat waves have been linked to several modes of climate variability, which influence large-scale dynamics leading to changes in moisture availability (Cai et al., 2009). Modes of inter-annual variability such as the El Nino- Southern Oscillation and the Indian Ocean Dipole have been shown to largely affect the rainfall in Australia (Jones et al., 2000; Cai et al., 2009; Williams et al., 2009). Such changes in rainfall can strongly influence soil moisture availability and have been linked to extreme heat-wave conditions (Jones et al., 2000; Cai et al., 2009; Perkins et al., 2015; Perkins-Kirkpatrick et al., 2016). Anomalies from the mean conditions in the land surface, in particular in soil moisture, have been recently studied with a focus on observational datasets in Europe (Hirschi et al., 2010) and globally (Mueller et al., 2012), and more recently in Australia (Herold et al., 2016).

The relationship between SPI and Tx90 has been previously investigated using observational data in Europe (Hirschi et al., 2010) and modelled data globally (Mueller et al.,

2012). Herold et al. (2016) conducted a continental scale analysis of Australia using the Standardized Precipitation Evaporative Index (SPEI) and found that during low soil moisture conditions there is a reduced likelihood of low heat wave temperatures. However, Herold et al. (2016) concluded that low soil moisture is necessary, but not a sufficient requirement, for heatwave days. Likewise, Kala et al. (2015) investigated the effects of soil moisture anomalies on the heat wave in the lead up to the "Black Saturday" fires in February 2009. They found that drier soils led to a higher maximum temperature at a lead-time of 5 days, whereas for longer time frames (10 and 15 days), a change in temperature did not necessarily coincide with a change in soil moisture. This further signifies the importance of investigating the effect of soil moisture of the conditions leading to forest fires and their intensity.

While these studies have investigated the magnitude and variability of this relationship between heat waves and soil moisture at various temporal scales, a direct comparison between a range of land surface moisture indices including soil moisture itself is yet to be undertaken. Likewise, these studies did not investigate the spatial variability of this relationship in context with different climate regimes and moisture/radiation partitioning across Australia.

The aim of this section is to substantially build on previous studies by investigating whether the relationship between soil moisture and Tx90 differs across the climate regimes of Australia and how this changes using various moisture indices. Moreover, the context of this relationship is examined and compared against the moisture/radiation partitioning across Australia, as explored previously in this chapter. Finally, this relationship is investigated at a higher spatial resolution (5km) compared to previous lower-resolution studies (50km) providing an insight into the local scale which has an impact on socio-economic aspects of regions prone to an increasing number of Tx90 under future climate change. This work will assist water management services to better allocate resources through the identification of regions where soil moisture can influence hot extremes.

5.2.2 Data and Methodology

The strength of the relationship between soil moisture indices and Tx90 is assessed using the same methods and metrics as in Chapter 4.1. In particular, the Pearson correlation, RMSE, and bias are all calculated in this section. As summer Tx90 are of particular interest, the DJF or austral summer period is used for analysis. Any additional methods are defined in the following subsections, below.

Hot days (Tx90)

As mentioned, the relationship between soil moisture indices and hot extremes is investigated here. Hot extremes can be calculated using several methods, these range from the number of consecutive days over a threshold temperature (Perkins et al., 2012) to the exceedance of a certain percentage of the time series (Mueller et al., 2012). For the purposes of this study, the number of Tx90 is defined as the number of days per month exceeding the 90th percentile of the entire temperature time series. The percentile for each day is calculated using a sliding 5-day window ($\pm 2\,days$). This is calculated for each day of the year providing 365 values. This method has been employed in similar studies which also related Tx90 to preceding precipitation deficits (Hirschi et al., 2010; Mueller et al., 2012; Fischer et al., 2007).

Modes of Climate Variability - ENSO

The focus of this analysis is on establishing the relationship between soil moisture and Tx90, but as heat waves have been linked to several modes of variability, namely the IOD, SAM, and in particular, ENSO, the effect of ENSO on this relationship is also included. Each of these influence the large-scale dynamical process leading to changes in moisture availability (Cai et al., 2009). Typically, ENSO is commonly investigated in relation to hot extremes as well as deficits in moisture and precipitation (Potter et al., 2009; Cai et al., 2011; Hallack-Alegria et al., 2012; Perkins et al., 2015; Yoon et al., 2015) and is considered the dominant mode of climate variability in the Southern Hemisphere (Wang et al., 2013), both directly, and due to its influence on SAM. Commonly, the intensity and phase of ENSO are defined in terms of the Southern Oscillation Index (SOI). The Troup SOI is used here to identify ENSO. This is defined as the difference in the Mean Sea Level Pressure (MSLP) anomaly in the central equatorial Pacific Ocean (between Darwin at $12.46°S\ 130.85°E$, and Tahiti at $17.65°S\ 149.43°W$), and is calculated by Eq. 5.3.

$$SOI, = \ 10\,\frac{[P_{diff} - \bar{P}_{diff}]}{\sigma_{(P_{diff})}} \tag{5.3}$$

where, P_{diff} is the difference between the MSLP of Tahiti and Darwin, $\bar{P}_{diff}$ is the long-term average of this difference, and $\sigma_{(P_{diff})}$ is the long-term standard deviation with values calculated monthly. Values above +7 and below -7 are considered strong ENSO phases (La Niña and El Niño, respectively), while values between are considered neutral. Strong positive values indicate El Niño events and are usually characterised by a warming of the central and eastern tropical Pacific Ocean and a decrease in Pacific 'trade winds'. This weakening of the trade winds causes a reduction in winter and spring precipitation in eastern Australia (Cai et al., 2011). Strong negative values indicate La Niña

events and are usually characterised by a warming of the western tropical Pacific Ocean and an increase in Pacific trade winds. This enhancing of the trade winds causes an increase in winter and spring precipitation in eastern Australia (Cai et al., 2011).

5.2.3 Results

Correlation between Moisture Indices and Tx90

The strength of the relationship between soil moisture and Tx90 has been investigated by calculating the Pearson correlation coefficient between each moisture index and Tx90. Figure 5.3 presents correlation coefficients spatially for Australia and the Köppen-Gieger climate regions for DJF (for the periods 1971 to 2015 and 2000 to 2015). These two periods are selected as they represent the whole time-series and the period of greatest warming to current (including the 'Millennial drought'). Average correlation coefficients for all months are summarised in Table 5.1.

Correlation coefficients are generally negative and on average between $-0.4 to -0.5$ for each index (Table 5.1). The strongest negative correlation is found in the southeast (semi-arid) and north (savanna) of Australia, with an inverse of this seen throughout parts of tropical Queensland, the Northern Territory, and South Australia. During the summer months (DJF; the monsoon season in the tropical North of Australia), any periods of significantly drier conditions appear to have a strong influence on Tx90, as is expected. There are considerably lower correlations around central Western Australia; this is due to the region not being represented well by AWAP as there is near zero precipitation (areas with precipitation less than 1 mm over this period are masked) during the time period, and also because of a high uncertainty in the accuracy of any precipitation estimates, due to a lack of rain gauges. Correlation coefficients are also generally very low along the coasts south-western and southern Australia.

These spatial observations are reflected in the averages seen in Table 5.1; the strongest correlation coefficients are seen in the semi-arid and savanna regimes. Regions that are considered within the transitional zone as expected show large correlation coefficients on average with values ranging between -0.48 and -0.56. API, MSDI, and s0 typically have the largest correlations in each climate regime and averaged across Australia.

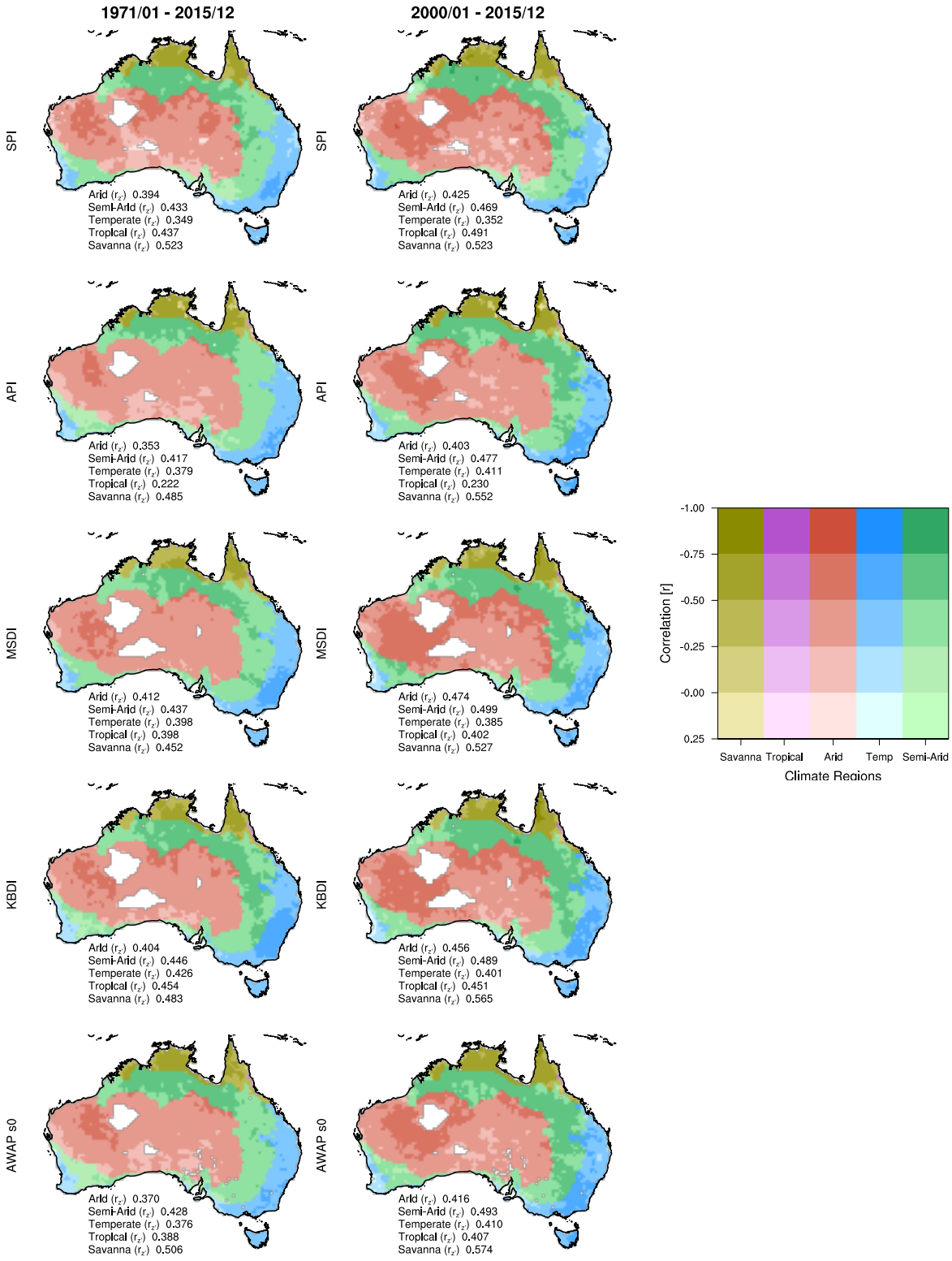

Figure 5.3: (rows) Pearson correlation coefficients between Tx90 and moisture indices for DJF months between 1971 and 2015 (left) and between 2000 to 2015 (right). The colour bar is separated into Köppen-Gieger climate regimes with each shading depicting a different region. Also shown are the mean correlation coefficients climate region using the Fisher-z transformation ($r_{z'}$).

Table 5.1: Summary of Pearson correlation coefficients between DJF Tx90 and SM indices for each climate regime and for the transitional regime. This is given as a spatial average for the period 1971-2015 (top) and 2000-2015 (bottom).

		Arid	Semi-Arid	Temperate	Tropical	Savanna	Transitional	Average
1971-2015	**SPI**	-0.383	-0.414	-0.345	-0.423	-0.498	-0.417	-0.394
	API	-0.359	-0.419	-0.395	-0.398	-0.532	-0.458	-0.396
	KBDI	-0.406	-0.448	-0.429	-0.419	-0.489	-0.456	-0.426
	MSDI	-0.412	-0.439	-0.404	-0.375	-0.457	-0.427	-0.419
	s0	-0.379	-0.428	-0.384	-0.378	-0.515	-0.448	-0.405
2000-2015	**SPI**	-0.445	-0.467	-0.354	-0.499	-0.529	-0.435	-0.443
	API	-0.406	-0.476	-0.417	-0.411	-0.603	-0.503	-0.444
	KBDI	-0.454	-0.485	-0.406	-0.445	-0.574	-0.480	-0.462
	MSDI	-0.471	-0.494	-0.390	-0.402	-0.534	-0.452	-0.467
	s0	-0.420	-0.491	-0.414	-0.426	-0.585	-0.494	-0.454

Figure 5.4 shows scatter plots of each moisture index with Tx90, along with quantile regression lines (0.1, 0.3, 0.5, 0.7, 0.9 in grey, mean and median regressions are denoted by blue and red dotted lines, respectively as well as the 95% confidence interval for the mean, shaded in grey). Each point represents the spatial average of one month in the period. Each moisture index is normalised between 0 and 1 for the purposes of comparison. However, API and s0, tend to have very low moisture, with median values near to zero. This is in contrast to SPI, KBDI, and MSDI which all have median values around 0.5. API appears to reflect patterns seen in s0, both, with a logarithmic distribution of increasing Tx90 with decreasing moisture. MSDI and KBDI appear to have a linear distribution over the domain. With each moisture index a distinct increase in Tx90 with decreasing moisture. SPI has the greatest divergence in regression lines and also the steepest gradient for each regression on average for all of Australia. Whilst SPI tends to have lower correlation coefficients than the other indices, this indicates that it tends to have the strongest difference between the number of Tx90 and a change in moisture, independent of climate regimes.

To investigate the differences in this relationship between the climate regimes, the slope of the linear regression at various quantiles for each moisture indices (Figure 5.4) was determined. The 95% confidence intervals of the estimated slopes are also shown and given as shading of the same colour as each climate regime. For each moisture index, we can see that the arid and semi-arid regions have a much more pronounced increase in the regression slope with increasing quantiles, signifying a much stronger relationship between low soil moisture and Tx90 in these regions. This is particularly noticeable for both API and s0 and to a lesser degree KBDI. When looking at values within the transi-

tional zone we can see that it is very similar to a mixture of the temperate and semi-arid regions.

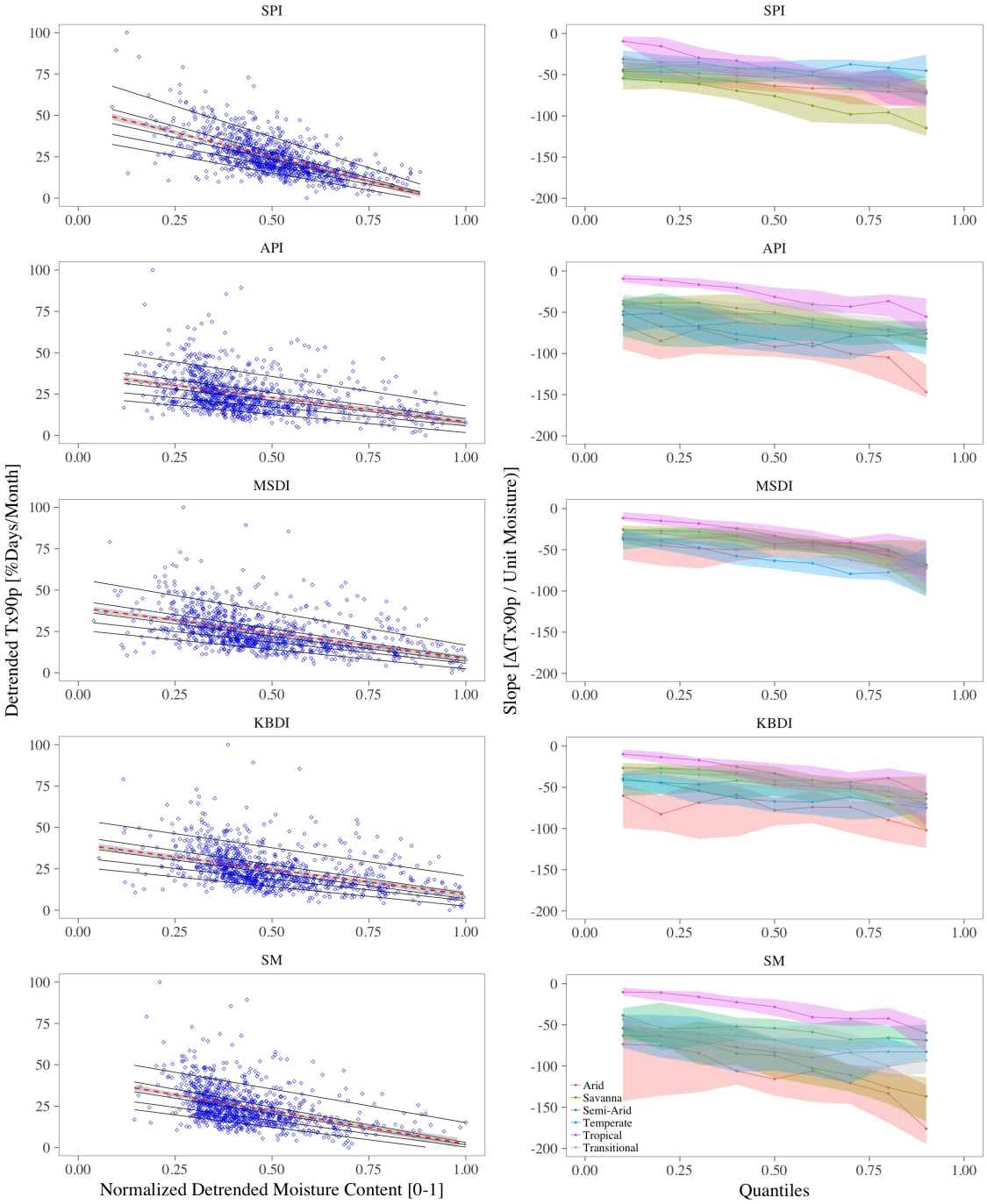

Figure 5.4: (Left) Scatter plots of monthly DJF Tx90p versus SPI, API, MSDI and KBDI. Soil moisture indices are normalised between 0 and 1. Also shown are linear regression lines for a selection of quantiles (0.1, 0.3, 0.5, 0.7, 0.9 and the median). (Right) Quantile regression slopes of monthly DJF Tx90 and SPI, API, MSDI and KBDI for each Köppen climate regime. The 95% confidence intervals of the calculated slopes for each climate regime are shaded . All data are spatially averaged for Australia and regions between 1971 and 2015.

Effect of ENSO on the SM-Tx90 relationship

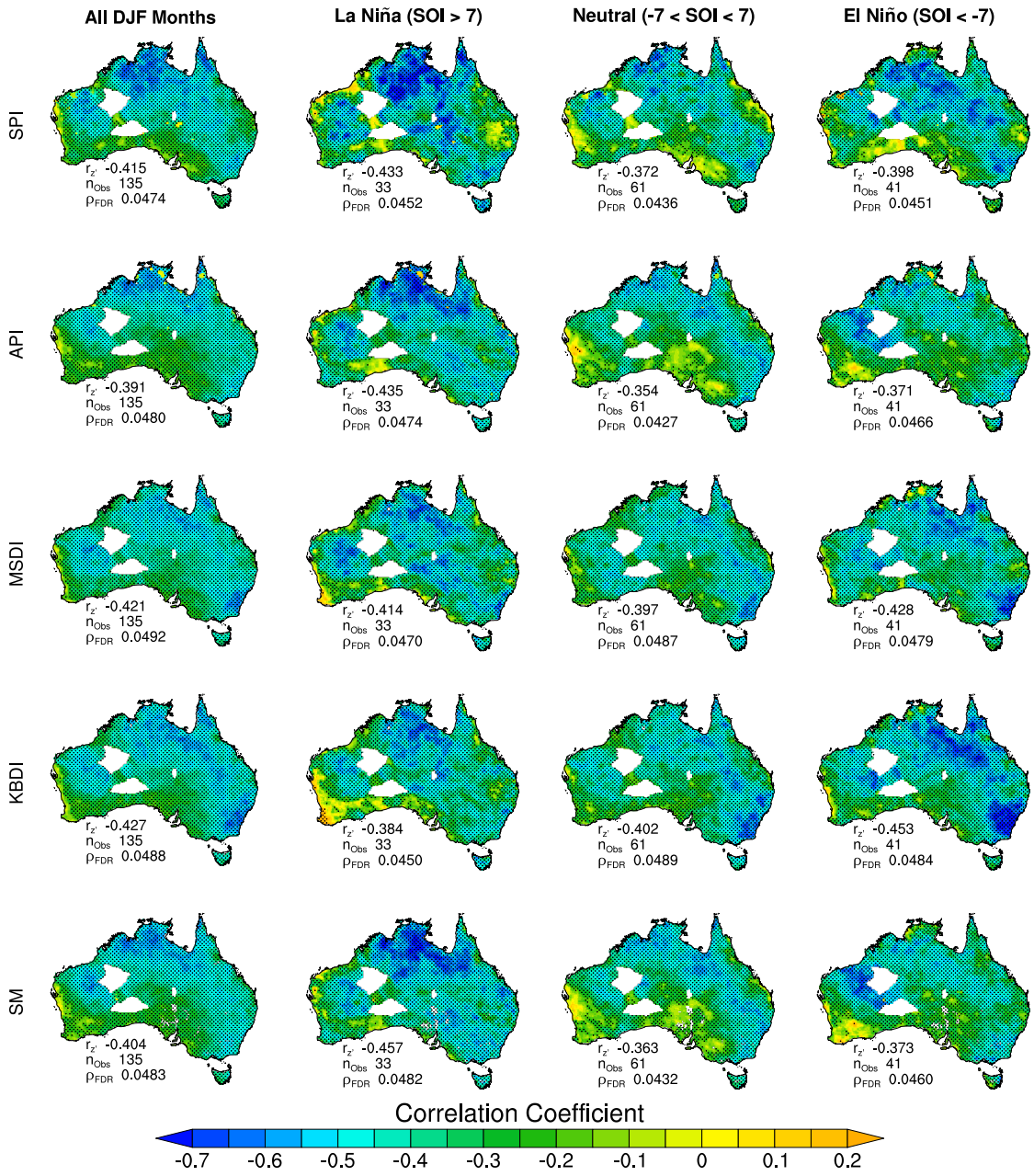

Figure 5.5: (rows) Pearson correlation coefficients between Tx90 and moisture indices for DJF months between 1971 and 2015 for Australia. (column 1) Calculated over time-series. (column 2) La Niña months with an SOI index greater than 7. (column 3) neutral months with an SOI index between -7 and 7. (column 4) El Ninõ months with an SOI index less than -7. Stippling is indicated for significant correlation coefficients using the False Discovery Rate transformation (level is denoted as ρFDR). Also shown are the mean correlation coefficients across Australia using the Fisher-z transformation ($r_{z'}$) and the number of observations (n_{Obs}) used for calculations.

In order to show the difference in the SM-Tx90 relationship due to the effect of ENSO, Figure 5.5 shows the spatially distributed Pearson correlation coefficients between Tx90 and SM for all DJF months and further for DJF months with an SOI exceeding +7, less

than -7 and from -7 and +7. Values above +7 and below -7 are considered strong ENSO phases (La Niña and El Niño, respectively) while values between are considered neutral. Stippling indicates regions which are statistically significant at the 95% level (two-sided t-test with the α level adjusted according to the FDR method).

Results show varying regions of mainly negative and some positive differences in the correlation coefficients for each La Niña, neutral and El Niño phases. El Niño and La Niña events generally have a larger negative-correlation on average, indicating that relationships between SM deficits and Tx90 are generally stronger during these periods. Typically, it is expected to find a larger amount of sensible heating and a stronger relationship in regions that have a lower than average winter and summer rainfall during El Niño phases, such as northern Australia, south-eastern Australia, and central-western Australia. However, correlation coefficients during El Niño phases in these regions generally show little change as these are already usually the driest months. One exception to this is in the tropical north, where DJF is the wet season. Therefore, intuitively, a breakdown of the Tx90-SM relationship should be expected, however, stronger negative-correlations are observed. This is due to the reduction in precipitation causing the region to move into the transitional zone. Conversely, during La Niña phases the opposite effect is observed, with much weaker correlation coefficients and a positive change in correlation coefficients in the tropical north.

During La Niña events, strong positive correlation coefficients are found across the southern portion of Australia as well as arid regions of Western Australia (La Niña events typically bring a larger number of precipitation events, particularly during winter months which could contribute to higher than usual SM in DJF in these regions). Arid regions are typically far too moisture limited and are not in the transitional regime, hence, increases in moisture would not necessarily lead to a decrease in Tx90. On the other hand, for temperate regions or regions within the transitional regime, a large increase in moisture results in these regions being radiation limited and an increase in Tx90 would not be attributed to changes in SM. The Nullarbor plain along the coast of the Great Australian Blight, and regions of south-west Western Australia tends to display large positive and negative changes during El Niño and La Niña phases, respectively, however, those are not statistically significant.

5.3 Discussion

The location in which changes in soil moisture largely affect the partitioning between sensible and latent heat, described as the transitional zone, was compared spatially across

Australia and for the five main Köppen-Gieger climate regimes therein. Seneviratne et al. (2010) and Fischer et al. (2007) indicate that the transitional zone lies within semi-arid regions within central and southern Europe, whereas Figure 5.1 indicates that for Australia, the transitional zone is actually a combination of the savanna, semi-arid and temperate Köppen-Gieger climate regimes. The generalisation of previous studies is not applicable to Australia, as catchments are not only in magnitude larger than other similar regions but also catchments in Australia often span several climate regimes. Beyond this, regions defined as semi-arid, through the Köppen-Gieger classification are dryer than other similarly defined regions, with evapotranspiration completely dependent on the available precipitation. This means that large areas of semi-arid regions more closely resemble arid conditions. Similarly, each Köppen-Gieger climate region tends to be shifted towards drier conditions throughout Australia resulting in the difference in the location of the transitional zone.

After establishing the position of the transitional zone, the degree of association between Tx90 and SM was investigated using high-resolution observationally-based data across Australia. Direct comparisons of various SM indices and the associated climate regimes were investigated providing an insight into the water balance in Australia which is expected to be indicative of other semi-arid and arid regions of the world. A clear correlation between the number of Tx90 and a decrease in SM during Austral summer months (DJF) was found, comparable to other studies in south-eastern Europe (Hirschi et al., 2010), Australia (Herold et al., 2016; Perkins et al., 2015), and globally (Mueller et al., 2012). Whilst these studies have previously assessed the correlation of this relationship and quantile regressions for a single SM index, this study analysed several additional indices, as well as the AWAP s0 dataset.

SM itself has recently been investigated in relation to heat wave days for Australia (Perkins, 2015; Perkins et al., 2015). However, this and the aforementioned studies have not investigated this relationship in context with the various climate regimes within Australia nor the partitioning of moisture and energy pertaining to the physical feedback process itself. Due to the significant range of climatological regimes across Australia and the differences in the moisture and energy partitioning, the spatial variation in the effect of SM on Tx90 is expected to differ vastly. Recent studies (Gibson et al., 2017a) have investigated this spatial inhomogeneity in relation to how global climate models simulate heatwaves. Gibson et al. (2017a) suggests that the physical origins for the observed differences could be due to land-atmosphere coupling and/or atmospheric circulation; to name a few possibilities. This study presents an analysis in terms of the physical drivers of the spatial variation seen in both Tx90 and SM indices in Australia, which may help inform other model evaluation studies.

The negative-correlation between SM and Tx90 was found to be particularly strong in regions falling within the semi-arid and temperate regimes. This is consistent with the physical feedback between low SM and an increase in sensible heating in the transitional regime. Here, the energy balance is strongly coupled with the water balance such that when a dry anomaly occurs, the following months will observe an increase in sensible heating resulting in a direct positive temperature anomaly. This observation was particularly strong in the southeast and northwest of Australia and was consistent with findings by both Herold et al. (2016) and Mueller et al. (2012). However, this relationship is much weaker in regions with little to no annual precipitation such as coastal southern Australia and large parts of inland Western Australia. This may be explained by the decoupling of surface SM with root zone SM under extreme dry conditions, as has been identified by Hirschi et al. (2014).

Williams et al. (2009) indicate that climate variation, in particular, in the south-east of Australia is largely influenced by large-scale atmospheric dynamics and inter-annual variability. Temperature extremes have been found to be directly influenced by large-scale atmospheric circulation through horizontal temperature advection (Pezza et al., 2011; Gibson et al., 2017a). Due to this, the relationship with ENSO is of particular interest as it modulates the circulation conditions giving rise to the relationship between itself and both temperature and precipitation. It has long been documented that there is a strong relationship between ENSO and both temperature and precipitation (Dai et al., 1997; Mullan, 1998; Evans et al., 2010; Hallack-Alegria et al., 2012).

Due to this, this chapter investigated the relationship between SM and Tx90 for summer months exceeding +7 and -7 SOI (an SOI above +7 is associated with strong La Niña events, while below -7 SOI with strong El Niño events). There appears to be a high level of spatial variability in the magnitude of correlation coefficients between SM and Tx90 associated with ENSO events across Australia (similar to those seen by Perkins et al. (2015)). Compared to non-DJF months, it was determined that overall, an increase in the correlation coefficients between SPI and Tx90 across Australia exists, but this cannot be solely attributed to the effect of ENSO on precipitation as there is a very large spatial variability in the Tx90-SM relationship. Along with the effect of the IOD, SAM and the Madden-Julian Oscillation (MJO) have on precipitation in Australia (Cai et al., 2009; Risbey et al., 2009), Williams et al. (2009) suggest that changes in precipitation (and hence SM) can be heavily influenced by the position of the southern hemisphere Hadley cell. Likewise, the latitudinal position of the sub-tropical high-pressure maximum over Australia is a significant mechanism influencing the inter-annual variability of precipitation rather than just solely ENSO (Pittock, 1971).

Chapter Summary

This chapter introduces the key mechanisms behind the relationships driving an increase in fire occurrence and intensity, namely, the location of the transitional zone, the strength of the correlation between various moisture indices and their effect of soil moisture on temperate extremes. Contrary to recent studies which indicate only semi-arid regions are within the transitional zone, here, we show that large parts of the temperate, semi-arid and savanna climate regions in Australia enter the transitional regime and are neither strongly moisture nor radiation limited (Figure 5.2a, 5.2b). Arid and semi-arid regions of Australia exhibit the strongest increase in the quantile regression slopes (from low to high percentiles), indicating that months with low SM are highly likely to experience a large number of Tx90 (Figure 5.4). However, Northern (savanna) and southeastern Australia (Temperate) observe the largest correlation coefficients between changes in moisture and Tx90. Again, API appears to best represent patterns seen with the AWAP s0 and has the largest negative-correlations with Tx90 in the transitional zone (Figure 5.5). In conclusion, we show that API and MSDI observe the largest correlation to surface soil moisture as well as a resulting increase in Tx90 with decreasing moisture. These results are particularly strong in the transitional zone which comprises of parts of the temperate, savanna and semi-arid regions in Australia. The following chapters will explore how the aforementioned results impact on fire danger, occurrence, and intensity.

CHAPTER 6

Improving Fire Risk Estimation by Investigating Fire Intensity, and Moisture and Temperature Extremes

Overview Understanding the mechanisms behind forest fires and quantifying their risk and scale is essential to mitigate their potential socioeconomic damage. The previously established relationship between soil moisture and extreme temperature is essential for understanding the energy and water balance within a region, particularly in temperate/transitional regimes. Consequently, forest fires are often linked to moisture deficits, extreme temperature, and low fuel moisture. However, soil moisture is yet to be investigated with context to the risk and likely intensity of forest fires. Fire Radiative Power (FRP) can be a useful tool to quantify the impact and severity of fires and is also dependent on temperature, moisture and vegetation conditions. Through these relations, fire risk and its intensity are analysed spatially across Australia in this chapter.

6.1 Introduction

Australia, and more specifically south-eastern Australia experiences a large number of forest fires and is generally considered one of the most fire-prone regions in the world (Hennessy et al., 2005). Understanding the mechanisms behind forest fires and quantifying their risk and scale is essential to mitigate their potential socio-economic damage. The interaction between forest fires and atmospheric conditions is relatively well studied (Pereira et al., 2005; Trigo et al., 2006; Potter, 2012). In Australia, an increase in fire danger is typically associated with high temperatures and strong winds ahead of cold fronts, with fire spread particularly correlated to fuel as well as wind speed and direction (Cheney et al., 1994; Mills, 2005). For example, in south-eastern Australia, high wind speeds may be sustained following a frontal passage if a front extends greatly into the troposphere. As a frontal passage passes, north-westerly winds can shift south-westerly, causing the fire to spread substantially as the previous fire-flank becomes the head (Mills, 2005). This coupled with massive energy releases can produce convection columns, also which accompanied by cyclonic winds in down-drafts, can exacerbate fire conditions through downwind spotting (Martin et al., 2016).

When assessing the likelihood or risk of fire in a region several terms can be used. Economical risk assessors consider 'risk' as the probability of fire, but also includes socio-economic loss and value. This is compared to fire management services which typically defines risk as the likelihood of ignition (Hardy, 2005). 'Hazard' is also used commonly used and refers to the state of the fuel load whilst 'severity' specifically describes the extent of a fire on the wildland system. In other words, the ecological impact (Hardy, 2005; Key et al., 2006; Keeley, 2009). Lastly, Beall (1946) describes fire 'danger' as including all the items which quantify how and whether fires will start, what the spread and damage are, and well as their containability.

Fire danger and risk can be defined using several metrics, and in general, spread, damage, and containability are pertinent to incipient fires and their conditions and do not present the likelihood of fire in a particular location. To this extent, typically, forest fire danger is described using indices that incorporate atmospheric conditions such as, surface air temperature, precipitation, relative humidity, wind speed, and fuel moisture. Various fire danger indices exist, including the McArthur Forest Fire Danger Index (FFDI; McArthur, 1967), the McArthur Grassland Fire Danger Index (GFDI; McArthur, 1967), the Canadian Fire Weather Index (FWI; Van Wagner, 1987), the United States National Fire Danger Ratings System (NFDRS; Deeming et al., 1972), the Fosberg Fire Weather Index (FFDI; Fosberg, 1978).

In Australia, the FFDI is used operationally by the Bureau of Meteorology and fire management services and is used in many studies to directly asses the level of forest fire risk. Recently, there has been a large effort to increase their accuracy using the methods mentioned previously and from various remotely sensed products. However, it has been found that there is a large variation in the categorical classification between such indices (FFDI and FWI) at low index values (Dowdy et al., 2009). More particularly, several studies have investigated improvements to the drought factor component of the FFDI, as such Griffiths (1998). This introduced a smoothing function for the drought factor and consequently, it is used in Australia. Alternate drought factors have also been investigated such as by Snyder et al. (2006), which presented a fuel dryness index based on biophysical principles associated with energy exchange, defined as the daily ratio of sensible heat to available energy. They determined that the index was more responsive to daily changes than most of the other indices, including the KBDI and the fuel moisture code in the FWI, providing more accurate fuel dryness conditions of live vegetation. Similarly, the KBDI (used within the drought factor) was modified for a better adaptation to Mediterranean conditions, also producing a faster response to daily to meteorological conditions (Petros et al., 2011).

Generally, these studies suggest:

1. The drought factor should have a cumulative form based on the drought conditions of the previous period (day), thus providing a faster response than the currently used KBDI.

2. This factor should be expressed as a function of potential evapotranspiration (PET). However, as PET is difficult to accurately measure, a simple function inferring PET through its formulation should be used.

3. The index should be initialised based on meteorological data and when the soil is near saturation and this level is reflected in its value.

Beyond this, the simplicity of such drought factors and fire danger indices has been questioned. (Sharples et al., 2009), investigated the use of a simpler fire danger index that is easy to calculate comparative to the FFDI indicating that they may be a useful pedagogical tool in the context of fire danger and fire weather. Likewise, Liu et al. (2003) substituted the API directly into the FFDI for the Goulburn River catchment in Australia over a short time period following a large forest fire in the region. It was shown that API, as a simple alternative to the drought factor, suitably represented the role of precipitation or soil moisture in the calculation of FFDI. As mentioned, certain indices (e.g. FFDI and GFDI) have been found to perform poorly when assessing the risk by high severity

fires (Harris et al., 2011). The current FFDI and various other indices can be used to determine the risk of the outbreak of forest fires, but such indices don't describe the risk of forest fires in terms of severity and intensity. Therefore particularly in Australia, the current indices don't provide the overall danger and risk of a fire for mitigation by local fire authorities. This has been addressed conceptually by Harris et al., 2011, in which a fire severity scale was proposed based on the size and rate of propagation of the fire. The idea is that as there is an increase in the rate of propagation or perimeter spread of the fire, a larger amount of fuel is consumed, releasing energy into the atmosphere. This rate of energy released from the fire determines the severity of the fire.

There are many methods to determine the amount of energy released by fires resulting from the combustion of fuels with a common method, fireline intensity being a measure of the energy released along the front of the fire itself (Byram, 1959). Quantification of most methods such as fireline intensity provides substantial challenges with large uncertainty in estimating, combustion efficiency, fuel load, and type and the spread or propagation of the fire itself. The severity and intensity resulting from the output of energy from fires can be described by the total Fire Radiative Power (FRP) and Fire Radiative Energy (FRE) of a fire. FRP is defined as the quantification of the radiant heat output from the fire (Roberts et al., 2005). FRP is a direct result of the combustion process, where carbon is oxidised to CO_2 (and other compounds) releasing energy stored in the fuel as heat (Wooster et al., 2005; Ellicott et al., 2009). Therefore, FRP is the rate of release of the radiative component that is, the higher the fuel consumption rate the greater the FRP. Despite a higher sensitivity at night (Maier et al., 2013) as remotely sensed retrievals improve, FRP and FRE are becoming more commonly used in studies to describe fire severity and intensity (Wooster et al., 2005; Roberts et al., 2005; Ellicott et al., 2009).

Independently, despite the long use of thematic mapping of FFDI and fire preconditions such as temperature, soil moisture etc., the effect of soil moisture on both FFDI and particularly FRP is not well studied. As investigated in Chapter 5, Hirschi et al. (2010) and Seneviratne et al. (2010) indicated a link between soil moisture deficits and hot extremes which is particularly strong in temperate climates potentially leading to exacerbated conditions for severe fire. This coupled with the soil and vegetation moisture, leading to the development, or drying vegetation can cause a greater fuel load and lead to higher FRP fires (Hudak et al., 2016). As soil moisture is a key component in each of these processes, this chapter aims to investigate its effect on both, comparing several commonly used moisture indices, as well as their potential use, through the drought factor in the currently used FFDI in Australia.

6.2 Data and Methodology

6.2.1 FRP

In order to validate the effectiveness of each FFDI formulation, the FRP from fire hotspots will be used. As mentioned in Chapter 3 can be used to derive both fire hotspots and FRP. For the purpose of this chapter, the MODIS Collection 6 datasets, which provides daily (from 8-daily) data at a resolution of 500 m are used. More specifically, the thermal anomalies/fire locations MCD14DL product is used for both FRP and fire hotspot retrieval. This product is derived from the swath products (MOD14/MYD14) rather than the tiled MOD14A1 and MYD14A1 products (Giglio, 2015). Likewise, the MODIS MOD13Q1 product is used for NDVI retrieval at 16-day intervals for a 250 m spatial resolution. Data for each product are obtained from the Land Processes Distributed Active Archive Center (LPDAAC; https://lpdaac.usgs.gov/), and are upscaled to 5 km and 25 km to match the spatial resolution of AWAP and the ESA CCI SM products, respectively.

6.2.2 ERA-INTERIM

The AWAP datasets do not include all input fields required for the formulation of the FFDI, and as such, relative humidity and wind speed have been sourced from the ERA-INTERIM (The European Centre for Medium-Range Weather Forecasts' re-analysis) dataset. Similarly, ERA-INTERIM (ERA-I) has previously been used by the CSIRO (the Australian Commonwealth Scientific and Industrial Research Organisation) to produce decadal FFDI between 2006-2096 (Leonard et al., 2016). Daily surface relative humidity, and the surface u and v wind components have been retrieved at a resolution of 25 km for Australia between 1979 to 2015. As these data are available at four time steps daily, the 6 am UTC (4 pm AET; Australian Eastern Time) time is used as this best corresponds to the maximum daily temperature, minimum daily relative humidity, and the highest likely instantaneous daily FFDI.

6.3 Results

As mentioned, fires are associated with warmer than normal temperatures, a high fuel loading and in regions which are in moisture deficit. Regions such as south-eastern and south-western Australia have a large number of summer (DJF) fires such as the Black Saturday fires in 2009 in Victoria, or the more recent fires of January and February 2014.

Each of these years experience extreme temperatures and moisture deficits throughout the summer period. In late January 2009 areas of Victoria observed 3 or more consecutive days above 40°, this was similarly the case in 2014 with 5 consecutive days above 40°. As mentioned fires such as these are the key motivation for investigating the preconditions leading to forest fires and how the FFDI and consequent FRP are affected. Section 3.5 describes how the FFDI is formulated based on the daily maximum temperature, the surface wind speed, the relative humidity and the KBDI through the drought factor. However, as established in Chapter 5, soil moisture plays a key role in influencing temperature extremes through its relationship with the partitioning of sensible and latent heating, particularly in the transitional zone. The location of the Black Saturday fires fall within this region, and as such, soil moisture, precipitation-driven indices, and temperature extremes are investigated in relation to fires and their FFDI.

Each of the moisture indices as well as the key variables used to calculate the FFDI are compared against each other for both Australia and for the Black Saturday fires in the following sections. The FFDI is calculated using each moisture indices (derived from AWAP), ERA-I data, and AWAP data for the 1979-2015 period. This temporal period has been further limited to match the temporal period of MODIS (MCD14DL) derived FRP and fire occurrence. All fires with a quality mask value greater than 70% (high certainty) have been included resulting in 916,457 fires between 2000 and 2015.

6.3.1 ERA-I/AWAP FFDI versus ERA-Interim FFDI

As mentioned above (Section 6.2.2), a combination of ERA-I and AWAP data has been used to produce FFDI. Despite the availability of temperature and precipitation among other variables in the ERA-I dataset, it was decided that the combination of the two products would achieve an FFDI dataset at a higher resolution than just using ERA-I data (AWAP available at 5km whereas ERA-I is only available at 25km). Whilst, this is not a "true" 5 km resolution dataset due to the aggregation of resolution the two products, it still provides FFDI at a higher resolution overall. A comparison between daily FFDI derived using only ERA-I data (API-driven) and ERA-I/AWAP (KBDI-driven) was produced to determine the degree of difference if any existed. Figure 6.1.a presents the Pearson correlation, RMSE, and bias between the two products, as well as, against ERA-I/AWAP (API-driven). The difference between API and KBDI driven FFDI is explored further in the following sections, however, from Figure 6.1.a there is little difference between the two. For AWAP API driven FFDI, the average correlation coefficient is 0.967 with a relative homogeneity across Australia, whilst for the ERA-I API product, the correlation is 0.952 on average, with slightly lower correlations seen in coastal Western

Australia. Both products have a low bias and RMSE with the main differences occurring in alpine south-east Australia. This is further exemplified in Figure 6.1.b, which shows the time series of the percentage change in the cumulative yearly FFDI for each of the three products. Again, there is a good agreement between the products with the largest differences occurring in 2000 and 2011. Both of these coincided with large negative FFDI anomalies primarily driven by high precipitation events resulting in a larger variation between products that use differing moisture components. Changes to input variables, like precipitation, can have a substantial influence on the resultant FFDI and as such the sensitivity of FFDI to its components is explored in the following section.

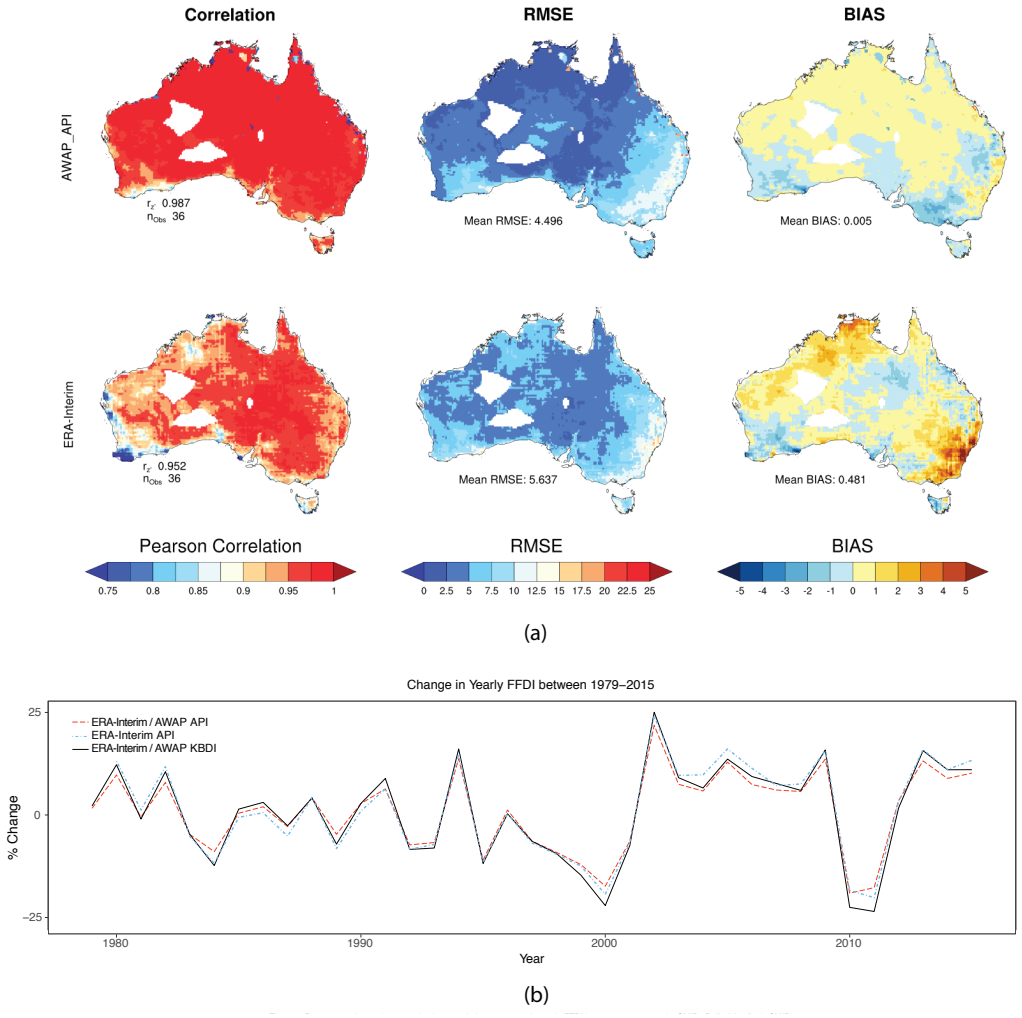

Figure 6.1: (a) Skill metrics of the comparison of daily ERA-interim API driven FFDI and ERA-interim/AWAP API driven FFDI against AWAP/ERA-Interim derived KBDI driven FFDI. Skill is based on the Pearson correlation (left column), RMSE (middle), and BIAS (right column). All data are compared between 1979 and 2015. (b) time series between 1979-2015 of the percentage change in cumulative yearly FFDI for ERA-I API driven FFDI (blue-dotted line), ERA-I/AWAP API driven FFDI (red-dashed line), and AWAP/ERA-I KBDI driven FFDI (black line).

6.3.2 Sensitivity of FFDI to its Components

As identified above, the FFDI differs varies both temporally and spatially due to changes in the variables used as input. This is particularly the case for each moisture index, temperature and wind speed. These changes are also strongly linked to the variation in FRP. The sensitivity of such changes in FFDI due to its input variables can be quantified both as a whole and spatially and are important to determine the contribution of each input variable in the FFDI. Respectively, Figure 6.2 and Figure 6.3 presents this sensitivity on average and spatially for Australia. In order to isolate changes in FFDI due to each variable, only one variable was changed whilst each other were kept constant at their respective median values. The FFDI was then computed using the 0.01, 0.05, 0.1, 0.2, 0.3, 0.4, 0.6, 0.7, 0.8, 0.9, 0.95 and 0.99 quantiles for the given variable and consequently the percentage change in FFDI from its median was determined.

The percentage change in FFDI (spatially averaged) versus quantile values is presented in Figure 6.2 for each of; the drought factor, relative humidity, maximum temperature, and the wind speed. Overall, across Australia, the FFDI has the greatest sensitivity to relative humidity with maximum temperature and the drought factor showing similar differences. The wind speed component has only a very small change (between -5% an 5%) in FFDI with increasing quantiles. Although linear regressions are produced for each variable, the change in FFDI substantially differs from this at each the high and low tails. Notably, the wind speed component increases from a change of 0% to about 60% between the 0.75 and 0.99 quantiles.

Similarly, the spatial variation of the sensitivity to each FFDI component is presented in Figure 6.3, however, only the difference between the median and 0.95 quantiles are shown. As in Figure 6.2, the relative humidity, and temperature components have the largest influence on FFDI on average, although there is a large amount of spatial variability. Much like what is seen in the spatial variability in the mean maximum temperature (see Figure 6.4c), there is a north-south gradient with an increasing change in FFDI due to temperature. As previously, the wind speed has a negligible change FFDI at the 0.95 quantile. The most substantial changes in FFDI occur for the drought factor and the relative humidity. Unlike Figure 6.2, the drought factor has changes in excess of 100%, however, regions in which this occurs are restricted to the south-east and the south-west of Australia. The sensitivity of FFDI to the drought factor is largely limited to the bias toward dry conditions. Few regions within Australia have a mean drought factor below 10 and therefore there are only marginal changes due to increasing percentiles (see Figure 6.4a).

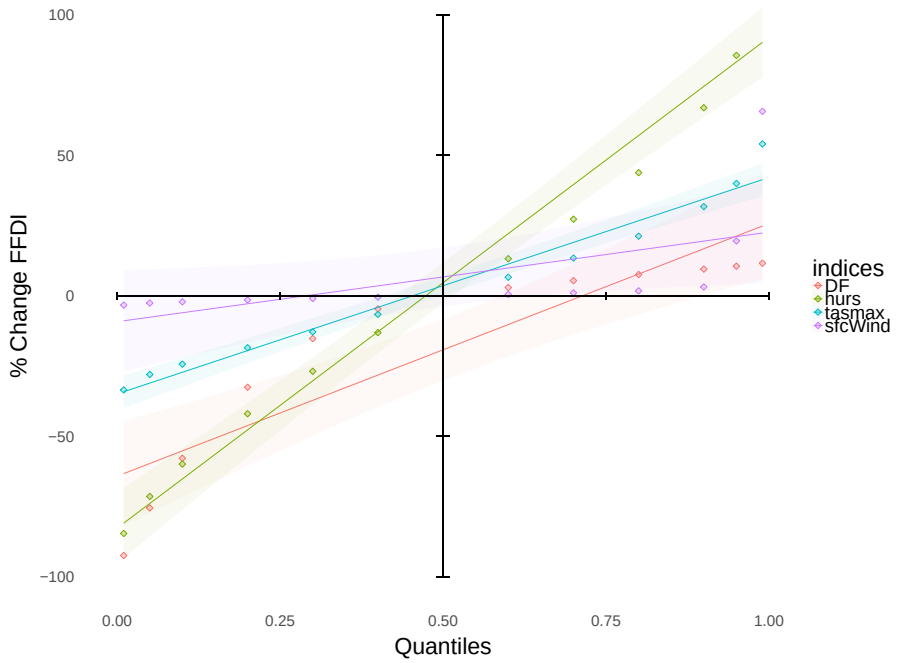

Figure 6.2: Percentage change in FFDI between median values (calculated between 2000 and 2015) and various quantiles values between 0 and 1 for drought factor (salmon), relative humidity, (green), maximum temperature (blue), and wind speed (magenta). Also shown are the linear least squares regression for each component and its 95% confidence interval (shaded).

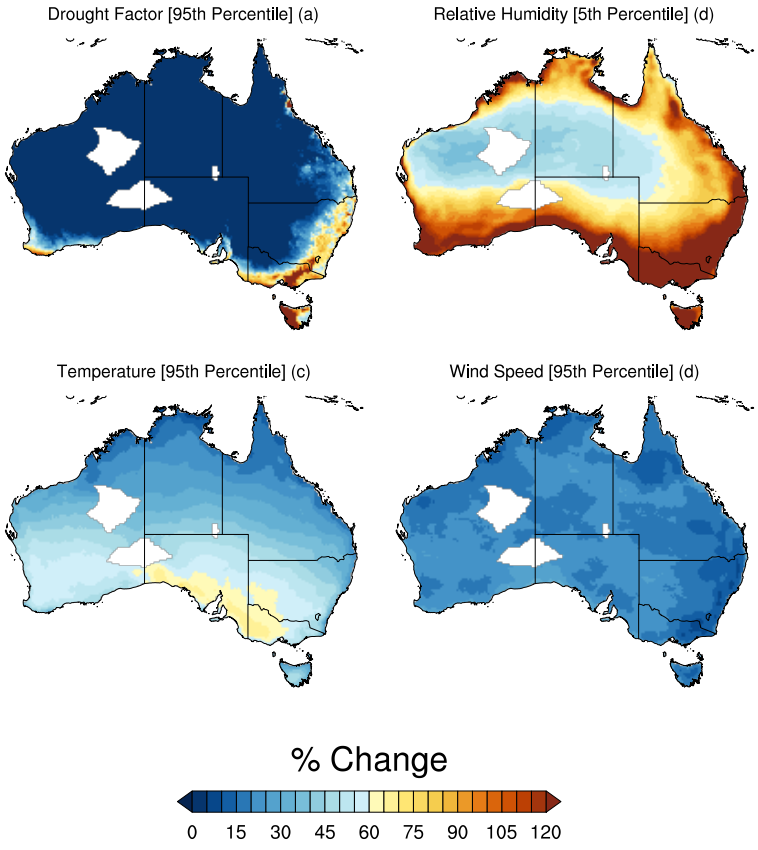

Figure 6.3: Percentage change in FFDI between median values (calculated using AWAP data between 2000 and 2015) and the 95th percentile (5th percentile for relative humidity) values for (a) drought factor, (b) relative humidity, (c) maximum temperature, and (d) wind speed.

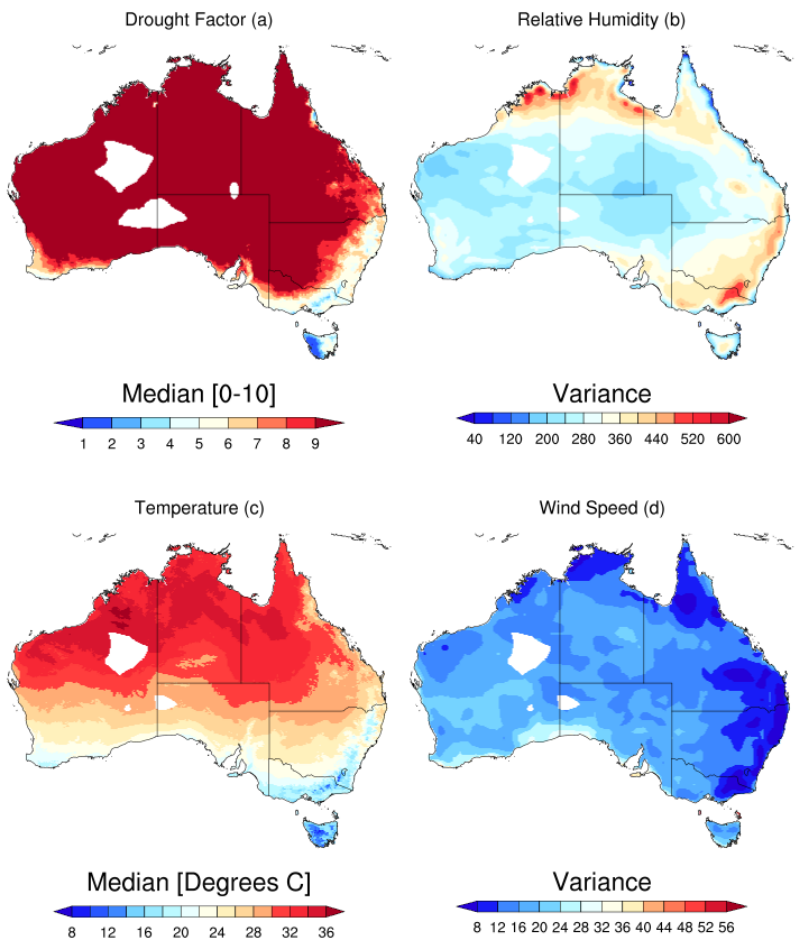

Figure 6.4: Drivers of spatial sensitivity of FFDI to its components. (a) Median drought factor, (b) relative humidity variance, (c) median maximum temperature, and (d) wind speed variance. Data are calculated using AWAP data between 2000 and 2015.

Conversely, there are widespread changes in FFDI in excess of 100% for large portions of Australia for the 0.95 quantile in relative humidity with the exception of central Australia. This is due to a very small variance in relative humidity (see Figure 6.4b) in central Australia as opposed to coastal Australia in which changes in relative humidity are driven by evaporation.

6.3.3 Temporal Variation in FFDI and FRP

The frequency and distribution of fires, as well as the strength of the FRP, and the FFDI spatially vary substantially, depending on the time of the year and the climate regime. Therefore, prior to assessing how these vary in relation to the temperature, soil moisture, and other metrics, the month [and season] in which the maximum FFDI, FRP and fire occurrence for a given location are presented in Figure 6.5. The left column displays the month and season of the maximum value spatially for Australia, whilst, the right col-

umn displays a time series of the distribution of maximum values for all spatial points separated into Köppen-Gieger climate regimes.

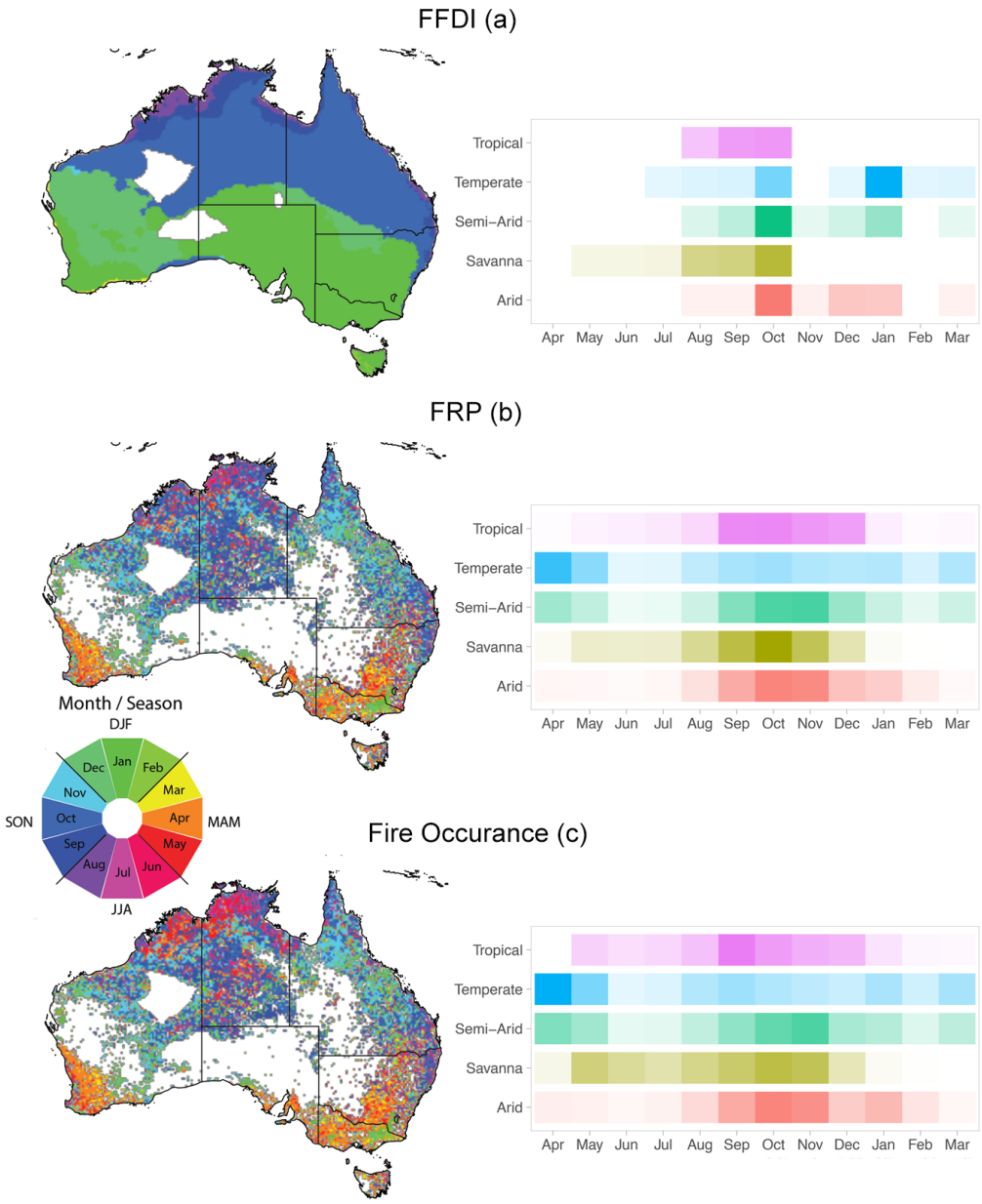

Figure 6.5: Month in which the maximum FFDI (a), maximum mean FRP (b) and number of fires (c) occur, for all fires detected by MODIS between 2000 and 2015. Also shown are density plots indicating the month of peak occurrence (pixel count) per Köeppen-Gieger Climate regimes (colour scheme is unrelated to maps).

Visually from Figure 6.5, there is a substantial difference between the months in which the maximum occurs for FFDI, FRP and fire occurrence. This is particularly noticeable between the FFDI and the two MODIS-derived metrics. The FFDI calculated using AWAP data as input indicates that there are three distinct seasons of fire danger. The maximum FFDI shifting from the far north-west in July, then southward through September and

October, eventually spanning the southern third portion of the continent by January. Largely homogeneous compared to FRP and fire occurrence, the differences in the maximum FFDI shows a similar pattern to previously documented seasonal changes in fire danger in Australia (Dowdy et al., 2009). There is also a strong similarity with the known monthly and seasonal trends in maximum daily temperature across Australia (Jones et al., 2000). This is highlighted by the lack of distinction between maximum FFDI according to Köppen-Gieger climate regimes. Each climate regime has peaks in FFDI in October with each regime having a varying distribution throughout the winter months. Only the temperate, semi-arid, and arid region have a further peak in January, again with the distribution spanning either side of this peak. As expected, this is most noticeable with the temperate regime, with the largest number of grid points with a maximum FFDI occurring in January.

As mentioned, the spatial variation in both FRP and fire occurrence is much more dispersed. Despite this, there are large spatial variations across Australia. However, there are still only minor differences between FRP and fire occurrence. The overall pattern for both is similar to FFDI, in which, the maximums, shift from JJA in the north-west of the country to DJF in the south-east and finally MAM in the south-west. Contrasting to FFDI, differences are noticed when comparing the Köppen-Gieger climate regimes. There are clear distinctions between the month and season in which maximum FRP and fire occurrence occur. The tropics and tropical savannas both have their maxima occurring during the dry season (JJA months), whilst the semi-arid and arid regimes have their maximums occurring during October, and to a lesser extent in April and January, respectively. Lastly, the temperate regime has its maximum occurring in April. The largest difference spatially between FRP and fire occurrence is observed in the tropical savannas, where the largest number of fires occur in June with the maximum FRP occurring between July and September. This observation is common to each climate regime, albeit to a lesser extent. That is, for each climate regime the maximum FRP occurs in the month proceeding the maximum fire occurrence. This is potentially due to the drying out of vegetation due to larger maximum temperatures and elevated fire conditions over an extended period, providing a drier, larger fuel load, producing larger more intense fires.

Similarly, the difference in seasonal FFDI compared to the climatological mean (between 1979-2015), as well as the frequency of fires and their respective FRP are shown for each climate regime in Figure 6.6. Seasonal anomalies are overlaid with both the total fire occurrences and mean FRP, with the degree of shading (purple) increasing with increasing occurrence and FRP. The seasonal variation in FFDI occurs regionally and coincides with the shifting changes in FFDI and mean FRP. Lower FRP fires typically occur during the

JJA northern fire season despite the larger number of fires overall. There is a north-south gradient in the change in FFDI for each season apart from autumn. In particular, during the austral summer, there is a strong positive change across the entire bottom two-thirds of the continent. The largest concentration of fires occurs throughout the Queensland hinterland and the Australian alpine region. Here, the highest intensity fires occur in alpine and south-west Australia. In autumn, despite only very small positive anomalies, fire occurrence shifts to Tasmania, Mallee N.S.W, non-alpine Victoria, southern South Australia, south-west Western Australia and the Kimberly region.

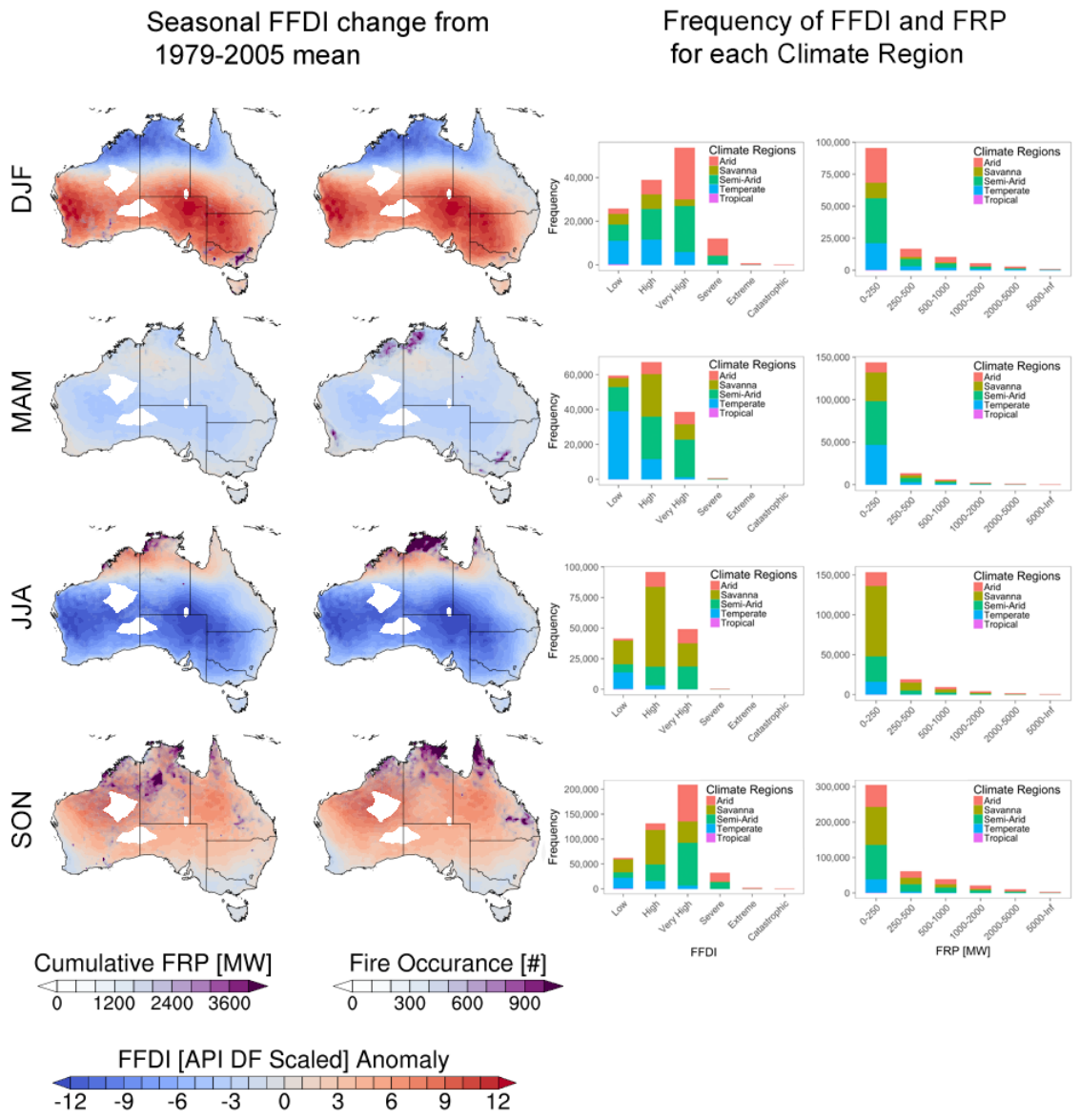

Figure 6.6: Seasonal FFDI anomaly (difference from mean) between 1979 and 2015 for Australia. Mean Fire Radiative Power for the total seasonal (left column) MODIS derived fire hotspots between 2000 and 2015 are also displayed as density contours (purple scale). Also shown are the total number of fires per season between 2000 and 2015 (right column).

During JJA, both a strong positive change in FFDI and the concentration of fires are almost entirely isolated to the tropical savanna north Australia. However, as mentioned, this does not necessarily translate to more intense fires. Typically, larger FRP fires occur during the SON season further towards the center of Australia. Finally, during spring, the savanna, semi-arid and arid regions of Australia observes a strong positive FFDI anomaly and the largest number of fires.

These changes are also reflected in Figure 6.6;right. Again, the largest number of fires occur at a relatively low FRP, with the total number of fires below 200 MW exceeding the combined number of fires exceeding 200 MW. This is particularly the case for the arid and savanna regions, which generally have the largest number of low-intensity fires occurring in DJF and SON, respectively. However, when comparing FFDI categories for each of the arid and savanna regimes, there is a larger number of fires occurring at a lower FFDI for the savanna regime than the arid regime. There is also a larger number of fires at higher index categories, particularly for both the arid and temperate regimes in the DJF period. This is also reflected in their respective FRP. Higher intensity of fires during this period occurs in each of the arid and temperate regimes.

From the total number of fires, there were 187817, 332437, 349741, 44399, 1970 and 93 fires from the low, high, very high, severe, extreme, and catastrophic FFDI categories, respectively. From this, we can see a clear skew of the data toward lower FFDI fires with 95% of the fires coming from the lower three categories. In particular, there are only 93 catastrophic fires during the 2000-2015 period. As discussed previously, Figure 6.6:right displays the frequency count of each FFDI category and increasing FRP categories (in 6 bins using the Jenks natural breaks classification). The number of fires is heavily skewed to the lower three FFDI categories, with a sudden drop thereafter. This is in contrast to FRP which observes an exponential decline in the number of fires with increasing FRP. Furthermore, the breakdown of each FFDI and FRP into the climate regimes is also contrasting. The proportion of fires across FFDI categories vary spatially, whereas the proportions for each FRP category are consistent. This is with the exception of the tropical regime which covers only a very small portion of Australia and likewise only a few fires occur during the temporal period.

6.3.4 Fire Preconditions

As identified in the previous section, the south-east of Australia observes the largest change in FFDI in DJF compared to the other seasons. Likewise, the largest FRP fires occur in this region during DJF. As mentioned, the Black Saturday fires are of particular interest as they fall within the transitional zone, where changes in soil moisture are ex-

pected to have the largest effect on temperature and consequently fires. Due to this, the time-series of API, SPI, KBDI, MSDI, s0, DF, FFDI, FRP, relative humidity, precipitation, surface wind, and maximum temperature are investigated here and shown in Figure 6.7.

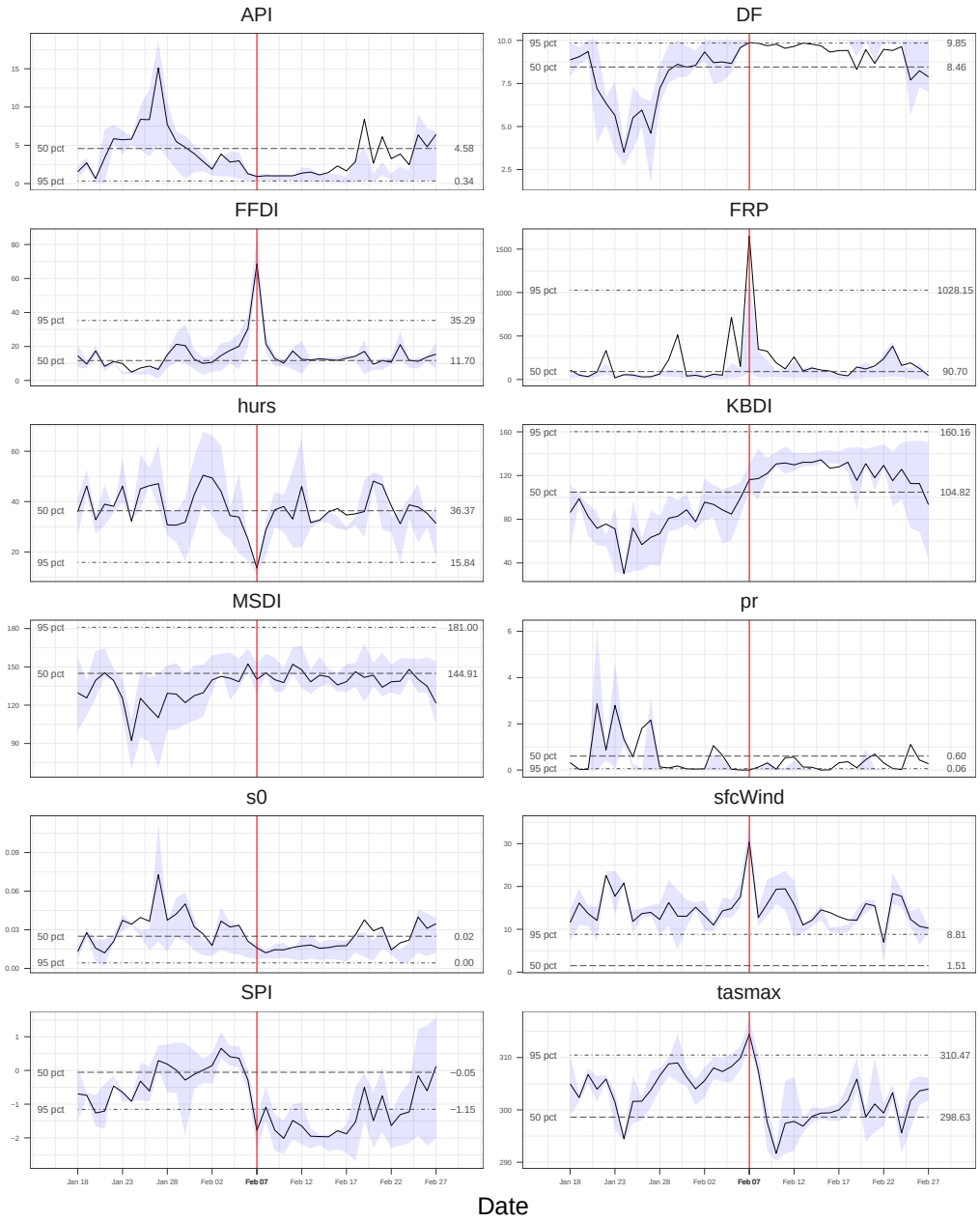

Figure 6.7: Time series of API, DF, FFDI, FRP, hurs (relative humidity), KBDI, MSDI, pr (precipitation), s0 (AWAP s0), sfcWind (surface wind speed), SPI, and tasmax (maximum temperature) $\pm$ 20 days either side of the Black Saturday fires in Victoria in February 2009. Also included are the climatological 95th (or 5th) and median percentiles for each variable between 2000 and 2015 (dotted and dot-dashed lines).

This depicts non-normalised values of each variable, plus and minus 20 days either side of February 7th, 2009 (red line). Also shown are the median, the 75th, and 25th confidence intervals (blue shading) from which averages were calculated (spatially averaged for Victoria), as well as the 95th (or 5th; dot-dashed line) and median (dashed line) percentiles of the climatology for Victoria between 2000 and 2015.

Each of, temperature, surface wind speed, relative humidity, and the drought factor were near or exceeding their respective median climatological values in the lead period to Black Saturday. Particularly for wind speed which was in excess of its 95th percentile for the entire period. This culminated on the 7th with each of these variables exceeding their 95th percentile climatological value. This resulted in an FFDI well in excess of the long-term 95th percentile value. Despite the drought factor also exceeding its climatological 95th percentile on the 7th, the KBDI only exceeds its median. Furthermore, in the lead up to the 7th, the KBDI is well below its climatological median value. This indicates that the soil moisture/drought conditions of the region were not above average in the lead up to the event. However, this observation is not accurately reflected in what is seen for the drought factor. Four moderate precipitation events occurred in the lead up to the 7th contributing to a higher moisture content, however, the dry-off period between precipitation events are underestimated in comparison to the other moisture indices. This is similar to what was observed in Chapter 4, in which, KBDI was found to be largely wet biased, overestimating moisture across various sites in Australia. Contrastingly, both API and SPI observe sharp decreases in moisture (rapid dry-off) in the days leading to the fires, relative to KBDI. Noticeably, MSDI presents a similar pattern to KBDI, whereas previously, MSDI had more closely resembled the patterns seen in API. Despite the strong link between moisture and FFDI, the largest influence during the Black Saturday fires is the surface wind speed, temperature, and relative humidity. Each of these show a sharp increases/decreases on the 7th, contributing to the substantial spike in FFDI (the sensitivity of these variables are shown later in this chapter). The increase in FRP is similarly observed during the 7th despite several fires burning prior to and after the event. Generally, the FRP is near or around the climatological median for each fire. However, the FRP was far in excess of the previous climatological maximum (post-2000) during the 7th.

The time series for each variable in Figure 6.7 presents an overview of the conditions leading to the fires and their relative values compared to the climatology. However, it does not indicate the spatial variability nor the location of the fires itself. Therefore, a spatial time-series for the seven days leading up to, and including the Black Saturday fires is presented in Figures 6.8 and 6.9. Each of the key contributing variables as well as each of the moisture indices has had their respective climatological 95th[5th] percentile (from between 2000 and 2015) removed. As before, intensity is given in the form of FRP (MW). The magnitude of FRP is indicated using increasing diamonds relative to their respective intensities. Figure 6.9 compares each of the moisture indices, whilst Figure 6.8 presents the remaining variables.

Similar to Figure 6.7, in the lead up to the 7th, the largest positive (negative) anomalies between the 95th (5th) percentile and daily values occur for wind speed, relative humidity, and temperature. Anomalies are particularly strong in the interior of the state with positive FFDI anomalies generally coinciding with positive wind speed anomalies. The location of fires and particularly higher intensity fires coincide with positive wind speed anomalies, as well as, temperature, and relative humidity anomalies. This is evident on the 7th, with all fires located in regions where the key variables observe strong positive (negative) anomalies with respect to their 95th (5th) percentiles.

Most notably, (with the exception of a region in the far north-east stretching to the south-east), the drought factor indicates small positive anomalies almost uniformly across the state in each of the days leading to the 7th. However, this is largely due to the finite scale, limiting values to a maximum of 10, compared to the continuous scales for each other variable (excluding relative humidity). I.e. as the 95th percentile occurs at near maximum potential values, exceedance will be limited in magnitude.

This is particularly noticeable in 6.9. Each of the moisture indices indicate small negative anomalies in moisture compared to their climatological 95th (5th) percentile during the 7th. However, in the lead up to the 7th most regions observe small positive anomalies in moisture, particularly in KBDI and MSDI. It has been highlighted previously that KBDI tends to over-estimate moisture compared to the other indices. It should be noted that for each moisture index, soils moisture is represented as extremely low, not just in comparison to their climatological 95th or 5th percentiles. Despite this, the location of fires coincides with regions of negative moisture anomalies. This is particularly strong for API and SPI on the 7th. The relationship between moisture indices and both FRP and FFDI are investigated further in the following sections.

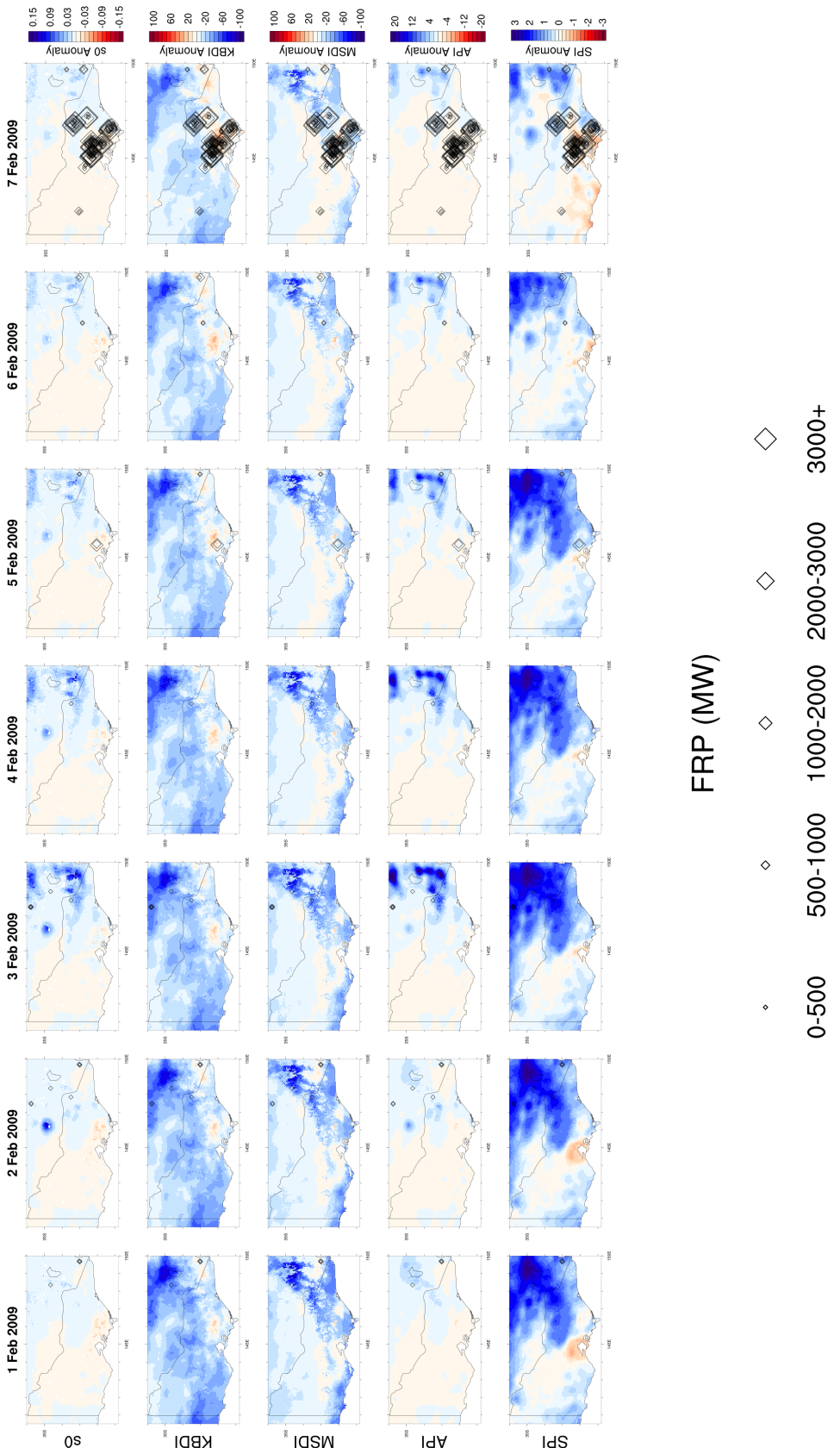

Figure 6.8: Time series of DF, FFDI, hurs (relative humidity), pr (precipitation), sfcWind (surface wind speed), and tasmax (maximum temperature) in the seven days leading to the Black Saturday fires in Victoria in February 2009. Each variable has had their respective climatological 95th[5th] percentiles (calculated between 2000 and 2015) removed. Fire intensity and location is given as FRP in MW and indicated as increasing diamonds relative to their size.

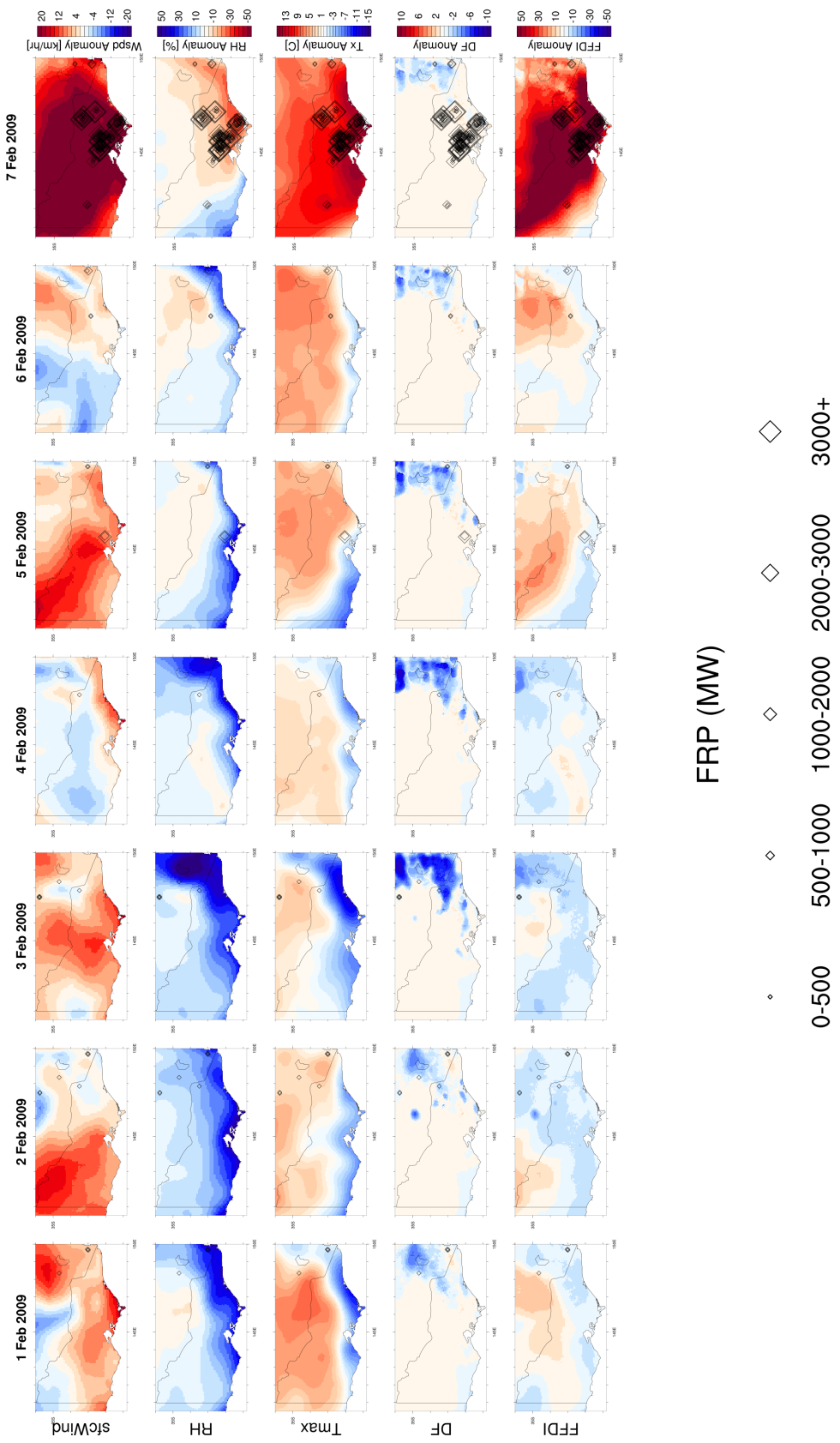

Figure 6.9: Time series of API, KBDI, MSDI, s0 (AWAP SM), and SPI in the seven days leading to the Black Saturday fires in Victoria in February 2009. Each variable has had their respective climatological 95th[5th] percentiles (calculated between 2000 and 2015) removed. Fire intensity and location is given as FRP in MW and indicated as increasing diamonds relative to their size.

6.3.5 Comparing FFDI computed using differing drought factors

Following on from the comparison between the moisture indices, each index has been used to compute the FFDI and compared against FRP and the original KBDI-derived FFDI. This has been done using two methods, i) through substituting each directly into the drought factor component of the FFDI scaling each to be equivalent to the KBDI (0-200) and, ii) through replacing the drought factor component by scaling each index to the drought factor itself (0-10). Figure 6.10 compares each of these methods against each other for the Black Saturday fires in Victoria on the 7th February 2009. Overlaid onto each panel is the relative FRP for each fire in MW.

From figure 6.10, there is little difference spatially (indices scaled to the DF) between each index with only minor differences in the low, moderate and high categories near Canberra. However, this is in contrast to figure 6.10 where a large difference in the FFDI occurs for each category and for each index. Where KBDI and SPI are scaled to the DF they tend to underestimate high FFDI index categories compared to the original formulation (non-scaled). In particular, in fire locations and towards the south-east coastline. Overall, both MSDI and API are the most similar to the actual FFDI. From previous studies (Kumar et al., 2017) and results indicated here, KBDI indicates a large wet bias throughout Australia, this appears to flow through to the FFDI calculation. Conversely, API which has a slight dry bias accurately depicts the KBDI-derived FFDI. This is partly because the API and the drought factor are calculated using a soil moisture decay component. This is in the form of the number of days since and the amount of the last rain event for the drought factor, and for the API, a decay factor derived from the maximum temperate modulating the current API value. As the API implicitly includes a decay component it tends to indicate the most similarities to the KBDI-derived FFDI. Not only does API best correspond to how the drought factor is calculated but as from previous results API shows the most similarities to the shallow layer soil moisture (*in situ* and AWAP derived).

The differences in the two methods for producing the FFDI as identified above are further investigated in Figure 6.11. This compares the number of fires per FFDI category produced using each of KBDI, MSDI, API, SPI, and s0 for the FFDI produced via replacement of the KBDI and for the FFDI produced via scaling each moisture index to the DF itself. As previously determined there is little difference when substituting each index in place of the KBDI. The greatest difference occurs at both the low and the catastrophic FFDI categories where the SPI and KBDI have the largest difference in the number of fires than the other three indices. This is most noticeable when comparing the FFDI produced by scaling to the drought factor.

In each category, SPI is substantially different to the other indices. More so, there are only very few fires occurring in the severe to catastrophic categories. However, it is observed that there is a large reduction in the number of fires for each index at higher severity categories than those produced by replacing with the KBDI. This suggests that the drought factor is skewed towards wetter conditions via this method and consequently fewer fires occur at higher FFDI values. In fact, for KBDI, MSDI, and SPI there are no fires occurring with an index category of catastrophic. As in Figure 6.10, API shares the most similarities between each method of producing the FFDI and the KBDI-derived FFDI.

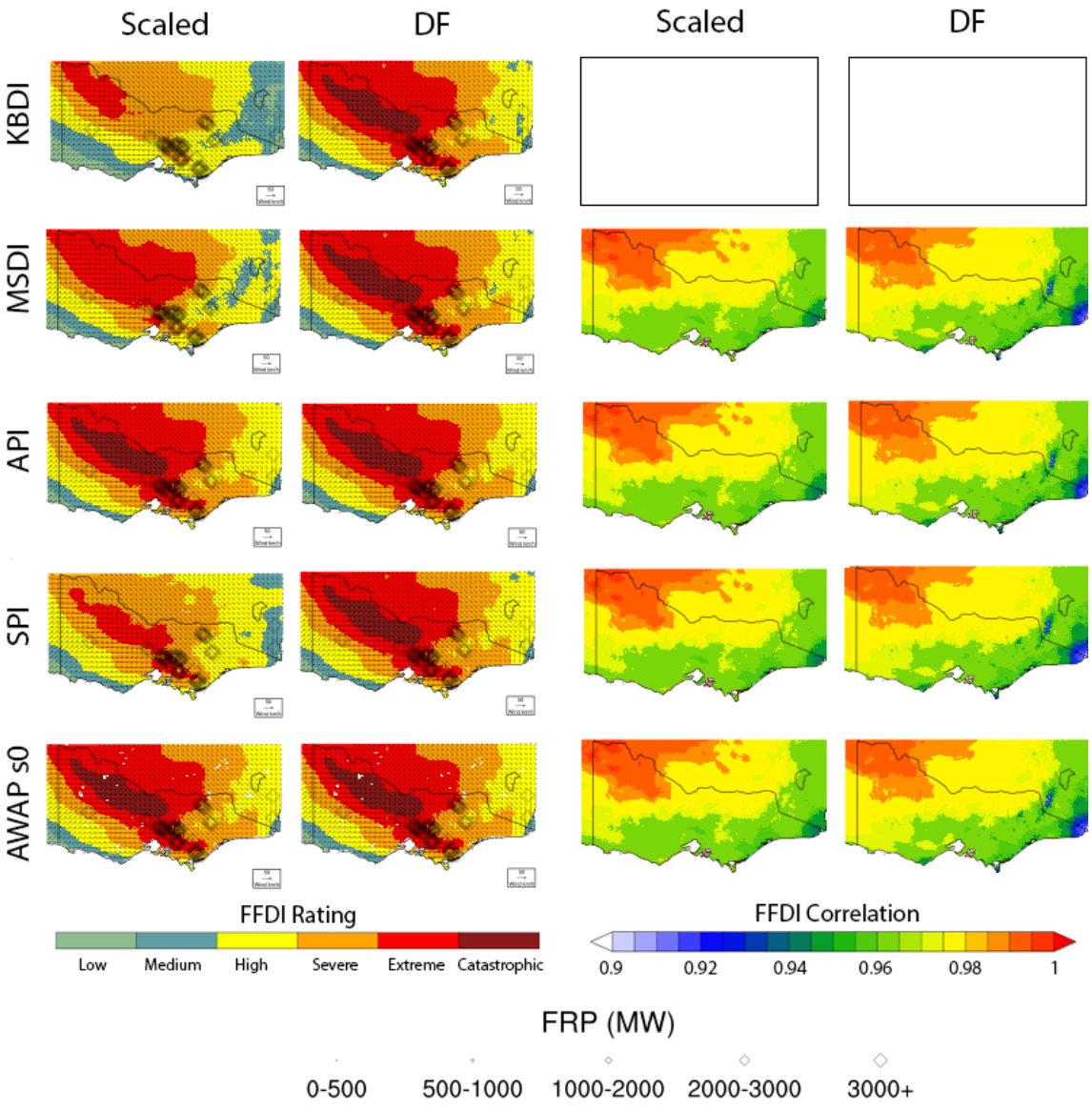

Figure 6.10: Maximum FFDI during the Black Saturday fires in Victoria on the 7th Feb 2009 calculated using API, SPI, MSDI and KBDI. Overlaid on each plot is the maximum FRP (in MW) of fires during the event with the relative size indicating the FRP scale. (a) Each moisture indices is scaled between 0-200 and replaced KBDI within the drought factor component of the FFDI. (b) Each moisture indices is scaled between 0-10 and replaces the drought factor altogether.

Similarly to Figure 6.11, Figure 6.12 presents the range of FRP values per FFDI category for each moisture index both from replacing the KBDI and from scaling to the DF. The FRP ranges are determined using the 25th and 75th percentile values in order to remove outliers in the data (due to the small number of fires at higher FFDI categories). As previously, there is little difference between the FRP ranges and FFDI categories when replacing the KBDI except for MSDI at the catastrophic category. Likewise, as before,

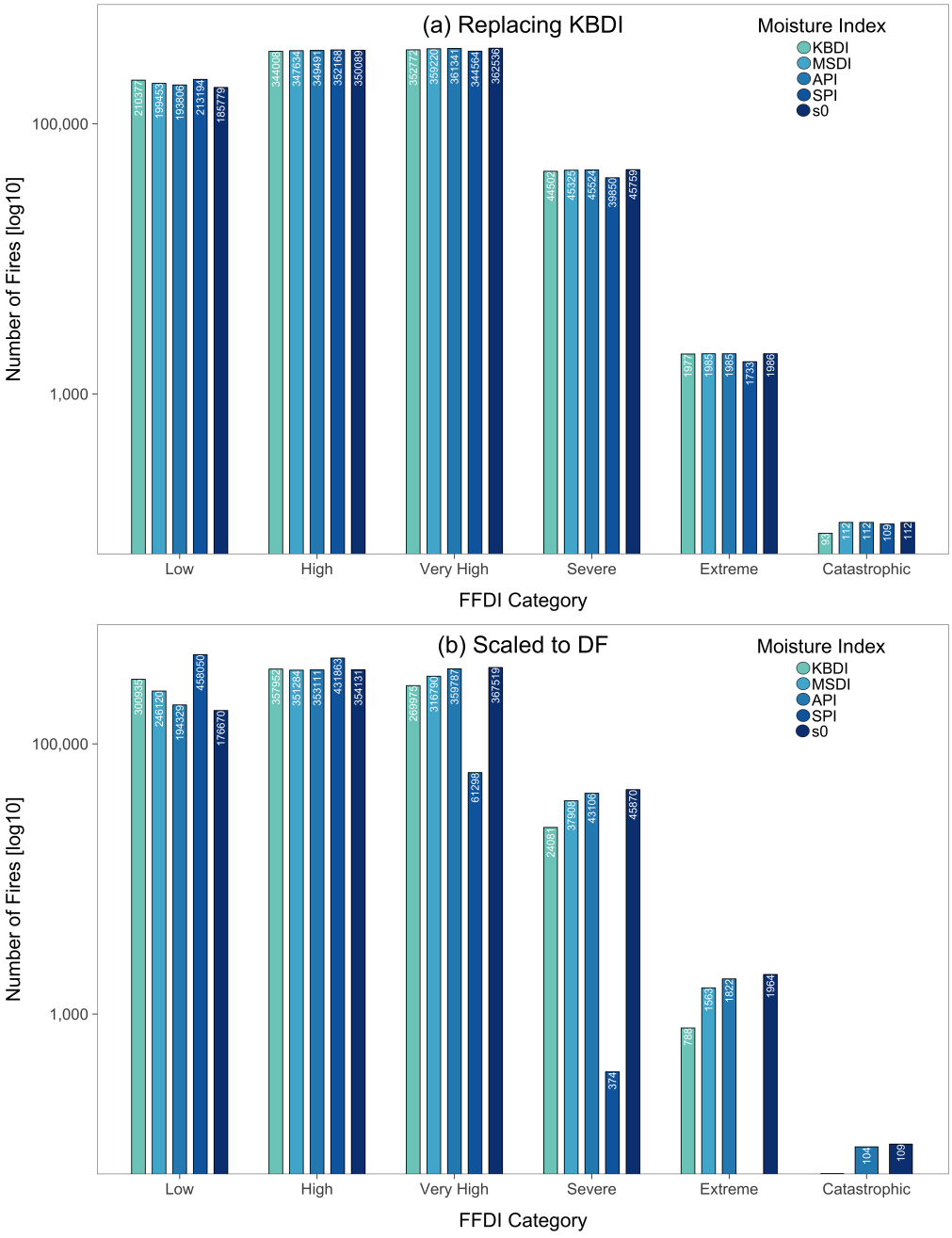

Figure 6.11: Comparison of the number of fires per FFDI category produced using each of KBDI, MSDI, API, SPI, and s0. (a) FFDI produced via replacement of the KBDI. (b) FFDI produced via scaling each moisture index to the DF itself. The y-axis uses a log base 10 scale and total counts are labelled for each index and each category. Data are for all fires in Australia between 2000 and 2015 (retrieved from MODIS).

there are much larger differences when comparing indices scaling to the drought factor. This is particularly the case for SPI. SPI consistently has a larger 75th percentile than each of the other indices with this difference increasing with increasing severity category. This increases from a factor of two to three between the severe and extreme categories, with no fires occurring at the catastrophic category for SPI. As previously, API shows the largest similarity with KBDI in all cases.

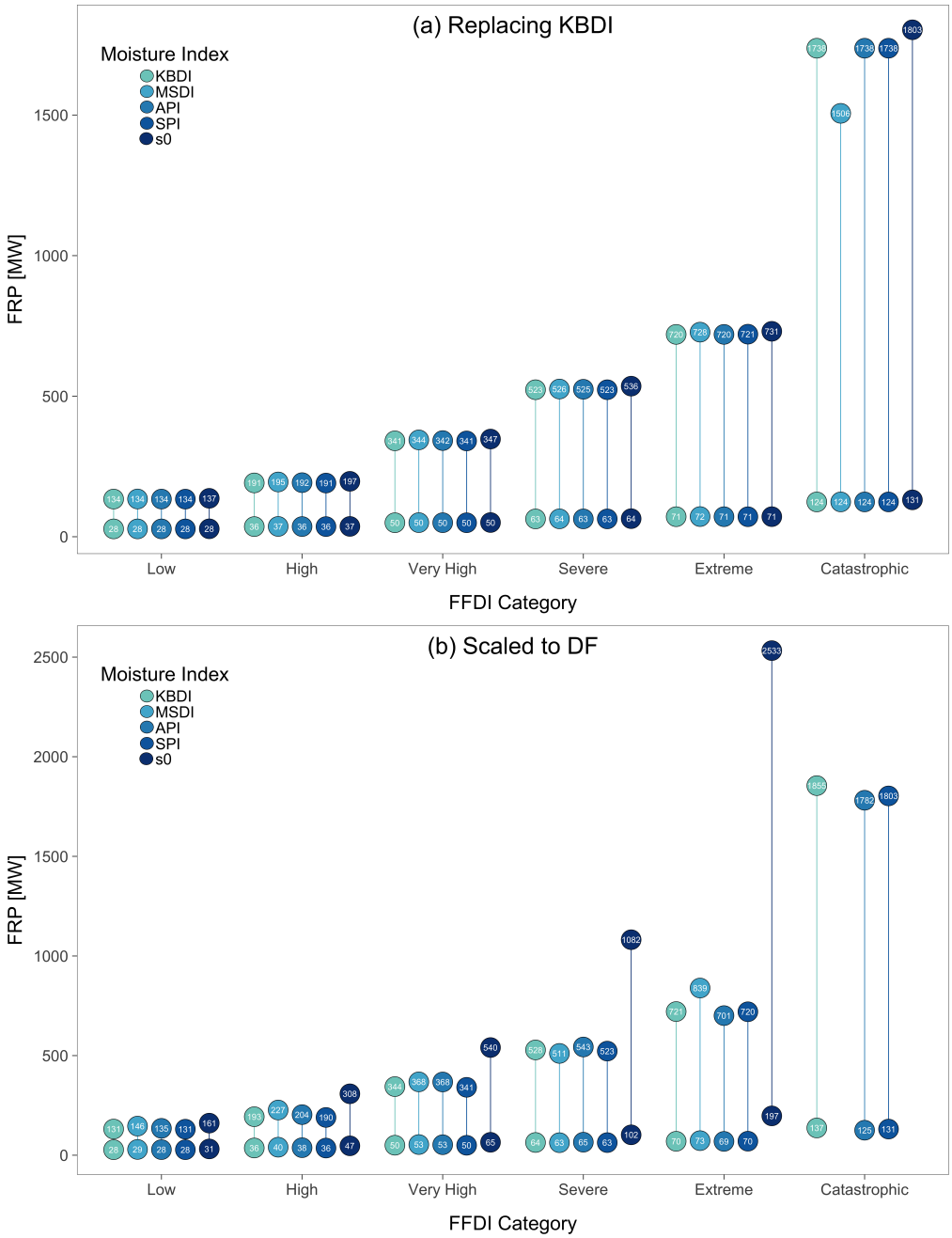

Figure 6.12: Comparison of the range in FRP (range between the 25th and 75th percentile values in FRP in MW) per FFDI category produced using each of KBDI, MSDI, API, SPI, and s0. (a) FFDI produced via replacement of the KBDI. (b) FFDI produced via scaling each moisture index to the DF itself. The 25th and 75th percentile values in FRP are labelled in the 'bell-ends' for each index and each category. Data are for all fires in Australia between 2000 and 2015 (retrieved from MODIS).

Table 6.1: Summary of the Pearson correlation coefficients between each moisture-index derived FFDI and the key components used to produce FFDI itself, as well as, FRP, and soil moisture.

Overall	FFDI	FRP	DF	Tmax	RH	Wind	pr	SM
FFDI API	0.993	0.182	0.356	0.582	-0.829	0.320	-0.139	-0.262
FFDI SPI	0.986	0.183	0.399	0.549	-0.815	0.323	-0.158	-0.308
FFD KBDI	1.000	0.182	0.407	0.588	-0.822	0.311	-0.135	-0.274
FFDI MSDI	0.997	0.182	0.376	0.583	-0.829	0.316	-0.135	-0.262
FFDI s0	0.992	0.182	0.335	0.584	-0.830	0.326	-0.134	-0.252
FFDI API Scaled	0.989	0.184	0.318	0.595	-0.836	0.324	-0.102	-0.248
FFDI SPI.scaled	0.951	0.191	0.3438	0.521	-0.817	0.336	-0.105	-0.284
FFD KBDI Scaled	0.928	0.153	0.367	0.642	-0.744	0.249	-0.060	-0.233
FFDI MSDI. Scaled	0.976	0.183	0.335	0.610	-0.808	0.291	-0.067	-0.228
FFDI s0 Scaled	0.980	0.184	0.255	0.601	-0.839	0.328	-0.073	-0.213
Temperate	FFDI	FRP	DF	Tmax	RH	Wind	pr	SM
FFDI API	0.979	0.171	0.405	0.664	-0.802	0.262	-0.114	-0.220
FFDI SPI	0.981	0.179	0.449	0.630	-0.784	0.257	-0.121	-0.259
FFDI KBDI	1.000	0.171	0.499	0.660	-0.779	0.235	-0.111	-0.240
FFDI MSDI	0.988	0.168	0.438	0.664	-0.800	0.251	-0.112	-0.221
FFDI s0	0.976	0.171	0.376	0.670	-0.809	0.266	-0.111	-0.205
FFDI API Scaled	0.976	0.172	0.377	0.685	-0.809	0.262	-0.085	-0.207
FFDI SPI Scaled	0.925	0.210	0.378	0.585	-0.751	0.263	-0.073	-0.238
FFDI KBDI Scaled	0.906	0.135	0.452	0.663	-0.691	0.182	-0.047	-0.163
FFDI MSDI Scaled	0.958	0.141	0.4016	0.691	-0.782	0.224	-0.054	-0.159
FFDI s0 Scaled	0.954	0.171	0.285	0.697	-0.821	0.273	-0.061	-0.162

Finally, these results are summarised in Table 6.1. This presents the Pearson correlation coefficients between each of the two FFDI methods for each index and KBDI-derived FFDI. Also shown are the correlation coefficients with the FRP, the drought factor, the maximum temperature, relative humidity, wind speed, precipitation, and soil moisture. The results observed previously are confirmed with very high correlation coefficients between each of the FFDI's and the original KBDI-derived FFDI. This is particularly strong for API which have coefficients of 0.993 and 0.989 (for all fires) for replaced and scaled, respectively. The KBDI has the lowest correlation of all the moisture indices when scaled to the drought factor at 0.928. This is exacerbated when comparing correlation coefficients for fires in only the temperate regime dropping to 0.906. Despite this correlations are still extremely high suggesting that there is little difference in what moisture index is used for producing the drought factor whether it be through direct substitution or by scaling to the drought factor.

As identified in Section 6.3.2, the FFDI is the most sensitive to changes in temperature,

drought factor, and in particular, relative humidity. Correlation coefficients are between -0.839 and -0.691 for relative humidity, whilst for temperature, they are between 0.697 and 0.521, and for the drought factor between 0.285 and 0.499. Correlation coefficients are far lower for FRP with values between 0.210 and 0.135. However, the relationship between the moisture indices and FRP are not directly related to the FFDI and are analysed further in the following section. On top of this, as mentioned in Chapter 2, the location of fires and the consequent FRP are also influenced by the ignition source, fuel load, and other mechanisms. As expected from the energy and moisture partitioning in Chapter 5, the strength of the correlation between FFDI and the drought factor stronger than the other FFDI components at locations within the transitional zone (by extension the temperate regime).

6.3.6 Changes in Soil Moisture Conditions

As mentioned previously, the relationship between FRP and soil moisture has not yet been studied. However, the preconditions leading to fires including soil moisture can have a large influence on the location and severity of fires. Through the previous sections and chapters, it has been established that deficits in moisture can lead to exacerbated temperatures and promote conditions for more intense fires. Therefore the relationship between API, SPI, KBDI, MSDI, and s0 and FRP (fire intensity) are shown in Figure 6.13. This displays normalised soil moisture values versus FRP from all fires in Australia between 2000 and 2015 (retrieved from MODIS). Each colour in Figure 6.13 represents the Köppen-Geiger climate regimes and the size of each point indicates the relative severity category in the FFDI. Also shown are the density distributions for both the x-axis and y-axis margins.

For API and s0 there is a clear logarithmic relationship between a decrease in moisture and an increase in FRP. This relationship is particularly strong in s0 with almost all fires occurring with a normalised soil moisture value of less than 0.5. Whilst similar in shape, the relationship in API is less pronounced. However, in either case, the distribution of fires occurs tending almost entirely to zero. This is in contrast to KBDI, which has been previously been shown to include a strong wet bias. The KBDI has an almost linearly decreasing moisture content with increasing FRP and a distribution more evenly spread throughout values, albeit skewed towards dry conditions. Interestingly, the MSDI shares similarities between both API, and s0 and KBDI. For MSDI there is a far less pronounced logarithmic relationship, particularly in the temperate regime, with a peak in the semi-arid regime at about 0.2, otherwise, with other regimes, this tends to zero. Due to the formulation of SPI (a fitted gamma distribution to the time series of rainfall), SPI observes

a gamma/normal distribution of fires with FRP slightly shifted to dry conditions. This is the clearest in both the semi-arid and the temperate regimes where there is a stronger shift to dry conditions.

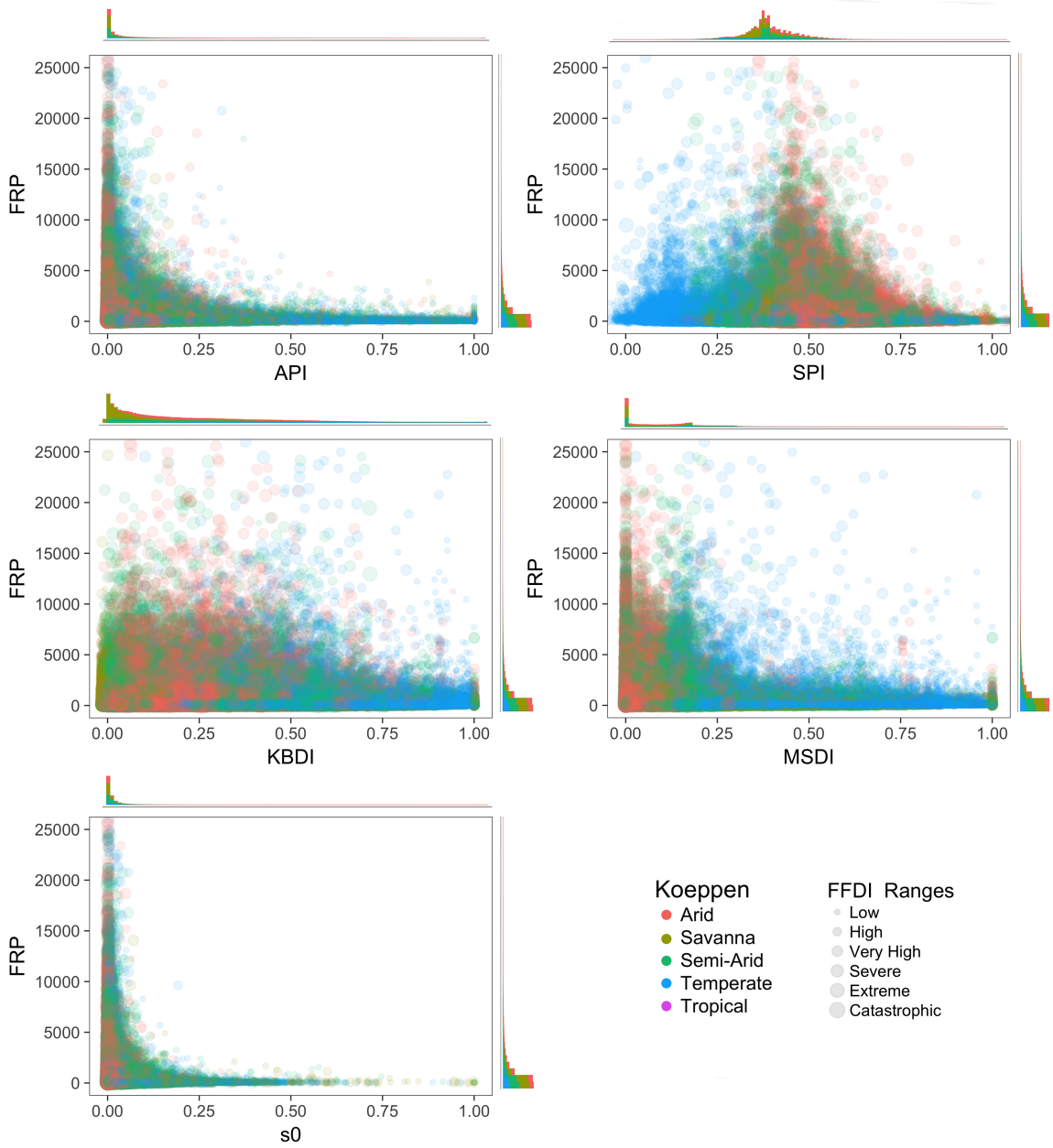

Figure 6.13: Normalised API, SPI, KBDI, MSDI, and s0 versus FRP (MW) for all fires in Australia between 2000 and 2015 (retrieved from MODIS). Each colour represents the Köppen-Geiger climate regimes and the size of each point indicates the relative severity category in the FFDI. Also shown are the density distributions for both the x-axis and y-axis margins.

For SPI there is a substantial difference in moisture between regimes in comparison to the other indices. Generally, observations are very similar throughout each climate regime with noticeable differences in the tropical (and to a lesser extent, temperate) regime due to the smaller overall number of fires. The differences between regimes are more clearly identified in Figure B.2 and Figure B.3. Also shown in Figure 6.13 are the FFDI severity

categories relative to increasing size. Generally, the higher severity categories are occurring at a low moisture content and at higher FRP values. This is most pronounced for API, s0, and MSDI whereas there is an even spread for all moisture and FRP values for SPI and KBDI. This is in agreement with the results of the previous sections and chapters.

6.4 Discussion

This chapter investigated the change in FFDI and FRP across Australia in relation to the temporal variation seasonally as well as the sensitivity of the input variables used to calculate the FFDI and how it is related to both FRP and the moisture indices introduced in Chapter 4. Typically, in Australia, an increase in fire danger is associated with high temperatures and strong winds (Cheney et al., 1994; Mills, 2005). This coupled with a deficit in soil and vegetation moisture can lead to the drying of vegetation causing a greater fuel load and lead to higher FRP fires (Chaparro et al., 2016; Hudak et al., 2016; Chaparro et al., 2017).

Due to this, the seasonality of fires was investigated by identifying the month and season of maximum FFDI and FRP across Australia, relative to their respective Köppen-Geiger climate regimes. This is similar to the work of Oliveira et al. (2015), which detected the seasonal differences in fire activity and intensity in tropical savannas of northern Australia. Similar to Oliveira et al. (2015), the seasonality of fire severity and burn area has been extensively studied for the tropical savannas of northern Australia (Williams et al., 1998; Russell-Smith et al., 2003a; Russell-Smith et al., 2006; Harris et al., 2008). Despite the spatial variation in changes in the fire season being investigated in Australia (Dowdy et al., 2009; Murphy et al., 2013) as well as their link to known monthly and seasonal trends in maximum daily temperature across Australia (Jones et al., 2000) seldom has the seasonality of FFDI nor FRP been investigated across Australia.

The results in this chapter indicate that fire activity was typically the largest throughout the northern Australia region particularly in the Northern Territory in the tropical savannas. This occurred during the late dry season (SON) with the higher FRP fires also occurring during this period. This also coincided with the maximum positive difference in FFDI compared to previous seasons. This is in agreement to Oliveira et al. (2015), which also indicated that for the Northern Territory median FRP was lower for early dry season fires (29 MW on average) than late dry season fires (56 MW) and that this was positively correlated with fire occurrence. This trend was similarly noticed spatially across Australia and throughout each climate regime. The season of the maximum FRP generally coincided with both maximum fire occurrence and maximum FFDI, although

lagging by approximately one month. For the temperate/transitional regimes, this occurred in February-April, whereas the maximum FFDI occurred in January. Overall the change in maximum FFDI shifts from the far north-west in July, then southward through September and October, eventually spanning the southern third portion of the continent by January. As mentioned in Chapter 2, the FRP is heavily influenced by the fuel and burn characteristics. Due to this, as the dry season (lowest relative humidity on average) progresses, fuel moisture decreases promoting fire activity and more intense fires (Key et al., 2006; Keeley, 2009; Chaparro et al., 2016; Hudak et al., 2016; Chaparro et al., 2017). Fire activity occurs throughout the year, also during the wet season. However, these occur at lower FFDI and FRP than in warmer conditions and are typically ignited by lightning strikes 'forcing' a fire to occur (Russell-Smith et al., 2003b). As the vegetation composition is largely made up of grassland in the tropical savanna (Russell-Smith et al., 2003a), the largest FRP fires occur in the temperate/transitional regime, particularly in alpine south-east Australia. However, these are typically characterised as having very few fires per year compared to the north of the country.

Following this, the sensitivity of the resultant FFDI to each input parameter was also assessed. It was found that generally across Australia, the FFDI is dominated by changes in the relative humidity. However, there is a large spatial variation in the sensitivity of parameters across Australia. This is particularly noticed in the south-east of Australia, in which changes in the FFDI are affected equally by changes in the drought factor and the relative humidity. This coincides with the temperate/transition zone, where it is expected that changes in soil moisture will significantly affect the energy partitioning of the region, as identified in Chapter 5. This is in contrast to (Dowdy et al., 2009), which found that the FFDI is most sensitive firstly to wind speed, then secondly to relative humidity and then thirdly to temperature. However, (Dowdy et al., 2009) also indicate that the FFDI is more sensitive to temperature and relative humidity, and less sensitive to wind speed, than other fire danger products. Furthermore, these sensitivities were produced using case studies from fires at six locations with distinct climate characteristics as opposed to spatially across Australia. Beyond this, as previously mentioned, the sensitivity of the FFDI to soil moisture is intrinsically limited by the drought factor. i.e. in regions with low average annual precipitation with infrequent events, the drought factor is often near maximum, meaning that changes in the drought factor in these regions will have a limited effect on the resultant FFDI.

Despite the differences to previous studies, the results shown here also indicate that there are large discrepancies between categorical classification at low and high index values when adjusting the input variable. This is in agreement with (Harris et al., 2011) and (Dowdy et al., 2009), who suggested that the current FFDI performed poorly when as-

sessing high-risk fires. This is highlighted when using various moisture indices to drive the drought factor. Both the SPI and s0 observe stark differences from the KBDI-derived FFDI at both the lowest and highest FFDI categories, in particular when scaling to the drought factor.

Finally, by substituting the KBDI with the API in the drought factor, the formulation of the FFDI is simplified greatly, requiring only temperature and precipitation (unlike studies that further add to the complexity of the FFDI, such as; Griffiths, 1998; Snyder et al., 2006). Beyond this, by using the API, the drought factor provides both a physical relationship with soil moisture, as well as providing a more direct response to daily variations in precipitation (as suggested by; Petros et al., 2011, and indicated in Chapter 4). This is in agreement with Liu et al. (2003), in which the exploratory analysis indicated that API suitably represented the role of precipitation or soil moisture in the FFDI. Results indicate that the API-derived FFDI (using an updated API compared to Liu et al. (2003)) has higher correlation coefficients than that of Liu et al. (2003) for maximum temperature, relative humidity, wind speed, and the drought factor. This indicates that not only is API a viable representation for soil moisture in the FFDI but that through the recent re-formulation of the API this has been improved upon. Furthermore, here, results indicate that despite the relatively small positive correlation between FFDI and FRP, there is a strong logarithmic relationship between decreasing moisture and increasing FRP. This logarithmic relationship occurs for API, MSDI, and the AWAP-derived s0.

Alternatively, results similarly show that the MSDI could also be used to represent soil moisture. However, not as directly related to antecedent conditions as the API, the MSDI allows for expressing the drought factor as a function of potential evapotranspiration (suggested as a requirement by; Petros et al., 2011) and is also simpler to produce that KBDI. Regardless which is used, both are simple to initialise at maximum moisture and provide evidence that they could be used to provide a physical relationship to the likely intensity of fire represented by FRP. Unlike previous studies (Sharples et al., 2009), the intention of this chapter is not to provide a complete overhaul of the FFDI system, but to provide fire managers with an accurate more physically related moisture component, that also provides information on the likelihood of the intensity of a fire. In doing so, a seamless transition between the currently used KBDI and API can be achieved operationally with minimal disruption.

Chapter Summary

Following Chapter 5, the precursory weather conditions leading to forest fire and its relative intensity in the form of FRP were investigated in this chapter. This was considered in relation to the previously established relationship between soil moisture and temperature extremes both spatially for Australia and specifically for the devastating Black Saturday fires. Typically, the FFDI varies temporally with the fire season shifting from north in the June/July months, progressively further south through SON, then to the south-east in DJF and the south-west later in the DJF season. This was similar to previous studies, however, unlike previously, the seasonality of maximum FFDI does not necessarily coincide with either the month of the maximum number of fires nor with the maximum FRP. Generally, both the number of fires and the FRP occurred succeeding the month of the maximum FFDI, with FRP lagging both marginally. Beyond this, the largest FRP fires occur in the temperate/transitional regime further underpinning the effect of soil moisture on temperature and relative humidity in these regions. This is also highlighted by the strong logarithmic relationship between a decrease in MSDI, API, and s0 and an increase in FRP, particularly in the temperate/transitional regime. Following this, the moisture indices were substituted in place of the KBDI and the DF within the FFDI calculation to determine the difference, if any, in the resultant FFDI. It was found that there was little difference in the resultant FFDI, particularly with API suggesting that the current formulation of FFDI is unnecessarily complex and replacing the drought factor with API would suffice. Consequently, the following chapter investigates the historical and projected changes in FFDI for various climate change scenarios, uses an API driven drought factor to produce FFDI.

CHAPTER 7

FFDI in a Changing Climate

Overview This chapter investigates historical and projected future changes in FFDI (scaling API to the drought factor component) and its components for Australia between 1979 and 2100. More specifically, historical CMIP5 model data used to derive FFDI are compared against historical AWAP-produced FFDI. Projections of two CMIP5 forcing pathways, namely, the RCP 4.5 (medium climate change forcing) and RCP 8.5 (high climate change forcing) pathways are also compared against each other. An ensemble of simulations from six global climate models each with a minimum of three simulations is analysed, resulting in 29 members for each forcing pathway. Anomalies in cumulative FFDI are assessed both on the seasonal and annual scale for the various climate regimes across Australia.

7.1 Introduction

Vast regions of Australia suffer from a large number of forest fires and are generally considered as some of the most fire-prone regions in the world (Hennessy et al., 2005). Therefore, understanding the mechanisms behind forest fires and quantifying their risk and scale are essential for mitigating their potential socio-economic damage. Forest fires are often linked to precipitation deficits, extreme temperature, increased wind speed, low fuel moisture, and as demonstrated in Chapter 6, soil moisture.

As discussed in Chapter 6, the relationship between forest fires and atmospheric conditions is relatively well understood (Pereira et al., 2005; Trigo et al., 2006; Potter, 2012). In particular, fire conditions can be heavily exacerbated due to changes in synoptic weather conditions, in particular, wind direction and speed. If fronts extend through the troposphere, high wind speeds ahead of cold fronts can be sustained through the front, often resulting in a strong change in wind direction causing a developing fire front to increase in size (Cheney et al., 1994; Turner et al., 1994). As projections of synoptic weather patterns have a relatively high uncertainty, the associated changes in fire danger are less well-studied (Clarke et al., 2011; Grose et al., 2014). However, changes in temperature and relative humidity are more accurately projected and in Australia are typically associated with changes in fire danger (defined here using FFDI). As introduced in Chapter 5, deficits in soil moisture are strongly related to an increase in temperature extremes and in the number of hot days. This can, in turn, exacerbate the aforementioned conditions, leading to a higher fire danger, as well as being directly related to an increase in fire intensity (quantified through FRP) as investigated in Chapter 6.

Fire risk is not only related to changes in synoptic weather conditions, but also to changes in the climate system as a whole (Hennessy et al., 2005). As the Earth's climate changes due to anthropogenic forcing (Charlson et al., 1992), it is expected that an increasing number of temperature extremes, precipitation deficits, and consequently the parameters associated with high fire risk will occur. Each is projected to change significantly in the future (Sherwood et al., 2010; Dai, 2013; Wang et al., 2013; Gibson et al., 2017b). It has been identified that in both observations and model simulations, that the spatial patterns and magnitude of changes in temperature extremes and precipitation differ between global and regional scales (Donat et al., 2017). Specifically, Seneviratne et al. (2016) used ensemble means of CMIP5 projections to show that changes in regional temperature extremes can differ significantly from the global mean. Partly, these regional increases in hot extremes have been identified as a result of the land-atmosphere feedbacks which amplify aridity over land (Berg et al., 2016). This is particularly the case with feedbacks of projected soil moisture decreases on land surface temperature, relative humidity, and

precipitation (Berg et al., 2016). This has also been identified by Seneviratne et al. (2013) using GLACE-CMIP5 projections, where projected soil moisture changes were found to substantially amplify temperature extremes in several regions in both boreal and austral summer. Therefore, it is essential to investigate regional differences in hot extremes, relative humidity, and precipitation deficits associated with an increase in fire risk and danger.

As mentioned in Chapter 2, several studies have investigated projected fire danger through the 21st century both globally and regionally (Liu et al., 2010; Flannigan et al., 2013; Stocks et al., 1998; Brown et al., 2004; Wotton et al., 2010) with Clarke et al. (2012), Hennessy et al. (2005), Pitman et al. (2007), and Clarke et al. (2011) investigating changes in the FFDI using GCM and RCMs across various locations in Australia. In each case, these studies have so far focused on a specific region within Australia or using data from local stations for comparisons across various climates within Australia and either looks into historical changes or future projects but not both consistently. Whilst there are global studies indicating the overall changes in fire danger for Australia, FFDI itself, which is used operationally, has yet to be studied using an ensemble of GCM's and RCM's. This shortcoming will be addressed in this chapter which assesses the changes in past and future projections of FFDI, for Australia between 1979 and 2100 using climate model simulations under the RCP 4.5 (medium climate change forcing) and RCP 8.5 (high climate change forcing) pathways from six modelling centres participating in the CMIP5 project. Cumulative FFDI produced from CMIP5 projections, as well as cumulative totals and means of its input variables, are compared against AWAP-derived FFDI and FRP. These are assessed both on the seasonal and annual scale for the different climate regimes across Australia.

Likewise, whilst various studies have compared historical changes in FFDI (Clarke et al., 2012), and projected changes in FFDI on a regional scale (Pitman et al., 2007; Fox-Hughes et al., 2014), this chapter addresses changes in fire danger, using a simple API-driven FFDI in the context of the spatial variability across Australia, as well as with the previously established relationship between soil moisture deficits, the number of hot days, and FRP (derived from MODIS). Furthermore, the accuracy of the ensemble mean projected FFDI is improved over previous studies by increasing the number of ensemble members, further reducing intrinsic biases from any particular model.

7.2 Data and Methodology

7.2.1 Fire Danger Index (FFDI)

The McArthur Forest Fire Danger Index as defined in Chapter 3 is produced here using monthly mean maximum temperature (C°), monthly mean wind speed ($km\,h^{-1}$), monthly mean relative humidity ($RH\%$), and the monthly mean Drought Factor (DF). The DF is typically driven by KBDI, however, as it was determined in Chapter 6 that API provides an accurate estimate for the DF, the FFDI is calculated using the monthly mean API. The API is scaled to between 0 and 10 to match the range of the DF, where 0 indicates minimum drought conditions and 10 indicates maximum drought conditions. Cumulative yearly FFDI and precipitation are calculated to reduce the seasonality of monthly totals, as is the yearly mean maximum temperature, the mean relative humidity and the mean yearly wind speed. Anomalies are relative to the 1979 to 2005 base period and are described as a percentage per year change (anomaly). It should be noted that in this chapter, the term "extreme" FFDI days does not refer to the"extreme" FFDI category.

7.2.2 CMIP5

Daily and monthly climate data for Australia of maximum temperature, mean surface wind speed, average surface relative humidity and total precipitation were retrieved from the World Climate Research Program's (WCRP) Coupled Model Intercomparison Project Phase 5 (CMIP5) multi-model dataset. Historical data between 1979 and 2005 as well as projected data from 2006 to 2100 were used to calculated FFDI as defined below. From the five main Representative Concentration Pathways (RCPs), the historical, RCP-4.5 (monthly only), and RCP-8.5 pathways were chosen as these represent the moderate and high anthropogenic radiative forcing scenarios.

For the purpose of this study six monthly GCM's, NCAR's CCSM4, NSF-DOE-NCAR's CESM1-CAM5, CSIRO-QCCCE's CSIRO-Mk3-6-0, MOHC's HadGEM2-ES, NASA-GISS's GISS-E2-H and MIROC's MIROC5 were used as these have smallest difference from the ensemble mean RMSE (ensemble of all available CMIP5 models) in key variables such as rainfall across Australia (Moise et al., 2015, for further details on CMIP5, refer to Chapter 3.2.3). Similarly, for the daily RCM's these were, the two CSIRO-BOM ACCESS models, UMR-CNRM's CNRM-CM5, NOAA-GFDL's GFDL-ESM2G and MIROC's MIROC5 model.

As FFDI is validated against fire occurrences which are available at 500 m resolution, the

spatial variation in FFDI at the regional scale is of interest. Models were selected that have a high spatial resolution and provide temperature, precipitation, relative humidity, and the u and v wind components and a minimum of three ensemble members per historical (for monthly), RCP-4.5 (monthly), and RCP-8.5 pathways. This resulted in 29 ensemble members from the six CMIP5 models per pathway for monthly data, and six models for historical and RCP-8.5 pathways for daily data (see Table 7.1). One caveat of daily CMIP5 data is the limited availability of both simulations and pathways. Access was limited to only one simulation per model and only the historical and RCP-8.5 pathways. However, the spatial resolution of each RCM is much higher than that of the GCM's and provides for a better comparison of local trends against the AWAP FFDI product. The FFDI is calculated under the assumption that the drought factor can be substituted with the simpler Antecedent Precipitation Index (API), requiring only precipitation and maximum temperature and is further detailed below. An overview of the models and their resolution is available in Table 7.1. A full list of the models and providers is available through the CMIP5 online portal (http://cmip-pcmdi.llnl.gov/cmip5/availability.html).

Table 7.1: List of models and number of ensemble members per scenario used in this study. Resolution in pixels, globally (GCMs) and Australia (RCMs).

Center	Model	Scale	Res	Hist	RCP 4.5	RCP 8.5
NCAR	CCSM4	Global	288x192	3	3	3
NSF-DOE-NCAR	CESM1-CAM5	Global	288x192	3	3	3
CSIRO-QCCCE	CSIRO-Mk3-6-0	Global	192x96	10	10	10
MOHC	HadGEM2-ES	Global	192x145	4	4	4
NASA-GISS	GISS-E2-H	Global	144x90	6	6	6
MIROC	MIROC5	Global	256x128	3	3	3
CSIRO-BOM	ACCESS1-3	Regional	145x192	1	0	1
CSIRO-BOM	ACCESS1-3	Regional	145x192	1	0	1
UMR-CNRM	CNRM-CM5	Regional	256x128	1	0	1
NOA A-GFDL	GFDL-ESM2G	Regional	144x90	1	0	1
MIROC	MIROC5	Regional	256x128	1	0	1

7.2.3 Regions

Unlike previous chapters, regions to be compared are defined based on the two regions of Australia with the highest fire occurrences and intensities. Northern Australia and south-eastern Australia are defined using the bounds of $10°S - 25°S, 120°E - 145°E$, and $45°S - 25°S, 135°E - 155°E$, respectively. As these are regions with seasonal fire occurrence, spatial averages have been produced using their respective fire seasons. i.e. for south-eastern Australia, this is DJF or the austral summer period and for northern Australia, this is the JJA, austral winter period.

7.3 Results

7.3.1 Historical and Seasonal Trends in FFDI between 1979 & 2015

The seasonal variation of fire activity has previously been proposed and maps of Australia indicating these variations have been produced by many sources including the Bureau of Meteorology and CSIRO (http://media.bom.gov.au/social/blog/50/australias-

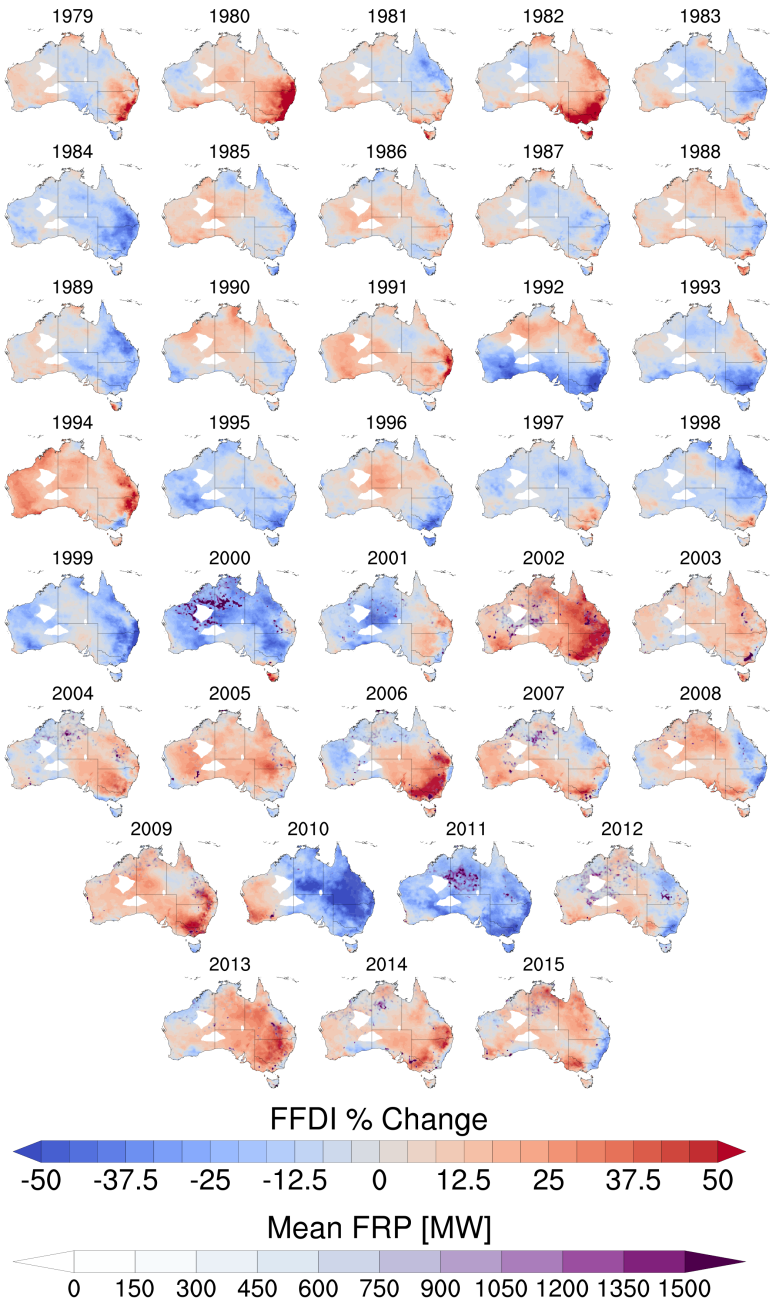

Figure 7.1: Percentage change (anomaly) in cumulative yearly FFDI compared with the 1979-2005 baseline. Mean Fire Radiative Power for the total yearly MODIS derived fire hotspots are also displayed as density contours (purple scale) between 2000 and 2015.

bushfire-seasons/ & Murphy et al., 2013). However, these have been seldom referenced in terms of the shift in FFDI, nor has MODIS been used to validate the observed fire occurrences. Leading on from Chapter 6, the change in FFDI over time has been investigated both with a decadal and seasonal context and referenced against FRP and fire occurrence. Figure 7.1, shows the time series of cumulative yearly AWAP derived FFDI as a percentage change (anomaly) compared to the 1979-2005 mean.

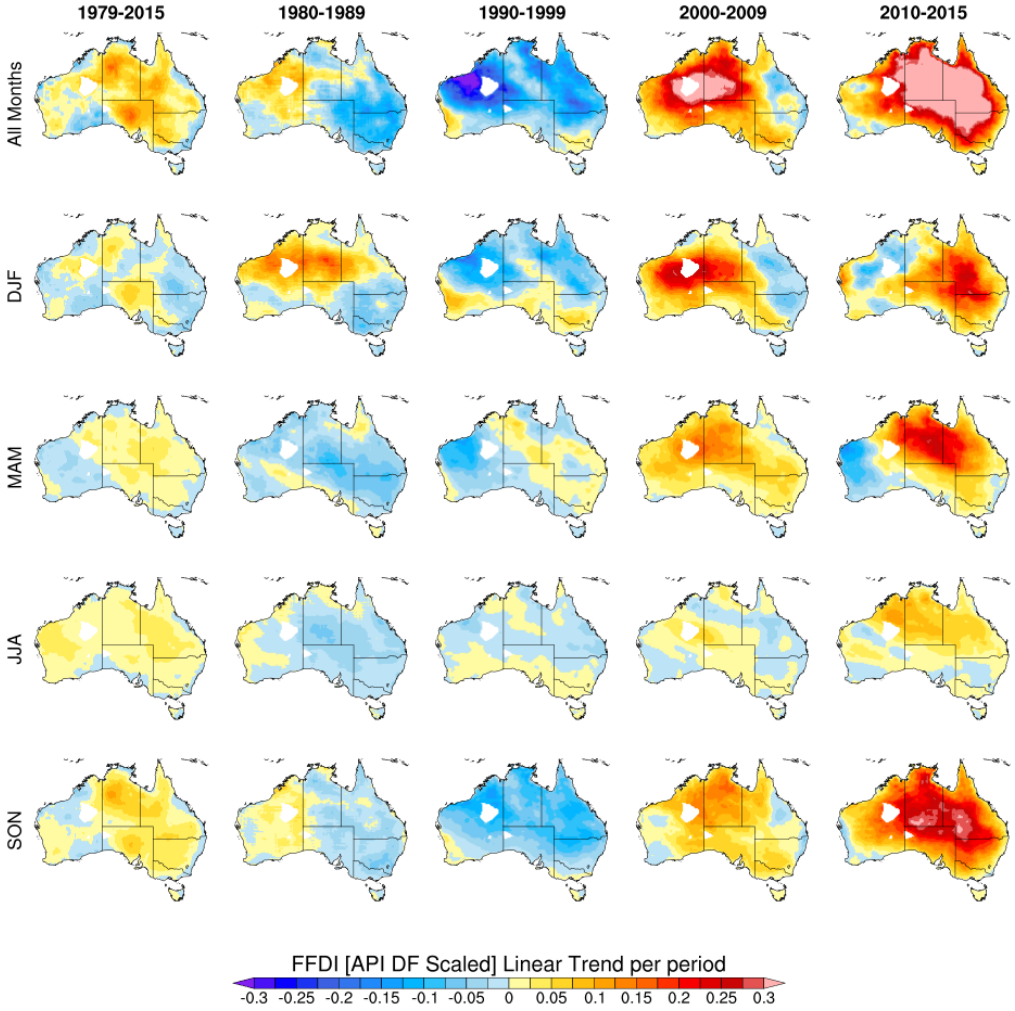

Figure 7.2: Decadal and seasonal FFDI trend for Australia for DJF, MAM, JJA, SON and 1980-1989, 1990-1999, 2000-2009, 2010-, as well as the overall trend between the period 1979-2015. The mean climatology has been subtracted for each period.

Overlaid on top of this are the mean FRP and the total yearly fire occurrences. Here we can see that there are distinct periods of positive and negative anomaly across the time series spatially. The most distinct period of warming occurs between 2002 to 2015 across Australia with the exception of 2010 and 2011, prior to this, differences are inter-annual with trends seldom lasting longer than one to four years. South-eastern Australia experiences the largest positive anomaly between 1979 to 1982 and in 2002, 2006 and 2009.

These years coincide with significant fire activity, particularly the Black Saturday fires in 2009, the 'Ash Wednesday fires' in 1983 (1979-1982 conditions culminated in exacerbated conditions leading into 1982) and the 'Great Divides' fires in 2006. Conversely, a large concentration of high-intensity fires is located in central Australia coinciding with periods of large negative anomalies, in 2000 and 2011. This may be due to the mechanisms explained in Chapter 6, in which, a lower FFDI is driven by a higher soil moisture assists in vegetation growth leading to a higher fuel load, and more intense fires during the JJA northern fire season.

Following this, the FFDI has been computed for the entire ERA-Interim period available, 1979-2015. From this, the seasonal and decadal trend has been calculated with the climatology removed (to remove the seasonal cycle). Figure 7.2 displays this for each season and the decadal periods 1980-1989, 1900-1999, 2000-2009, 2010-, as well as for the total trend. All trends are given per period. The trend for the 1979-2015 period is also given in Figure 7.3, however, this shows both the time series and maps for the trend in the JJA (northern Australia) and DJF (south-eastern Australia) seasons/regions, as well as, overall. It is seen that in Figure 7.3 the FFDI is generally increasing for the entire period and throughout each season of the year, almost evenly. This is particularly the case for the millennial period, which observes very strong trends, this period coincides with the 'Millennial Drought' which exacerbated FFDI conditions considerably. Despite this, there is a small negative trend in the Queensland hinterland, most noticeably, in DJF. The opposite is seen during the 1990's decade, which observes large negative trends, most noticeably in the north of the continent with little to no trend is seen in the 1980's apart from in the north-west of Australia in DJF.

Interestingly, large portions of coastal Australia observes a negative trend in FFDI overall, with Broome and coastal NSW showing particularly strong trends. When breaking this up into seasonal trends, the spring period has the largest positive trend which accounts for the majority of the overall observed tend, whilst to a far lesser degree, both DJF and MAM show a mixture of positive and negative trends. During the WA fire season (as established previously), in autumn, almost the entire state observes a decreasing trend in the FFDI, particularly, during the 1990's and the 2010-2015 period.

These trends are further examined in Figure 7.3. Here, the percentage change (compared to the 1979-2005 base period; anomaly) of cumulative FFDI between 1979 and 2015 are averaged for all months, DJF months and JJA months. The most prominent fire occurrences and differential in FFDI occur in the north of Australia in JJA and in the south-east of Australia in DJF (Figure 6.6; Murphy et al., 2013), due to this averages are calculated using DJF and JJA months, from the south-east and northern Australia regions, respec-

tively. This confirms the patterns seen from Figure 7.2 in which in the 1980's and 1990's there are small negative trends with the post-millennial period observing an increase in FFDI. This is partly due to the limited scope of the base period, i.e. only a 26 year period spanning the beginning of the time-series. Interestingly, the overall FFDI trend for DJF has a slightly negative trend of 0.114% per year compared to the JJA period of positive

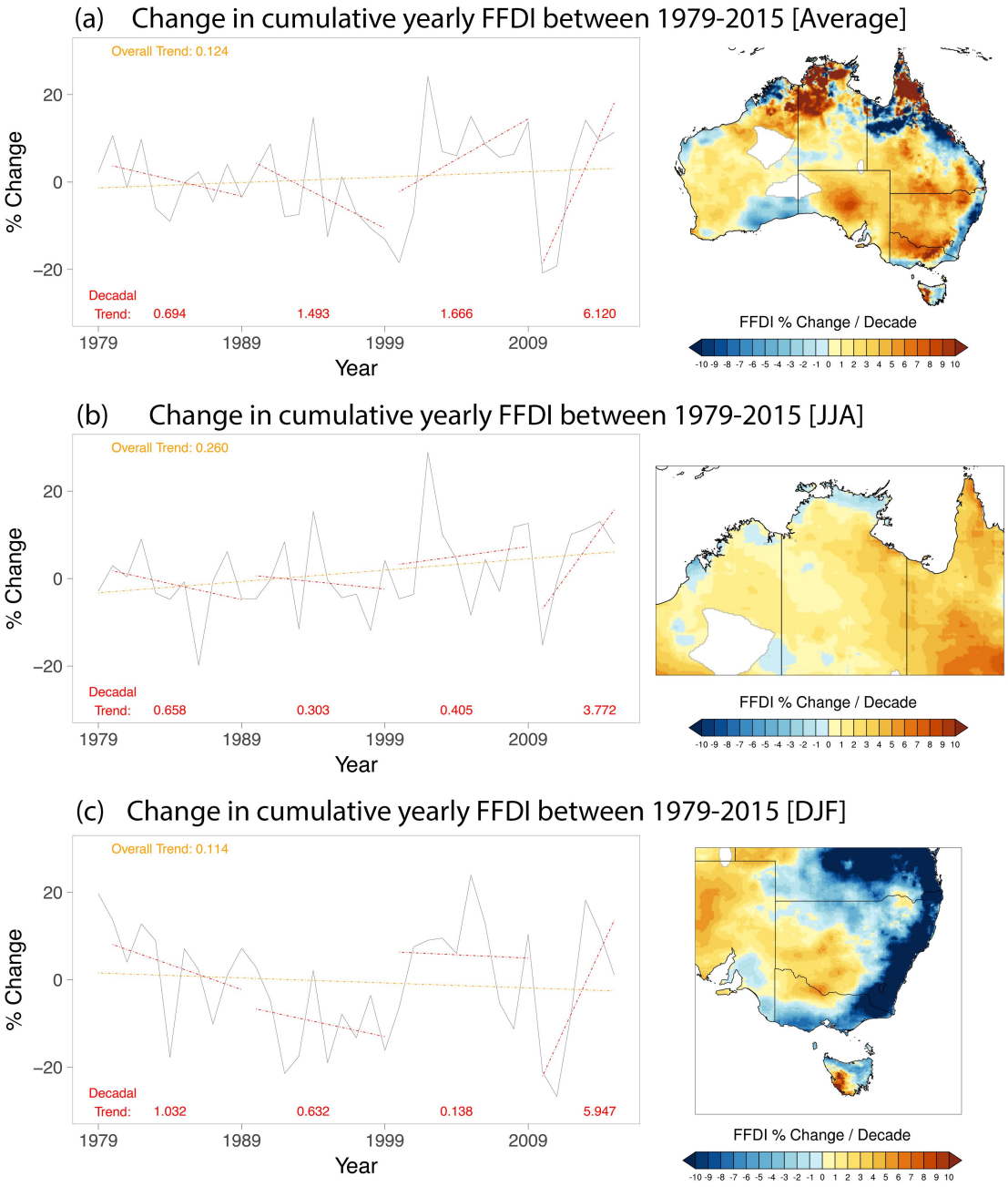

Figure 7.3: Percentage change (compared to the 1979-2005 base period; anomaly) in yearly FFDI between 1979-2015 averaged across Australia for all months (a), averaged across northern Australia for JJA months (b), and averaged across south-eastern Australia for DJF months (c). FFDI are derived from AWAP observations (black line). Also shown are the overall (dashed orange line), and decadal (dashed red line) trends. Trend values are displayed per decadal period as well as for the overall timeseries.

0.260%. This can be attributed to the substantially large FFDI decrease in 2010 and 2011, particularly in coastal regions, biasing results. This is less prominent in JJA and hence a strong positive trend is seen. This large negative anomaly also accounts for the very large positive trend seen in the 2010-2015 period, as subsequent years each have positive anomalies in FFDI. Due to the length of the record, it may be more suitable to compare the overall trend rather than just decadal anomalies.

Following comparing the trend the cumulative yearly FFDI, the trend in extreme fire danger days the is also explored and shown in Figure 7.4. Not only is the overall trend of FFDI important to the likely increased activity of fire due to climate change, however, as mentioned in Chapter 2.4, the extremes of temperature, precipitation, soil moisture, and consequent extreme FFDI days are also likely to change substantially. Figure 7.4 shows the trend overall and seasonally, in the number of days exceeding an FFDI of either 25 or 50. This is done both spatially across Australia (Figure 7.4.b, c, e, f) and also on average (7.4.a, d).

Similarly to Chapter 6, there are few days in which FFDI exceeds the severe category (>50). Here, anomalies vary between $\pm$ 8 days and consequently the trend in extreme days is as little as $\pm$ 1-2 days per decade. However, there is a clear positive trend in days >50 FFDI both overall and across Australia, as well as, during each season. This trend is spatially and seasonally dependent with the smallest and in some cases, negative trends, occurring in W.A in MAM and in JJA overall. As identified in Chapter 6, typically, fires in the northern regions of Australia occur at a lower FRP and also lower FFDI due to a lower extreme maximum temperature than in the south of the country.

This trend is exacerbated when considering the number of days exceeding the 'very high' FFDI category (i.e. FFDI >25). Here, there are more extreme days in MAM and JJA than when the FFDI exceeds 50. This is particularly the case post-2000, where there are years with substantial differences between the two anomalies. As previously identified in this chapter, both 2000 and 2011 have substantial negative anomalies in contrast to the overall positive trend. This contributes to a much smaller linear trend seen overall in the 1979-2015 period. The largest trends tend to occur inland, particularly in SON and DJF. Overall this contributes to a trend in excess of 10 days with an FFDI >25 in some regions. Despite the high variation in daily FFDI and potentially extreme FFDI days, there is little difference in the trend observed when comparing extreme FFDI days and monthly/yearly cumulative FFDI, albeit at a lower magnitude (discussed in the following sections).

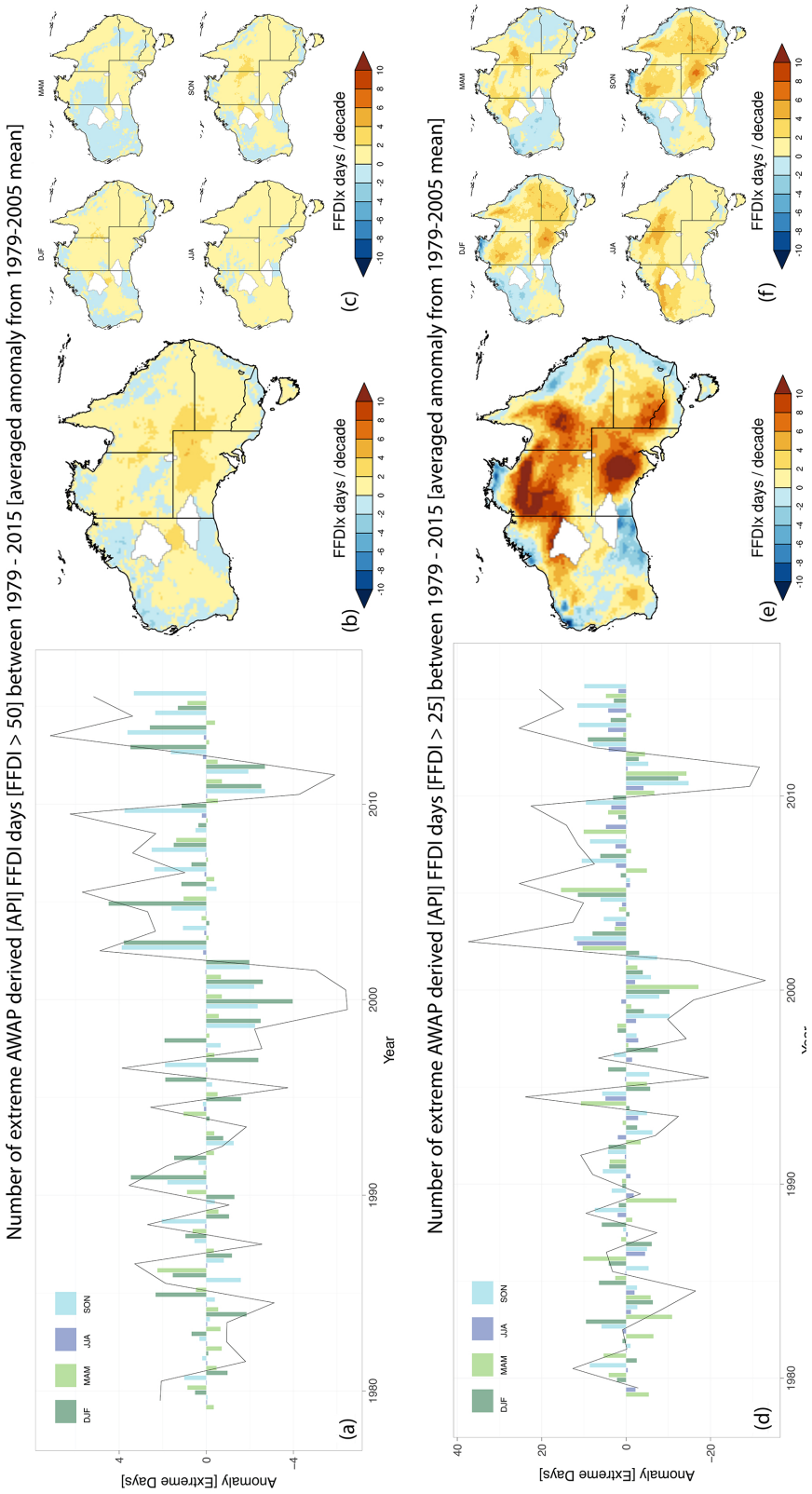

Figure 7.4: (a) Number of AWAP derived extreme FFDI days [FFDI > 50] between 1979-2015 (anomaly from 1979-2005 mean) averaged for Australia. Anomaly per year (black line), anomaly per season (dark green: DJF; light green: MAM; dark blue: JJA; light blue: SON). The mean FFDIx from the CMIP5 ensemble is derived from daily historical and RCP 8.5 data. (d) same as (a) for the number of days with FFDI > 25. Maps of the trend in FFDIx per year between 1979 âĂŞ 2015 for FFDI > 50 (b) and FFDI > 25 (e), and per season for FFDI > 50 (c) and FFDI > 25 (f).

7.3.2 Trends in FFDI between 1979 & 2100

Using projections from the CMIP5 models, the FFDI record can be extended to provide an overview of the potential change in FFDI during the 21st century. Similarly to the previous section, monthly and yearly trends of FFDI (compared to the 1979-2005 base period) were produced for CMIP5-derived FFDI (both daily and monthly CMIP5) for Australia. Both the percentage change (anomaly) in FFDI, as well as, the difference in the number of days exceeding an FFDI of 25 and 50 were produced. The northern and south-eastern regions are separated into their respective JJA and DJF fire seasons in section 7.3.2. As mentioned previously, unless otherwise specified, extreme FFDI refers to FFDI in excess of either 25 or 50.

Prior to investigating trends in FFDI, daily and monthly CMIP5 products have been compared against AWAP and ERA-Interim data to assess the skill and accuracy of projections. Due to the uncertainty in precipitation projections, it is expected that there be considerable differences between products and the computed FFDI overall. This is outlined in Figure 7.5, which assess the skill of precipitation, maximum temperature, relative humidity, and surface wind speed using the Pearson correlation, RMSE, and bias as metrics. As with previous studies (see Chapter 2), there is little agreement spatially and on average between AWAP and CMIP5 (monthly means) precipitation. This is similarly the case with relative humidity and surface wind speed. However, it should be noted that there are differences between the measurement periods between the ERA-Interim and CMIP5 products. Both the relative humidity and surface wind speed are instantaneous measurements that are aggregated to monthly means, whilst, for the CMIP5 data, these are averages as produced by model output. There is a stronger agreement between monthly means of maximum daily temperatures, with correlation coefficients in excess of 0.2 for large portions of the country and on average a correlation of 0.126. Despite the discrepancy between the products, with the exception of precipitation, for each variable, there is a negligible bias and only a minimal RMSE.

Following this, the FFDI was computed for both the CMIP5-daily (denoted as CMIP5d) and CMIP5-monthly (denoted as CMIP5m) data and the cumulative yearly FFDI was produced. In the following analysis, CMIP5d is averaged monthly for comparison to AWAP and CMIP5m data. For example, cumulative yearly FFDI is calculated by multiplying by the number of days per month by the monthly mean for each product. As shown in Figure 7.6.a, the agreement between AWAP and CMIP derived cumulative yearly FFDI is fairly low, particularly with the daily product which has an average correlation coefficient of -0.054, whereas the monthly product has a correlation of 0.215 on average across Australia. Most noticeably, in the south-east of Australia, the correlation coefficient is

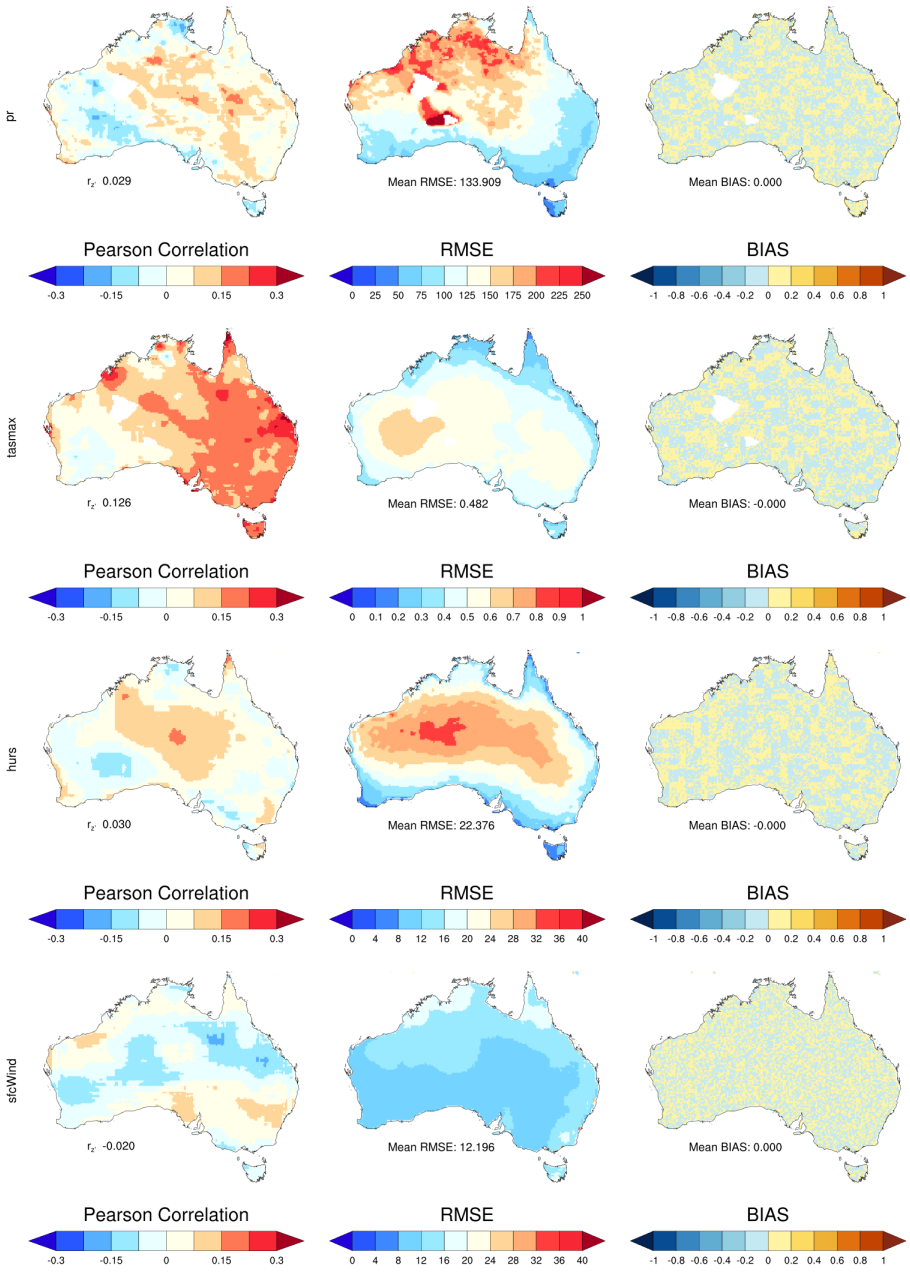

Figure 7.5: Skill metrics comparing monthly CMIP5 and AWAP input variables used to derive FFDI. Skill is based on the Pearson correlation (left column), RMSE (middle), and BIAS (right column). All data are compared between 1979 and 2005. (top row) precipitation, (middle-top row) maximum daily temperature, (middle-bottom) relative humidity, and (bottom) surface wind speed.

as high as 0.5. Again, the bias between the products is minimal, particularly with the monthly product, which slight overestimates cumulative yearly FFDI. The daily product tends to underestimate FFDI across Australia and has a relatively large RMSE compared to the monthly product (21.32 compared to 16.65). From the time series in Figure 7.6.b it can be seen that whilst there are some years in which the percentage change in yearly cumulative FFDI resembles AWAP, on a whole, there are large differences between the

products. However, at first glance, there are much closer similarities between trends over the 1979-2015 periods. As the following sections investigate, there is often a strong agreement between trends produced by AWAP derived FFDI and that from the CMIP5 data, particularly with the extreme FFDI days trends. These results indicate that there is some work to produce accurate projections of FFDI for forecasting purposes. Partly these differences can be attributed to the aggregation of means due to the differences in spatial and temporal resolution. However, due to the consistency in the use of the variables used to produce FFDI from CMIP5 data it is acceptable for the purpose of trend assessment.

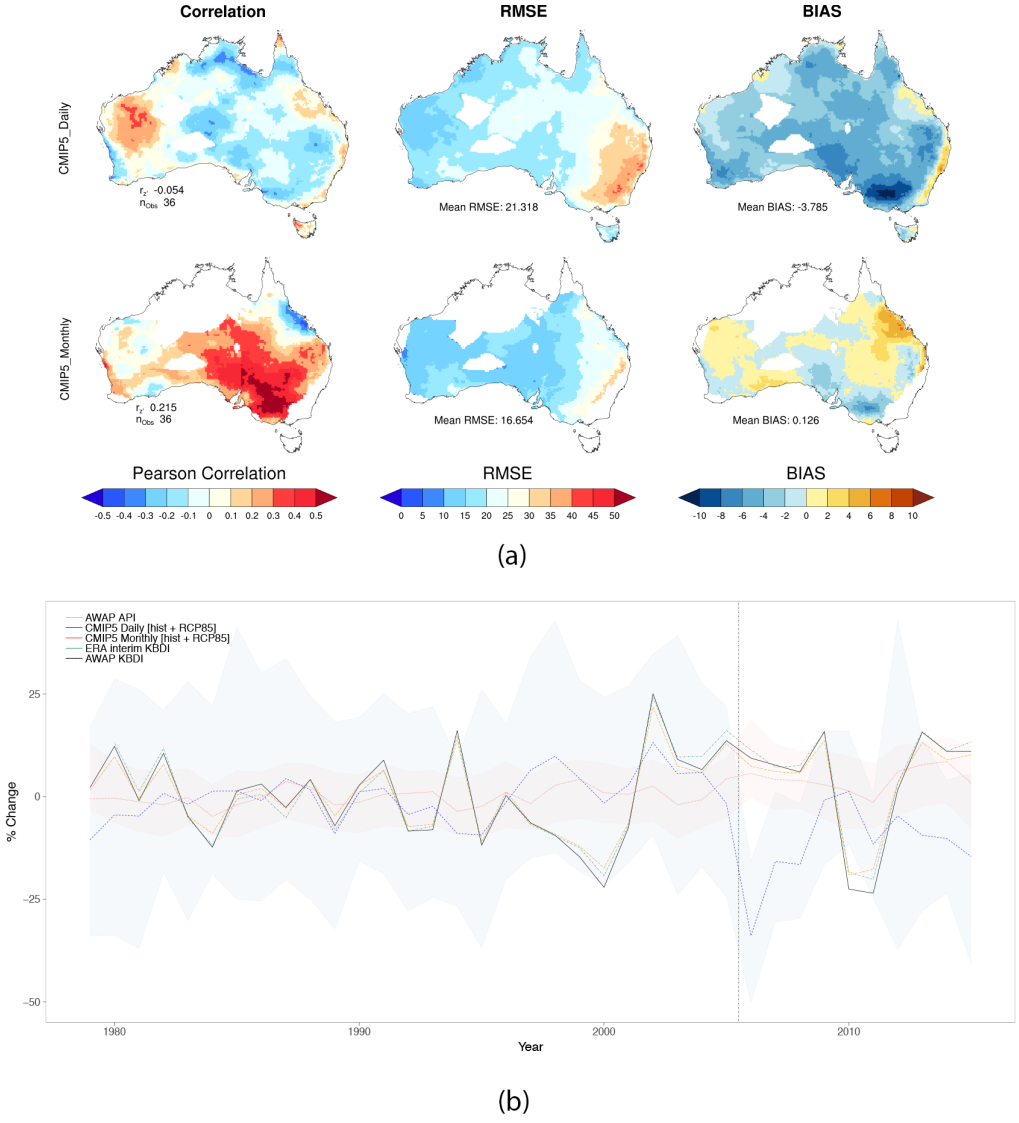

Figure 7.6: (a) Skill metrics of the comparison between AWAP derived cumulative yearly FFDI and both CMIP5 daily and CMIP5 monthly products. Skill is based on the Pearson correlation (left column), RMSE (middle), and BIAS (right column). All data are compared between 1979 and 2005. (b) time series of the percentage change in cumulative yearly FFDI between various products including CMIP5 daily and CMIP5 monthly driven FFDI. CMIP5 time series includes the historic and RCP 8.5 pathway betwen 1979 and 2015.

Daily & Monthly FFDI trends between 1979 & 2100

Following from the previous section, the trend monthly FFDI between 1979 and 2100 have been compared between the AWAP, CMIP5d and CMIP5m derived products. Figure 7.7 shows these trends for Australia (all months; Figure 7.7.a), for the northern Australia region (JJA months; Figure 7.7.b), and for the south-east region of Australia (DJF months; Figure 7.7.c).

As with previous AWAP-derived FFDI trends, there is a strong negative trend of between -6 to -10 % per decade across the coastal south-east of Australia as well as coastal Western Australia and the Kalgoorlie region (extending into the Nullabor plains) with large positive trends seen throughout inland Australia (in excess of 10% per decade), particularly in Queensland (Figure 7.7.a). In CMIP5m-derived historical FFDI, there are small positive trends in the south-east of the country extending into the semi-arid and arid regions (inland) with the small negative trends being observed in the Broome (north-west) and Kalgoorlie regions. Interestingly, in each case a smaller trend in FFDI for Tasmania compared to mainland Australia is seen. Similarly, a negative trend is seen for CMIP5d-derived historical data, albeit, with a magnitude more similar to AWAP, particularly in Queensland. However, in contrast to CMIPm, there is actually a very small positive trend in FFDI. With the exception of south-west Australia, the CMIP5d product most closely resembles the trends seen in the AWAP product between 1979 and 2005. Both RCP 4.5 and RCP 8.5 (CMIP5m and CMIP5d) pathways show large positive trends across Australia, with the largest trends seen in CMIP5d's RCP.5 projections.

As mentioned before, seasonal trends were also produced for the DJF and JJA regions, shown in Figure 7.7.b and 7.7.c. These show contrasting patterns to the overall trends seen across Australia for all months. For JJA months, the largest FFDI trends are seen in northern Queensland for both the historical and the observational datasets. A similar pattern is observed between the three datasets, however, the magnitude of the trend is far smaller in the CMIP5m produced FFDI compared to CMIPd and AWAP. Partly, this difference can be attributed to the larger variance in FFDI values from the AWAP and CMIP5d datasets as daily maximum wind speed, as opposed to monthly mean wind speed, is used as input. In addition, CMIP5 is also produced from an ensemble of models and simulations, further reducing variation, as well as, the aggregation of contrasting values due to the lower resolution of the products. Furthermore, differences in the observed patterns between datasets are largely dependent on the moisture or drought component (precipitation-based) used to drive FFDI, which as discussed previously, incur large uncertainties.

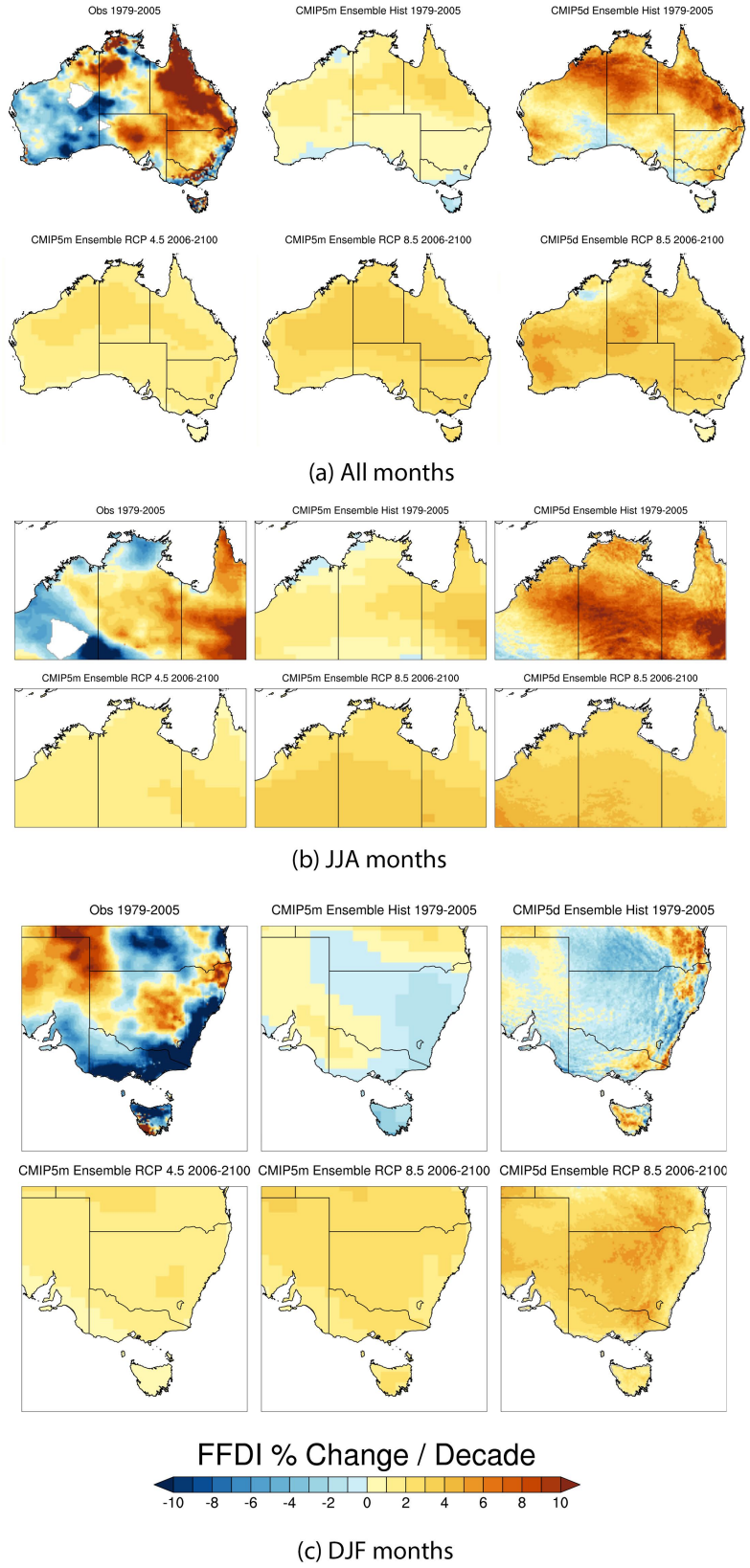

Figure 7.7: Linear trend in monthly percentage change (anomaly) in FFDI between 1979-2100 across Australia for all months (a), northern Australia in JJA (b) and for south-eastern Australia in DJF (c); for AWAP observations between 1979-2005, as well as, daily (CMIP5d) and monthly (CMIP5m) CMIP5 simulations from historical, RCP 4.5, and RCP 8.5 pathways. CMIP5m data are based on an average ensemble of 29 members from 6 model outputs. CMIP5d data are based on an ensemble of 6 model. Anomalies are defined as the percentage change from the 1979-2005 mean per year.

From Figure 7.7.b and 7.7.c, there is distinctly negative trend in DJF in southern Queensland and northern New South Wales is shown for each of the historical datasets. Each shows similar patterns, however, some differences can be seen in the south-east coast and in Tasmania. Both the RCP pathways observe positive trends in FFDI across the entire region, particularly for the RCP 8.5 pathway and as previously the CMIP5d product has an increase in the magnitude of trends compared to CMIP5m. The strongest trends are seen in the arid center portions of the region.

Differences in RCP 4.5 and RCP 8.5 derived FFDI trends between 1979 & 2100

CMIP5m projections of monthly total precipitation, maximum mean temperature, mean relative humidity, and maximum mean wind speed is used to produce monthly API and consequently FFDI. This is used to assess the change in FFDI using two climate pathways (RCP 4.5 and RCP 8.5), indicating a medium and large effect on climate change due to radiative forcing. As only the CMIP5m product has both the RCP 4.5 and RCP 8.5 pathways (due to availability), this is used for the following analysis. Both the historical CMIP5m and observationally based AWAP data have been used to produce FFDI using similar monthly values as previously discussed and used to reference against projected changes. API is again used to drive the drought factor component of the FFDI to remain consistent when comparing against projected values. As AWAP and CMIP5m datasets differ in the magnitude of FFDI, the cumulative yearly FFDI is calculated as an anomaly compared to the 1979-2005 base period (anomaly) and has been derived for the entire time-series for each dataset. Likewise, the mean yearly relative humidity, the mean yearly wind speed, the mean yearly temperature, and the cumulative yearly precipitation are also computed and compared for each dataset.

Figure 7.8, shows each of the four variables used to calculated FFDI for the 1979-2100 period. The percentage change (anomaly) of the historical, observational, RCP 4.5 and RCP 8.5 are averaged for Australian. Also included are the .25 and .75 ensemble percentiles bounds for each of the RCP 4.5 and RCP 8.5 pathways. From Figure 7.8 we can see that there is a substantial negative trend in the relative humidity and cumulative precipitation across the entire 1979-2015 with similar trends noticed for each RCP pathway. Conversely, there appears to be a very small negative trend in surface winds if at all, with no difference between pathways. There is a consistent positive trend in maximum temperature which is consistent with other studies investigating changes in maximum temperature. The projected trend in RCP 8.5 continues to increase throughout the 21st century deviating slightly from the RCP 4.5 pathway which stabilises at about 2075. These variables combine to produce a noticeable trend in FFDI throughout the time series.

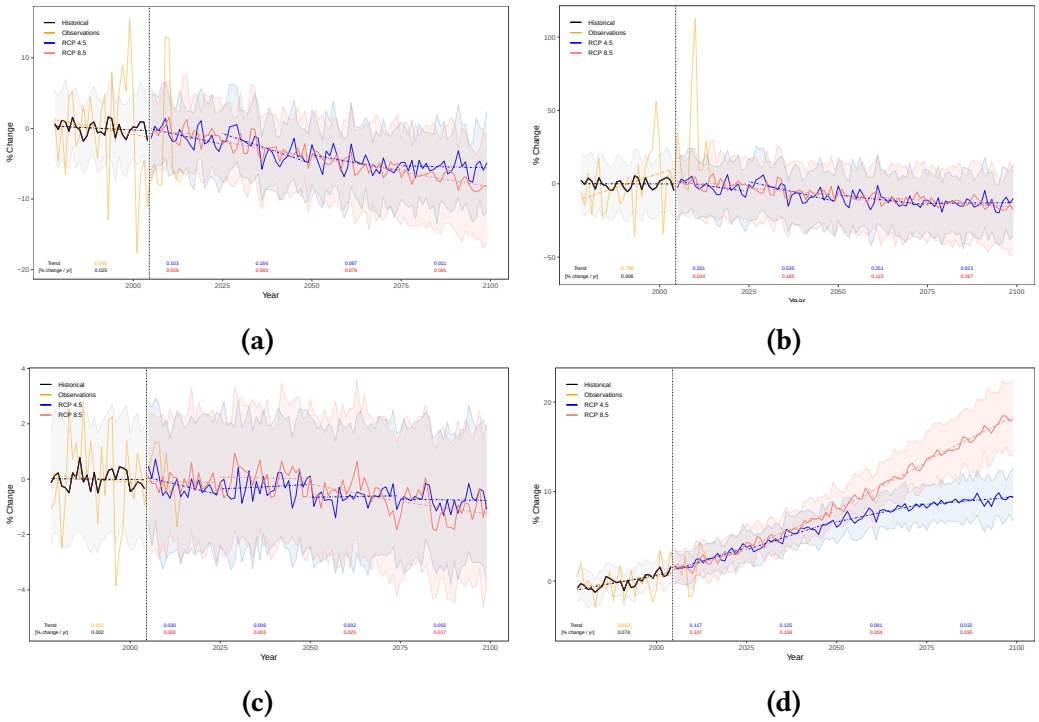

Figure 7.8: Percentage change (compared to base period: 1979-2005; anomaly) in yearly mean relative humidity (a), cumulative precipitation (b), mean surface winds (c), mean maximum temperature (d), between 1979-2100 averaged for Australia for historical (black line), RCP 4.5 (blue line), RCP 8.5 (red line) ensemble CMIP5m models. Also shown are observational fields derived from AWAP (orange line). Shaded areas indicate the 75th and 25th percentiles of the ensembles. Trend values are displayed per decadal period for RCP pathways and for the total period for historical and observational data. In total 29 ensemble members are used from six CMIP5 model outputs

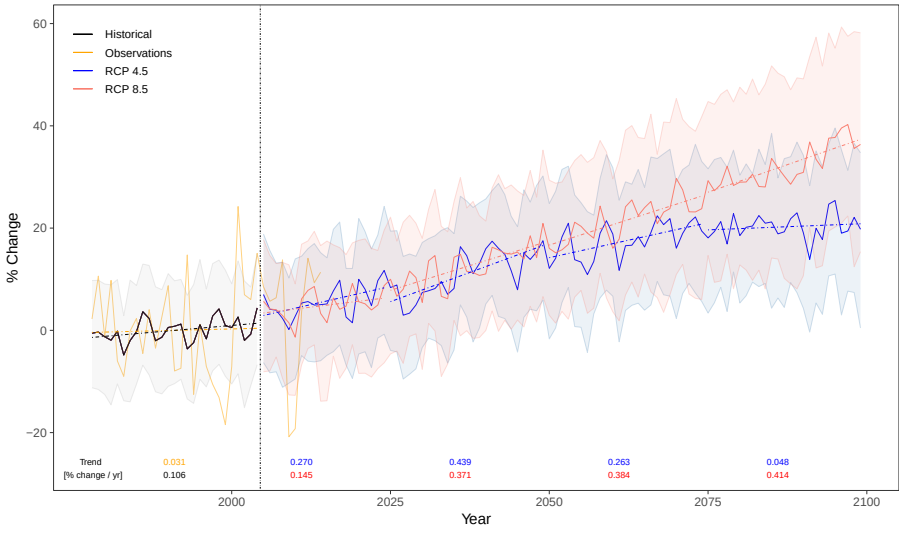

Figure 7.9: Percentage change (compared to base period: 1979-2005; anomaly) in yearly cumulative FFDI between 1979-2100 averaged for Australia for historical (black line), RCP 4.5 (blue line), RCP 8.5 (red line) ensemble CMIP5m models. Also shown are observational FFDI derived from AWAP with the drought component driven by KBDI (orange line). Trend values are displayed per decadal period for RCP pathways and for the total period for historical and observational data. Shaded areas indicate the 75th and 25th percentiles of the ensembles. In total 29 ensemble members are used from 6 CMIP5m model outputs.

The average anomaly in cumulative yearly FFDI for observational, historical and climate pathway datasets is shown in Figure 7.9, presenting similar trends to Figure 7.8. As expected due to the trends in each of the variables driving FFDI, a strong positive trend is also reflected in FFDI. This is particularly noticeable for the RCP 8.5 pathway which exhibits an increase in FFDI of up to 35% by the end of the century, similarly, the RCP 4.5 pathway indicates a positive anomaly of up to 20%. The majority of this difference is during the latter 50 years where there is a large difference in the trends, with values decreasing from over 0.3 % per year to 0.043% for RCP 4.5, while for RCP 8.5, trends are continuing to increase throughout the century nearing 0.4% per year. There is also a larger difference in the percentile bounds of model values by the end of the century. This indicates that there are a greater variation and uncertainty in model output in the RCP 8.5 pathway increasing in time.

Similarly, figure 7.10 compares the FFDI calculated at JJA months and DJF months for the northern-Australian and the south-eastern Australian regions, respectively. Again, in each case the general trend is increasing for each climate pathway, however, the JJA months in northern Australia appear to have a larger positive anomaly by the end of 2100. This is also noticed when comparing the observational FFDI between the two seasons. Despite a large negative anomaly difference in cumulative FFDI in 1986 and 1995 in JJA, there is a positive trend of 0.157 which compares favourably to the historical CMIP5m trend of 0.194, whereas, there is a far greater variation in the FFDI seen in the observations for DJF. This can be partly explained by the effect of precipitation deficits due to the millennial drought, which was far more prominent in south-eastern Australia than northern Australia (van Dijk et al., 2013). Here the trend is 0.007 compared to 0.169 for the historical CMIP5m based FFDI. This is largely due to the influence of the large negative trend in observations in the late 1980's and in the 1990's as mentioned in the previous section. When comparing the climate pathways a similar pattern is seen for both seasons, in which both pathways appear to increase at a similar rate until the latter part of the 21st century, most noticeably in the last 10-15 years in DJF. Interestingly there is a slight negative trend in DJF for RCP 4.5 in the last 25 years of the 21st century. Some of these differences can be attributed to the seasonal variation in the models selected as well as the spatial variation in FFDI between models, as detailed further, below.

The monthly variation in the change in FFDI at 2050 and 2100 for each model on average and for the northern and south-eastern Australia regions are presented in Figure 7.11. The mean of the 10 years leading up to 2050 and 2100 are used to indicated mid-and end-of-century change. The most significant difference seen in Figure 7.11 is between the CSIRO-Mk3-6-0 and HadGEM2-ES models compared to the other four models. The former predicts a far larger anomaly for each month, particularly the CSIRO-Mk3-6-0

model shows high levels of differences to the others, both in magnitude and in inter-annual patterns. Generally, there is a substantial difference between months across all models with a large contrast seen between the northern and south-eastern regions. Typically, the south-eastern region has the largest differences in spring whilst, the largest differences in the northern region occur in summer and autumn seasons, however, as established these are not necessarily aligned with the fire seasons. Likewise, as men-

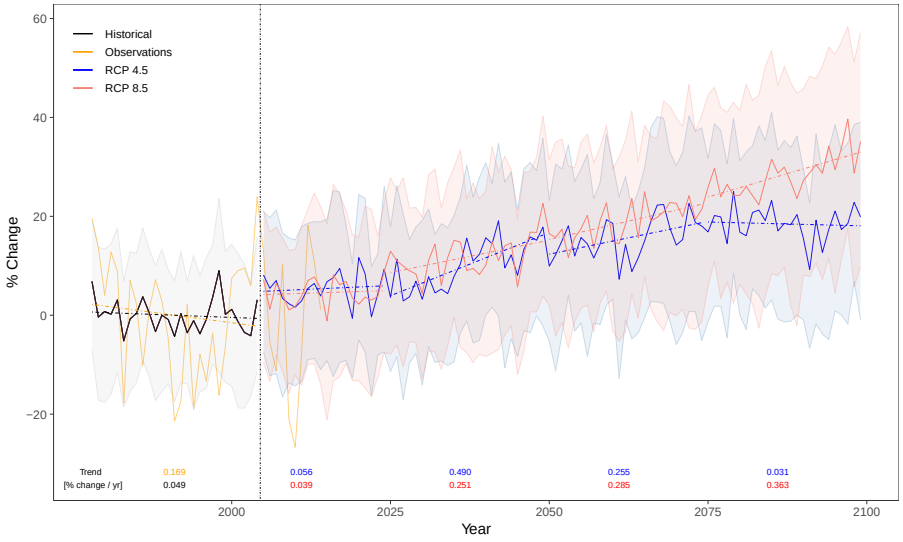

(a)

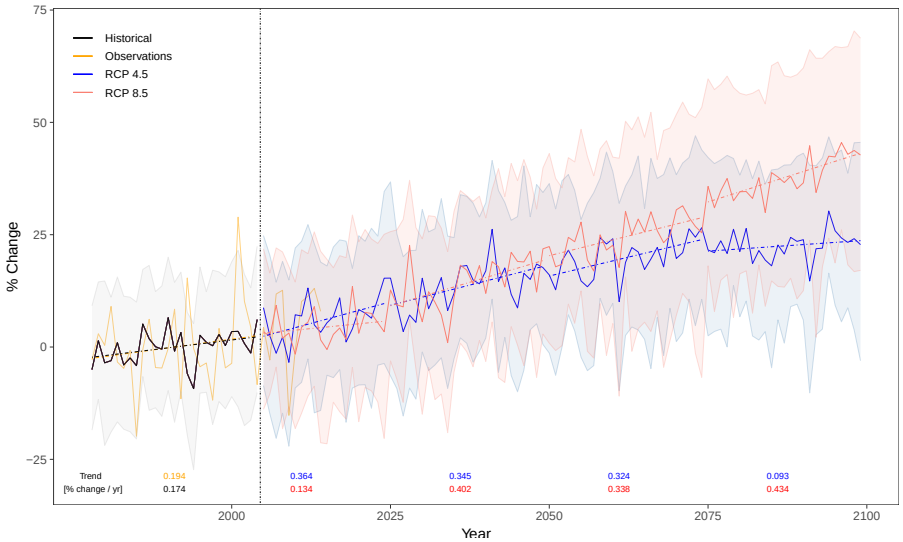

(b)

Figure 7.10: Percentage change (compared to base period: 1979-2005; anomaly) in cumulative yearly FFDI, between 1979-2100 averaged for DJF in South-Eastern Australia (a) and JJA in Northern Australia (b). Shown are averages of; historical (black line), RCP 4.5 (blue line), RCP 8.5 (red line) ensemble CMIP5m models. Also shown are observational fields derived from AWAP (orange line). Shaded areas indicate the 75th and 25th percentiles of the ensembles. Trend values are displayed per decadal period for RCP pathways and for the total period for historical and observational data. In total 29 ensemble members are used from 6 CMIP5m model outputs

tioned previously, the largest temporal variation between the models is seen in the RCP 8.5 pathway. Not only is there a large variation in overall change in FFDI but also a large difference between 2050 and 2100 values. It should also be noted that there are some months with negative anomalies for GISS-E2-H in the RCP 8.5 pathway, particularly in the summer and autumn months.

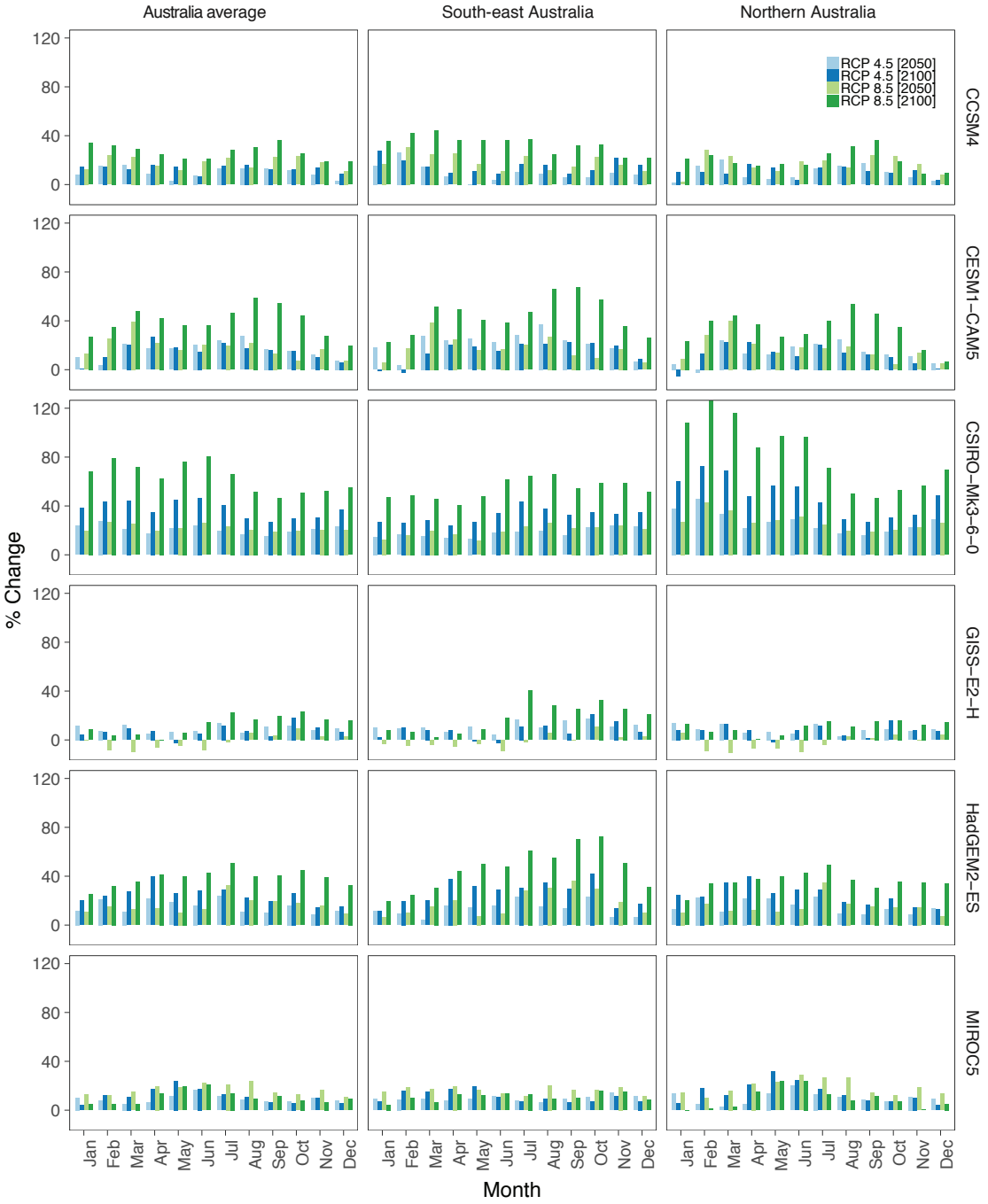

Figure 7.11: Percentage change in monthly FFDI (compared to 1979-2005 baseline; anomaly) at 2050 (mean 2040-2049) and 2100 (mean 2090-2099) for both RCP 4.5 and RCP 8.5 CMIP5m pathways. FFDI is averaged for Australia (left), south-eastern Australia (middle), and northern Australia (right) based on defined bounds. Data are separated into ensemble means of each model.

Trend in extreme FFDI days between 1979 & 2100

Despite the previous section primarily using monthly FFDI being to determine trends in seasonally and yearly cumulative FFDI, daily CMIP5d projections were used to investigate the trend in extreme FFDI days (similarly to 7.3.1). Again, extreme FFDI days were defined as days with an FFDI exceeding a value of either 25 & 50. Figure 7.12 shows the trend in the number of days exceeding an FFDI of either 25 or 50 between 1979 and 2100 (seasonally and overall). The combined time range includes only the historical and RCP 8.5 pathways due to the limited availability of data as discussed previously. However, for this analysis, the highest emission pathway providing the most extreme FFDI conditions are of particular interest as this will likely reflect the largest difference in extremes. As with Figure 7.4, this is done both spatially across Australia (Figure 7.12.b, c, e, f) and also on average (Figure 7.12.a, d). As with all previous analysis, anomalies are given as a difference from the 1979-2005 mean.

Similarly to Figure 7.4, there is a clear difference in the magnitude between the two extremes as noted previously. This is $\pm$ three for days with an FFDI>50 and $\pm$ 20 for days with an FFDI>25 over the 1979-2100 period. Beyond this, like the previous section, it is important to note that the magnitude of trends is substantially lower than AWAP derived FFDI for the same period (1979-2015). This is primarily due to the reduced resolution of the CMIP5d product causing the aggregation of local extremes. Despite this, the CMIP5d product again reflects features seen in Figure 7.4. Most noticeably, there is a similar negative anomaly in 2000 and 2011 for both plots. However, unlike the AWAP product, there is also a very large negative anomaly in 2006. This may be due to the underestimation of FFDI, particularly in DJF which drives the FFDI anomaly in the AWAP data for this year. Overall, there is a clear upward trend in the extreme FFDI days anomaly post-2020 for both FFDI>25 and FFDI>50. As with the RCP 8.5 projections from monthly FFDI, this again increases exponentially as the end of the century nears with anomalies in excess of two days per year and 15 days per year for FFDI>50 and FFDI>25, respectively. This increase in trend is far less pronounced in FFDI > 25 which experiences a more gradual linear increase from 2006. Spatially, there are similar patterns for both plots, albeit with a lower magnitude than AWAP derived extreme FFDI days. Likewise, the largest trend is in excess of two days per decade ($\approx$ one day for FFDI>50) and is experienced in central Australia (particularly South Australia) with small localised negative trends along coastal south-east Australia and north-western Australia.

Even more pronounced than with the AWAP data is the difference in the trend and anomalies seen between seasons. For both FFDI > 25 and FFDI >50, DJF and SON tend to drive trends due to their larger contribution to the yearly anomaly. In both DJF and

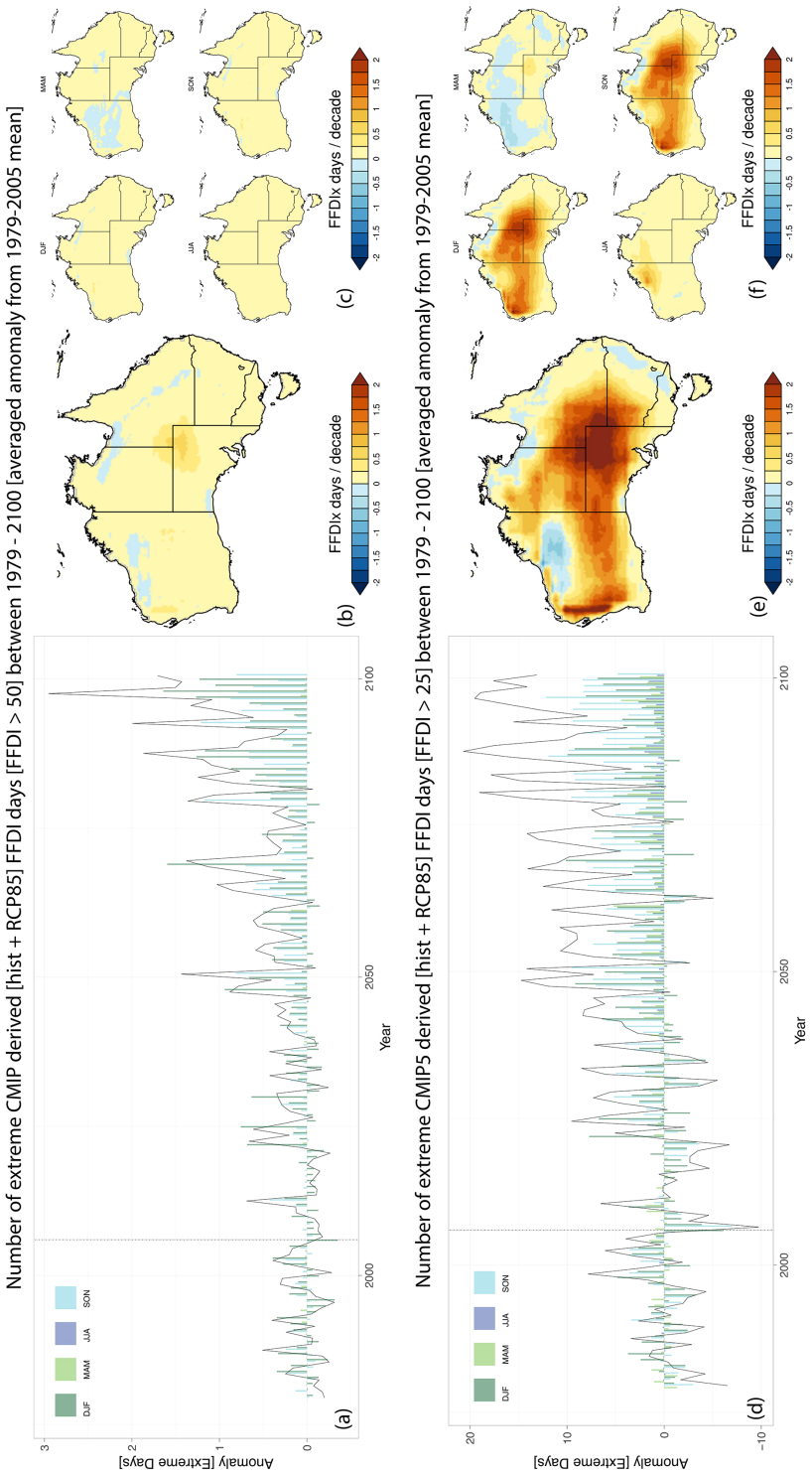

Figure 7.12: (a) Number of CMIP5d derived extreme FFDI days [FFDI > 50] between 1979-2100 (anomaly from 1979-2005 mean) averaged for Australia. Anomaly per year (black line), anomaly per season (dark green: DJF; light green: MAM; dark blue: JJA; light blue: SON). The mean FFDIx from the CMIP5d ensemble is derived from daily historical and RCP 8.5 data. (d) same as (a) for the number of days with FFDI > 25. Maps of the trend in FFDIx per year between 1979 - 2100 for FFDI > 50 (b) and FFDI > 25 (e), and per season for FFDI > 50 (c) and FFDI > 25 (f).

SON, this is relatively uniform spatially, with large positive trends experienced in central Australia and only a very small negative trend seen in far north coastal Australia. As with Figure 7.4, the strongest negative trends are seen in MAM. However, on average, Australia experiences an increase of about 1-1.5 days with the FFDI exceeding 25 per decade (0.5-1 days per decade with FFDI>50). To put this into context, from these projections, it is expected that by 2100 there to be on average up to 10 to 15 more days with an FFDI exceeding at least the very high danger category. Considering the vast majority of extreme FFDI days occur in a five month period, this is quite substantial.

7.4 Discussion

The temporal FFDI trends derived in this chapter from both observationally based AWAP data and CMIP5 ensemble data show different patterns in the historical and modelled analysis. Historically based trends were assessed between 1979 and 2015 whilst CMIP5 RCP 4.5 (monthly only) and RCP 8.5 pathways were used to project FFDI between 2006 and 2100. Numerous studies have previously compared trends in fire danger globally and regionally (Liu et al., 2010; Flannigan et al., 2013; Stocks et al., 1998; Brown et al., 2004; Wotton et al., 2010) as well as for regions within Australia (Hennessy et al., 2005; Pitman et al., 2007; Clarke et al., 2012; Fox-Hughes et al., 2014).

One caveat of comparing the historical trends of FFDI (and associated variables) derived from AWAP and ERA-I to CMIP5 is that CMIP5 simulations are forced by time-varying greenhouse gas concentrations and aerosols, whereas, AWAP and ERA-I modelled observations are driven by annually-varying atmospheric circulation and sea surface temperatures. Despite trend and temporal similarities between the products this explains the near-zero Pearson correlations noticed spatially in Figure 7.5 and Figure 7.6. Beyond this, this could contribute to differences in the magnitude of trends in FFDI between products.

Similarly to Clarke et al. (2012), the anomaly in cumulative FFDI between 1979 to 2015 (Clarke et al. (2012) used 1973 to 2010), however, using gridded AWAP data rather than single station data was investigated. It was found that generally there was a strong positive trend in FFDI over time, however, there were regions with small negative trends, particularly along coastal regions. This is contrasting to Clarke et al. (2012), which indicates only positive trends from its 38 station sites with strong positive anomalies generally located at sites in arid and semi-arid regions. Part of the observed difference in coastal regions can be attributed to the very large negative anomalies in FFDI in both 2011 and 2012, which, are not included in Clarke et al. (2012) analysis. Clarke et al. (2012) indicate that overall 16 if the 38 sites observe significant positive trends, of sites

with non-significant trends, 13 out of 20 are located in coastal regions and observe only small positive trends.

When comparing decadal and seasonal trends it is apparent that there is substantial spatial variability across Australia and even within similar climate regimes. Similarly to Clarke et al. (2012), when comparing seasonal trends, DJF observes the most widespread negative anomalies, particularly in southern Australia with northern Australia observing strong positive trends. The greatest positive trends are observed in the SON season, particularly in south-eastern Australia. Despite the generally positive trends, an increase in FFDI does not necessarily translate to an increase in fire occurrence nor fire intensity. For example, in several years (2000 and 2011), there is actually a large increase in both the number of fires and in FRP despite negative anomalies in FFDI during these years (Figure 7.1), as suggested, these are largely dependent on the local fire dynamics as well as the climate regime and fuel conditions at the time. As (Forkel et al., 2017) suggests fire activity is dependent on the combined influence of climate and vegetation variability. In particular, (Forkel et al., 2017) concludes that, in south-eastern Australia, fire is largely controlled by vegetation whereas in arid Australia fire is controlled by a combination of climate and vegetation conditions. The contrasting trends, or state, in both climatic conditions and vegetation conditions, may contribute to the larger fire activity experienced during years with negative FFDI anomalies. Conversely, the Black Saturday fires, among other notable fires, appear to be as a direct result of the positive anomaly and trend both prior to and during these years (Tolhurst, 2009; Clarke et al., 2012). However, this observation may, in fact, be the culmination of extreme negative anomalies in vegetation moisture for the years prior to these events. Furthermore, regions of Australia which experienced negative trends in fire activity and FFDI may be as a result of the expansion and intensification of agricultural land use and its effect on vegetation (Andela et al., 2017). Beyond this, changes in both FFDI trends and fire activity may also be strongly influenced by inter-annual variability, namely, ENSO (Williams et al., 1999; Xu et al., 2014) as well as soil moisture conditions (Liu et al., 2003).

These observed positive trends and changes in monthly and yearly cumulative FFDI were also seen in projections from an ensemble of CMIP5 models both for RCP 4.5 and RCP 8.5 pathways. CMIP5 models replicated the spatial patterns of AWAP observational data between 1979 to 2005, particularly with daily CMIP5, however, with some notable exceptions. These included the negative trends in the coastal regions of eastern and to a lesser extent southern Australia as well as in Tasmania. There was also a large discrepancy between the magnitude of trends seen between AWAP and the CMIP5 products. However, daily CMIP5 data tended to show a better agreement. This is partly because the aggregation of data due lower resolution data, reducing the overall variance, and partly

due to the reduction in variance when comparing differing temporal resolutions. There were substantial similarities between AWAP and CMIP5 derived FFDI, when separating into seasonally defined regions. For example, for RCP 4.5 and RCP 8.5 projections, in general, there was an increase in FFDI of between 0.2 to 0.5 % per year, with all of Australia experiencing positive trends. This was particularly noticeable when considering the change in the number of extreme FFDI days, where both DJF and SON seasons experienced similar trends for both AWAP and CMIP5 derived FFDI. However, there were some regions with little or minor negative trends such as alpine south-eastern Australia. Typically, the positive trends are principally driven by warming and reductions in relative humidity through the drought component of the FFDI. This is in agreement with Pitman et al. (2007), who investigated the change in FFDI and GDFI using gridded data produced by RCPs for 2050 and 2100. Similarly, projected FFDI has been studied at station sites by Hennessy et al. (2005), regionally by Clarke et al. (2011) and in Tasmania by Fox-Hughes et al. (2014). Hennessy et al. (2005) investigated the change in FFDI and GFDI using two RCMs as input for climate change scenarios for 2020 and 2050 across 17 sites, whereas, Clarke et al. (2011) investigated the seasonal change in 2050 and 2100 FFDI projections in four specific east-coast regions of Australia.

Generally, the results presented here are in agreement with Hennessy et al. (2005), Pitman et al. (2007), Clarke et al. (2011), and Fox-Hughes et al. (2014) that there is an increase in FFDI in both 2050 and 2100. However, here, we indicate a higher magnitude of trends, continuously increasing in the RCP 8.5 pathway while flattening off towards the end of the 21st century for the RCP 4.5. Conversely to Clarke et al. (2011), the onset of the positive trend in FFDI is already present early on, increasing throughout the 21st century (RCP 8.5). Overall, changes in the FFDI and trends appear to be seasonally dependent for both the model and the regions selected, with the largest differences occurring in the CSIRO and HadGEM2 models between SON and JJA for monthly data, whilst the largest trends occurred during DJF and SON for daily data. Similarly, these results do not necessarily coincide with previous studies, particularly with Clarke et al. (2011), using only point data, which may result in representativeness issues. This is due to the difference in the number of grid cells used to average FFDI across regions as well as the regions selected by Clarke et al. (2011), which all fall in similar climate regimes along coastal south-eastern Australia.

Chapter Summary

Chapter 7 assesses the change in FFDI derived from past and future projections of selected CMIP5 models (scaling API to the drought factor component), for Australia between 1979 and 2100. Changes in FFDI are projected to increase substantially throughout the twenty-first century, particularly if the radiative forcing of the RCP 8.5 pathway is realised. However, these changes are expected to vary greatly across Australia and seasonally, in line with observations from current trends in FFDI. These positive trends do not necessarily correspond to an increase in fire occurrence nor higher FRP fires as similarly stated in the previous chapter.

CHAPTER 8

Conclusions and Future Work

Overview This thesis investigates the relationship between various soil moisture indices and temperature extremes, and their effect on fire intensity (FRP) and fire danger (FFDI) across Australia. This has been achieved through four analysis chapters (Chapters 4-7), with the first two focusing on a comparison between soil moisture indices as well as their relation to the number of hot-days (Tx90), and the second two investigating the relationship in context with FRP and FFDI as well as past and projected changes in FFDI. Each of these chapters uses gridded data to compare spatial variability across a range of climate regimes in Australia but Chapter 4 also includes *in situ* station sites. Appendix A also includes a case study investigating the minimum sampling frequency used to determine fire severity from remotely sensed and ground-truthing data. Therefore, this chapter summarises the specific research outcomes of this Ph.D. thesis and its conclusions, as well as potential opportunities for future work.

8.1 Summary of Research Conclusions

8.1.1 Conclusions from Chapter 4: Comparison of Soil Moisture Proxies Across Australia

Chapter 4 presented a comparison of a variety of soil and climate characteristics to better understand how the performance of soil moisture indices compares to a reference soil moisture and how these vary across Australia. More particularly, four moisture indices and 64 *in situ* soil moisture sites were compared from the OzNet, OzFlux and CosmOz networks in Australia. They were then compared against ESA CCI remotely sensed soil moisture observations across Australia. This expanded on previous studies which used a limited number of *in situ* sites representing only few climate regimes across Australia, as well as adding a gridded analysis to provide an overview of spatial trends. Beyond this, the temporal range was expanded and included moisture indices pertinent to fire danger. The Pearson correlation coefficient, bias, and RMSE were the primary statistics used for measuring the degree of association between products and were primarily compared against for the 2000 (1979 for gridded data) to 2015 period.

Similar to other studies, there is a strong agreement between various soil moisture products and the reference soil moisture across both *in situ* sites and observations for large parts of Australia. It was found that API and MSDI show the highest correlation to *in situ* surface soil moisture (normalised and normalised anomaly) with the highest correlations observed in the OzNet network. Also, API and MSDI tend to resemble the gridded reference soil moisture the closest with little bias towards either wetter or drier conditions. Both KBDI and 14-day SPI observe a large wet bias across all sites and AWAP surface soil moisture shows a large dry bias compared to *in situ* sites. However, these results are not reflected in deeper soil moisture layers with KBDI and MSDI best-representing soil moisture at 30, 60, and 90 cm compared to API, SPI and AWAP s0. Average correlation coefficients between *in situ* sites and both KBDI and MSDI are generally consistent with varying depths indicating that these might be better suited for root zone studies. These results are consistent with the comparison of gridded products, but, spatial variations appear to be largely due to the soil and climate characteristics. Correlation coefficients are particularly strong in the south-east and north of the country coinciding with regions within the transitional regime (savanna, temperate and semi-arid regimes) as well as in soils with strong filtration properties (low porosity) and regions with a lower vegetation density (VOD). This indicates that the performance of moisture indices is heavily influenced by spatial variability due to soil and climate characteristics. These differences should be observed and considered when choosing an appropriate index for any particular application. Chapter 4 highlights the strength of API as a proxy for soil moisture as

it represents a parsimonious model that accomplishes the desired level of accuracy relying on only precipitation and temperature data using a relatively simple drying model.

From Chapter 4 we can conclude that:

1. API and MSDI show the largest correlation to *in situ* surface soil moisture (normalised daily, normalised daily anomaly and monthly data) with the highest correlations seen in the OzNet network.

2. Both KBDI and SPI14 show a large wet bias across all sites and AWAP surface soil moisture observes a large dry bias compared to *in situ* sites.

3. KBDI and MSDI correlate best to *in situ* soil moisture at 30, 60, and 90 cm depths compared to API, SPI and AWAP s0.

4. Regions within the transitional zone experience the largest correlation between the soil moisture indices and ESA CCI soil moisture apart from the south-east coast.

5. Soil type, porosity, VOD and climate regime significantly influence correlations between each product and the reference soil moisture.

8.1.2 Conclusions from Chapter 5: Variability of Soil Moisture Proxies and Hot Days

The transitional zone paradigm as introduced by Seneviratne et al. (2010), explains the influence of soil moisture on the overlying energy partitioning between sensible and latent heat in context with evapotranspiration drivers (Teuling et al., 2009) and vegetation conditioning (Seneviratne et al., 2010). This has long been implied through the interpretation of the commonly used Köppen-Gieger climate regimes Köppen (1884), Kottek et al. (2006), and Peel et al. (2007), but an explicit inter-comparison has only been identified at either the global (Greve et al., 2014; Greve et al., 2016) or catchment (Carmona et al., 2016) scales. Due to the size of Australia and its catchments, they are spanning several climate regimes meaning that it is not accurate to generalise conditions for all regions. Chapter 5 clearly identifies a difference between both the established climate regimes and also recent Budyko studies (Greve et al., 2014; Greve et al., 2016) for Australia using the AWAP dataset at 25 km spatial resolution.

As mentioned, Chapter 5 introduces the key mechanisms behind the relationships driving an increase in fire occurrence and intensity, but also the strength of the correlation between various moisture indices and their effect of soil moisture on temperate extremes.

Contrary to recent studies (Seneviratne et al., 2010; Fischer et al., 2007) which indicate that the transitional zone lies within semi-arid regions within central and southern Europe, whereas we indicate in Figure 5.1, that for Australia, the transitional zone is actually a combination of the savanna, semi-arid and temperate Köppen-Gieger climate regimes. More specifically in 34 out of 46 years, the semi-arid regime exceeds the dryness index threshold for the transitional zone and rather is moisture limited. This is in agreement with Figure 5.2 (top), which indicates that in the majority of the semi-arid region evapotranspiration is completely dependent on the available precipitation as is the case for the arid regime. This indicates that in general, these regimes are dryer than similarly classified regimes presented in previous studies. Similarly, these results differ from Greve et al. (2014) and Greve et al. (2016) which used a variation of the definition of the transitional zone using a smaller aridity range $2 < PET/P > 2$, compared to $1 < PET/P > 3$. However, this does not account for the changes seen in Figure 5.1 as the transitional zone would be further narrowed to exclude the semi-arid region completely. Likewise, this would not account for the observed aridity values seen for the savanna regime. Finally, greater detail of regions within the transitional zone is noted here including regions in the east of Tasmania, southern West Australia and around alpine Australia.

Chapter 5 also clearly identifies the strength and mechanisms of the relationship between monthly SM and temperature anomalies in Australia. Generally, it is found that there is a significant negative relationship between various SM indices and Tx90 for large parts of Australia. More particularly, arid and semi-arid regions of Australia exhibit the strongest increase in the quantile regression slopes (from low to high percentiles), indicating that months with low SM are highly likely to experience a large number of Tx90 (Figure 5.4). However, northern (savanna) and southeastern Australia (temperate) observe the largest correlation coefficients between changes in moisture and Tx90. Again, API appears to best represent patterns seen with the AWAP s0 and has the largest negative-correlations with Tx90 in the transitional zone (Figure 5.3).

Finally, the effect of inter-annual variability in the form of ENSO was introduced in Chapter 5 and there appears to be a high level of spatial variability in the magnitude of correlation coefficients between SM and Tx90 associated with ENSO events across Australia (similar to those seen by Perkins et al., 2015). Compared to non-DJF months, it was determined that overall, an increase in the correlation coefficients between SPI and Tx90 across Australia exists, but this cannot be solely attributed to the effect of ENSO on precipitation as there is a very large spatial variability in the Tx90-SM relationship.

To summarise, Chapter 5 confirms that:

1. In 34 out of 46 years, the semi-arid region is moisture limited, indicating that the semi-arid regime is largely not within the transitional zone. This is further highlighted in Figure 5.2 (top/bottom), where, large areas of the temperate, savanna, and to a lesser extent semi-arid (compared with as expected) climate regions in Australia enter the transitional regime and are neither strongly moisture nor radiation limited.

2. Arid and semi-arid regions of Australia exhibit the strongest increase in the quantile regression slopes (from low to high percentiles), indicating that months with low SM is highly likely to experience a large number of Tx90 (Figure 5.4).

3. Northern (savanna) and southeastern Australia (Temperate) observes the largest correlation coefficients between changes in moisture and Tx90. Conversely, regions with near-zero precipitation tend to have little to no correlation. (Figure 5.4).

4. API appears to best represent patterns seen with the AWAP s0 and has the largest negative-correlations with Tx90 in the transitional zone (Figure 5.3).

8.1.3 Conclusions from Chapter 6: Improving Fire Risk Estimation by Investigating Fire Intensity, and Moisture and Temperature Extremes

Following from the previous section, fire intensity in the form of FRP was investigated in the context of the land-climate interactions, particularly the relationship between soil moisture and temperate extremes. This was then compared to the FFDI produced for each moisture index and well as being compared against the key variables leading to fire conditions. As with previous studies, it was found that the seasonality of maximum FFDI was highly variable across Australia with the fire season shifting from the north in the in June/July progressively further south through SON, to the south-east in DJF and the south-west later in this season. Similarly, the fire seasons were determined with respect to the climate regimes in Australia with maximum FFDI occurring for the temperate and semi-arid regimes in DJF and all other regimes peaking in October. This analysis was also performed for MODIS-derived FRP and fire occurrence, producing starkly contrasting results to that of maximum FFDI. Our results indicate that the month in which the maximum FRP occurs does not necessarily coincide with the maximum number of fire occurrences. This is particularly noticeable in the savanna and tropical regimes where the maximum number of fires occurs prior to the maximum FRP. Furthermore, the largest FRP fires appear to occur in the temperate/transitional regime, particularly in alpine south-east Australia and are typically characterised as having very few fires

per year compared to the north of the country.

Following this, it was found that there is a clear relationship between both an increasing number of fires and an increase in FRP with decreasing moisture. This was consistent for each moisture index, however, the change in moisture between the lead-up and post-fire events such as the Black Saturday fires were far more prominent for API, SPI, and s0. This was translated in the pattern seen in the drought factor which was consistently at near maximum levels throughout these periods. Due to this the resultant FFDI and its change during this event appears to be more closely associated with changes in wind speed, temperature, and relative humidity than the moisture component. Considering the strong logarithmic relation between a decrease in soil moisture and FRP, this suggests that KBDI and MSDI may not be the most appropriate indicators for representing the increase in fire intensity through the FFDI. This is confirmed in the comparison of the change in each moisture index and the resulting change in both FRP and FFDI. More so, when directly replacing the KBDI with each moisture index, there was little difference in the resultant FFDI, particularly with API. This was also the case when scaling each of the indices to the drought factor, further suggesting that the current formulation of FFDI is unnecessarily complex and replacing the drought factor with API would suffice. Along with this, it was found that the changes in FFDI do not reflect the changes in the maximum observed FRP.

Key findings from Chapter 6 include:

1. Both the number of fires and FRP increase with decreasing soil moisture for each index.

2. As observed with previous results, both MSDI and API best correspond to observed changes in the relationship between observationally based soil moisture and FRP. i.e. there is a clear logarithmic increase in FRP with decreasing moisture.

3. KBDI again does not represent the observed changes well, with only a small linear increase in FRP with decreasing moisture.

4. A high concentration of fire occurrences does not necessarily correlate to a larger FRP. The highest maximum observed FRP is located in alpine Victoria and N.S.W. These results again correspond with the transitional zone, indicating that significant differences in soil moisture from the mean in these regions will provide an increase in fire conditions and intensity.

5. Changes in FRP are not reflected in the respective change in the FFDI or the current categories.

6. There is a very strong agreement between ERA-I/AWAP (combined product) KBDI driven FFDI and API driven FFDI derived from ERA-I data alone. Furthermore, there is a negligible difference between API and KBDI driven FFDI products.

7. There is minimal difference in FFDI when substituting different indices into the current drought factor component of the FFDI. The DF is principally driven by the decay component and therefore, API provides a suitable replacement for the drought component completely (Figure 6.10).

8.1.4 Conclusions from Chapter 7: FFDI in a Changing Climate

Chapter 7 assesses the change in FFDI derived from past and future projections of selected CMIP5 models (scaling API to the drought factor component), for Australia between 1979 and 2100. Overall, FFDI is projected to increase substantially throughout the twenty-first century, particularly for the RCP 8.5 pathway. However, these changes are expected to vary greatly across Australia and seasonally, in line with observations from current trends in FFDI. More specifically, the eastern and southern coastal regions of Australia, are expected to have a far smaller increase in FFDI, particularly in summer compared to arid and semi-arid regions. This is also the case in northern Australia in the winter (JJA) months. Comparing the variables used to drive FFDI, changes are shown to be primarily related to an increase in maximum temperature and reduction in relative humidity through the drought factor. These results are in agreement with previous studies, combining to produce an overall view of the temporal and spatial variation across Australia throughout the current century. This chapter provides a further analysis of trends in FFDI for Australia both historically and projected using two different forcing pathways from an expanded 29 ensemble members from six CMIP5 models (six ensembles from six models for daily CMIP5 data). Changes in FFDI and the number of extreme FFDI days were spatially compared at a monthly, seasonal and at the yearly temporal scale providing an overview of the potential change in fire risk under moderate and high-end climate change conditions.

More specifically, from this chapter, we can conclude that:

1. With the exception of coastal eastern and southern Australia, the majority of Australia has experienced an increase in FFDI between 1979 and 2015. The largest positive changes in FFDI have occurred during the last 15 years with changes being observed almost uniformly across Australia.

2. Positive trends in FFDI do not necessarily correspond to an increase in fire occurrence nor higher FRP fires, with 2000 and 2011 being noticeable examples. How-

ever, in 2002, 2006 and in 2009 the fire activity is heavily influenced by strong positive changes in FFDI (particularly the "Black Saturday" fires.)

3. Changes in FFDI are principally driven by warming and reductions in relative humidity through the drought factor.

4. By the end of the century, the change in FFDI is likely to increase by about 20% and 30% for climate pathways, RCP 4.5 and RCP 8.5, respectively.

5. The change in FFDI over the 21st century is not uniform, spatially nor seasonally, with the largest changes being observed in central Australia during SON and DJF. This is similarly noticed with the change in the number of extreme FFDI days.

6. It is expected that there will be on average up to 10 to 15 more days with an FFDI exceeding at least the very high danger category (FFDI > 25) by 2100.

8.2 Outlook and Future Work

There are several opportunities for future research arising from this thesis. Chapter 4, introduced the comparison of various soil moisture indices, primarily at the surface soil layer but also at several deeper layers, which may be better associated with actual soil moisture in studies investigating longer-term droughts. This was done using *in situ* observations. However, with improvements to the accuracy of land surface models (LSM's) such as the Joint UK Land Environment Simulator (JULES; currently being implemented in Australia), further work could include a gridded analysis of the spatial variation between JULES and moisture indices. This work could eventually be conducted at a higher spatial resolution than presented in this study, for example, at 1 km to improve the spatial representation and temporal stability (Minet et al., 2013; Zhou et al., 2007). However, despite improvements in the accuracy of LSM's, Yang et al. (2014) concluded that they need to include lateral soil moisture/water flow, and to use more accurate prescriptions of the hydraulic and thermal properties of the soil to achieve a better simulation of soil moisture.

As mentioned, Chapter 5 identifies the strength and mechanisms of the relationship between monthly SM and temperature anomalies in Australia, providing an extended insight beyond previous studies. This involved introducing inter-annual variability in the form of ENSO through the SOI. However, various other modes of variability have been proven to have a strong effect on precipitation in the region (Cai et al., 2009; Williams et al., 2009; Risbey et al., 2009), specifically, the Indian Ocean Dipole (IOD), the Southern-Annular Mode (SAM) and the Madden-Julian Oscillation (MJO) which account for the

three largest explained differences in the variance of precipitation across Australia (Montazerolghaem et al., 2016). The IOD, SAM, and MJO could be investigated in the context of large-scale dynamics along with the spatial distribution of precipitation and evapotranspiration across Australia. Similarly to Chapter 5, this could then be put into context with the observed spatial variation due to the energy partitioning as well as climate variability itself.

Another consideration in Chapter 5, is to note that as the depletion rate in the calculation of API, KBDI and MSDI considers the contribution of maximum daily temperature, the resultant relationship between these indices and Tx90 could include a bias due to the dependency on temperature. Similarly, as analyses are based on monthly data, data may not accurately reflect monthly trends where influenced by extreme daily moisture anomalies. For example, despite a sustained dry period during a month, the overall anomaly may be positive due to an extreme precipitation event. Thus any hot-days associated with the dry events could be masked. Rather than investigating the effect of soil moisture on Tx90 or heat wave days, further research could benefit from investigating the difference in day-to-day temperature or daily anomalies in order to isolate the change in temperature due to changes in soil moisture.

Following Chapter 6, FFDI has been calculated for each moisture index and compared against both the key variables leading to fire conditions and also FRP. It was found that the current formulation of FFDI is unnecessarily complex and replacing the drought factor with API would suffice. Along with this, it was found that the changes in FFDI do not necessarily reflect the changes in the maximum observed FRP. Further investigation into the change in FFDI reveals that there is a positive trend in the last two decades, however, this trend is spatially dependent which is not represented in the current categories of FFDI.

In addition, some indices (FFDI and GFDI) have been found to perform poorly when assessing the risk of high severity fires (Harris et al., 2011). The current FFDI and various other indices can be used to determine the risk of the outbreak of forest fires, but such indices cannot describe the risk of forest fires in terms of severity and intensity. Therefore, current indices cannot provide the overall danger and risk of a fire for mitigation by local fire authorities, particularly for the conditions found in Australia. This has been addressed conceptually by Harris et al. (2011), in which a fire severity scale was proposed based on the size and rate of propagation of the fire. The idea is that as there is an increase in the rate of propagation or perimeter spread of the fire, a larger amount of fuel is consumed, releasing energy into the atmosphere. This rate of energy released from the fire determines the severity of the fire.

Through the literature review for Chapter 6, there are many methods to determine the amount of energy released by fires due to the combustion of fuels with a common method; fire-line intensity being a measure of the energy released along the front of the fire itself (Byram, 1959). However, due to improvements in the retrieval of remotely sensed products, FRP provides an accurate estimation of the amount of energy released and is explored in this thesis. Little research has been conducted on the use of FRP, not only to determine minimum fire detection thresholds but also to be included in a fire danger index to produce a scaling of fire intensity and severity. This potential use of forecasting fire intensity in fire risk indices is similar in approach to many other natural hazard scales and risks' such as the case for hurricanes and cyclones (Saffir scale), earthquakes (Richter scale) and avalanches (e.g. European danger scale) but such approaches have been seldom studied in relation to forest fire. As such, further research could consider implementing the FRP into a modified FFDI, providing the scale as well as the risk of ignition (as current). Furthermore, the drought factor in this modified FFDI could be further simplified using either the API or a similar simple moisture index modulated by a moisture decay function.

As with previous chapters, ideally FFDI, FRP and moisture conditions should be compared at the daily scale. However, due to the availability and large uncertainty in the simulated projections of the variables used to calculated FFDI, primarily monthly means, and yearly totals are used to assess trends here (Chapter 7). This chapter could benefit from a more comprehensive comparison of the uncertainty between daily and monthly produced FFDI and to what degree this would effect the spatial variability seen across Australia. More specifically, the difference between daily and monthly RCP pathways and their affect on both extreme FFDI days, as well as, the overall trends could be further investigated. Ideally, the RCP 4.5 (and possibly RCP 6.5) would be added to the daily analysis, as well as, an expansion of the simulations used for ensemble means. Similarly, a comparison between FFDI derived using various moisture driven indices would add further information on the effect of soil moisture of projected FFDI trends.

Finally, as precipitation, temperature, surface wind, and relative humidity, as well as evapotranspiration and potential evapotranspiration (implemented in the hydrological models), originate from the same model, they are assumed to be physically consistent. For the purposes of this work, it was assumed that inter-model comparisons are valid and do not contain intrinsic differences. However, it is likely that the performance relating to the hydroclimatological processes differs between model members of the CMIP5 climate project. Due to this, the Budyko framework introduced in Chapter 5 could be

used to assist in selecting specific climate models that represent hydroclimatological processes better than others. This will not only result in more accurate projections of FFDI, but also allow for more accurate ensemble averages, and allow for better comparisons between the models themselves. Furthermore, the models used for projected changes in dryness/wetness (moisture indices) could be validated against the observations in the historical period similar to what has been done in Chapter 7.

APPENDIX A

Determining the Minimum Sampling Frequency for Ground Measurements of Burn Severity

This appendix has been included as additional work conducted in review of the methods for "burn severity" mapping, however, as it is not directly related to the aims or contents, it has not been included in the main body of work. This is a published work as declared in the preamble of the thesis as: Holmes, A., C. Rüdiger, S. Harris, and N. Tapper (2018). "Determining the Minimum Sampling Frequency for Ground Measurements of Burn Severity." International Journal of Wildland Fires (*in press*).

Overview Understanding burn severity is essential to provide an overview of the precursory conditions leading to fires as well as understanding the constraints placed on fire management services when mitigating their effects. Determining the minimum sampling frequency for ground measurements of achieved burn efficiency is not only essential for accurately assessing burn severity, but also for fire managers to better allocate resources and reduce the time and costs associated with sampling. In this study, field sampling methods for assessing burn severity are analysed statistically for ten burn sites across Victoria, Australia with varying burn extents, topography, and vegetation. Random and transect sampling methods are compared against each other using a Monte-Carlo simulation to determine the minimum sample size needed for a difference of 0.02 (2%) in the severity classes proportions, relative to the population proportions. We show that on average transect sampling requires a sampling rate of 3.16% compared to 0.59% for random sampling. We also find that sites smaller than 400 hectares require a sampling rate of between 1.4 and 2.8 times that of sites greater than 400 hectares to achieve the same error. The information obtained from this study will assist fire managers to better allocate resources for assessing burn severity.

A.1 Introduction

Forest fires occur regularly on a large scale across semi-arid regions such as south-eastern Australia. These fires cause significant strain on forest management services attempting to mitigate their impact on both community and the economy. Forest and fire management services throughout the world have long used vegetation management, in the form of controlled burning, to minimise fuel load and to mitigate potential fire danger in a region at risk. Forest fires, either through long or short term ecological impact, alter the vegetation and soil attributes from burning of surface litter to changing the species composition throughout a forest (Cocke et al., 2005; Keeley, 2009), and if applied as a preventive measure, reduce future large-scale fire risks. "Fire severity" or “burn severity” (current literature uses “burn severity” and is used hereafter) describes the immediate effects of a fire on organic matter such as vegetation, soil, and litter (Key et al., 2006; Keeley, 2009). In other words, burn severity is a function of the ecological change due to fire (Cocke et al., 2005) Due to this, improving the techniques and methods used by management services to quantify and map burn severity is essential to improve fire danger mitigation and manage the vegetation-fuel load. In particular, for controlled burns, it is essential to have knowledge on the effectiveness of the fire, i.e. how well it has reduced the fuel load, for which burn severity is taken as the quantifiable indicator. However, manual sampling is subjective and cannot be used for assessments across large areas, hence remote sensing techniques have been developed to estimate the fire severity from such data.

As mentioned, fire alters the vegetation, soil, and litter composition as well as exposing and altering the colour and brightness of the surface soil. This causes changes in the spectral response and as such can be detected through the visible near-infrared and mid-infrared wavelengths via remote sensing satellites (van Wagtendonk et al., 2004; Chuvieco et al., 2006). Currently, burn severity is determined using a combination of both remotely sensed and ground sampled data. As the accuracy of remotely sensed data has improved during recent years, it has become a more commonly deployed approach to determine burn severity (Keeley, 2009). Various satellite sensors (e.g. MODIS, ASTER, Landsat, RapidEye) have previously been compared against field measurements. The Landsat Thematic Mapper has been identified as the most accurate and commonly used instrument to estimate burn severity (van Wagtendonk et al., 2004; Brewer et al., 2005; Cocke et al., 2005; Chuvieco et al., 2006; Kokaly et al., 2007; French et al., 2008). This is achieved using various techniques. One such index is known as the differenced Normalized Burn Ratio (dNBR) (Brewer et al., 2005; Cocke et al., 2005; Miller et al., 2007) that is often used in the USA.

$$NBR = \frac{(R_4 - R_7)}{(R_4 + R_7)} \times 1000$$
$$dNBR = NBR_{prefire} - NBR_{postfire} \tag{A.1}$$

Equation A.1 describes the NBR and dNBR. Where R_4 and R_7 is the reflectance for bands 4 (0.76-0.9 μm wavelength) and 7 (2.08-2.35 μm wavelength) of the imagery, respectively. R is determined using the solar irradiance, the per-pixel brightness value, the grain and bias, the earth's eccentricity and the solar zenith angle. The dNBR can simply be described as the difference in the reflectance between pre-fire and post-fire images. In the USA, Burn Area Emergency Rehabilitation (BAER) assessors commonly use the dNBR to determine burn severity due to the speed and accuracy at which BARC (Burned Area Reflectance Classification) maps can be produced. Fire management services are yet to use NBR in Australia; however, recent studies have also used dNBR for determining burn severity, in particular, Boer et al. (2008) who used the leaf area index as a proxy for dNBR to determine burn severity patterns in southwestern Australia. They concluded that reductions in forest leaf area index were consistent with observed changes in flame length, scorch height and fire intensity (Boer et al., 2008). Many studies have indicated a strong correlation between burn severity classes produced with BARC and those produced from field assessments (Cocke et al., 2005; Miller et al., 2007). In order to ensure an acceptable quality, burn severity assessments using BARC maps should be conducted as soon as possible, post-burn, in order to correctly describe changes due to the fire. One limitation is that satellite "overpasses" will not necessarily coincide with either clear skies or the appropriate time (Keeley, 2009) and it is possible that several days to weeks may pass before an image can be acquired. Therefore, it is necessary for BAER assessors to continue assessing burn severity from field surveys. Also, field sampling is still needed to validate remotely sensed burn data. In order to limit resources expenditure, the sampling techniques need to be optimised, which is the focus of this paper.

Field sampling requires BAER assessors to record burn severity based on the proportion of burned area of organic matter from a sample area (Key et al., 2006). Globally, management services use various approaches to record burn severity. One such approach is the composite burn index (CBI), which is often used in the USA and Canada. It quantifies the proportion burned based on various organic metrics (vegetation, soil, litter, etc.). Key et al. (2006), proposed sample plots in which the CBI was to be assessed. These plots include all burn information within a 15m radius of a predetermined location that is to be assessed, expanding to 30m when burn effects are complex or it is too difficult to walk through. Similarly, in southeastern Australia DELWP (the Department of En-

vironment, Land, Water, and Planning) assess burn severity using plots, however, with a 10 m radius (DEPI, 2013b). DELWP indicate that the severity must be uniform for a minimum radius of 20m. This is required to reduce qualitative error and errors caused by positional inaccuracies with GPS devices. It is usually recommended that a range of vegetation and aspect (hill-slope and elevation), as well as burn patterns, are assessed to capture the spatial variability within a burn (Key et al., 2006; DEPI, 2013b).

Key et al. (2006) determine that depending on site size and complexity, 50 to 100 plots per burn are adequate in most cases. Nevertheless, if the total burn area is larger than 1000 hectares, the site exhibits large variability in burn severity such that the number of plots may need to be larger. Conversely, smaller burns tend to have a low spatial variability and it may be sufficient to record as few as 20 to 40 plots. DELWP provides its own guideline to determining the number of plots necessary and suggest that all sites should include at least ten plots per severity class where possible (DEPI, 2013b), further specifying that sampling be taken at a rate of between 0.5% and 4% (of the total area) depending on the size of a site. Generally, for operational assessments, a sampling rate of between 0.5% and 1% is used (DEPI, 2013b). In either case, field sampling is recommended to be recorded in transects throughout burn sites.

Field sampling requires extensive time and resources to accurately depict the severity of any given fire due to the size of burn sites and accessibility of plots, the amount of information recorded and occupational health and safety procedures (Key et al., 2006; Keeley, 2009; DEPI, 2013a; DEPI, 2013b). As a result, there is a large variation in sampling techniques between different fire authorities in different countries (e.g. the U.S Department of Agriculture using the CBI, and in Victoria, Australia, DELWP and the Country Fire Authority defining their own method), however, there are no specific studies to quantitatively determine the rate at which field sampling should be recorded to produce an accurate representation of burn severity. This paper addresses this, and the results could be applied globally regardless of the burn severity assessment tool used.

This sampling rate is determined here by statistically analysing the differences between transect sampling and random sampling within a region. The objective of this study is to determine the minimum sampling rate at any given burn site for the random and transect sampling to reduce the time and resources for fire managers to collect field data.

A.2 Study Sites and Datasets

A.2.1 Study Sites

This study presents a burn severity analysis of ten burn sites across Victoria, Australia. The burn sites are located within national forests (see Figure A.1. The sites were chosen due to the completeness of records and access to the data as it was supplied through DELWP. These sites have been part of the fire assessment from prescribed burns between 2012 and 2013. Each site varies significantly in size and topography, ranging between 223 ha (Gembrook) and 3,613 ha (Valencia Creek). A summary of the sites, their individual name, location, size and burn class percentages are given in Table A.1. The vegetation within each site also varies substantially with vegetation ranging from wet sclerophyll forests with a high canopy and fern understory to dense, dry sclerophyll forests with a much lower canopy height.

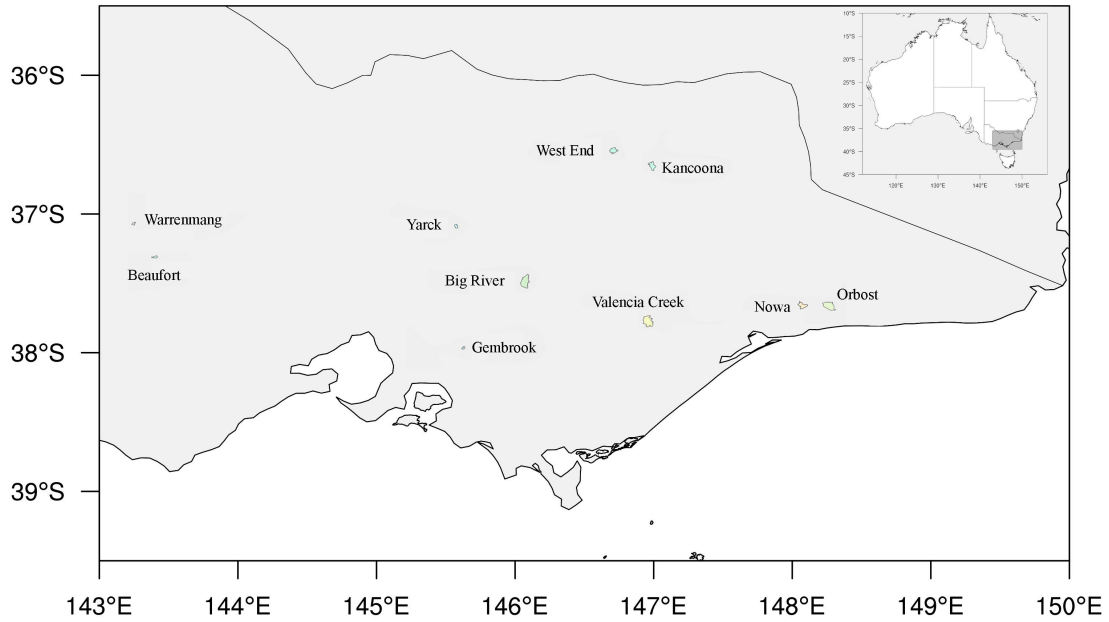

Figure A.1: Locations of burn sites and their relative size within Victoria. Inset map of Australia, indicating the region where sites are located.

Table A.1: Summary of burn sites. Size, location, burn class percentages and sampling rate for both random and transect sampling methods are shown. Minimum iterations required are calculated using the formula: $n = [\frac{(Z_{\alpha/2}S_d)}{E}]^2$, where, Z is the critical value for a given statistical significance (given as α, it is equal to 0.05 for 95% significance; resulting in a Z value of 1.96), Sd is the populations standard deviation and E is the standard desired error (5% in this case).

Site	Lat	Lon	Size	Minimum	Burn Proportions [%]				Random [% Sampled				Transect [% Sampled]			
				Iterations	1	2	3	4	1	2	3	4	1	2	3	4
Beaufort	37.29 S	143.38 E	327.5	901	57.3	30.7	9.4	2.5	1.55	1.26	0.5	0.06	6.64	3.58	1.93	0.22
Big River	37.52 S	146.0 E	3,513.50	917	21.6	36.2	42.1	0.1	0.09	0.13	0.22	NA	1.14	1.63	2.71	NA
Gembrook	37.96 S	145.6 E	222.9	781	53.4	33.4	13	0.1	1.98	1.73	0.99	NA	17.13	7.13	14	NA
Kancoona	36.66 S	146.96 E	1,632.60	863	42.9	38.1	18.9	0.1	0.37	0.38	0.16	NA	3.33	1.64	2.06	NA
Nowa	37.67 S	148.03 E	1,491.90	649	63	28.3	8.7	0.3	0.38	0.28	0.14	NA	2.46	1.34	0.41	NA
Orbost	37.68 S	148.22 E	2,951.20	991	48.5	31.3	19.1	1.1	0.11	0.15	0.05	NA	2.89	1.22	2.17	0.02
Valencia	37.8 S	146.92 E	3,612.70	1108	35.3	40.7	19.5	4.5	0.21	0.15	0.07	0.17	1.51	1.13	0.67	0.23
Warrenmang	37.05 S	143.2 E	280.7	1072	36.6	38.3	22.2	2.9	2.03	1.78	1.32	0.13	8.06	4.17	4.6	0.67
West-End	36.49 S	146.74 E	1,369.90	929	9.4	36.9	45.4	8.3	0.34	0.56	0.76	0.12	0.78	2.17	2.16	0.97

A.2.2 Remotely Sensed Data

Burn severity classes can be derived through the use of high-resolution remotely sensed data. Many BARC related studies (van Wagtendonk et al., 2004; Miller et al., 2007; Keeley, 2009) use a variety of remotely sensed products to produce dNBR, namely, Landsat, ASTER (Advanced Spaceborne Thermal Emission and Reflection Radiometer), MODIS (Moderate Resolution Imaging Spectroradiometer) and MASTER (MODIS-ASTER). However, in Victoria, DELWP uses the RapidEye product to produce burn severity through the Burn Severity Assessment Tool (BSAT). Similar to the aforementioned products, RapidEye provides the required multi-spectral images from the red, green, blue, red-edge and NIR bands through its constellation's five satellites. At 5-10 m, RapidEye has a much higher spatial resolution than Landsat (15-30 m), MODIS (250m), and ASTER (15-30 m). RapidEye also has a geolocation accuracy of 10 m, and a revisit time of 1-5.5 days (Arnett et al., 2015).

A.2.3 Severity Classification

Remotely Sensed Products

The US Forest Service specifically developed the BARC to produce severity classes based on remotely sensed optical imagery. As mentioned, satellite reflectance values are used to characterise burn severity through Equation A.1, to produce the dNBR. Where available (otherwise NBR is used) dNBR is scaled to the dynamic range of 8-bit data (0-255) to produce the BARC-Adjustable (BARC-A) product from which BARC maps are derived. Jenks Natural Breaks logic is used to classify the BARC-A product into four classes, 0-75 (unburnt), 76-109 (low), 110-187 (moderate) and 188-255 (high) (Key and Benson 2006).

Similarly, DELWP produces severity maps from remotely sensed data using the BSAT. As with BARC, BSAT is a semi-automated GIS tool designed specifically for use with RapidEye satellite imagery. Differently from the BARC product, the BSAT calculates the Differenced Normalized Difference Vegetation Index (dNDVI) using RapidEye images. dNDVI is calculated using:

$$\begin{aligned} NDVI &= \frac{(NIR - Red)}{(NIR + Red)} \\ dNDVI &= NDVI_{prefire} - NDVI_{postfire} \end{aligned} \tag{A.2}$$

where, Red and NIR are the spectral reflectance measurements acquired from the visible-red (0.63-0.685 μm) and near-infrared (0.76-0.85 μm) wavelengths, respectively. From this, four classes of severity are produced using a Jenks Natural Breaks logic adjusted to match visual observations (detailed in DEPI (2013a)).

Field Observations

Due to the varied composition of forests, burn severity may be difficult to ascertain and compared against in different locations. Due to this, in Victoria, DELWP divides severity into four classes to match those produced using the BARC and BSAT methodologies. In plots where the canopy is more than 50% burnt, vegetation is black and disintegrates easily, are defined as the most severe (Black). Plots in which the canopy is less than 50% burnt but the combined scorch and burnt area exceeds 50%, are described as the second most severe (Brown), and those that are less than 50% burnt and scorched, are the third most severe class (Green). The final unburnt class (Blue) is defined as a plot where the surface vegetation is 100% unburned. To reflect variation in vegetation type and density it is suggested that samples are taken across plots with a relatively uniform vegetation across a radius of 10 m (DEPI, 2013a).

A.2.4 Sampling

As the aim of this paper is to estimate the minimum number of samples in a given area to provide an accurate classification of the overall burn site through sub-sampling, two sampling techniques, random sampling, and transect sampling were tested as described below (both of which are commonly employed by DELWP for sampling). This was done by comparing the populations' proportions (determined by calculating the fraction of the number points per class divided by the total number of points per burn site) to the sampled proportions for each possible sample size.

This difference is expressed as the mean absolute error (MAE) between each severity class's proportion from sampled points and from the overall population for each severity classification.

$$MAE = \frac{1}{k}\sum_{j=1}^{k} |(Severity_{i,population} - Severity_{i,sample})| \tag{A.3}$$

Where, *Severity* is the proportion of the given severity class i calculated for the population and for the number of samples used, j. Where k is the total number of iterations.

This approach has been applied to determine the minimum samples needed to accurately represent the population proportions for each severity class.

Random Sampling

Random samples were taken from the overall population starting from one sample to the total number of samples available in the population. This enabled the computation of the difference (MAE) between sampled proportions and the overall populations' proportion, at each sample size. As there is a large variation in the possible combinations of samples and proportions per sample size, a Monte-Carlo-type method was applied (Metropolis et al., 1949). That is, the aforementioned process was repeated 1000 times from which a mean value for the sample severity proportion was obtained. The number of iterations per sample size was chosen to sufficiently minimise the variation in proportions per sample size as per the Monte-Carlo convergence (Cowles et al., 1996). This was chosen as 1000 iterations exceeded the average minimum number of iterations (see Table A.1 for a summary of the minimum number of iterations per site) required so that the mean value is within an accuracy of 5% at 95% confidence (Driels et al., 2004). The main difference between a classic Monte-Carlo method and the method used here is that samples are taken without replacement. Whilst used for a different field of study, statistically, this is intrinsically similar to the Monte-Carlo sampling approach used in a study by Hale et al. (2012). Here, the minimum samples needed to represent the population proportion of allele frequencies (gene mutations) for various animal species within a mean error of 0.02 were calculated. By using this method at an error of 0.02, Hale et al. (2012). were able to accurately estimate the proportions of samples.

This approach produced an exponential decay at which the mean absolute error in the sampled burn severity proportion approaches zero with increasing sample size, as it would be expected in a randomly distributed population. From this, the minimum number of samples needed to achieve an accurate (less than 0.02 error) depiction of the population proportions can be determined. Sample size estimation of multinomial populations from stratified random sampling has been investigated by Thompson (1987) and Cochran (1977). Both provide sample size estimates between unknown population proportions and sample proportions, suggesting possible values for the difference d (error) at various significance levels (99%, 95%, 90%, etc.). Typically, they suggest using a difference of 0.01 or 0.02 and 0.02 or 0.05 for Thompson (1987) and Cochran (1977), respectively, as well as a significance level 95% in most cases. This general estimation provides a worst-case sampling rate in excess of what is practical for recording observations. The 0.02 error used in this study has been chosen to remain consistent with the current practices of DELWP and with the studies of Thompson (1987), Cochran (1977), and Hale et al.

(2012).

Transect Sampling

As an alternative to random sampling, transect sampling follows a predefined sampling path, with regularly spaced samples taken. Transects were taken along every horizontal and vertical grid line (in one direction) with sampling taken at the desired resolution. Similarly, as with random sampling, 1000 combinations of transects were sampled (selected at random with replacement) in order to provide robust results. This method is intrinsically similar to Barabesi et al. (2012) of sub-sampled data, in which the difference between transect-point and transect-line sampling methods were analysed.

As before, the MAE was calculated for each burn severity class and each combination of transects. That is, the total count of each severity classification for each combination of transects was divided by the number of points in each combination of transects. Following this, the mean difference between the samples severity proportion and the population proportions were calculated.

A.3 Results

The direct comparison between random and transect sampling for the Gembrook burn site is shown in Figure A.2. As expected, when the sampling rate of the burn site increases, the mean absolute difference in the proportion decreases exponentially. For all severity classes (except class 4), the mean fractional difference asymptotes below 0.01 when the sampling rate reaches roughly 50% of the overall points. At the Gembrook burn site, the random sampling method reaches the 0.02 MAE baseline at a lower sampling rate than that of the transect sample method for the severity classes 1-3. Severity class 4 occurs in few locations, resulting in a much smaller total number of points and consequently a negligible mean difference. This analysis shows that to reach the minimum error in the representation of severity class 1, sampling rates of 1.98% and 17.36% are needed for random and transect sampling, respectively. Likewise, a sampling rate of 1.73 (7.13) and 1.00 (14.00) would be required for severity classes 2 and 3 for random (transect) sampling.

Similarly, Figure A.3 shows the comparison of classes and sites over and under 400 Ha for the average of all sites. Where each panel shows the mean, per class, for sites under 400 Ha and above 400 Ha as well as for transect and random sampling methods. Shown as a shaded ribbon are the 0.25 and 0.75 quantile ranges of all the sites. Following Cleveland et al. (1988) the fitted locally weighted regression or LOESS (Locally weighted scatterplot smoothing) fit is fitted to each site as per Figure A.2 (Gembrook), in the form of :

$$y = a \times log(b \times x) + c \tag{A.4}$$

However, this is a non-parametric regression providing a multivariate smoothing by applying a fitted function of the variables locally (Cleveland et al., 1988). This LOESS regression applies a low-degree polynomial fit at each point in the range, producing multiple shape, intercept, and scale parameters to determine predictive statistics for the relationship. From Equation 4, and using the LOESS regression we obtained the sampling rate for an MAE of 0.02 for each site and sampling methods. A summary of the results is also available in Table A.1. Here, results are consistent with observed values, with Beaufort, Gembrook, and Yarck-Terrip requiring the largest sampling rate, in the order of twice the magnitude of the other sites. In general, the sampling rate needed for an MAE of 0.02 is 0.59% and 3.16% for random and transect sampling respectively (Figure A.3). On average, transect sampling would, therefore, require 5.35 times the sampling rate of random sampling to produce a 0.02 MAE.

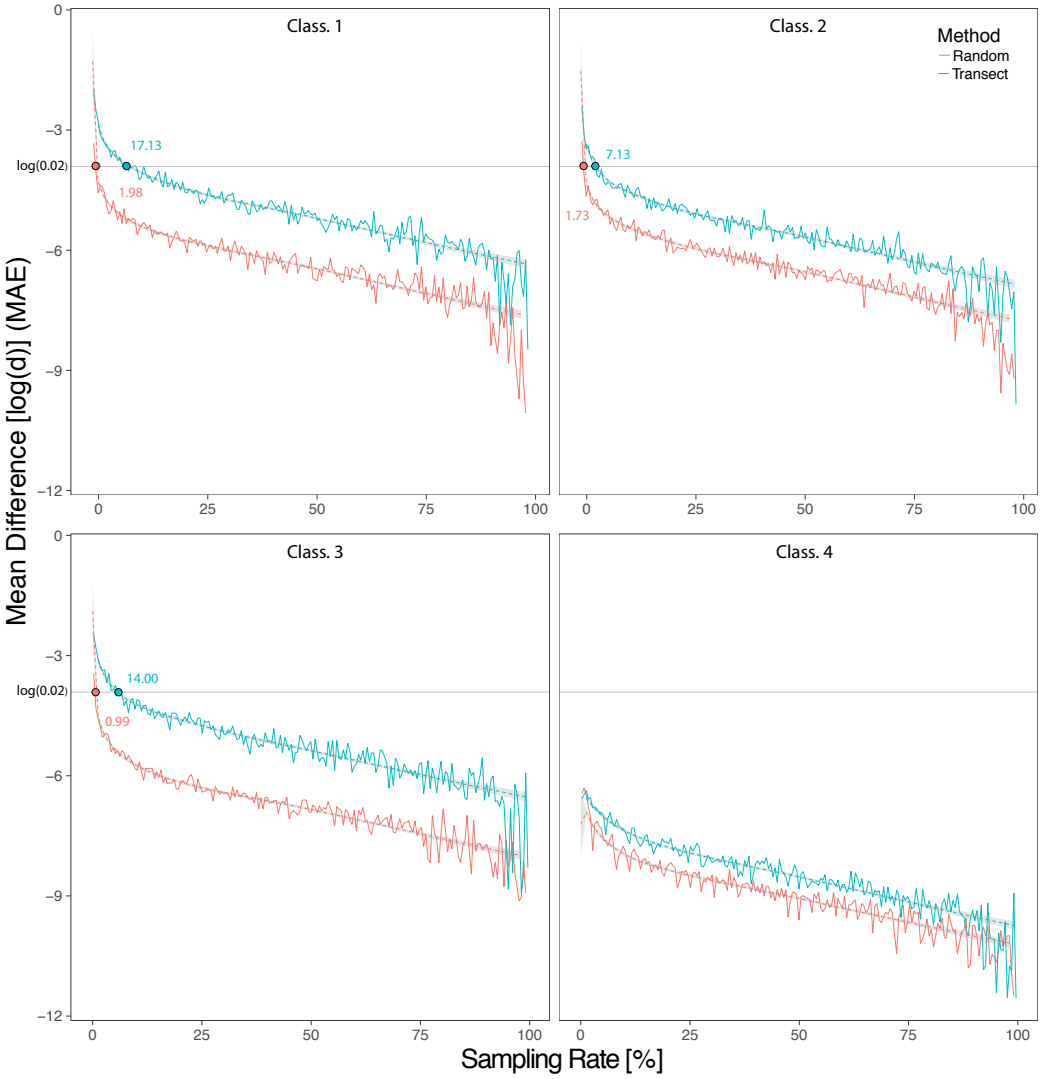

Figure A.2: Mean Absolute Error (MAE) or mean difference in classification proportion (y-axis) versus the sampling rate (x-axis) for the Gembrook site. Random (blue) and transect (pink) sampling are compared directly against each other for each severity classification. The minimum sample required for a maximum difference of 0.02 is given for both random and transect sampling (excluding the most severe class). Also shown are the fitted nonlinear least squares regression curves and 0.02 MAE intercepts and the 0.02 MAE intercepts.

Lastly, the sampling rate for all severity classes for sites over 400 hectares and below 400 hectares has been compared (Figure A.4). This threshold has been chosen to remain consistent with DELWP's standard sampling practices, which state two different sampling rates for sites smaller and larger than 400 Ha. On average, sites smaller than 400 hectares require a sampling rate of 4.15% and 16.41% to achieve a maximum MAE of 0.02 for random and transect sampling, respectively, compared to 1.49% and 11.52% for sites larger than 400 hectares (Figure A.4). In general, sites that are smaller than 400 hectares require 1.4 and 2.8 times more points to be sampled than for sites over 400 hectares. This

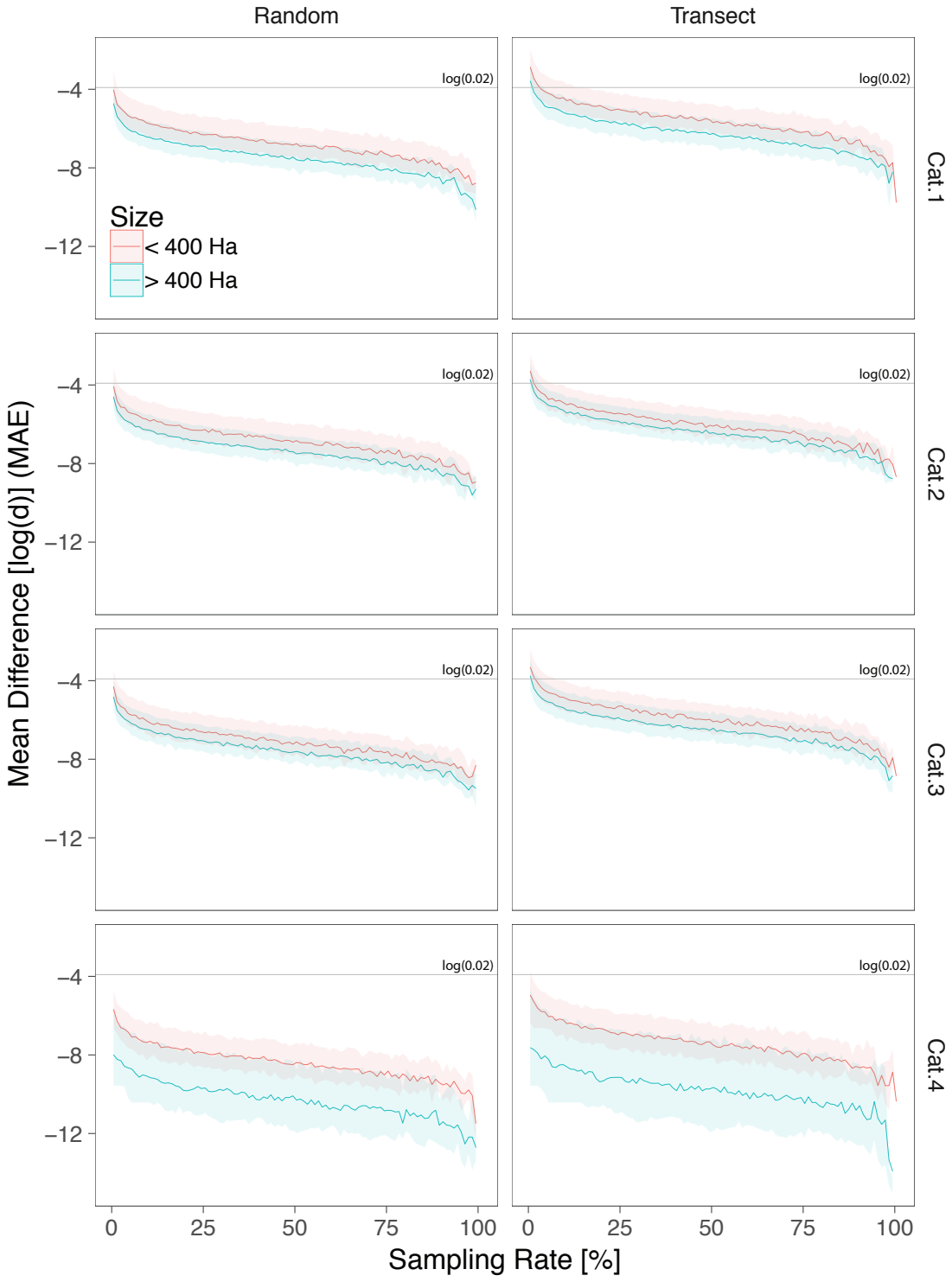

Figure A.3: Mean Absolute Error (MAE) or mean difference in classification proportion (y-axis) versus the sampling rate (x-axis) averaged for all sites. Each panel represents the severity classes for both random and transect sampling methods. Also shown are the 0.25 to 0.75 quantile bounds for the range of MAE values for all sites (shaded). Each colour represents sites greater than 400 Ha (pink) and less than 400 Ha (blue).

is somewhat to be expected as the data are discrete categories. This means that as the data's population decrease (the site size) the standard deviation increases considerably compared to larger sites, therefore providing larger inaccuracies. It is also found that there is a large difference between the median and mean sampling rates for transect sampling, which is due to the variability in the accuracy of the sampling method in contrast with random sampling. Values range between a sampling rate of 0.04% and 2.02% and between 0.02% and 17.35% for random and transect sampling, respectively. This highlights that for transect sampling, the sampling rate needed for a mean difference of 0.02 is consistently higher than that achieved using the random sampling method, irrespective of the site, its overall burn severity, and the severity proportion of the achieved burn.

As with the Gembrook site, the number of points per class affects the sampling rate required for an MAE of 0.02 for each of the burn sites. It should be noted that classes with a very small number of points will have a near-zero proportion which may differ substantially from the populations' proportion. Where classes do not have any samples, the proportion is denoted as NA in Table A.1. Due to this, it is often the case that Class 4 has much lower errors than the other classes. As there is a large error in the population proportions depending on the number of plots recorded per class, a locally weighted regression was fitted to both the random and transect methods for each class.

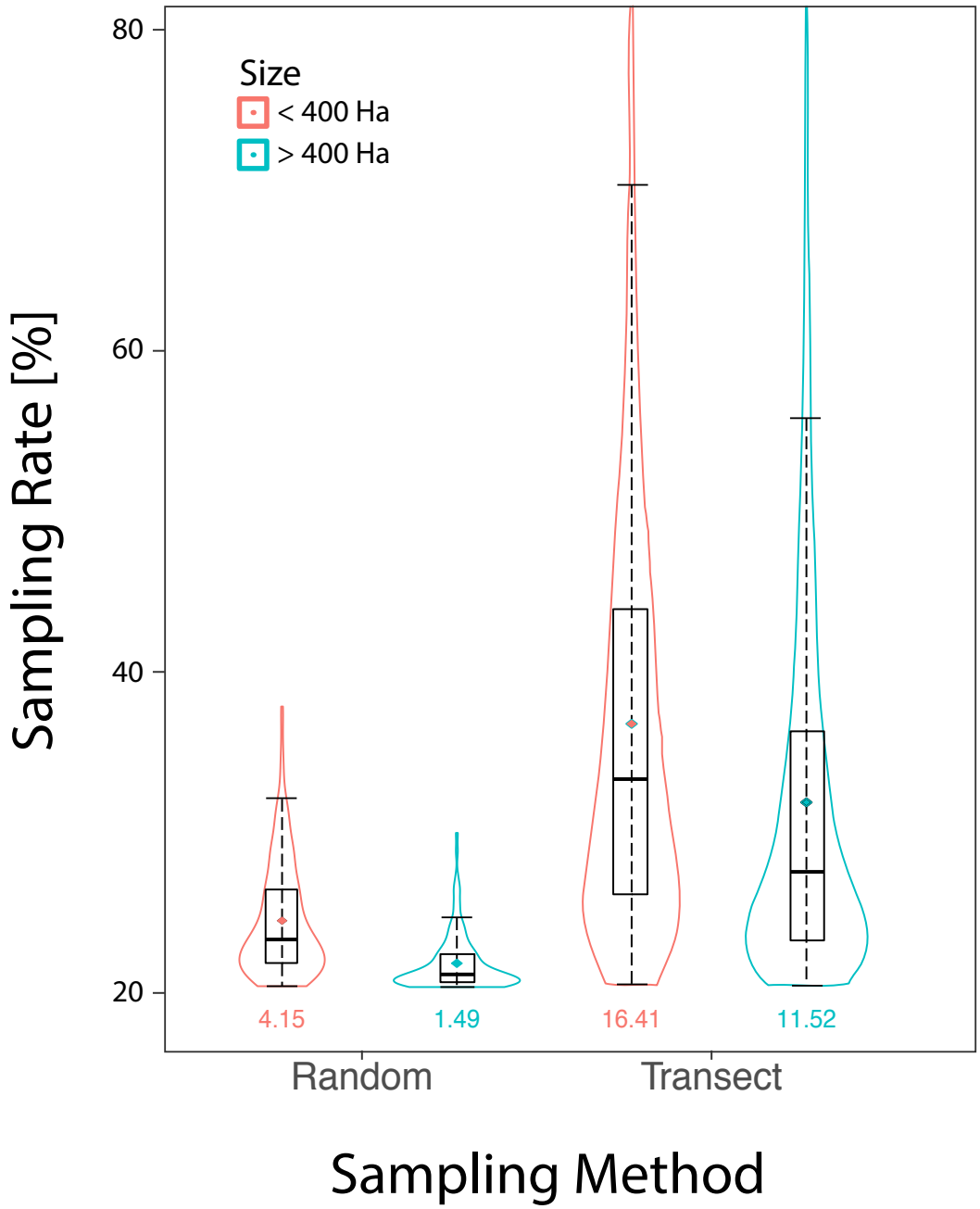

Figure A.4: Comparison of the sampling rate (y-axis) at sites greater than 400 Ha (pink) versus at sites less than 400 Ha (blue) for both random and transect sampling methods (x-axis). All points $\pm$ 0.0005 of the 0.02 Mean Absolute Error (MAE) calculated from raw values overlayed onto the boxplots. The shape of the violin plot reflects the relative density. Also shown is the mean sampling rate as calculated from the fitted loess curve at an MAE of 0.02.

A.4 Discussion and Conclusions

Recommendations of "good practices" for the accurate assessment of remotely sensed data products refer to estimations of sample size of "strata" or classes from Thompson (1987) and Cochran (1977) (Olofsson et al., 2014). These generally provide rough estimates of worst-case scenarios which often over- or underestimate sampling rates used for stratified random sampling, only. This does not allow for the consideration of geographical differences between study sites nor does it take into account a comparison of various sampling techniques such as transect and random sampling. Due to economic, methodological and other constraints, government organisations such as DELWP often are required to assess the "good practices" of ground measurements such as with fire severity.

To determine the minimum sampling rate for effective and efficient ground measurements of burn severity across forests, this study presents a comparison between two different sampling techniques, drawing spatially distributed data from remotely sensed severity assessments. The accuracy from which a sample size was drawn from a burn site to depict the overall classification characteristics was estimated using both random sampling and sampling along transects. The minimum sampling rate required to achieve a difference of less than 0.02 between the sample classification and the overall burn classification was compared across ten managed burn sites across Victoria, Australia.

We find that random sampling requires much lower sampling rates for an MAE of 0.02 or less for the ten burn sites compared to transect sampling. This is also the case for each of the severity classes, however, accuracy is generally limited by the number of points within the class itself. As the number of points within a class increases, the MAE decreases. As a consequence, larger sites require a much lower spatial sampling rate than smaller sites, to obtain the same MAE. At the same time, burnt areas become more homogeneous at larger scales, reducing the small-scale patchiness of the burns. However, it must be noted that the total number of samples needed will also be higher. Both random and transect sampling follow an exponential decay with increasing sampling rates which is observed for all sites and severity classes.

The results shown here indicate that across all sites, sampling is required at a rate of 0.58% and 5.35% for random and transect sampling. Furthermore, our results show that for sites smaller than 400 hectares, sampling would be required at a rate of 0.89% and 5.35% for random and transect sampling, respectively. Sites larger than 400 hectares would require a sampling rate of 0.73% and 3.4% for random and transect sampling, respectively. These results highlight that random sampling requires a lower number of

points per hectare sampled and also that the sampling rate is dependent on the size of a site.

Overall, the results suggest that the current sampling rate specified by DELWP may not be sufficient to accurately depict burn severity. DELWP indicates that sampling should be made at a rate of 4% for sites smaller than 400 ha and 2% for sites over 400 ha. Considering transect sampling only, our results indicate that the sampling rate of sites smaller than 400 hectares should be a minimum of 5.35% compared with the 4% designated by DELWP, however, for sites larger than 400 hectares, sampling is only required at 3.4% compared to 2% Note that the required sampling rate would substantially reduce by selecting an MAE smaller than 0.02 (2%).

One caveat of this work is that further studies are necessary to determine the cost-benefit or efficiency of employing the random sampling method compared to transect sampling. It may not be realistic to apply random sampling across a large site where the time taken walking between random plot locations could be greater than the time taken to record data where plot locations are in a straight transect. In such cases, recording data using transects could prove more cost-effective than using random sampling. This is also dependent on the number of observers, the size, and type of data recorded as well as other factors that are not considered as factors in this study, which focused purely on the differences in sampling requirements of burn sites.

APPENDIX B

Additional Content

Overview Any additional figures, tables or equations referred to in text but not discussed in detail are to be presented in this appendix chapter.

B.1 Figures

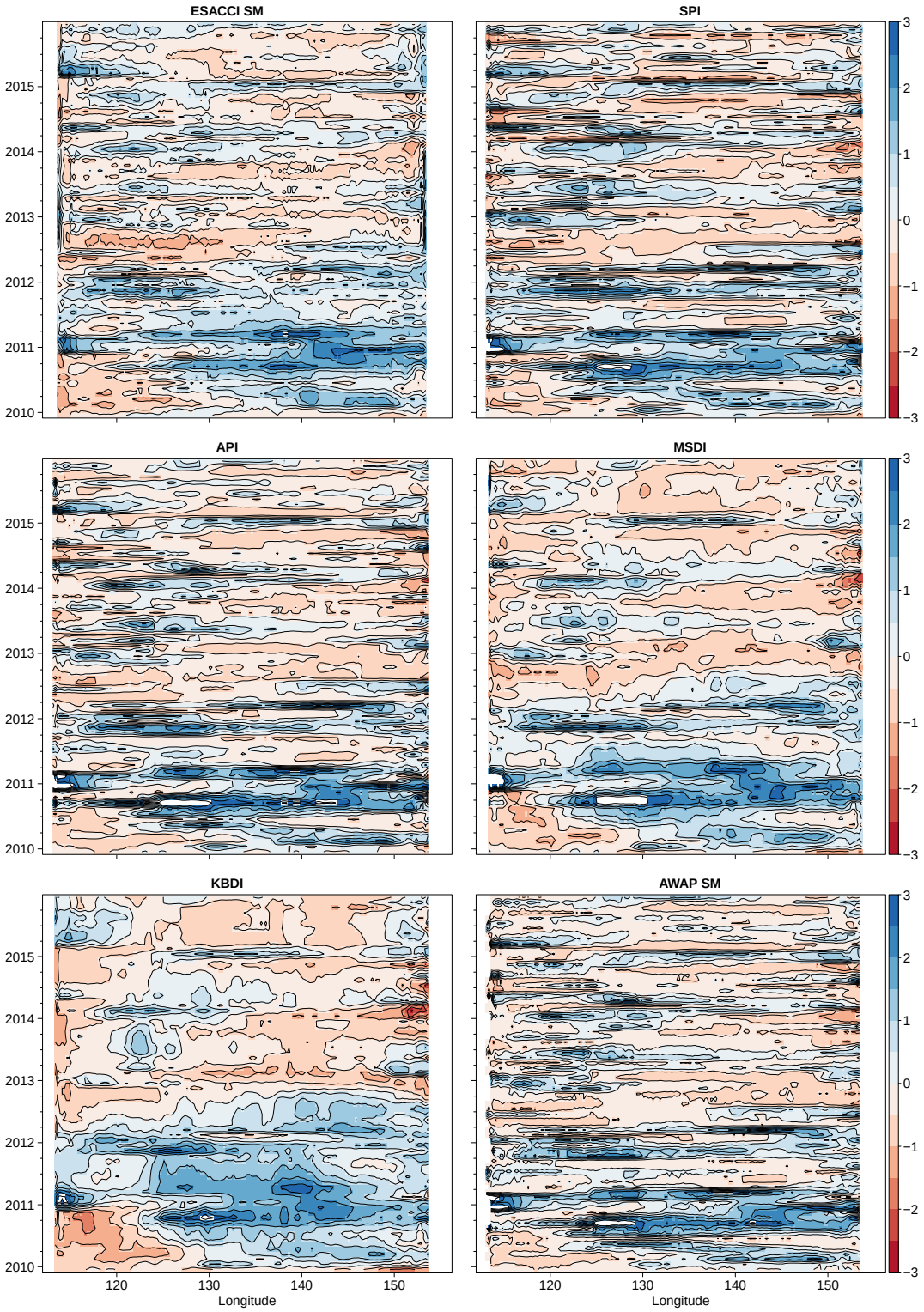

Figure B.1: Time-longitude Hovmöller diagrams of anomalous monthly soil moisture (compared to the 1979-2015 climatological mean) for each moisture index averaged between $10°S$ and $44.5°S$ latitudes during the 2010-2015 period.

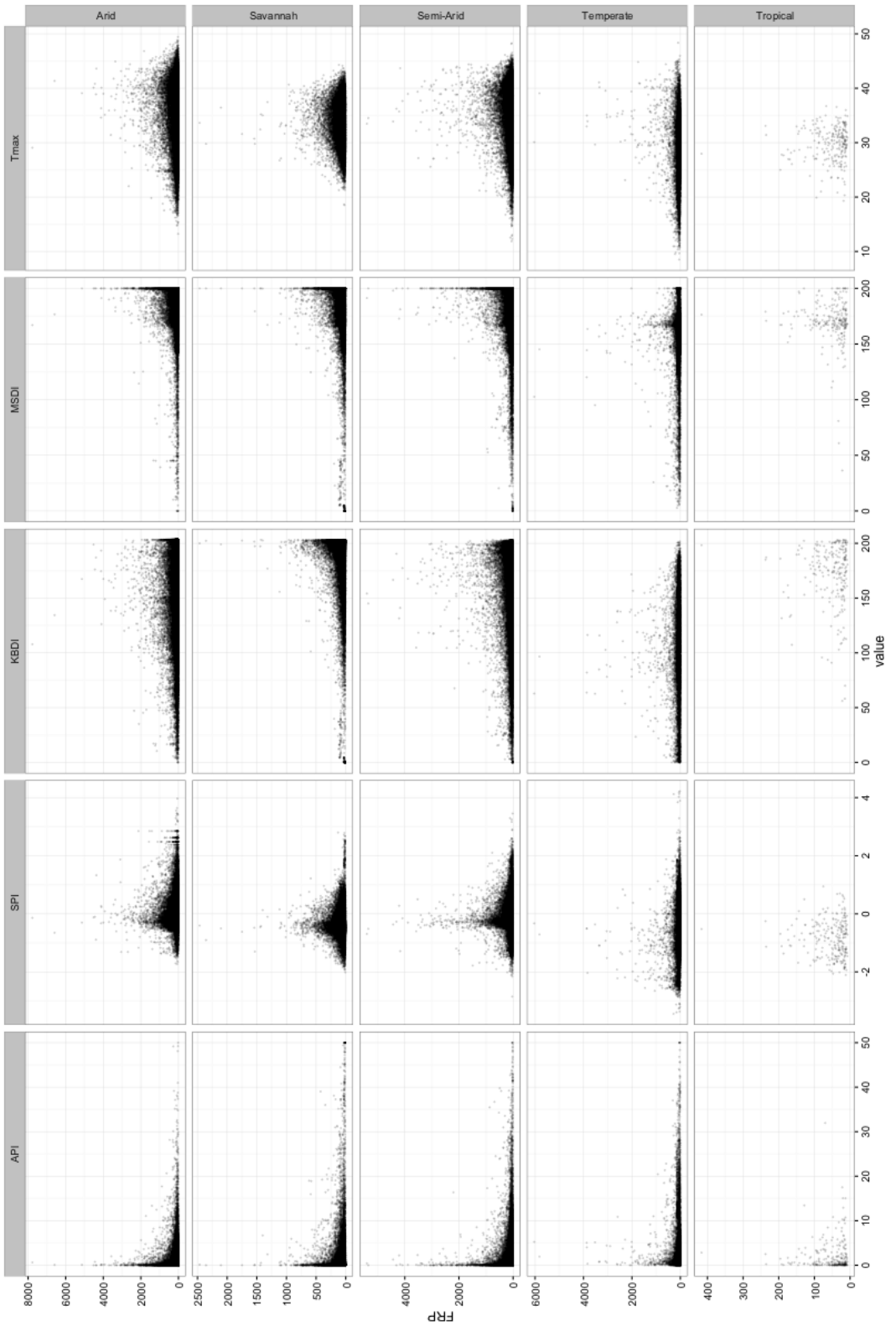

Figure B.2: API, SPI, KBDI, MSDI, and maximum temperature versus FRP (MW) for all fires in Australia between 2000 and 2015 (retrieved from MODIS) separated by Köppen-Geiger climate regimes.

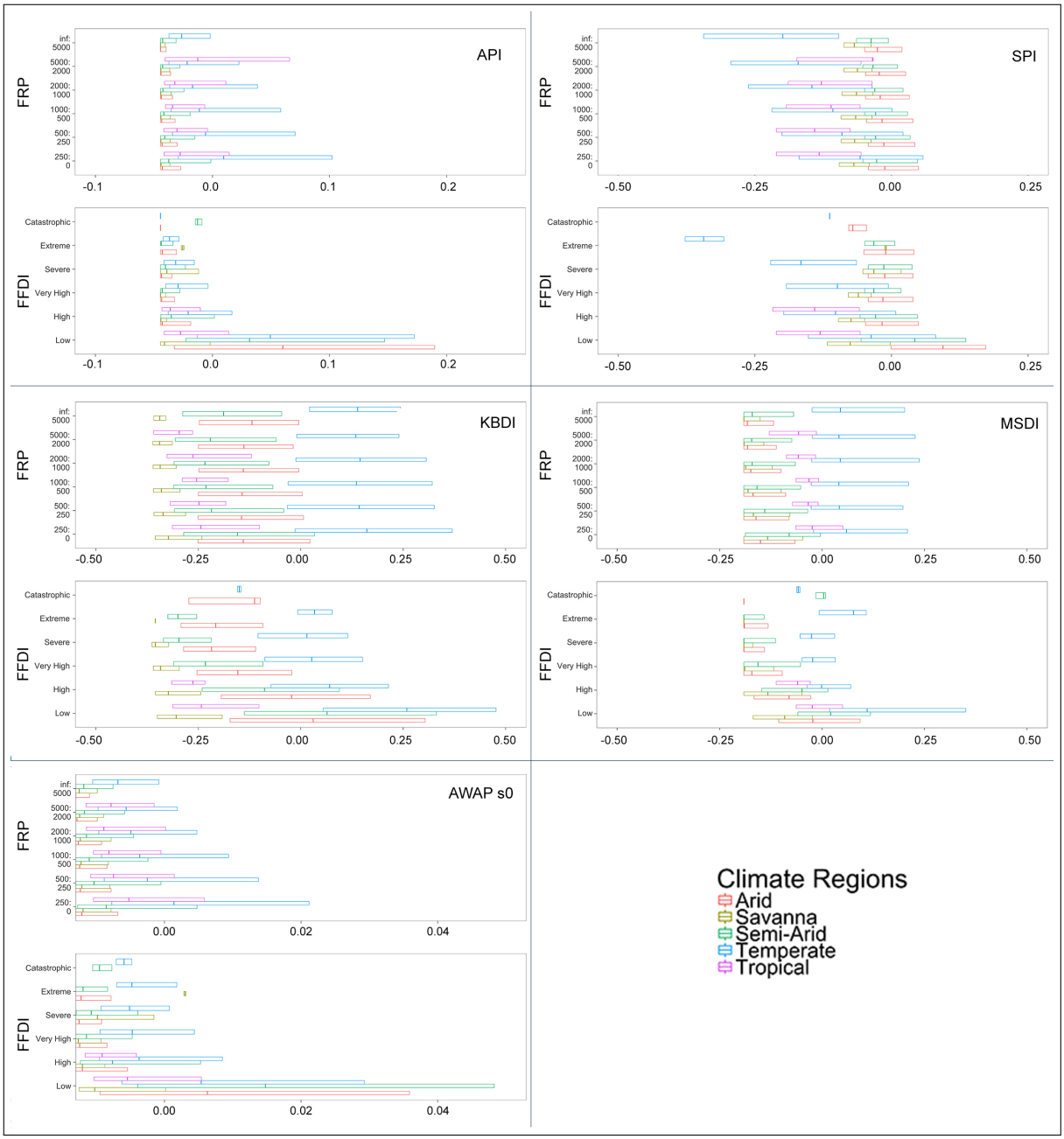

Figure B.3: Boxplots of moisture indices versus FRP and FFDI for each Köppen-Geiger climate regime. FRP is given in ranges of MW and the scale of each moisture index indicates the anomaly of normalised values. Data are for all fires in Australia between 2000 and 2015 (retrieved from MODIS)

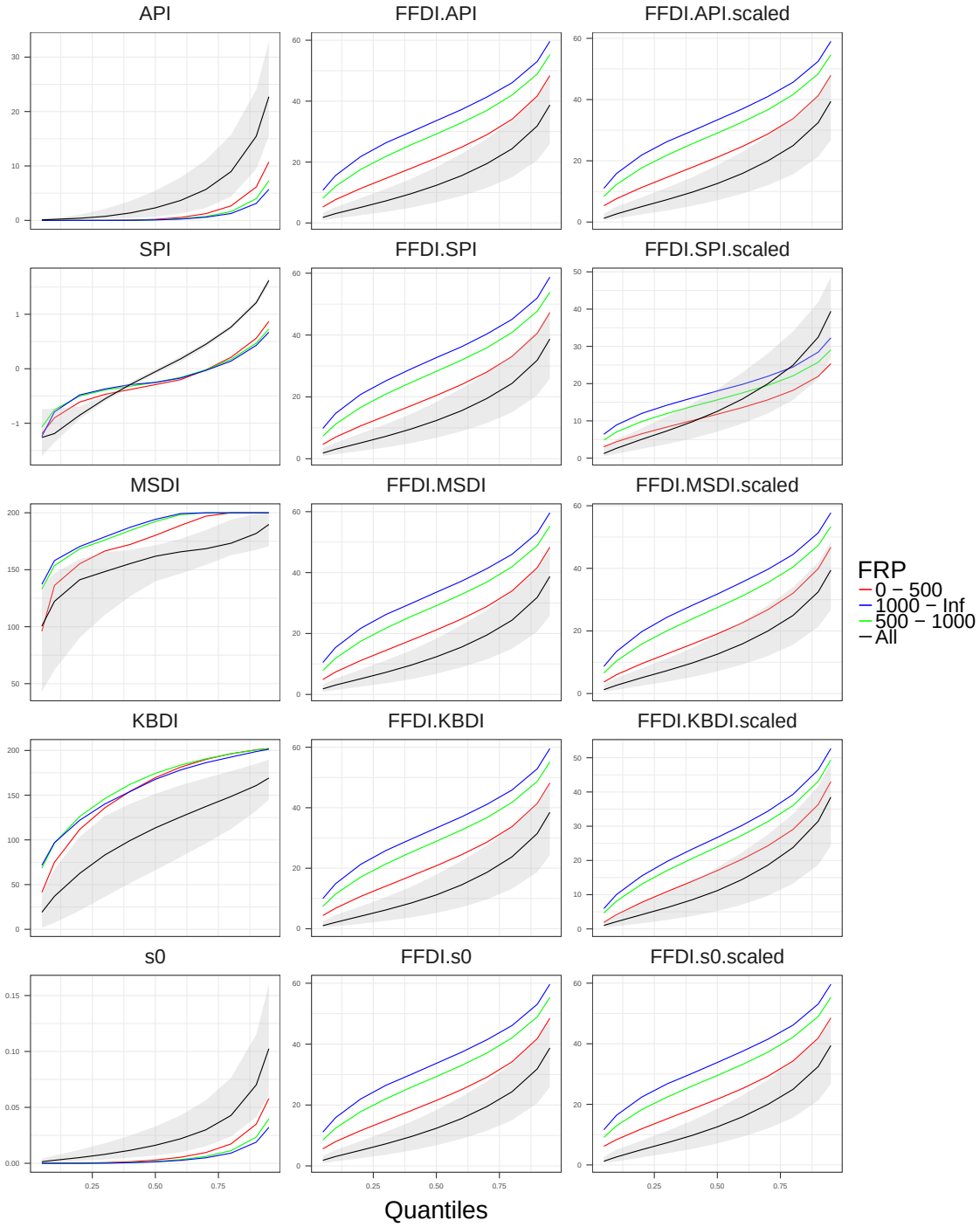

Figure B.4: Difference in FRP quantiles for FRP ranges; 0-500 MW, 500-1000 MW, 1000+ MW, and all fires and each moisture index, scaled FFDI's and for the KBDI replaced FFDI's. Y-axis indicates the variables non-normalised values and the x-axis indicates the quantile.

References

1. Abramowitz, M. and I. A. Stegun (1964). *Handbook of mathematical functions with formulas, graphs, and mathematical tables*. 64060036 edited by Milton Abramowitz and Irene A. Stegun. illus. 27 cm. Bibliographical footnotes. Washington, U.S. Govt. Print. Off., xiv, 1046 p.

2. Ainuddin, N. and J. Ampun (2008). "Temporal analysis of the Keetch-Byram Drought Index in Malaysia: Implications for Forest Fire Management". In: *Journal of Applied Science* 8.21, pp. 3991–3994.

3. Albergel, C., W. Dorigo, R. H. Reichle, G. Balsamo, P. de Rosnay, J. Muñoz-Sabater, L. Isaksen, R. de Jeu, and W. Wagner (2013). "Skill and Global Trend Analysis of Soil Moisture from Reanalyses and Microwave Remote Sensing". In: *Journal of Hydrometeorology* 14.4, pp. 1259–1277. ISSN: 1525-755X 1525-7541. DOI: 10.1175/jhm-d-12-0161.1.

4. Albergel, C., P. de Rosnay, C. Gruhier, J. Muñoz-Sabater, S. Hasenauer, L. Isaksen, Y. Kerr, and W. Wagner (2012). "Evaluation of remotely sensed and modelled soil moisture products using global ground-based in situ observations". In: *Remote Sensing of Environment* 118, pp. 215–226. ISSN: 00344257. DOI: 10.1016/j.rse.2011.11.017. URL: http://www.sciencedirect.com/science/article/pii/S0034425711004147.

5. Andela, N., D. C. Morton, L. Giglio, Y. Chen, G. R. van der Werf, P. S. Kasibhatla, R. S. DeFries, G. J. Collatz, S. Hantson, S. Kloster, D. Bachelet, M. Forrest, G. Lasslop, F. Li, S. Mangeon, J. R. Melton, C. Yue, and J. T. Randerson (2017). "A human-driven decline in global burned area". In: *Science* 356.6345, pp. 1356–1362. DOI: 10.1126/science.aal4108. URL: http://science.sciencemag.org/content/sci/356/6345/1356.full.pdf.

6. Andreae, M. O. and P. Merlet (2001). "Emission of trace gases and aerolsols from biomass burning". In: *Global Biogeochemical Cycles* 15.4, pp. 955–966.

7. Armstrong, S. and F. Collopy (1992). "Error Measures For Generalizing About Forecasting Method: Empirical Comparisons". In: *International Journal of Forecasting* 8, pp. 69–80.

8. Arndt, S. (2013). *Wombat State Forest OzFlux tower site OzFlux: Australian and New Zealand Flux Research and Monitoring hdl: 102.100.100/14237*. Dataset.

9. Arnett, J. T. T. R., N. C. Coops, L. D. Daniels, and R. W. Falls (2015). "Detecting forest damage after a low-severity fire using remote sensing at multiple scales". In: *International Journal of Applied Earth Observation and Geoinformation* 35, pp. 239–246. ISSN: 03032434. DOI: 10.1016/j.jag.2014.09.013.

10. Balling Jr, R. C., G. A. Mayer, and S. G. Wells (1992). "Relation of Surface Climate and Burned Area in Yellowstone National Park". In: *Agricultural and Forest Meteorology*.

11. Barabesi, L. and L. Fattorini (2012). "Random versus stratified location of transects or points in distance sampling: theoretical results and practical considerations". In: *Environmental and Ecological Statistics* 20.2, pp. 215–236. ISSN: 1352-8505 1573-3009. DOI: 10.1007/s10651-012-0216-1.

12. Barbosa, P. M., D. Stoppiana, and J.-M. Gregoire (1999). "An assessment of vegetation fire in Africa (1981-1991): Burned areas, burned biomass, and atmospheric emissions". In: *Global Biogeochemical Cycles* 13.4, pp. 933–950.

13. Barnes, W. L., T. S. Pagano, and V. V. Salomonson (1998). "Prelaunch Characteristics of the Moderate Resolution Imaging Spectroradiometer (MODIS) on EOS-AM1". In: *IEEE Transactions on Geoscience and Remote Sensing* 36.4, pp. 1088–1100.

14. Bartsch, A., H. Balzter, and C. George (2009). "The influence of regional surface soil moisture anomalies on forest fires in Siberia observed from satellites". In: *Environmental Research Letters* 4.4, p. 045021. ISSN: 1748-9326. DOI: 10.1088/1748-9326/4/4/045021.

15. Beall, H. W. (1946). *Forest fire danger tables (provisional)*. Report. Dominion Forest Service.

16. Berg, A., K. Findell, B. Lintner, A. Giannini, S. I. Seneviratne, B. van den Hurk, R. Lorenz, A. Pitman, S. Hagemann, A. Meier, F. Cheruy, A. Ducharne, S. Malyshev, and P. C. D. Milly (2016). "Land–atmosphere feedbacks amplify aridity increase over land under global warming". In: *Nature Climate Change* 6.9, pp. 869–874. ISSN: 1758-678X 1758-6798. DOI: 10.1038/nclimate3029.

17. Beringer, J. (2013a). *Howard Springs OzFlux tower site OzFlux: Australian and New Zealand Flux Research and Monitoring hdl: 102.100.100/14234*. Dataset.

18. Beringer, J. (2013b). *Sturt Plains OzFlux tower site OzFlux: Australian and New Zealand Flux Research and Monitoring hdl: 102.100.100/14217*. Dataset.

19. Beringer, J. (2013c). *Wallaby Creek OzFlux tower site OzFlux: Australian and New Zealand Flux Research and Monitoring hdl: 102.100.100/14231*. Dataset.

20. Beringer, J. (2013d). *Whroo OzFlux tower site OzFlux: Australian and New Zealand Flux Research and Monitoring hdl: 102.100.100/14232*. Dataset.

21. Beringer, J. (2014). *Riggs Creek OzFlux tower site OzFlux: Australian and New Zealand Flux Research and Monitoring hdl: 102.100.100/14246*. Dataset.

22. Blumenstock, G. (1947). *Drought in the United States Analyzed by Means of the Theory of Probability*. Report. United States Department of Agriculture.

23. Boer, M., C. Macfarlane, J. Norris, R. Sadler, J. Wallace, and P. Grierson (2008). "Mapping burned areas and burn severity patterns in SW Australian eucalypt forest using remotely-sensed changes in leaf area index". In: *Remote Sensing of Environment* 112.12, pp. 4358–4369. ISSN: 00344257. DOI: 10.1016/j.rse.2008.08.005.

24. Bonaccorso, B., I. Bordi, A. Cancelliere, G. Rossi, and A. Sutera (2003). "Spatial Variability of Drought: An Analysis of the SPI in Sicily". In: *Water Reseources Management* 17, pp. 273–296.

25. Brewer, K. C., C. J. Winne, R. L. Redmond, S. W. Opitz, and M. V. Mangrich (2005). "Classifying and Mapping Wildfire Severity: A Comparison of Methods". In: *Photogrammetric Engineering and Remote Sensing* 71.11, pp. 1311–1320.

26. Brocca, L., S. Hasenauer, T. Lacava, F. Melone, T. Moramarco, W. Wagner, W. Dorigo, P. Matgen, J. Martínez-Fernández, P. Llorens, J. Latron, C. Martin, and M. Bittelli (2011). "Soil moisture estimation through ASCAT and AMSR-E sensors: An intercomparison and validation study across Europe". In: *Remote Sensing of Environment* 115.12, pp. 3390–3408. ISSN: 00344257. DOI: 10.1016/j.rse.2011.08.003.

27. Brocca, L., F. Melone, T. Moramarco, and R. Morbidelli (2009). "Soil moisture temporal stability over experimental areas in Central Italy". In: *Geoderma* 148.3-4, pp. 364–374. ISSN: 00167061. DOI: 10.1016/j.geoderma.2008.11.004.

28. Brown, G. W. (1947). "On Small-Sample Estimation". In: *The Annals of Mathematical Statistics* 18.4, pp. 582–585.

29. Brown, T. J., B. L. Hall, and A. L. Westerling (2004). "The Impact of Twenty-First Century Climate Change on Wildland Fire Danger in the Western United States: An Applications Perspective". In: *Climatic Change* 62, pp. 365–388.

30. Budyko, M. I. (1974). *Climate and Life (English ed.)* New York, U.S.A.: Academic Press. DOI: ISBN0-12-139450-6..

31. Byram, G. M. (1959). *Combustion of forest fuels.* New York: McGaw-Hill, pp. 61–89.

32. Cai, W., T. Cowan, and M. Raupach (2009). "Positive Indian Ocean Dipole events precondition southeast Australia bushfires". In: *Geophysical Research Letters* 36.19. ISSN: 0094-8276. DOI: 10.1029/2009gl039902.

33. Cai, W., P. van Rensch, S. Borlace, and T. Cowan (2011). "Does the Southern Annular Mode contribute to the persistence of the multidecade-long drought over southwest Western Australia?" In: *Geophysical Research Letters* 38.14, pp. 1–5. ISSN: 00948276. DOI: 10.1029/2011gl047943.

34. Calperum-Tech (2013). *Calperum Chowilla OzFlux tower site OzFlux: Australian and New Zealand Flux Research and Monitoring hdl: 102.100.100/14236.* Dataset.

35. Carmona, A. M., G. Poveda, M. Sivapalan, S. M. Vallejo-Bernal, and E. Bustamante (2016). "A scaling approach to Budyko's framework and the complementary relationship of evapotranspiration in humid environments: case study of the Amazon River basin". In: *Hydrology and Earth System Sciences* 20.2, pp. 589–603. ISSN: 1607-7938. DOI: 10.5194/hess-20-589-2016.

36. Certini, G. (2005). "Effects of fire on properties of forest soils: a review". In: *Oecologia* 143.1. Certini, Giacomo eng Review Germany 2005/02/03 09:00 Oecologia. 2005 Mar;143(1):1-10. doi: 10.1007/s00442-004-1788-8. Epub 2005 Feb 2., pp. 1–10. ISSN: 0029-8549 (Print) 0029-8549 (Linking). DOI: 10.1007/s00442-004-1788-8. URL: https://www.ncbi.nlm.nih.gov/pubmed/15688212.

37. Chaparro, D., M. Piles, M. Vall-llossera, and A. Camps (2017). "Surface moisture and temperature trends anticipate drought conditions linked to wildfire activity in the Iberian Peninsula". In: *European Journal of Remote Sensing* 49.1, pp. 955–971. ISSN: 2279-7254. DOI: 10.5721/EuJRS20164950.

38. Chaparro, D., M. Vall-llossera, M. Piles, A. Camps, C. Rüdiger, and R. Riera-Tatche (2016). "Predicting the Extent of Wildfires Using Remotely Sensed Soil Moisture and Temperature Trends". In: *IEEE Journal of Selected Topics in Applied Earth Observations and Remote Sensing* 9.6, pp. 2818–2829. ISSN: 1939-1404 2151-1535. DOI: 10.1109/jstars.2016.2571838.

39. Charlson, R. J., S. E. Schwartz, J. M. Hales, R. D. Cess, J. J. A. Coakley, J. E. Hansen, and D. J. Hofmann (1992). "Climate Forcing by Anthropogenic Aerosols". In: *Science* 255.5043, pp. 423–430.

40. Chatfield, C. (1988). "Apples, Oranges and Mean Square Error". In: *International Journal of Forecasting* 4, pp. 515–518.

41. Cheney, N. P., J. S. Gould, and W. R. Catchpole (1994). "The Influence of Fuel, Weather and Fire Shape Variables on Fire-Spread in Grasslands". In: *International Journal of Wildland Fire* 3.1, pp. 31–44.

42. Choudhury, B. J. (1999). "Evaluation of an empirical equation for annual evaporation using field observations and results from a biophysical model". In: *Journal of Hydrology* 216, pp. 99–110.

43. Christidis, N., G. S. Jones, and P. A. Stott (2014). "Dramatically increasing chance of extremely hot summers since the 2003 European heatwave". In: *Nature Climate Change* 5.1, pp. 46–50. ISSN: 1758-678X 1758-6798. DOI: 10.1038/nclimate2468.

44. Chuvieco, E., I. Aguado, S. Jurdao, M. L. Pettinari, M. Yebra, J. Salas, S. Hantson, J. de la Riva, P. Ibarra, M. Rodrigues, M. Echeverría, D. Azqueta, M. V. Román, A. Bastarrika, S. Martínez, C. Recondo, E. Zapico, and F. J. Martínez-Vega (2014). "Integrating geospatial information into fire risk assessment". In: *International Journal of Wildland Fire* 23.5, p. 606. ISSN: 1049-8001. DOI: 10.1071/wf12052.

45. Chuvieco, E. and R. G. Congalton (1989). "Application of Remote Sensing and Geographic Information Systems to Forest Fire Hazard Mapping". In: *Remote Sensing of the Environment* 29, pp. 147–159.

46. Chuvieco, E., D. Riaño, F. M. Danson, and P. Martin (2006). "Use of a radiative transfer model to simulate the postfire spectral response to burn severity". In: *Journal of Geophysical Research: Biogeosciences* 111.G4, pp. 1–15. ISSN: 01480227. DOI: 10.1029/2005jg000143.

47. Chuvieco, E., D. Cocero, D. Riaño, P. Martin, J. Martínez-Vega, J. de la Riva, and F. Pérez (2004). "Combining NDVI and surface temperature for the estimation of live fuel moisture content in forest fire danger rating". In: *Remote Sensing of Environment* 92.3, pp. 322–331. ISSN: 00344257. DOI: 10.1016/j.rse.2004.01.019.

48. Chuvieco, E. and E. S. Kasischke (2007). "Remote sensing information for fire management and fire effects assessment". In: *Journal of Geophysical Research* 112.G1. ISSN: 0148-0227. DOI: 10.1029/2006jg000230.

49. Clarke, H. G., C. Lucas, and P. L. Smith (2012). "Changes in Australian fire weather between 1973 and 2010". In: *International Journal of Climatology* 33.4, pp. 931–944. ISSN: 08998418. DOI: 10.1002/joc.3480.

50. Clarke, H. G., P. L. Smith, and A. J. Pitman (2011). "Regional signatures of future fire weather over eastern Australia from global climate models". In: *International Journal of Wildland Fire* 20, pp. 550–562.

51. Cleveland, W. S. and S. J. Devlin (1988). "Locally Weighted Regression: An Approach to Regression Analysis by Local Fitting". In: *Journal of the American Statistical Association* 83.403, pp. 596–610.

52. Cleverly, J. (2011). *Alice Springs Mulga OzFlux tower site: Australian and New Zealand Flux Research and Monitoring hdl: 102.100.100/14217*. Dataset.

53. Cleverly, J. (2013). *Ti Tree East OzFlux tower site OzFlux: Australian and New Zealand Flux Research and Monitoring hdl: 102.100.100/14225*. Dataset.

54. Cochran, W. (1977). *Sampling Techniques*. 3rd ed. New York: John Wiley and Sons, pp. 1–10.

55. Cocke, A. E., P. Z. Fulé, and J. E. Crouse (2005). "Comparison of burn severity assessment using Differenced Normalized Burn Ration adn ground data". In: *International Journal of Wildland Fire* 14, pp. 189–198.

56. Cook, B. I., J. E. Smerdon, R. Seager, and S. Coats (2014). "Global warming and 21st century drying". In: *Climate Dynamics* 43.9-10, pp. 2607–2627. ISSN: 0930-7575 1432-0894. DOI: 10.1007/s00382-014-2075-y.

57. Corey, D. M., W. P. Dunlap, and M. J. Burke (1998). "Averaging correlations: Expected values and bias in combined Pearson rs and Fishers z transformations". In: *The Journal of General Psychology* 125.3, pp. 245–261.

58. Cowan, T., A. Purich, S. Perkins, A. Pezza, G. Boschat, and K. Sadler (2014). "More Frequent, Longer, and Hotter Heat Waves for Australia in the Twenty-First Century". In: *Journal of Climate* 27.15, pp. 5851–5871. ISSN: 0894-8755 1520-0442. DOI: 10.1175/jcli-d-14-00092.1.

59. Cowles, K. M. and B. P. Carlin (1996). "Markov Chain Monte Carlo Convergence Diagnostics: A Comparative Review". In: *Journal of the American Statistical Association* 91.434, pp. 883–904.

60. Crow, W. T., R. Bindlish, and T. J. Jackson (2005). "The added value of spaceborne passive microwave soil moisture retrievals for forecasting rainfall-runoff partitioning". In: *Geophysical Research Letters* 32.18, pp. 1–5. ISSN: 00948276. DOI: 10.1029/2005gl023543.

61. Crow, W. T., S. V. Kumar, and J. D. Bolten (2012). "On the utility of land surface models for agricultural drought monitoring". In: *Hydrology and Earth System Sciences* 16.9, pp. 3451–3460. ISSN: 1607-7938. DOI: 10.5194/hess-16-3451-2012.

62. Cruz, M. G., M. Alexander, and P. Fernandes (2007). *Development of a model system to predict wildfire behaviour in pine plantations*. Conference Paper.

63. Dai, A. (2011a). "Characteristics and trends in various forms of the Palmer Drought Severity Index during 1900–2008". In: *Journal of Geophysical Research* 116.D12. ISSN: 0148-0227. DOI: 10.1029/2010jd015541.

64. Dai, A. (2011b). "Drought under global warming: a review". In: *Wiley Interdisciplinary Reviews: Climate Change* 2.1, pp. 45–65. ISSN: 17577780. DOI: 10.1002/wcc.81.

65. Dai, A. (2013). "Increasing drought under global warming in observations and models". In: *Nature Climate Change* 3.1, pp. 52–58. DOI: 10.1038/nclimate1633. URL: http://www.nature.com/nclimate/journal/v3/n1/abs/nclimate1633.html#supplementary-information.

66. Dai, A., I. . Fung, and A. . Del Genio (1997). "Surface Observed Global Land Precipitaiton Variations during 1900-88". In: *Journal of Climate* 10.Novmber, pp. 2943–2962.

67. de Jeu, R. A. M., W. Wagner, T. R. H. Holmes, A. J. Dolman, N. C. van de Giesen, and J. Friesen (2008). "Global Soil Moisture Patterns Observed by Space Borne Microwave Radiometers and Scatterometers". In: *Surveys in Geophysics* 29.4, pp. 399–420. ISSN: 1573-0956. DOI: 10.1007/s10712-008-9044-0. URL: https://doi.org/10.1007/s10712-008-9044-0.

68. Dee, D. P., S. M. Uppala, A. J. Simmons, P. Berrisford, P. Poli, S. Kobayashi, U. Andrae, M. A. Balmaseda, G. Balsamo, P. Bauer, P. Bechtold, A. C. M. Beljaars, L. van de Berg, J. Bidlot, N. Bormann, C. Delsol, R. Dragani, M. Fuentes, A. J. Geer, L. Haimberger, S. B. Healy, H. Hersbach, E. V. Hólm, L. Isaksen, P. Kållberg, M. Köhler, M. Matricardi, A. P. McNally, B. M. Monge-Sanz, J. J. Morcrette, B. K. Park, C. Peubey, P. de Rosnay, C. Tavolato, J. N. Thépaut, and F. Vitart (2011). "The ERA-Interim reanalysis: configuration and performance of the data assimilation system". In: *Quarterly Journal of the Royal Meteorological Society* 137.656, pp. 553–597. ISSN: 00359009. DOI: 10.1002/qj.828.

69. Deeming, J. E., J. W. Lancaster, M. A. Fosberg, W. R. Furman, and C. Sch textquotedblrightroeder M. Jar (1972). *The National Fire-Danger Rating System*. Report. U.S. Department of Agriculture, Forest Service, Rocky Mountain Forest and Range Experiment Station.

70. Delmas, R., J. P. Laxaux, and D. Brocard (1995). "Determination of Biomass Burning Emission Factors: Methods and Results". In: *Environmental Monitoring and Assessment* 38, pp. 181–204.

71. DEPI (2013a). *Methods used to map planned burn extent and severity within DEPI*. Report. DEPI Internal Report, Department of Primary Industries and Environment.

72. DEPI (2013b). *Remote Sensing of Fire Severity for Planned Burns: Development Field Assessment*. Report. DEPI Internal Report, Bushfire Monitoring, Evaluation and Research Unit.

73. Dharssi, I., K. J. Bovis, B. Macpherson, and C. P. Jones (2011). "Operational assimilation of ASCAT surface soil wetness at the Met Office". In: *Hydrology and Earth System Sciences* 15.8, pp. 2729–2746. ISSN: 1607-7938. DOI: 10.5194/hess-15-2729-2011.

74. Didan, K. (2015). *MOD13Q1 MODIS/Terra Vegetation Indices 16-Day L3 Global 250m SIN Grid V006*. Web Page. DOI: https://doi.org/10.5067/modis/mod13q1.006. URL: https://doi.org/10.5067/modis/mod13q1.006.

75. Dirmeyer, P. A., J. Wu, H. E. Norton, W. A. Dorigo, S. M. Quiring, T. W. Ford, J. A. Santanello, M. G. Bosilovich, M. B. Ek, R. D. Koster, G. Balsamo, and D. M. Lawrence (2016). "Confronting Weather and Climate Models with Observational Data from Soil Moisture Networks over the United States". In: *Journal of Hydrometeorology* 17.4, pp. 1049–1067. ISSN: 1525-755X 1525-7541. DOI: 10.1175/jhm-d-15-0196.1.

76. Doesken, N. J., T. B. McKee, and J. Kleist (1991). *Development of a Surface Wawter Supply Index for the Western United States*. Report. Colorado Climate Center.

77. Dolling, K., P.-S. Chu, and F. Fujioka (2005). "A climatological study of the Keetch/Byram drought index and fire activity in the Hawaiian Islands". In: *Agricultural and Forest Meteorology* 133.1-4, pp. 17–27. ISSN: 01681923. DOI: 10.1016/j.agrformet.2005.07.016.

78. Donat, M. G., A. J. Pitman, and S. I. Seneviratne (2017). "Regional warming of hot extremes accelerated by surface energy fluxes". In: *Geophysical Research Letters* 44, pp. 7011–7019. DOI: 10.1002/.

79. Dorigo, W. A., A. Gruber, R. A. M. De Jeu, W. Wagner, T. Stacke, A. Loew, C. Albergel, L. Brocca, D. Chung, R. M. Parinussa, and R. Kidd (2015). "Evaluation of the ESA CCI soil moisture product using ground-based observations". In: *Remote Sensing of Environment* 162, pp. 380–395. ISSN: 00344257. DOI: 10.1016/j.rse.2014.07.023.

80. Dorigo, W., W. Wagner, C. Albergel, F. Albrecht, G. Balsamo, L. Brocca, D. Chung, M. Ertl, M. Forkel, A. Gruber, E. Haas, P. D. Hamer, M. Hirschi, J. Ikonen, R. de Jeu, R. Kidd, W. Lahoz, Y. Y. Liu, D. Miralles, T. Mistelbauer, N. Nicolai-Shaw, R. Parinussa, C. Pratola, C. Reimer, R. van der Schalie, S. I. Seneviratne, T. Smolander, and P. Lecomte (2017). "ESA CCI Soil Moisture for improved Earth system understanding: State-of-the art and future directions". In: *Remote Sensing of Environment* 203, pp. 185–215. ISSN: 00344257. DOI: 10.1016/j.rse.2017.07.001.

81. Douville, H., J. Colin, E. Krug, J. Cattiaux, and S. Thao (2016). "Midlatitude daily summer temperatures reshaped by soil moisture under climate change". In: *Geophysical Research Letters* 43, pp. 812–818. DOI: 10.1002/.

82. Douville, H., A. Ribes, B. Decharme, R. Alkama, and J. Sheffield (2012). "Anthropogenic influence on multidecadal changes in reconstructed global evapotranspiration". In: *Nature Climate Change* 3.1, pp. 59–62. ISSN: 1758-678X 1758-6798. DOI: 10.1038/nclimate1632.

83. Dowdy, A. J., G. A. Mills, K. Finkele, and W. de Groot (2009). *Australian fire weather as represented by the McArthur Forest Fire Danger Index and the Canadian Forest Fire Weather Index*. Report. The Center for Australian Weather and Climate Research.

84. Draper, C. S., R. H. Reichle, R. de Jeu, V. Naeimi, R. M. Parinussa, and W. Wagner (2013). "Estimating root mean square errors in remotely sensed soil moisture over continental scale domains". In: *Remote Sensing of Environment* 137, pp. 288–298. DOI: 0.1016/j.rse.2013.06.013.

85. Draper, C. S., J. P. Walker, P. J. Steinle, R. A. M. de Jeu, and T. R. H. Holmes (2009). "An evaluation of AMSR–E derived soil moisture over Australia". In: *Remote Sensing of Environment* 113.4, pp. 703–710. ISSN: 00344257. DOI: 10.1016/j.rse.2008.11.011.

86. Driels M, R. and Y. S. Shin (2004). *Determining the number of iterations for Monte Carlo simulations of weapon effictiveness*. Report. Naval Postgraduate School.

87. Edwards, D. (1997). "Characteristics of 20th century drought in the United States at multiple time scales". Thesis.

88. Ellicott, E., E. Vermote, L. Giglio, and G. Roberts (2009). "Estimating biomass consumed from fire using MODIS FRE". In: *Geophysical Research Letters* 36.13. ISSN: 0094-8276. DOI: 10.1029/2009gl038581.

89. Evans, J. P. and M. F. McCabe (2010). "Regional climate simulation over Australia's Murray-Darling basin: A multitemporal assessment". In: *Journal of Geophysical Research* 115.D14. ISSN: 0148-0227. DOI: 10.1029/2010jd013816.

90. Feng, J. and Z. Wang (2013). "A satellite-based energy balance algorithm with reference dry and wet limits". In: *International Journal of Remote Sensing* 34.8, pp. 2925–2946. ISSN: 0143-1161 1366-5901. DOI: 10.1080/01431161.2012.748990.

91. Finkele, K., G. A. Mills, G. Beard, and D. A. Jones (2006). "National gridded drought factors and comparison of two soil moisture deficit formulations used in prediction of Forest Fire Danger Index in Australia". In: *Australian Meteorological Magazine* 55, pp. 183–197.

92. Fischer, E. M., S. I. Seneviratne, P. L. Vidale, D. Lüthi, and C. Schär (2007). "Soil Moisture–Atmosphere Interactions during the 2003 European Summer Heat Wave". In: *Journal of Climate* 20.20, pp. 5081–5099. ISSN: 0894-8755 1520-0442. DOI: 10.1175/jcli4288.1.

93. Flannigan, M. D., B. M. Wotton, G. A. Marshall, W. J. de Groot, J. Johnston, N. Jurko, and A. S. Cantin (2015). "Fuel moisture sensitivity to temperature and precipitation: climate change implications". In: *Climatic Change* 134.1-2, pp. 59–71. ISSN: 0165-0009 1573-1480. DOI: 10.1007/s10584-015-1521-0.

94. Flannigan, M., A. S. Cantin, W. J. de Groot, M. Wotton, A. Newbery, and L. M. Gowman (2013). "Global wildland fire season severity in the 21st century". In: *Forest Ecology and Management* 294, pp. 54–61. ISSN: 03781127. DOI: 10.1016/j.foreco.2012.10.022.

95. Forkel, M., W. Dorigo, G. Lasslop, I. Teubner, E. Chuvieco, and K. Thonicke (2017). "A data-driven approach to identify controls on global fire activity from satellite and climate observations (SOFIA V1)". In: *Geoscientific Model Development* 10.12, pp. 4443–4476. ISSN: 1991-9603. DOI: 10.5194/gmd-10-4443-2017.

96. Fosberg, M. A. (1978). "Weather in Wildland Fire Management - Fire Weather Index". In: *Bulletin of the American Meteorological Society* 59.3, pp. 341–341.

97. Fox-Hughes, P., R. Harris, G. Lee, M. Grose, and N. Bindoff (2014). "Future fire danger climatology for Tasmania, Australia, using a dynamically downscaled regional climate model". In: *International Journal of Wildland Fire* 23, pp. 309–321. DOI: 0.1071/WF13126.

98. Freeborn, P. H., M. J. Wooster, W. M. Hao, C. A. Ryan, B. L. Nordgren, S. P. Baker, and C. Ichoku (2008). "Relationships between energy release, fuel mass loss, and trace gas and aerosol emissions during laboratory biomass fires". In: *Journal of Geophysical Research* 113.D1. ISSN: 0148-0227. DOI: 10.1029/2007jd008679.

99. French, N. H. F., E. S. Kasichke, R. J. Hall, K. A. Murphy, D. L. Verbyla, E. E. Hoy, and J. L. Allen (2008). "Using Landsat data to assess fire and burn severity in the North American boreal forest region: an overover and summary of results". In: *International Journal of Wildland Fire* 17, pp. 443–462.

100. French, N. H. F. (2004). "Uncertainty in estimating carbon emissions from boreal forest fires". In: *Journal of Geophysical Research* 109.D14. ISSN: 0148-0227. DOI: 10.1029/2003jd003635.

101. Fu, X., Z. Yu, L. Luo, H. Lü, D. Liu, Q. Ju, T. Yang, F. Xu, H. Gu, C. Yang, J. Chen, and T. Wang (2013). "Investigating soil moisture sensitivity to precipitation and evapotranspiration errors using SiB2 model and ensemble Kalman filter". In: *Stochastic Environmental Research and Risk Assessment* 28.3, pp. 681–693. ISSN: 1436-3240 1436-3259. DOI: 10.1007/s00477-013-0781-3.

102. Gaiser, P. W., K. M. St Germain, E. M. Twarog, G. A. Poe, W. Purdy, D. A. Richardson, W. Grossman, W. Lindwood-Jones, D. Spencer, G. Golba, J. Cleveland, L. Choy, R. M. Bevilacqua, and P. S. Chang (2004). "The WindSat Spaceborne Polarimetric Microwave Radiometer: Sensor Description and Early Orbit Performance". In: *IEEE TRANSACTIONS ON GEOSCIENCE AND REMOTE SENSING* 42.11, pp. 2347–2361. DOI: 0.1109/TGRS.2004.836867.

103. Garcia-Prats, A., D. C. Antonio, F. J. G. Tarcísio, and M. J. Antonio (2015). "Development of a Keetch and Byram—Based drought index sensitive to forest management in Mediterranean conditions". In: *Agricultural and Forest Meteorology* 205, pp. 40–50. ISSN: 01681923. DOI: 10.1016/j.agrformet.2015.02.009.

104. GCOS (2010). *Implementation Plan for the Global Observing System for Climate in support of the UNFCCC: (2010 update)*. Report.

105. Gellie, N., K. Gibos, and K. Johnson (2010). *Relationship between Severe Landscape Dryness and Large Destructive Fires in Victoria*. Conference Paper.

106. Gibson, P. B., S. E. Perkins-Kirkpatrick, L. V. Alexander, and E. M. Fischer (2017a). "Comparing Australian heat waves in the CMIP5 models through cluster analysis". In: *Journal of Geophysical Research: Atmospheres*. ISSN: 2169897X. DOI: 10.1002/2016jd025878.

107. Gibson, P. B., S. E. Perkins-Kirkpatrick, P. Uotila, A. S. Pepler, and L. V. Alexander (2017b). "On the use of self-organizing maps for studying climate extremes". In: *Journal of Geophysical Research: Atmospheres* 122.7, pp. 3891–3903. ISSN: 2169897X. DOI: 10.1002/2016jd026256.

108. Giglio, L. (2015). *MOD14A1 MODIS/Terra Thermal Anomalies/Fire Daily L3 Global 1km SIN Grid V006*. Web Page. DOI: https://doi.org/10.5067/modis/mod14a1.006. URL: https://doi.org/10.5067/modis/mod14a1.006.

109. Giglio, L., I. Csiszar, Á. Restás, J. T. Morisette, W. Schroeder, D. Morton, and C. O. Justice (2008). "Active fire detection and characterization with the advanced spaceborne thermal emission and reflection radiometer (ASTER)". In: *Remote Sensing of Environment* 112.6, pp. 3055–3063. ISSN: 00344257. DOI: 10.1016/j.rse.2008.03.003.

110. Giglio, L., J. Descloitres, C. O. Justice, and Y. J. Kaufman (2003). "An Enhanced Contextual Fire Detection Algorithm for MODIS". In: *Remote Sensing of Environment* 87.2-3, pp. 273–282. ISSN: 00344257. DOI: 10.1016/s0034-4257(03)00184-6.

111. Greve, P., L. Gudmundsson, B. Orlowsky, and S. I. Seneviratne (2016). "A two-parameter Budyko function to represent conditions under which evapotranspiration exceeds precipitation". In: *Hydrology and Earth System Sciences* 20.6, pp. 2195–2205. ISSN: 1607-7938. DOI: 10.5194/hess-20-2195-2016.

112. Greve, P., B. Orlowsky, B. Mueller, J. Sheffield, M. Reichstein, and S. I. Seneviratne (2014). "Global assessment of trends in wetting and drying over land". In: *Nature Geoscience* 7.10, pp. 716–721. ISSN: 1752-0894 1752-0908. DOI: 10.1038/ngeo2247.

113. Griffiths, D. (1998). *Improved Formulae for the McArthur Forest Fire Danger Meter*. Report. Bureau of Meteorology, Meteorological.

114. Grose, M. R., P. Fox-Hughes, R. M. B. Harris, and N. L. Bindoff (2014). "Changes to the drivers of fire weather with a warming climate – a case study of southeast Tasmania". In: *Climatic Change* 124.1-2, pp. 255–269. ISSN: 0165-0009 1573-1480. DOI: 10.1007/s10584-014-1070-y.

115. Gruber, A., W. A. Dorigo, W. Crow, and W. Wagner (2017). "Triple Collocation-Based Merging of Satellite Soil Moisture Retrievals". In: *IEEE Transactions on Geoscience and Remote Sensing* 55.12, pp. 6780–6792. ISSN: 0196-2892 1558-0644. DOI: 10.1109/tgrs.2017.2734070.

116. Guttman, N. (1998). "Comparing the Palmer Drought Index and the Standardized Precipitation Index". In: *Journal of the American Water Resources Association* 34.1, pp. 113–121.

117. Guttman, N. (1999). "Accepting the Standardized Precipitation Index: A Calculation Algorithm". In: *Journal of the American Water Resources Association* 35, pp. 311–322.

118. Hale, M. L., T. M. Burg, and T. E. Steeves (2012). "Sampling for microsatellite-based population genetic studies: 25 to 30 individuals per population is enough to accurately estimate allele frequencies". In: *PLoS One* 7.9. Hale, Marie L Burg, Theresa M Steeves, Tammy E eng Research Support, Non-U.S. Gov't 2012/09/18 06:00 PLoS One. 2012;7(9):e45170. doi: 10.1371/journal.pone.0045170. Epub 2012 Sep 12., e45170. ISSN: 1932-6203 (Electronic) 1932-6203 (Linking). DOI: 10.1371/journal.pone.0045170. URL: https://www.ncbi.nlm.nih.gov/pubmed/22984627.

119. Hallack-Alegria, M., J. Ramirez-Hernandez, and D. W. Watkins (2012). "ENSO-conditioned rainfall drought frequency analysis in northwest Baja California, Mexico". In: *International Journal of Climatology* 32.6, pp. 831–842. ISSN: 08998418. DOI: 10.1002/joc.2310.

120. Han, E., W. T. Crow, T. Holmes, and J. Bolten (2014). "Benchmarking a Soil Moisture Data Assimilation System for Agricultural Drought Monitoring". In: *Journal of Hydrometeorology* 15.3, pp. 1117–1134. ISSN: 1525-755X 1525-7541. DOI: 10.1175/jhm-d-13-0125.1.

121. Hardy, C. C. (2005). "Wildland fire hazard and risk: Problems, definitions, and context". In: *Forest Ecology and Management* 211.1-2, pp. 73–82. ISSN: 03781127. DOI: 10.1016/j.foreco.2005.01.029.

122. Harris, S., A. Anderson, M. Kilinc, and L. Fogarty (2011). *Establishing a link between the power of fire and community loss: the first step towards developing a bushfire severity scale.* Report. Victorian Government: Department of Sustainability and Environment.

123. Harris, S., N. Tapper, D. Packham, B. Orlove, and N. Nicholls (2008). "The relationship between the monsoonal summer rain and dry-season fire activity of northern Australia". In: *International Journal Of Wild land Fires* 17, pp. 674–684.

124. Hawdon, A., D. McJannet, and J. Wallace (2014). "Calibration and correction procedures for cosmic-ray neutron soil moisture probes located across Australia". In: *Water Reseources Research* 50.6, pp. 5029–5043. DOI: 10.1002/2013WR015138.

125. Hayes, M. J., M. D. Scvoboda, D. A. Wilhite, and O. V. Vanyarkho (1999). "Monitoring the 1996 Drought Using the Standardized Precipitation Index". In: *Bulletin of the American Meteorological Society*, pp. 429–438.

126. Heim, R. (2002). "A Review of Twentieth-Century Drought Indicies Used in the United States". In: *American Meteorological Society* 1, pp. 1149–1165.

127. Hennessy, K., C. Lucas, N. Nicholls, J. Bathols, R. Suppiah, and J. Ricketts (2005). *Climate Change Impacts on Fire-Weather in South-East Australia*. Report. CSIRO Marine and Atmospheric Research.

128. Herold, N., J. Kala, and L. V. Alexander (2016). "The influence of soil moisture deficits on Australian heatwaves". In: *Environmental Research Letters* 11.6, p. 064003. ISSN: 1748-9326. DOI: 10.1088/1748-9326/11/6/064003.

129. Hirschi, M., B. Mueller, W. Dorigo, and S. I. Seneviratne (2014). "Using remotely sensed soil moisture for land–atmosphere coupling diagnostics: The role of surface vs. root-zone soil moisture variability". In: *Remote Sensing of Environment* 154, pp. 246–252. ISSN: 00344257. DOI: 10.1016/j.rse.2014.08.030.

130. Hirschi, M., S. I. Seneviratne, V. Alexandrov, F. Boberg, C. Boroneant, O. B. Christensen, H. Formayer, B. Orlowsky, and P. Stepanek (2010). "Observational evidence for soil-moisture impact on hot extremes in southeastern Europe". In: *Nature Geoscience* 4.1, pp. 17–21. ISSN: 1752-0894 1752-0908. DOI: 10.1038/ngeo1032.

131. Holgate, C. M., R. A. M. De Jeu, A. I. J. M. van Dijk, Y. Y. Liu, L. J. Renzullo, Vinodkumar, I. Dharssi, R. M. Parinussa, R. Van Der Schalie, A. Gevaert, J. Walker, D. McJannet, J. Cleverly, V. Haverd, C. M. Trudinger, and P. R. Briggs (2016). "Comparison of remotely sensed and modelled soil moisture data sets across Australia". In: *Remote Sensing of Environment* 186, pp. 479–500. ISSN: 00344257. DOI: 10.1016/j.rse.2016.09.015.

132. Hubbard, K. G., J. You, and E. D. Hunt (2007). "Development of the Soil Moisture Index to Quantify Agricultural Drought and Its "User Friendliness"in Severity-Area-Duration Assessment". In: *Journal of Hydrometeorology* 9, pp. 660–676. DOI: 0.1175/2007JHM892.1.

133. Hudak, A. T., M. B. Dickinson, B. C. Bright, R. L. Kremens, E. L. Loudermilk, J. J. O'Brien, B. S. Hornsby, and R. D. Ottmar (2016). "Measurements relating fire radiative energy density and surface fuel consumption – RxCADRE 2011 and 2012". In: *International Journal of Wildland Fire* 25.1, p. 25. ISSN: 1049-8001. DOI: 10.1071/wf14159.

134. Hunt, E. D., K. G. Hubbard, D. A. Wilhite, T. J. Arkebauer, and A. L. Dutcher (2009). "The development and evaluation of a soil moisture index". In: *International Journal of Climatology* 29.5, pp. 747–759. ISSN: 08998418 10970088. DOI: 10.1002/joc.1749.

135. Ichoku, C., J. V. Martins, Y. J. Kaufman, M. J. Wooster, P. H. Freeborn, W. M. Hao, S. Baker, C. A. Ryan, and B. L. Nordgren (2008). "Laboratory investigation of fire radiative energy and smoke aerosol emissions". In: *Journal of Geophysical Research* 113.D14. ISSN: 0148-0227. DOI: 10.1029/2007jd009659.

136. IPCC (2013a). *Climate Change 2013: The Physical Science Basis. Contribution of Working Group I to the Fifth Assessment Report of the Intergovernmental Panel on Climate Change*. Cambridge, United Kingdom and New York, NY, USA: Cambridge University Press, p. 1535. ISBN: ISBN 978-1-107-66182-0. DOI: 10.1017/CBO9781107415324. URL: www.climatechange2013.org.

137. IPCC (2013b). "Summary for Policymakers". In: *Climate Change 2013: The Physical Science Basis. Contribution of Working Group I to the Fifth Assessment Report of the Intergovernmental Panel on Climate Change*. Ed. by T. Stocker, D. Qin, G.-K. Plattner, M. Tignor, S. Allen, J. Boschung, A. Nauels, Y. Xia, V. Bex, and P. Midgley. Cambridge, United Kingdom and New York, NY, USA: Cambridge University Press. Chap. SPM, pp. 1–30. ISBN: ISBN 978-1-107-66182-0. DOI: 10.1017/CBO9781107415324.004. URL: www.climatechange2013.org.

138. Johnson, M. B. and G. Forthum (2001). "Spatial mapping of KBDI for the southeast United States". In: *Proceedings of the 4th Symposium on Fire and Forest Meteorology*.

139. Jones, D., I. Grant, W. Wang, R. Fawcett, and D. Barratt (2007). *Meteorological and Remotely Sensed Datasets for Hydrological Modelling: A Contribution to the Australian Water Availability Project*. Report. Bureau of Meteorology.

140. Jones, D. and B. Trewin (2000). "The spatial structure of monthly temperature anomalies over Australia". In: *Australian Meteorological Magazine* 49, pp. 261–276.

141. Jones, D., W. Wang, and R. Fawcett (2009). "High-quality spatial climate data-sets for Australia". In: *Australian Meteorological and Oceanographic Journal* 58, pp. 233–248.

142. Jung, I. and H. Chang (2012). "Climate change impacts on spatial patterns in drought risk in the Willamette River Basin, Oregon, U.S.A." In: *Theoretical and Applied Climatology* 108, pp. 355–371.

143. Kala, J., J. P. Evans, and A. J. Pitman (2015). "Influence of antecedent soil moisture conditions on the synoptic meteorology of the Black Saturday bushfire event in southeast Australia". In: *Quarterly Journal of the Royal Meteorological Society* 141.693, pp. 3118–3129. ISSN: 00359009. DOI: 10.1002/qj.2596.

144. Kaufman, Y. J., C. O. Justice, L. P. Flynn, J. D. Kendall, E. M. Prins, L. Giglio, D. E. Ward, W. P. Menzel, and A. W. Setzer (1998). "Potential global fire monitoring from EOS-MODIS". In: *Journal of Geophysical Research: Atmospheres* 103.D24, pp. 32215–32238. ISSN: 01480227. DOI: 10.1029/98jd01644.

145. Keeley, J. E. (2009). "Fire intensity, fire severity and burn severity: a breif review and suggested usage". In: *International Journal of Wildland Fire* 18, pp. 116–126.

146. Keetch, J. J. and G. M. Byram (1968). "A Drought Index for Forest Fire Control". In: *Forest Service Research Paper* 38, p. 32.

147. Key, C. and N. Benson (2006). *Landscape Assessment (LA) Sampling and Analysis Methods*. Report RMRS-GTR-164-CD. USDA Forest Service.

148. Keyantash, J. and J. A. Dracup (2002). "The Quantification of Drought: An Evaluation of Drought Indices". In: *Bulletin of the American Meteorological Society* 83, pp. 1167–1180. DOI: https://doi.org/10.1175/1520-0477(2002)083<1191:TQODAE>2.3.CO;2.

149. Kim, J. and T. Reichler (2015). "How well do Climate Models Simulate Todays Climate?" In: *Proceedings of the Autumn Meeting of KMS*.

150. Knutti, R. and J. Sedláček (2012). "Robustness and uncertainties in the new CMIP5 climate model projections". In: *Nature Climate Change* 3.4, pp. 369–373. ISSN: 1758-678X 1758-6798. DOI: 10.1038/nclimate1716.

151. Kohler, M. A. and R. K. Linsley (1951). "Predicting the Runoff from Storm Rainfall". In: *National Oceanic and Atmospheric Administration Weather Bureau Research Papers* 34, pp. 1–13.

152. Kokaly, R. F., B. W. Rockwell, S. L. Haire, and T. V. V. King (2007). "Characterization of post-fire surface cover, soils, and burn severity at the Cerro Grande Fire, New Mexico, using hyperspectral and multispectral remote sensing". In: *Remote Sensing of Environment* 106.3, pp. 305–325. ISSN: 00344257. DOI: 10.1016/j.rse.2006.08.006.

153. Köppen, W. (1884). "Die Wärmezonen der Erde, nach der Dauer der heissen, gemässigten und kalten Zeit und nach der Wirkung der Wärme auf die organische Welt betrachtet (The thermal zones of the earth according to the duration of hot, moderate and cold periods and to the impact of heat on the organic world)". In: *Meteorologische Zeitschrift* 1.3, 215–226, (translated and edited by Volken, E. and S. Brönnimann), Meteorologische Zeitschrift, 20 (2011), 351–350. ISSN: 09412948. DOI: 10.1127/0941-2948/2011/105.

154. Korontzi, S., D. Roy, C. J. Justice, and D. E. Ward (2004). "Modeling and sensitivity analysis of fire emission in southern Africa during SAFARI 2000". In: *Remote Sensing of Environment* 92.2, pp. 255–275.

155. Koster, R. D., Y. Chang, and S. D. Schubert (2014). "A Mechanism for Land–Atmosphere Feedback Involving Planetary Wave Structures". In: *Journal of Climate* 27.24, pp. 9290–9301. ISSN: 0894-8755 1520-0442. DOI: 10.1175/jcli-d-14-00315.1.

156. Koster, R. D., Y. Chang, H. Wang, and S. D. Schubert (2016). "Impacts of Local Soil Moisture Anomalies on the Atmospheric Circulation and on Remote Surface Meteorological Fields during Boreal Summer: A Comprehensive Analysis over North America". In: *Journal of Climate* 29.20, pp. 7345–7364. ISSN: 0894-8755 1520-0442. DOI: 10.1175/jcli-d-16-0192.1.

157. Koster, R. D., Z. Guo, R. Yang, P. A. Dirmeyer, K. Mitchell, and M. J. Puma (2009). "On the Nature of Soil Moisture in Land Surface Models". In: *Journal of Climate* 22.16, pp. 4322–4335. ISSN: 0894-8755 1520-0442. DOI: 10.1175/2009jcli2832.1.

158. Koster, R. D., M. J. Suarez, R. W. Higgins, and H. M. Van den Dool (2003). "Observational evidence that soil moisture variations affect precipitation". In: *Geophysical Research Letters* 30.5, n/a–n/a. ISSN: 00948276. DOI: 10.1029/2002gl016571.

159. Kottek, M., J. Grieser, C. Beck, B. Rudolf, and F. Rubel (2006). "World Map of the Köppen-Geiger climate classification updated". In: *Meteorologische Zeitschrift* 15.3, pp. 259–263. ISSN: 09412948. DOI: 10.1127/0941-2948/2006/0130.

160. Kumar, V., I. Dharssi, J. Bally, P. Steinle, D. McJannet, and J. Walker (2017). "Comparison of soil weness from multiple models over Australia with observations". In: *Water Reseources Research* 53, pp. 633–646. DOI: 10.1002/2015WR017738.

161. Leblanc, M. J., P. Tregoning, G. Ramillien, S. O. Tweed, and A. Fakes (2009). "Basin-scale, integrated observations of the early 21st century multiyear drought in southeast Australia". In: *Water Resources Research* 45.4, n/a–n/a. ISSN: 00431397. DOI: 10.1029/2008wr007333.

162. Leonard, J., K. Opie, and C. Wang (2016). *Decadal Forest Fire Danger Index (2006-2096). v1.* Dataset. DOI: http://doi.org/10.4225/08/5745ABC131831.

163. Liddell, M. (2013a). *Cape Tribulation OzFlux tower site OzFlux: Australian and New Zealand Flux Research and Monitoring hdl: 102.100.100/14242.* Dataset.

164. Liddell, M. (2013b). *Cow Bay OzFlux tower site OzFlux: Australian and New Zealand Flux Research and Monitoring hdl: 102.100.100/14244.* Dataset.

165. Liu, C. and R. P. Allan (2013). "Observed and simulated precipitation responses in wet and dry regions 1850–2100". In: *Environmental Research Letters* 8.3, p. 034002. ISSN: 1748-9326. DOI: 10.1088/1748-9326/8/3/034002.

166. Liu, S., L. Leslie, M. Speer, and R. Bunker (2003). "Predicting Forest Fire Danger Using Improved Model Derived Soil Moisture and Antecedent Precipitation". In: *Proceedings of International Congress of Modelling and Simulation*, pp. 642–647.

167. Liu, W. T. and F. N. Kogan (1996). "Monitoring regional drought using the Vegetation Condition Index". In: *International Journal of Remote Sensing* 17.14, pp. 2761–2782. ISSN: 0143-1161 1366-5901. DOI: 10.1080/01431169608949106.

168. Liu, Y. Y., W. A. Dorigo, R. M. Parinussa, R. A. M. de Jeu, W. Wagner, M. F. McCabe, J. P. Evans, and A. I. J. M. van Dijk (2012). "Trend-preserving blending of passive and active microwave soil moisture retrievals". In: *Remote Sensing of Environment* 123, pp. 280–297. ISSN: 00344257. DOI: 10.1016/j.rse.2012.03.014.

169. Liu, Y. Y., R. M. Parinussa, W. A. Dorigo, R. A. M. De Jeu, W. Wagner, A. I. J. M. van Dijk, M. F. McCabe, and J. P. Evans (2011). "Developing an improved soil moisture dataset by blending passive and active microwave satellite-based retrievals". In: *Hydrology and Earth System Sciences* 15.2, pp. 425–436. ISSN: 1607-7938. DOI: 10.5194/hess-15-425-2011.

170. Liu, Y., J. Stanturf, and S. Goodrick (2010). "Trends in global wildfire potential in a changing climate". In: *Forest Ecology and Management* 259, pp. 685–697. DOI: 0.1016/j.foreco.2012.10.022.

171. Livada, I. and V. D. Assimakopoulos (2006). "Spatial and temporal analysis of drought in greece using the Standardized Precipitation Index (SPI)". In: *Theoretical and Applied Climatology* 89.3-4, pp. 143–153. ISSN: 0177-798X 1434-4483. DOI: 10.1007/s00704-005-0227-z.

172. Lorenz, R., D. Argüeso, M. G. Donat, A. J. Pitman, B. van den Hurk, A. Berg, D. M. Lawrence, F. Chéruy, A. Ducharne, S. Hagemann, A. Meier, P. C. D. Milly, and S. I. Seneviratne (2016). "Influence of land-atmosphere feedbacks on temperature and precipitation extremes in the GLACE-CMIP5 ensemble". In: *Journal of Geophysical Research: Atmospheres* 121.2, pp. 607–623. ISSN: 2169897X. DOI: 10.1002/2015jd024053.

173. Lorimer, C. G. and W. R. Gough (1988). "Frequency of drought and sever fire weather in north-eastern Wisconsin". In: *Journal of Environment Management* 26.3, pp. 203–219.

174. Maier, S. W., J. Russell-Smith, A. C. Edwards, and C. Yates (2013). "Sensitivity of the MODIS fire detection algorithm (MOD14) in the savanna region of the Northern Territory, Australia". In: *ISPRS Journal of Photogrammetry and Remote Sensing* 76, pp. 11–16. ISSN: 09242716. DOI: 10.1016/j.isprsjprs.2012.11.005.

175. Martin, J. and T. Hillen (2016). "The Spotting Distribution of Wildfires". In: *Applied Sciences* 6.6, p. 177. ISSN: 2076-3417. DOI: 10.3390/app6060177.

176. McArthur, A. G. (1967). *Fire behaviour in eucalypt forests*. Canberra : Forestry and Timber Bureau, p. 36.

177. McEvoy, D. J., J. L. Huntington, J. T. Abatzoglou, and L. M. Edwards (2012). "An Evaluation of Multiscalar Drought Indices in Nevada and Eastern California". In: *Earth Interactions* 16.18, pp. 1–18. ISSN: 1087-3562. DOI: 10.1175/2012ei000447.1.

178. McKee, T. B., N. J. Doesken, and J. Kleist (1993). "The relationship of drought frequency and duration to time scales". In: *Journal of Hydrology* 179, pp. 17–22. URL: http://ccc.atmos.colostate.edu/relationshipofdroughtfrequency.pdf.

179. Metropolis, N. and S. Ulam (1949). "The Monte Carlo Method". In: *American Statistical Association Journal* 44, p. 8.

180. Miller, J. D. and A. E. Thode (2007). "Quantifying burn severity in a heterogeneous landscape with a relative version of the delta Normalized Burn Ratio (dNBR)". In: *Remote Sensing of Environment* 109.1, pp. 66–80. ISSN: 00344257. DOI: 10.1016/j.rse.2006.12.006.

181. Mills, G. A. (2005). *On the sub-synoptic scale meteorology of two extreme fire weather days during the Eastern Australian fires of January 2003*. Report. Bureau of Meteorology Research Center.

182. Minet, J., N. E. C. Verhoest, S. Lambot, and M. Vanclooster (2013). "Temporal stability of soil moisture patterns measured by proximal ground-penetrating radar". In: *Hydrology and Earth System Sciences Discussions* 10.4, pp. 4063–4097. ISSN: 1812-2116. DOI: 10.5194/hessd-10-4063-2013.

183. Miralles, D. G., M. J. van den Berg, A. J. Teuling, and R. A. M. de Jeu (2012). "Soil moisture-temperature coupling: A multiscale observational analysis". In: *Geophysical Research Letters* 39.21, n/a–n/a. ISSN: 00948276. DOI: 10.1029/2012gl053703.

184. Miralles, D. G., M. J. van den Berg, J. H. Gash, R. M. Parinussa, R. A. M. de Jeu, H. E. Beck, T. R. H. Holmes, C. Jiménez, N. E. C. Verhoest, W. A. Dorigo, A. J. Teuling, and A. Johannes Dolman (2013). "El Niño–La Niña cycle and recent trends in continental evaporation". In: *Nature Climate Change* 4.2, pp. 122–126. ISSN: 1758-678X 1758-6798. DOI: 10.1038/nclimate2068.

185. Miralles, D. G., A. J. Teuling, and C. C. van Heerwaarden (2008). "Mega-heatwave temperatures due to combined soil desiccation and atmospheric heat accumulation". In: *Nature Geoscience* 7.5, pp. 345–349. DOI: 0.1038/ngeo2141.

186. Mishra, A. K. and V. P. Singh (2010). "A review of drought concepts". In: *Journal of Hydrology* 391.1-2, pp. 202–216. ISSN: 00221694. DOI: 10.1016/j.jhydrol.2010.07.012.

187. Mohammad Amin Asadi, Z., B. Sivakumar, and A. Sharma (2015). "Droughts in a warming climate: A global assessment of Standardized precipitation index (SPI) and Reconnaissance drought index (RDI)". In: *Journal of Hydrology* 526, pp. 183–195. ISSN: 00221694. DOI: 10.1016/j.jhydrol.2014.09.071.

188. Moise, A., L. Wilson, M. Grose, P. Whetton, I. Watterson, J. Bhend, J. Bathols, L. Hanson, T. Erwin, T. Bedin, C. Heady, and T. Rafter (2015). "Evaluation of CMIP3 and CMIP5 Models over the Australian Region to Inform Confidence in Projections". In: *Australian Meteorological and Oceanographic Journal* 65.1, pp. 19–53.

189. Montazerolghaem, M., W. Vervoort, B. Minasny, and A. McBratney (2016). "Long-term variability of the leading seasonal modes of rainfall in south-eastern Australia". In: *Weather and Climate Extremes* 13, pp. 1–14. ISSN: 22120947. DOI: 10.1016/j.wace.2016.04.001.

190. Morak, S., G. C. Hegerl, and J. Kenyon (2011). "Detectable regional changes in the number of warm nights". In: *Geophysical Research Letters* 38.17, n/a–n/a. ISSN: 00948276. DOI: 10.1029/2011gl048531.

191. Morak, S., G. C. Hegerl, and N. Christidis (2013). "Detectable Changes in the Frequency of Temperature Extremes". In: *Journal of Climate* 26.5, pp. 1561–1574. ISSN: 0894-8755 1520-0442. DOI: 10.1175/jcli-d-11-00678.1.

192. Moreno, M. V. and E. Chuvieco (2013). "Characterising fire regimes in Spain from fire statistics". In: *International Journal of Wildland Fire* 22.3, p. 296. ISSN: 1049-8001. DOI: 10.1071/wf12061.

193. Mount, A. B. (1972). *The derivation and testing of a soil dryness index using run-off data*. 4th ed. Tasmanian Foresty Commission.

194. Mueller, B., M. Hirschi, C. Jimenez, P. Ciais, P. A. Dirmeyer, A. J. Dolman, J. B. Fisher, M. Jung, F. Ludwig, F. Maignan, D. G. Miralles, M. F. McCabe, M. Reichstein, J. Sheffield, K. Wang, E. F. Wood, Y. Zhang, and S. I. Seneviratne (2013). "Benchmark products for land evapotranspiration: LandFlux-EVAL multi-data set synthesis". In: *Hydrology and Earth System Sciences* 17.10, pp. 3707–3720. ISSN: 1607-7938. DOI: 10.5194/hess-17-3707-2013.

195. Mueller, B. and S. I. Seneviratne (2012). "Hot days induced by precipitation deficits at the global scale". In: *Proceedings of the National Academy of Sciences of the United States of America* 109.31, pp. 12398–403. ISSN: 1091-6490 (Electronic) 0027-8424 (Linking). DOI: 10.1073/pnas.1204330109. URL: http://www.ncbi.nlm.nih.gov/pubmed/22802672.

196. Mullan, A. (1998). "Southern Hemisphere Sea-Surface Temperatures and Their Contemporary and Lag Association with New Zealand Temperature and Precipitation". In: *International Journal of Climatology* 18, pp. 817–840.

197. Munger, T. (1916). "Graphic Mehtod of Representing and Comparing Drought Intensities". In: *Monthly Weather Review* 44, pp. 642–643.

198. Murphy, B. P., R. A. Bradstock, M. M. Boer, J. Carter, G. J. Cary, M. A. Cochrane, R. J. Fensham, J. Russell-Smith, G. J. Williamson, D. M. J. S. Bowman, and P. Ladiges (2013). "Fire regimes of Australia: a pyrogeographic model system". In: *Journal of Biogeography* 40.6, pp. 1048–1058. ISSN: 03050270. DOI: 10.1111/jbi.12065.

199. Myneni, R. Y. K. (2015). "MCD15A2H MODIS/Terra+Aqua Leaf Area Index/FPAR 8-day L4 Global 500m SIN Grid V006". In: *NASA EOSDIS Land Processes DAAC*. DOI: https://doi.org/10.5067/modis/mcd15a2h.006.

200. Naresh Kumar, M., C. S. Murthy, M. V. R. Sesha Sai, and P. S. Roy (2009). "On the use of Standardized Precipitation Index (SPI) for drought intensity assessment". In: *Meteorological Applications* 16.3, pp. 381–389. ISSN: 13504827 14698080. DOI: 10.1002/met.136.

201. Nicolai-Shaw, N., M. Hirschi, H. Mittlebach, and S. I. Seneviratne (2015). "Spatial representativeness of soil moisture using in situ, remote sensing, and land reanalysis data." In: *Journal of Geophysical Research: Atmospheres* 120, pp. 9955–9964. DOI: 0.1002/2015JD023305.

202. Njoku, E. G. (2004). *AMSR-E/Aqua Daily L3 Surface Soil Moisture, Interpretive Parameters, and QC EASE-Grids, Version 2*. Web Page.

203. Nobel, I. R., G. A. V. Bary, and A. M. Gill (1980). "McArthur fire danger meters expressed as equations". In: *Australian Journal of Ecology* 5, pp. 201–203.

204. Oladipo, O. E. (1985). "A Comparitive Performance Analysis of Three Meteorolgical Drought Indices". In: *Journal of Climatology* 5, pp. 655–664.

205. Oliveira, S. L. J., S. W. Maier, J. M. C. Pereira, and J. Russell-Smith (2015). "Seasonal differences in fire activity and intensity in tropical savannas of northern Australia using satellite measurements of fire radiative power". In: *International Journal of Wildland Fire*. ISSN: 1049-8001. DOI: 10.1071/wf13201.

206. Olofsson, P., G. M. Foody, M. Herold, S. V. Stehman, C. E. Woodcock, and M. A. Wulder (2014). "Good practices for estimating area and assessing accuracy of land change". In: *Remote Sensing of Environment* 148, pp. 42–57. ISSN: 00344257. DOI: 10.1016/j.rse.2014.02.015.

207. Palmer, W. W. (1965). "Meteorologic Drought". In: *US Department of Commerce, Weather Bureau* 45, p. 58.

208. Peel, M. C., B. L. Finlayson, and T. A. McMahon (2007). "Updated world map of the Koppen-Geiger climate classification". In: *Hydrology and Earth Systems Sciences* 11, pp. 1333–1644.

209. Pendall, E. (2015). *Cumberland Plain OzFlux tower site: Australian and New Zealand Flux Research and Monitoring hdl: 102.100.100/25164*. Dataset.

210. Pereira, M. G., R. M. Trigo, C. C. da Camara, J. M. C. Pereira, and S. M. Leite (2005). "Synoptic patterns associated with large summer forest fires in Portugal". In: *Agricultural and Forest Meteorology* 129.1-2, pp. 11–25. ISSN: 01681923. DOI: 10.1016/j.agrformet.2004.12.007.

211. Perkins, S. E., L. V. Alexander, and J. R. Nairn (2012). "Increasing frequency, intensity and duration of observed global heatwaves and warm spells". In: *Geophysical Research Letters* 39.20. ISSN: 00948276. DOI: 10.1029/2012gl053361.

212. Perkins, S. E. (2015). "A review on the scientific understanding of heatwaves—Their measurement, driving mechanisms, and changes at the global scale". In: *Atmospheric Research* 164-165, pp. 242–267. ISSN: 01698095. DOI: 10.1016/j.atmosres.2015.05.014.

213. Perkins, S. E., D. Argüeso, and C. J. White (2015). "Relationships between climate variability, soil moisture, and Australian heatwaves". In: *Journal of Geophysical Research: Atmospheres* 120.16, pp. 8144–8164. ISSN: 2169897X. DOI: 10.1002/2015jd023592.

214. Perkins-Kirkpatrick, S. E., C. J. White, L. V. Alexander, D. Argüeso, G. Boschat, T. Cowan, J. P. Evans, M. Ekström, E. C. J. Oliver, A. Phatak, and A. Purich (2016). "Natural hazards in Australia: heatwaves". In: *Climatic Change* 139.1, pp. 101–114. ISSN: 0165-0009 1573-1480. DOI: 10.1007/s10584-016-1650-0.

215. Petros, G., A. Mantzavelas, and M. Tsakaldimi (2011). "Development of an adapted empirical drought index to the Mediterranean conditions for use in forestry". In: *Agricultural and Forest Meteorology* 151.2, pp. 241–250. ISSN: 01681923. DOI: 10.1016/j.agrformet.2010.10.011.

216. Pezza, A. B., P. van Rensch, and W. Cai (2011). "Severe heat waves in Southern Australia: synoptic climatology and large scale connections". In: *Climate Dynamics* 38.1-2, pp. 209–224. ISSN: 0930-7575 1432-0894. DOI: 10.1007/s00382-011-1016-2.

217. Phillips, A. (2015). *Warra OzFlux tower site OzFlux: Australian and New Zealand Flux Research and Monitoring hdl: 102.100.100/14266*. Dataset.

218. Pike, J. (1964). "The estimation of annual runoff from meteorological data in a tropical climate". In: *Journal of Hydrology* 2, pp. 116–123.

219. Pitman, A. J., G. T. Narisma, and J. McAneney (2007). "The impact of climate change on the risk of forest and grassland fires in Australia". In: *Climatic Change* 84.3, pp. 383–401. ISSN: 1573-1480. DOI: 10.1007/s10584-007-9243-6. URL: https://doi.org/10.1007/s10584-007-9243-6.

220. Pittock, A. (1971). *Rainfall and the general circulation*. Conference Paper.

221. Potter, B. E. (2012). "Atmospheric interactions with wildland fire behaviour - II. Plume and vortex dynamics". In: *International Journal of Wildland Fire* 21.7, p. 802. ISSN: 1049-8001. DOI: 10.1071/wf11129.

222. Potter, N. J. and L. Zhang (2009). "Interannual variability of catchment water balance in Australia". In: *Journal of Hydrology* 369.1-2, pp. 120–129. ISSN: 00221694. DOI: 10.1016/j.jhydrol.2009.02.005.

223. Purich, A., T. Cowan, S.-K. Min, and W. Cai (2013). "Autumn Precipitation Trends over Southern Hemisphere Midlatitudes as Simulated by CMIP5 Models". In: *Journal of Climate* 26.21, pp. 8341–8356. ISSN: 0894-8755 1520-0442. DOI: 10.1175/jcli-d-13-00007.1.

224. Quiring, S. M. and S. Ganesh (2010). "Evaluating the utility of the Vegetation Condition Index (VCI) for monitoring meteorological drought in Texas". In: *Agricultural and Forest Meteorology* 150.3, pp. 330–339. ISSN: 01681923. DOI: 10.1016/j.agrformet.2009.11.015.

225. Rebel, K. T., R. A. M. de Jeu, P. Ciais, N. Viovy, S. L. Piao, G. Kiely, and A. J. Dolman (2012). "A global analysis of soil moisture derived from satellite observations and a land surface model". In: *Hydrology and Earth System Sciences* 16.3, pp. 833–847. ISSN: 1607-7938. DOI: 10.5194/hess-16-833-2012.

226. Risbey, J. S., M. J. Pook, P. C. McIntosh, M. C. Wheeler, and H. H. Hendon (2009). "On the Remote Drivers of Rainfall Variability in Australia". In: *Monthly Weather Review* 137.10, pp. 3233–3253. ISSN: 0027-0644 1520-0493. DOI: 10.1175/2009mwr2861.1.

227. Roberts, G., M. J. Wooster, G. L. W. Perry, N. Drake, L. M. Rebelo, and F. Dipotso (2005). "Retrieval of biomass combustion rates and totals from fire radiative power observations: Application to southern Africa using geostationary SEVIRI imagery". In: *Journal of Geophysical Research* 110.D21. ISSN: 0148-0227. DOI: 10.1029/2005jd006018.

228. Robinson, D. A., C. S. Campbell, J. W. Hopmans, B. K. Hornbuckle, S. B. Jones, R. Knight, F. Ogden, J. Selker, and O. Wendroth (2008). "Soil Moisture Measurement for Ecological and Hydrological Watershed-Scale Observatories: A Review". In: *Vadose Zone Journal* 7.1, p. 358. ISSN: 1539-1663. DOI: 10.2136/vzj2007.0143.

229. Ropelewski, C. F. and P. D. Jones (1987). "An Extension of the Tahiti–Darwin Southern Oscillation Index". In: *Monthly Weather Review* 115.9, pp. 2161–2165. DOI: 10.1175/1520-0493(1987)115<2161:aeotts>2.0.co;2. URL: http://journals.ametsoc.org/doi/abs/10.1175/1520-0493%281987%29115%3C2161%3AAEOTTS%3E2.0.CO%3B2.

230. Rouholahnejad, E. and J. W. Kirchner (2016). "A Budyko framework for estimating how spatial heterogeneity and lateral moisture redistribution affect average evapotranspiration rates as seen from the atmosphere". In: *Hydrology and Earth System Sciences Discussions*, pp. 1–28. ISSN: 1812-2116. DOI: 10.5194/hess-2016-424.

231. Rowlings, D. (2011). *Samford OzFlux tower site OzFlux: Australian and New Zealand Flux Research and Monitoring hdl: 102.100.100/14219*. Dataset.

232. Rüdiger, C., J.-C. Calvet, C. Gruhier, T. R. H. Holmes, R. A. M. de Jeu, and W. Wagner (2009). "An Intercomparison of ERS-Scat and AMSR-E Soil Moisture Observations with Model Simulations over France". In: *Journal of Hydrometeorology* 10.2, pp. 431–447. ISSN: 1525-755X 1525-7541. DOI: 10.1175/2008jhm997.1.

233. Rüdiger, C., A. W. Western, J. P. Walker, A. B. Smith, J. D. Kalma, and G. R. Willgoose (2010). "Towards a general equation for frequency domain reflectometers". In: *Journal of Hydrology* 383.3-4, pp. 319–329. ISSN: 00221694. DOI: 10.1016/j.jhydrol.2009.12.046.

234. Russell-Smith, J. and A. C. Edwards (2006). "Seasonality and fire severity in savanna landscapes of monsoonal northern Australia". In: *International Journal of Wildland Fire* 15, pp. 541–550.

235. Russell-Smith, J., C. Yates, A. C. Edwards, G. E. Allan, G. D. Cook, P. Cooke, R. Craig, B. Heath, and R. Smith (2003a). "Seasonal Changes in Fire Behaviour in a Tropical Savanna in Northern Australia". In: *International Journal of Wildland Fire* 12, pp. 283–297.

236. Russell-Smith, J., A. C. Edwards, and G. D. Cook (2003b). "Reliability of biomass burning estimates from savanna fires: Biomass burning in northern Australia during the 1999 Biomass Burning and Lightning Experiment B field campaign". In: *Journal of Geophysical Research: Atmospheres* 108.D3, n/a–n/a. ISSN: 01480227. DOI: 10.1029/2001jd000787.

237. Sahr, K., D. White, and A. Kimerling (2002). "Geodesic Discrete Global Grid Systems". In: *Cartography and Geographic Information Science* 30, pp. 121–134.

238. Schroder, I. (2014). *Arcturus Emerald OzFlux tower site OzFlux: Australian and New Zealand Flux Research and Monitoring hdl: 102.100.100/14249*. Dataset.

239. Schubert, S. D., R. E. Stewart, H. Wang, M. Barlow, E. H. Berbery, W. Cai, M. P. Hoerling, K. K. Kanikicharla, R. D. Koster, B. Lyon, A. Mariotti, C. R. Mechoso, O. V. Müller, B. Rodriguez-Fonseca, R. Seager, S. I. Seneviratne, L. Zhang, and T. Zhou (2016a). "Global Meteorological Drought: A Synthesis of Current Understanding with a Focus on SST Drivers of Precipitation Deficits". In: *Journal of Climate* 29.11, pp. 3989–4019. ISSN: 0894-8755 1520-0442. DOI: 10.1175/jcli-d-15-0452.1.

240. Schubert, S., Y. Chang, H. Wang, R. Koster, and M. Suarez (2016b). "A Modeling Study of the Causes and Predictability of the Spring 2011 Extreme U.S. Weather Activity". In: *Journal of Climate* 29.21, pp. 7869–7887. ISSN: 0894-8755 1520-0442. DOI: 10.1175/jcli-d-15-0673.1.

241. Seaman, R. (1989). "Tuning the Barnes Objective Analysis Parameters by Statistical Interpolation Theory". In: *Journal of Atmospheric and Oceanic Technology* 6, pp. 993–1000.

242. Seiler, W. and P. J. Crutzen (1980). "Esitmates of Gross and Net Fluces of Carbon Between the Biospher and the Atmosphere from Biomass Burning". In: *Climate Change* 2, pp. 207–247.

243. Seneviratne, S. I., M. G. Donat, A. J. Pitman, R. Knutti, and R. L. Wilby (2016). "Allowable CO2 emissions based on regional and impact-related climate targets". In: *Nature* 529.7587. Seneviratne, Sonia I Donat, Markus G Pitman, Andy J Knutti, Reto Wilby, Robert L eng Research Support, Non-U.S. Gov't Research Support, U.S. Gov't, Non-P.H.S. England 2016/01/21 06:00 Nature. 2016 Jan 28;529(7587):477-83. doi: 10.1038/nature16542. Epub 2016 Jan 20., pp. 477–83. ISSN: 1476-4687 (Electronic) 0028-0836 (Linking). DOI: 10.1038/nature16542. URL: https://www.ncbi.nlm.nih.gov/pubmed/26789252.

244. Seneviratne, S. I., T. Corti, E. L. Davin, M. Hirschi, E. B. Jaeger, I. Lehner, B. Orlowsky, and A. J. Teuling (2010). "Investigating soil moisture–climate interactions in a changing climate: A review". In: *Earth-Science Reviews* 99.3-4, pp. 125–161. ISSN: 00128252. DOI: 10.1016/j.earscirev.2010.02.004.

245. Seneviratne, S. I., M. Wilhelm, T. Stanelle, B. van den Hurk, S. Hagemann, A. Berg, F. Cheruy, M. E. Higgins, A. Meier, V. Brovkin, M. Claussen, A. Ducharne, J.-L. Dufresne, K. L. Findell, J. Ghattas, D. M. Lawrence, S. Malyshev, M. Rummukainen, and B. Smith (2013). "Impact of soil moisture-climate feedbacks on CMIP5 projections: First results from the GLACE-CMIP5 experiment". In: *Geophysical Research Letters* 40.19, pp. 5212–5217. ISSN: 00948276. DOI: 10.1002/grl.50956.

246. Shafer, B. A. and L. E. Dezman (1982). "Development of a Surface Water Supply Index (SWSI) to Assess the Severity of Drought Conditions in Snowpack Runoff Areas". In: *The Western Snow Conference*, pp. 146–175.

247. Sharples, J. J., R. H. D. McRae, R. O. Weber, and A. M. Gill (2009). "A simple index for assessing fire danger rating". In: *Environmental Modelling and Software* 24.6, pp. 764–774. ISSN: 13648152. DOI: 10.1016/j.envsoft.2008.11.004.

248. Sheffield, J., E. F. Wood, and M. L. Roderick (2012). "Little change in global drought over the past 60 years". In: *Nature* 491.7424. Sheffield, Justin Wood, Eric F Roderick, Michael L eng Research Support, Non-U.S. Gov't Research Support, U.S. Gov't, Non-P.H.S. England 2012/11/16 06:00 Nature. 2012 Nov 15;491(7424):435-8. doi: 10.1038/nature11575., pp. 435–8. ISSN: 1476-4687 (Electronic) 0028-0836 (Linking). DOI: 10.1038/nature11575. URL: https://www.ncbi.nlm.nih.gov/pubmed/23151587.

249. Sherwood, S. C. and M. Huber (2010). "An adaptability limit to climate change due to heat stress". In: *Proc Natl Acad Sci U S A* 107.21. Sherwood, Steven C Huber, Matthew eng Research Support, Non-U.S. Gov't Research Support, U.S. Gov't, Non-P.H.S. 2010/05/05 06:00 Proc Natl Acad Sci U S A. 2010 May 25;107(21):9552-5. doi: 10.1073/pnas.0913352107. Epub 2010 May 3., pp. 9552–5. ISSN: 1091-6490 (Electronic) 0027-8424 (Linking). DOI: 10.1073/pnas.0913352107. URL: https://www.ncbi.nlm.nih.gov/pubmed/20439769.

250. Sherwood, S. and Q. Fu (2014). "A Drier Future?" In: *Science* 343, pp. 737–739.

251. Silberstein, R. (2015). *Gingin OzFlux tower site: Australian and New Zealand Flux Research and Monitoring hdl: 102.100.100/14217*. Dataset.

252. Sims, A. P., D. d. S. Niyogi, and S. Raman (2002). "Adopting drought indices for estimating soil moisture: A North Carolina case study". In: *Geophysical Research Letters* 29.8, pp. 1183–1187. ISSN: 00948276. DOI: 10.1029/2001gl013343.

253. Sippel, S., Z. J., M. Heimann, H. Lange, M. D. Mahecha, G. J. van Oldenborgh, F. E. L. Otto, and M. Reichstein (2017). "Have precipitation extremes and annual totals been increasing in the worlds dry regions over the last 60 years?" In: *Hydrology and Earth System Sciences* 21, pp. 441–458.

254. Smith, A. B., J. P. Walker, A. W. Western, R. I. Young, K. M. Ellett, R. C. Pipunic, R. B. Grayson, L. Siriwardena, F. H. S. Chiew, and H. Richter (2012). "The Murrumbidgee soil moisture monitoring network data set". In: *Water Resources Research* 48.7, n/a–n/a. ISSN: 00431397. DOI: 10.1029/2012wr011976.

255. Snyder, R. L., D. Spano, P. Duce, D. Baldocchi, L. Xu, and K. T. Paw U (2006). "A fuel dryness index for grassland fire-danger assessment". In: *Agricultural and Forest Meteorology* 139.1-2, pp. 1–11. ISSN: 01681923. DOI: 10.1016/j.agrformet.2006.05.006.

256. Stocks, B. J., M. A. Fosberg, T. J. Lynham, L. Mearns, B. M. Wotton, Q. Yang, J.-Z. Jin, K. Lawrence, G. R. Hartley, J. A. Mason, and D. W. McKenney (1998). "Climate Change and Forest Fire Potential in Russian and Canadian Boreal Forests". In: *Clmatic Change* 38, pp. 1–13.

257. Su, C.-H., D. Ryu, R. I. Young, A. W. Western, and W. Wagner (2013). "Inter-comparison of microwave satellite soil moisture retrievals over the Murrumbidgee Basin, southeast Australia". In: *Remote Sensing of Environment* 134, pp. 1–11. ISSN: 00344257. DOI: 10.1016/j.rse.2013.02.016.

258. Tannehill, I. R. (1947). *Drought,: Its Causes and Effects*. Princton University: Oxford University Press.

259. Taylor, K. E., R. J. Stouffer, and G. A. Meehl (2012). "An Overview of CMIP5 and the Experiment Design". In: *Bulletin of the American Meteorological Society* 93.4, pp. 485–498. ISSN: 0003-0007 1520-0477. DOI: 10.1175/bams-d-11-00094.1.

260. Teague, B., R. Mcleod, and S. Pascoe (2010). "FINAL REPORT: Summary". In: *2009 Victorian Bushfires Royal Commission*.

261. Tebaldi, M., S. Biscaglia, A. Pecoraro, M. Fineschi, and G. Campo (2016). "Fractional flow reserve implementation in daily clinical practice: A European survey". In: *Int J Cardiol* 207. Tebaldi, Matteo Biscaglia, Simone Pecoraro, Alessandro Fineschi, Massimo Campo, Gianluca eng Letter Netherlands 2016/01/25 06:00 Int J Cardiol. 2016 Mar 15;207:206-7. doi: 10.1016/j.ijcard.2016.01.097. Epub 2016 Jan 9., pp. 206–7. ISSN: 1874-1754 (Electronic) 0167-5273 (Linking). DOI: 10.1016/j.ijcard.2016.01.097. URL: https://www.ncbi.nlm.nih.gov/pubmed/26803245.

262. Teuling, A. J., M. Hirschi, A. Ohmura, M. Wild, M. Reichstein, P. Ciais, N. Buchmann, C. Ammann, L. Montagnani, A. D. Richardson, G. Wohlfahrt, and S. I. Seneviratne (2009). "A regional perspective on trends in continental evaporation". In: *Geophysical Research Letters* 36.2, pp. 1–5. ISSN: 00948276. DOI: 10.1029/2008gl036584.

263. Teuling, A. J., S. I. Seneviratne, C. Williams, and P. A. Troch (2006). "Observed timescales of evapotranspiration response to soil moisture". In: *Geophysical Research Letters* 33.23. ISSN: 0094-8276. DOI: 10.1029/2006gl028178.

264. Thompson, S. K. (1987). "Sample Size for Estimating Multinomial Proportions". In: *The American Statistician* 41.1, pp. 42–46. ISSN: 0003-1305 1537-2731. DOI: 10.1080/00031305.1987.10475440.

265. Thornthwaite, C. W. (1948). "An Approach toward a Rational Classification of Climate". In: *Geographical Review* 38.1, pp. 55–94.

266. Tian, F., M. Brandt, Y. Y. Liu, A. Verger, T. Tagesson, A. A. Diouf, K. Rasmussen, C. Mbow, Y. Wang, and R. Fensholt (2016). "Remote sensing of vegetation dynamics in drylands: Evaluating vegetation optical depth (VOD) using AVHRR NDVI and in situ green biomass data over West African Sahel". In: *Remote Sensing of Environment* 177, pp. 265–276. ISSN: 00344257. DOI: 10.1016/j.rse.2016.02.056.

267. Tolhurst, K. (2009). *Report on the Physical Nature of the Victorian Fires occurring on 7th February 2009*. Report. University of Melbourne.

268. Trenberth, K. E., A. Dai, G. v. d. Schrier, P. D. Jones, J. Barichivich, K. R. Biriffa, and J. Sheffield (2013). "Global warming and changes in drought". In: *Nature Climate Change* 4. DOI: 0.1038/NCLIMATE2067.

269. Trigo, R. M., J. M. C. Pereira, M. G. Pereira, B. Mota, T. J. Calado, C. C. Dacamara, and F. E. Santo (2006). "Atmospheric conditions associated with the exceptional fire season of 2003 in Portugal". In: *International Journal of Climatology* 26.13, pp. 1741–1757. ISSN: 08998418 10970088. DOI: 10.1002/joc.1333.

270. Turco, M., J. von Hardenberg, A. AghaKouchak, M. C. Llasat, A. Provenzale, and R. M. Trigo (2017). "On the key role of droughts in the dynamics of summer fires in Mediterranean Europe". In: *Sci Rep* 7.1. Turco, Marco von Hardenberg, Jost AghaKouchak, Amir Llasat, Maria Carmen Provenzale, Antonello Trigo, Ricardo M eng Research Support, Non-U.S. Gov't England 2017/03/03 06:00 Sci Rep. 2017 Mar 6;7(1):81. doi: 10.1038/s41598-017-00116-9., p. 81. ISSN: 2045-2322 (Electronic) 2045-2322 (Linking). DOI: 10.1038/s41598-017-00116-9. URL: https://www.ncbi.nlm.nih.gov/pubmed/28250442.

271. Turner, M. and W. H. Romme (1994). "Landscape dynamics in crown fire ecosystems". In: *Landscape Ecology* 9.1, pp. 59–77.

272. Urbieta, I. R., G. Zavala, J. Bedia, J. M. Gutiérrez, J. S. Miguel-Ayanz, A. Camia, J. E. Keeley, and J. M. Moreno (2015). "Fire activity as a function of fire–weather seasonal severity and antecedent climate across spatial scales in southern Europe and Pacific western USA". In: *Environmental Research Letters* 10.11, p. 114013. ISSN: 1748-9326. DOI: 10.1088/1748-9326/10/11/114013.

273. van Dijk, A. I. J. M., L. J. Renzullo, Y. Wada, and P. Tregoning (2014). "A global water cycle reanalysis (2003-2012) merging satellite gravimetry and altimetry observations with a hydrological multi-model ensemble". In: *Hydrology and Earth System Sciences* 18.8, pp. 2955–2973. ISSN: 1607-7938. DOI: 10.5194/hess-18-2955-2014.

274. van Dijk, A. I. J. M., H. E. Beck, R. S. Crosbie, R. A. M. de Jeu, Y. Y. Liu, G. M. Podger, B. Timbal, and N. R. Viney (2013). "The Millennium Drought in southeast Australia (2001-2009): Natural and human causes and implications for water resources, ecosystems, economy, and society". In: *Water Resources Research* 49.2, pp. 1040–1057. ISSN: 00431397. DOI: 10.1002/wrcr.20123.

275. Van Rooy, M. P. (1965). "A Rainfall Anomaly Index Independent of Time and Space". In: *Notos* 14, pp. 43–48.

276. Van Wagner, C. E. (1987). *Development and Structure of the Canadian Forest Fire Weather Index System*. Report. Petawawa National Forestry Institute.

277. van Wagtendonk, J. W., R. R. Root, and C. H. Key (2004). "Comparison of AVIRIS and Landsat ETM+ detection capabilities for burn severity". In: *Remote Sensing of Environment* 92.3, pp. 397–408. ISSN: 00344257. DOI: 10.1016/j.rse.2003.12.015.

278. Verbesselt, J., P. Jonsson, S. Lhermitte, J. van Aardt, and P. Coppin (2006). "Evaluating satellite and climate data-derived indices as fire risk indicators in savanna ecosystems". In: *IEEE TRANSACTIONS ON GEOSCIENCE AND REMOTE SENSING* 44.6, pp. 1622–1632.

279. Vicente-Serrano, S. M., S. Beguería, and J. I. López-Moreno (2010). "A Multiscalar Drought Index Sensitive to Global Warming: The Standardized Precipitation Evapotranspiration Index". In: *Journal of Climate* 23.7, pp. 1696–1718. ISSN: 0894-8755 1520-0442. DOI: 10.1175/2009jcli2909.1.

280. Wagner, W., W. A. Dorigo, R. de Jeu, D. Fernandez, J. Benveniste, E. Haas, and M. Ertle (2012). *Fusion of Active and Passive Microwave Observations to Create an Essential Climate Variable Data Record on Soil Moisture*. Conference Paper. ISPRS Annals of the Photogrammerty, Remote Sensing and Spatial Information Sciences.

281. Wanders, N., D. Karssenberg, A. de Roo, S. M. de Jong, and F. P. Bierkens (2014). "The suitability of remotely sensed soil moisture for improving operational flood forecasting". In: *Hydrology and Earth System Sciences* 18, pp. 2343–2357. DOI: 0.5194/hess-18-2343-2014.

282. Wang, G. and W. Cai (2013). "Climate-change impact on the 20th-century relationship between the Southern Annular Mode and global mean temperature". In: *Sci Rep* 3. Wang, Guojian Cai, Wenju eng Research Support, Non-U.S. Gov't England 2013/06/21 06:00 Sci Rep. 2013;3:2039. doi: 10.1038/srep02039., p. 2039. ISSN: 2045-2322 (Electronic) 2045-2322 (Linking). DOI: 10.1038/srep02039. URL: https://www.ncbi.nlm.nih.gov/pubmed/23784087.

283. Wang, K., R. E. Dickinson, M. Wild, and S. Liang (2010). "Evidence for decadal variation in global terrestrial evapotranspiration between 1982 and 2002: 2. Results". In: *Journal of Geophysical Research* 115.D20. ISSN: 0148-0227. DOI: 10.1029/2010jd013847.

284. Werf, G. R. van der, J. T. Randerson, L. Giglio, G. J. Collatz, P. S. Kasibhatla, and A. F. Arellano Jr (2006). "Interannual variability in global biomass burning emissions from 1997 to 2004". In: *Atmos. Chem. Phys.* 6.11. ACP, pp. 3423–3441. ISSN: 1680-7324. DOI: 10.5194/acp-6-3423-2006. URL: https://www.atmos-chem-phys.net/6/3423/2006/.

285. Westerling, A. L., H. G. Hidalgo, D. R. Cayan, and T. W. Swetnam (2006). "Warming and earlier spring increase western U.S. forest wildfire activity". In: *Science* 313.5789. Westerling, A L Hidalgo, H G Cayan, D R Swetnam, T W eng 2006/07/11 09:00 Science. 2006 Aug 18;313(5789):940-3. Epub 2006 Jul 6., pp. 940–3. ISSN: 1095-9203 (Electronic) 0036-8075 (Linking). DOI: 10.1126/science.1128834. URL: http://www.ncbi.nlm.nih.gov/pubmed/16825536.

286. Wilks, D. S. (2006). "On "Field Significance"and the False Discovery Rate". In: *Journal of Applied Meteorology and Climatology* 45, pp. 1181–1189.

287. Williams, A. A. J. and D. J. Karoly (1999). "Extreme fire weather in Australia and the impact of the El Nino Southern Oscillation". In: *Australian Meteorological Magazine* 48, pp. 15–22.

288. Williams, A. A. J., D. J. Karoly, and N. Tapper (2001). "The Sensitivity of Australian Fire Danger to Climate Change". In: *Climate Change* 49, pp. 171–191.

289. Williams, A. and R. Stone (2009). "An assessment of relationships between the Australian subtropical ridge, rainfall variability and high-latitude circulation patterns". In: *International Journal of Climatology* 29, pp. 661–709.

290. Williams, R. J., A. M. Gill, and P. H. R. Moore (1998). "Seasonal Changes in Fire Behaviour in a Tropical Savanna in Northern Australia". In: *International Journal Of Wildland Fires* 8.4, pp. 227–239.

291. Wooster, M. J., G. Roberts, G. L. W. Perry, and Y. J. Kaufman (2005). "Retrieval of biomass combustion rates and totals from fire radiative power observations: FRP derivation and calibration relationships between biomass consumption and fire radiative energy release". In: *Journal of Geophysical Research* 110.D24. ISSN: 0148-0227. DOI: 10.1029/2005jd006318.

292. Wotton, B. M., C. A. Nock, and M. D. Flannigan (2010). "Forest fire occurrence and climate change in Canada". In: *International Journal of Wildland Fire* 19, pp. 253–271.

293. Xu, W., M. J. Wooster, T. Kaneko, J. He, T. Zhang, and D. Fisher (2017). "Major advances in geostationary fire radiative power (FRP) retrieval over Asia and Australia stemming from use of Himarawi-8 AHI". In: *Remote Sensing of Environment* 193, pp. 138–149. ISSN: 00344257. DOI: 10.1016/j.rse.2017.02.024.

294. Xu, Z. and G. C. van Kooten (2014). "The El Nino Southern Oscillation index and wildfire prediction in British Columbia". In: *The Forestry Chronicle* 90.5, pp. 592–598.

295. Yang, Y., M. Uddstrom, M. Revell, and S. Moore (2014). "Soil moisture simulation by JULES in New Zealand: verification and sensitivity tests". In: *Meteorological Applications* 21.4, pp. 888–897. ISSN: 13504827. DOI: 10.1002/met.1426.

296. Yoon, J.-H. and R. L. Leung (2015). "Assessing the relative influence of surface soil moisture and ENSO SST on precipitation predictability over the contiguous United States". In: *Geophysical Research Letters* 42, pp. 5005–5013. DOI: 10.1002/2015GL064139.

297. Zeng, Z., S. Piao, X. Lin, G. Yin, S. Peng, P. Ciais, and R. B. Myneni (2012). "Global evapotranspiration over the past three decades: estimation based on the water balance equation combined with empirical models". In: *Environmental Research Letters* 7.1, p. 014026. ISSN: 1748-9326. DOI: 10.1088/1748-9326/7/1/014026.

298. Zeng, Z., T. Wang, F. Zhou, P. Ciais, J. Mao, X. Shi, and S. Piao (2014). "A worldwide analysis of spatiotemporal changes in water balance-based evapotranspiration from 1982 to 2009". In: *Journal of Geophysical Research: Atmospheres* 119.3, pp. 1186–1202. ISSN: 2169897X. DOI: 10.1002/2013jd020941.

299. Zhou, X. and Q. Zhu (2007). "Temporal stability of soil moisture spatial variability at two scales and its implication for optimal field monitoring". In: *Hydrology and Earth System Sciences* 4, pp. 1185–1214.

300. Zreda, M. (2016). "Land-surface hydrology with cosmic-ray neutrons: principles and applications". In: *Journal of the Japanses Society of Soil Physics* 132, pp. 25–30.